Neural Plasticity

Neural Mechanisms of Autonomic Dysfunction in Neurological Diseases

Lead Guest Editor: Depei Li
Guest Editors: Yulong Li, Jianhua Li, and Sheng Wang

Neural Mechanisms of Autonomic Dysfunction in Neurological Diseases

Neural Plasticity

Neural Mechanisms of Autonomic Dysfunction in Neurological Diseases

Lead Guest Editor: Depei Li
Guest Editors: Yulong Li, Jianhua Li, and Sheng Wang

Editorial Board

Contents

Hindawi
Neural Plasticity
Volume 2017, Article ID 2050191, 2 pages
https://doi.org/10.1155/2017/2050191

Editorial

Neural Mechanisms of Autonomic Dysfunction in Neurological Diseases

De-Pei Li,[1] Yu-Long Li,[2] Jianhua Li,[3] and Sheng Wang[4]

[1]*Department of Critical Care, The University of Texas, MD Anderson Cancer Center, Houston, TX, USA*
[2]*Department of Emergency Medicine, University of Nebraska Medical Center, Omaha, NE, USA*
[3]*Department of Medicine, Penn State College of Medicine, Hershey, PA, USA*
[4]*Department of Physiology, Hebei Medical University, Shijiazhuang, Hebei, China*

Correspondence should be addressed to De-Pei Li; dpli@mdanderson.org

Received 7 December 2017; Accepted 7 December 2017; Published 27 December 2017

Autonomic nervous system innervates internal organs and plays a crucial role in maintaining hemostasis of cardiovascular, respiratory, energy metabolism, balance of water, electrolyte, and body fluid, and so forth. Dysfunction of the autonomic nervous system is associated with many neurological diseases including neurogenic hypertension, stroke, Alzheimer's disease, Parkinson's disease, and depression. Autonomic dysfunction is also observed in metabolic diseases such as diabetes, obesity, and metabolic syndrome. Many efforts have been made to elucidate the neuronal mechanisms underlying dysautonomia of the cardiovascular system such as hypertension [1]. Overactivation of the sympathetic nervous system is associated with several types of hypertension such as essential hypertension, salt-sensitive hypertension, and obesity-related hypertension, as well as renal hypertension [1, 2]. It has been shown that presympathetic neurons in autonomic nuclei in the hypothalamus and rostral ventrolateral medulla provide excitatory drive to sympathetic outflow in hypertension. Thus, the neural plasticity in these presympathetic neurons and related factors that regulate the excitability of these neurons are crucially important to affect blood pressure and sympathetic vasomotor tone. In this special issue of "Neural Mechanisms of Autonomic Dysfunction in Neurological Diseases," studies addressed brain stem and hypothalamus mechanisms involved in the regulation of sympathetic outflow and blood pressure.

H. Zheng et al. studied hypothalamic mechanisms in the context of sympathetic activation in hypertension related to obesity or type II diabetes mellitus. They reported that the expression levels of leptin receptor and *N*-methyl-*D*-aspartate receptor (NMDAR) subunit NR1 in the hypothalamus were significantly elevated in a rat model of type II diabetes mellitus induced by high-fat diet and low-dose streptozotocin. They also found that leptin receptors interact with NMDARs in the regulation of sympathetic outflow. The mechanisms associated with the development of hypertension identified in this study may contribute to the elevated sympathetic outflow and provide a potential target to develop a novel treatment for hypertension in type II diabetes mellitus.

A variety of factors may lead to autonomic dysfunction involved in the overactivation of the sympathetic nervous system including diet ingredients and environmental factors. M.-F. Zhong et al. reported in this special issue that homocysteine, a dietary amino acid, in the rostral ventrolateral medulla in the brain stem increased blood pressure and sympathetic outflow. This observed response is mediated by an induction of oxidative stress in the autonomic brain nucleus. A. D. Chapp et al. reported that high-salt diet was an independent risk factor for the development of salt-sensitive hypertension through suppressing small conductance calcium-activated potassium channels and subsequently increasing excitability of presympathetic neurons in the hypothalamus. These findings could significantly improve our understanding of the role of dilatory ingredients in the development of dysautonomia in hypertension. Glutamate is a major excitatory neurotransmitter in the vertebrate

nervous system, and glutamatergic synaptic inputs innervate the presympathetic neurons located in the autonomic nucleus in the brain stem and hypothalamus. Enhancement of these excitatory glutamatergic inputs can result in sympathetic overactivation in various animal models of hypertension [1]. W. Wang et al. reported that glutamatergic inputs to the rostral ventrolateral medulla in the brain stem were enhanced, contributing to neuropathic pain-induced high blood pressure.

The purpose of this special issue is to publish findings focusing on neural plasticity of dysautonomia in neurological diseases. Although most of the accepted manuscripts reported neural plasticity in dysfunction of the autonomic nervous system in the regulation of sympathetic activity and blood pressure, these mechanisms may also apply to autonomic dysfunction during other neurological diseases. Therefore, the studies compiled in this special issue may promote research activities of neural mechanisms underlying autonomic dysfunction in neurological diseases.

Acknowledgments

We are grateful to all the authors for their informative contributions and the reviewers for their support and constructive critiques in making this special issue possible.

De-Pei Li
Yu-Long Li
Jianhua Li
Sheng Wang

References

[1] D. P. Li and H. L. Pan, "Glutamatergic regulation of hypothalamic presympathetic neurons in hypertension," *Current Hypertension Reports*, vol. 19, no. 10, p. 78, 2017.

[2] A. M. Allen, "Inhibition of the hypothalamic paraventricular nucleus in spontaneously hypertensive rats dramatically reduces sympathetic vasomotor tone," *Hypertension*, vol. 39, no. 2, pp. 275–280, 2002.

Hindawi
Neural Plasticity
Volume 2017, Article ID 7282834, 10 pages
https://doi.org/10.1155/2017/7282834

Research Article

Long-Term High Salt Intake Involves Reduced SK Currents and Increased Excitability of PVN Neurons with Projections to the Rostral Ventrolateral Medulla in Rats

Andrew D. Chapp,[1] Renjun Wang,[1,2] Zixi (Jack) Cheng,[3] Zhiying Shan,[1] and Qing-Hui Chen[1]

[1]*Department of Kinesiology and Integrative Physiology, Michigan Technological University, Houghton, MI 49931, USA*
[2]*Department of Biotechnology, School of Life Science, Jilin Normal University, Siping, Jilin 136000, China*
[3]*Biomolecular Science Center, Burnett School of Biomedical Sciences, College of Medicine, University of Central Florida, Orlando, FL 32816, USA*

Correspondence should be addressed to Qing-Hui Chen; qinghuic@mtu.edu

Received 19 July 2017; Accepted 11 September 2017; Published 6 December 2017

Academic Editor: Depei Li

Evidence indicates that high salt (HS) intake activates presympathetic paraventricular nucleus (PVN) neurons, which contributes to sympathoexcitation of salt-sensitive hypertension. The present study determined whether 5 weeks of HS (2% NaCl) intake alters the small conductance Ca^{2+}-activated potassium channel (SK) current in presympathetic PVN neurons and whether this change affects the neuronal excitability. In whole-cell voltage-clamp recordings, HS-treated rats had significantly decreased SK currents compared to rats with normal salt (NS, 0.4% NaCl) intake in PVN neurons. The sensitivity of PVN neuronal excitability in response to current injections was greater in HS group compared to NS controls. The SK channel blocker apamin augmented the neuronal excitability in both groups but had less effect on the sensitivity of the neuronal excitability in HS group compared to NS controls. In the HS group, the interspike interval (ISI) was significantly shorter than that in NS controls. Apamin significantly shortened the ISI in NS controls but had less effect in the HS group. This data suggests that HS intake reduces SK currents, which contributes to increased PVN neuronal excitability at least in part through a decrease in spike frequency adaptation and may be a precursor to the development of salt-sensitive hypertension.

1. Introduction

Elevated sympathetic outflow is a characteristic of salt-sensitive hypertension (SSH). The increased sympathetic outflow elicited by elevated dietary consumption of sodium chloride (NaCl) has been well documented to underlie the neural mechanisms of SSH, although many other stressors contribute to the development of SSH. Recent reports from our lab [1–4] and others [5–8] have demonstrated that the development of SSH is at least in part, neurogenic in nature. Indeed, numerous studies have demonstrated a link between elevated extracellular NaCl and the development of exaggerated sympathetic outflow [2, 9–12] as well as central hyperosmotic NaCl challenge consistently increases SNA [2, 9–14]. However, how HS intake activates the sympathetic nervous system (SNS) neurogenically has not been well studied.

While there are many areas in the brain that contribute to the sympathetic activation and development of SSH, the paraventricular nucleus (PVN) of the hypothalamus has numerous projections to downstream brain regions such as the nucleus solitary tract [15], rostral ventrolateral medulla [3, 4] (RVLM), and spinal cord [16, 17]. These downstream brain regions are capable of regulating and/or initiating

sympathetic outflow which contributes to hypertension. A key pathway in the neuronal circuitry for the development of hypertension is neurons originating in the PVN which have a monosynaptic projection to the RVLM (PVN-RVLM) [1, 3, 4]. The RVLM has pathway projecting to the spinal intermediolateral column (IML) [18] which has high regulatory control on sympathoexcitation. As such, any alterations in PVN-RVLM neuronal excitability can have a profound effect on the sympathoexcitation.

Like other central nervous system (CNS) regions, PVN neuronal activity is regulated not only by synaptic activity but also by intrinsic membrane properties and excitability. Small conductance Ca^{2+}-activated K^+ (SK) channels have been documented in brain regions as a major regulator of neuronal excitability [19–22]. It has been demonstrated that the SK channels also play an important role in controlling the *in vitro* excitability of presympathetic PVN-RVLM neurons and *in vivo* sympathetic outflow in rats [3, 23]. Moreover, we have reported that downregulation of SK channel function among the PVN neurons contributed to the sympathoexcitation in rats with chronic HS intake (5 weeks of 2% NaCl) [24]. Furthermore, our recent study indicates that depletion of endoplasmic reticulum (ER) Ca^{2+} store likely plays a role in increasing PVN-RVLM neuronal excitability, which may underlie the mechanisms of sympathoexcitation in rats with HS intake [24]. Due to the fact that Ca^{2+} release from the ER is a prominent activator of SK channels to mediate neuronal excitability [25], we hypothesize that reduced SK currents may contribute to the increased excitability of PVN-RVLM neurons in rats with HS intake, which may underlie the neural mechanism of sympathoexcitation. This in turn may be a precursor and contributing factor to the development of SSH through alterations of the intrinsic properties of presympathetic PVN-RVLM neurons.

2. Methods

2.1. Animal Preparation and High Salt Diet. Male Sprague-Dawley rats ($n = 21$, 250–400 gm, Taconic) were individually housed in a temperature-controlled room (22-23°C) with a 14 h : 10 h light-dark cycle. Rats were age matched and placed on either high salt (HS, 2% NaCl) or normal salt (NS, 0.4% NaCl). Diets were identical in calories from fat and protein and also total carbohydrate and sucrose (Harlan). All experimental and surgical procedures were carried out under the guidelines of the National Institutes of Health Guide for the Care and Use of Laboratory Animals with approval by the Institutional Animal Care and Use Committee of Michigan Technological University.

2.2. Retrograde Labeling of PVN-RVLM Neurons. Rats on HS diet were labeled after 5 weeks of HS feed, and NS rats were age matched and labeled as needed. PVN neurons were retrogradely labeled from the ipsilateral RVLM as previously described [1, 3, 16]. Briefly, rats were anesthetized with intraperitoneal sodium pentobarbital (50 mg/kg body weight) and placed in a stereotaxic frame, and a small burr hole drilled to expose the cerebellum. A glass micropipette was lowered into the pressor region of the RVLM (coordinates: −13.0 mm caudal to bregma, 1.8 mm lateral to midline, and 9.2 mm below the skull) and 100 nL of red fluosphere microspheres (Life Technologies) injected. Each animal received daily injections of penicillin G (30,000 U/100 gm body weight, subcutaneously) and meloxicam (1 mg/kg body weight) for 3 days after surgery. Location of the tracer was verified postmortem in histological sections through the RVLM (Figure 1). Identical surgeries were performed on rats on a NS diet.

2.3. Electrophysiology. To perform whole-cell patch clamp recordings, methods utilized were adapted from our and others' previous publications [1, 4, 26]. Briefly, five to seven days following retrograde labeling, rats were anesthetized with isoflurane (5% in O_2) and decapitated. Brains were rapidly removed and submerged in ice-cold cutting solution (~3 min) containing (in mM) 206 sucrose, 2 KCl, 2 $MgSO_4$, 1.25 NaH_2PO_4, 26 $NaHCO_3$, 1 $CaCL_2$, 1 $MgCl_2$, 10 D-glucose, and 0.4 ascorbic acid. Osmolality and pH were adjusted to 290–302 mosmol/L and 7.32–7.40, respectively. Cutting solution pH and pO_2 were maintained by continuous gassing with 95% O_2–5% CO_2. A brain block containing the hypothalamus was cut and fixed on a vibrating microtome (Leica VT 1000S; Leica, Nussloch, Germany). Coronal slices through the PVN were cut at a thickness of 250 μm. Slices were incubated at 30°C for 1 h in artificial cerebrospinal fluid (ACSF) containing (in mM) 125 NaCl, 2 KCl, 2 $MgSO_4$, 1.25 NaH_2PO_4, 26 $NaHCO_3$, 2 $CaCl_2$, 10 D-glucose, and 0.4 ascorbic acid (osmolality: 295–302 mosmol/L, pH 7.32–7.40). Slices were transferred to a glass-bottomed recording chamber and viewed through an upright microscope (Nikon) equipped with DIC optics, epifluorescence, an infrared (IR) filter, and an IR-sensitive video camera (C2400, Hamamatsu, Bridgewater, NJ). An appropriate filter was used to visualize neurons retrogradely labeled with the red fluospheres (Figure 1).

Patch electrodes were pulled (Flaming/Brown P-97, Sutter Instrument, Novato, CA) from borosilicate glass capillaries and polished to a tip resistance of 4–8 MΩ as previously described [1, 4, 26]. Electrodes were filled with a solution containing (in mM) 135 K-gluconate, 10 HEPES, 0.1 EGTA, 1.0 $MgCl_2$, 1.0 NaCl, 2.0 Na_2ATP, and 0.5 Na_2GTP (osmolality: 280–285 mosmol/L, pH 7.3). Our intracellular solution contains a low concentration of EGTA (0.1 mM) to allow the accumulation of intracellular Ca^{2+} during membrane depolarization for the activation of SK channels [3, 16]. Once a GΩ seal was achieved in whole-cell configuration, cell capacitance (C_m), access resistance, and resting membrane potential (V_m) were monitored until stable. Cells that met the following criteria were included in the analysis: action potential amplitude ≥50 mV from threshold to peak, input resistance (R_{input}) ≥ 0.5 GΩ (determined by injection of −20 pA from a holding potential of −80 mV), resting V_m negative to −50 mV. Recordings were made using an Axopatch 200B amplifier and pCLAMP software (10, Axon Instruments, Union City, CA). Signals were filtered at 1 kHz, digitized at 10 kHz (Digidata 1400A, Axon Instruments), and saved on a computer for off-line analysis.

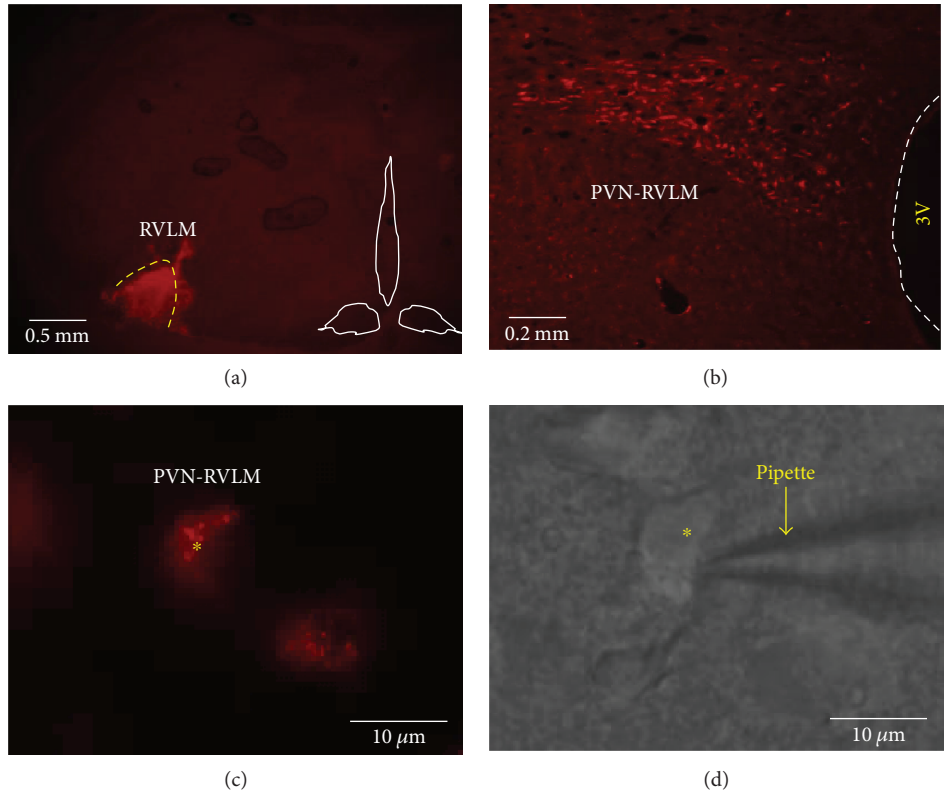

Figure 1: Identification of PVN-RVLM neurons in brain slice for whole-cell patch clamp recording. (a) Red fluorescent tracers were microinjected (100 nL) into the RVLM. (b) Retrograde labeling of the ipsilateral PVN was observed in the dorsal and ventrolateral subnuclei. (c) Image viewed with fluorescence illumination shows a recorded PVN-RVLM neuron containing retrograde tracer. (d) Infrared-DIC image shows the patch electrode positioned on the same PVN-RVLM neuron as (c). 3V: third ventricle.

2.4. Recording SK Current. To study SK current, voltage-clamp recordings were performed as previously described [1, 4], with intracellular solution containing a cAMP analogue 8-(4-chlorophenylthio) 3,5′-cyclic adenosine monophosphate (8CPT-cAMP, 50 μM) to block the slow afterhyperpolarization current [1]. Recordings were performed in the presence of tetrodotoxin (TTX, 1.0 μM) to block voltage-gated sodium channels and tetraethylammonium (TEA, 1.0 mM) to block voltage-gated potassium channels. Membrane potential was clamped at −60 mV and stepped to +10 mV for 100 ms. On returning V_m to −60 mV, an outward tail current was recorded. A time control was performed at 5, 10, and 15 min. After time control tail currents, apamin (100 nM) was bath applied to selectively block SK channels and again recorded at 5, 10, and 15 min postapamin treatment. The tail current recorded during treatment was subtracted from the corresponding control tail current to isolate the apamin-sensitive SK current. Decay of the SK current was analyzed by fitting the subtracted current with a one-phase exponential.

2.5. Testing Neuronal Excitability. Excitability of neurons from NS and HS rats was studied in a current-clamp mode in the absence of TTX, TEA, or 8CPT-cAMP as was previously described [1, 4, 26], with slight modification. With membrane potential adjusted to −80 mV by continuous negative current injection, a series of square-wave current injections was delivered in steps of +25 pA, each for a duration of 800 ms. To determine the action potential voltage threshold (V_t), ramp current injections (0.2 pA ms^{-1}, 1000 ms) were made from a potential of −80 mV. Square wave and ramp current injections were made in the same neurons. For the depolarizing R_{input}, a +25 pA current injection was made for 800 ms and the voltage change measured. The depolarizing R_{input} was calculated using Ohms' law ($V = (I/R)$). It must be noted that current and voltage-clamp recordings were made from different groups of PVN-RVLM neurons.

2.6. Chemicals. All chemicals were obtained from Sigma-Aldrich (St Louis, MO, USA) except for TTX (Tocris Bioscience, UK) and TEA (Fluka BioChemika, Switzerland).

2.7. Data Analysis. Summary data are reported as means ± SEM. Depending on the experiment, group means were compared using an unpaired test, a one-way or a two-way ANOVA with post hoc analysis. When differences were found, the Newman-Keuls multiple comparison test was used for comparison test (GraphPad Prism, v5.0). Differences between means were considered significant at $P < 0.05$.

Table 1: Properties of PVN-RVLM neurons.

Group	n	V_m (mV)	C_m (pF)	R_{input} (GΩ)	V_t (mV)
NS	6	-57.8 ± 3.2	51.2 ± 4.7	0.54 ± 0.03	-42.8 ± 2.8
NS apamin	5	-55.8 ± 1.7	44.8 ± 3.3	0.78 ± 0.11	-38.0 ± 1.3
HS	6	-59.3 ± 1.5	47.0 ± 4.3	0.83 ± 0.08	-40.4 ± 1.8
HS apamin	6	-58.0 ± 1.0	41.2 ± 2.4	0.96 ± 0.11	-41.0 ± 2.1

V_m: resting membrane potential; C_m: membrane capacitance; R_{input}: depolarizing input resistance; V_t: subthreshold of membrane potential to fire action potential.

3. Results

3.1. Comparison of Passive Membrane Properties. Resting membrane potential (V_m), depolarizing R_{input}, whole-cell capacitance (C_m), and voltage threshold for firing action potentials (V_t) of PVN-RVLM neurons from NS controls and the HS group were compared, and no significant differences were identified either in the absence or presence of bath application of apamin (Table 1).

3.2. High Salt Diet Reduces SK Currents in PVN-RVLM Neurons. Our lab has previously demonstrated that HS diet and subcutaneous infusion of ang II induce a diseased state model of SSH in male SD rats. This hypertensive model shows reduced SK currents and increased PVN-RVLM neuronal excitability [1]. To determine whether HS alone is capable of altering PVN-RVLM SK currents, we performed whole-cell voltage-clamp recordings of SK currents in PVN-RVLM neurons from NS and HS diet-treated SD rats at a holding potential of −60 mV. Our results show that SK currents in HS rats were significantly reduced compared to NS rats (12.9 ± 6.9 pA versus 37.1 ± 6.5 pA, $P < 0.05$). Figure 2(a) shows a representative SK current trace from the same neuron of before apamin, a SK channel blocker in NS (black), after treatment of apamin in NS (red), and the subtracted total SK current in NS (*inset*). Figure 2(b) shows a representative SK current trace from the same neuron in HS rats, before apamin (blue), after apamin (purple), and the subtracted total SK current (*inset*). Figure 2(c) is summary data of SK currents in NS (black, $n = 5$) and HS (blue, $n = 6$). Figure 2(d) is summary data for SK current density between NS (black) and HS (blue). The SK current density was calculated by the total SK current divided by the cell capacitance.

3.3. High Salt Intake and Role of SK Channels in Regulating Neuronal Excitability. To test whether HS intake alters excitability and whether reduced SK currents underlie the mechanisms of HS intake induced an increase in excitability, PVN-RVLM neurons from NS and HS-treated rats were subjected to sequential depolarizing current injections (0–200 pA, positive). Graded current injections evoked graded increases in firing frequency and reached saturation at +200 pA current in NS neurons. This data confirms our previous findings regarding PVN-RVLM neuronal excitability between NS and HS-treated rats [24]. Apamin, a potent SK channel blocker, significantly increased neuronal firing frequency in NS neurons compared to NS neurons without apamin (+200 pA, 49.4 ± 3.2 versus 18.5 ± 2.5 Hz, $P < 0.05$). Figure 3 shows representative traces of NS control (Figure 3(a), black), NS with apamin (Figure 3(a), red), HS control (Figure 3(a), blue), and HS with apamin (Figure 3(a), purple) to +200 pA current injection. A current injection stimulus response was constructed between NS and NS with apamin over the sequential depolarizing current injections (0–200 pA). Significant increases ($^*P < 0.05$) in excitability were observed at 100, 150, and 200 pA current injection in NS with apamin (Figure 3(b), left, red line, two-way ANOVA) compared to NS control (Figure 3(b), left, black line, two-way ANOVA). A linear regression of the current injection response was well fit and showed an increased slope of the line in NS with apamin compared to NS control (Figure 3(c), 0.25 ± 0.013 versus 0.10 ± 0.004, $^*P < 0.05$ versus NS). Likewise, PVN-RVLM neurons from HS rats showed a significant increase in firing frequency compared to NS neurons (30.0 ± 4.8 versus 18.5 ± 2.5 Hz, $P < 0.05$). SK channel blockade with apamin in HS PVN-RVLM neurons increased neuronal excitability compared to HS control (45.4 ± 5.4 versus 30.0 ± 4.8 Hz, $P < 0.05$) but did not show a difference when compared to NS with apamin (45.4 ± 5.4 versus 49.4 ± 3.2 Hz). A current injection stimulus-response curve was constructed for HS control and HS with apamin PVN-RVLM neurons over the depolarizing current injections (0–200 pA). A significant ($\dagger P < 0.05$) difference in excitability was noticed at 200 pA current injection in HS control (Figure 3(b), right, blue line, two-way ANOVA) compared to HS with apamin (Figure 3(b), right, purple line, two-way ANOVA). A linear regression of the current injection response was well fit and showed an increased slope of the line in HS with apamin compared to HS control (Figure 3(c), 0.28 ± 0.010 versus 0.18 ± 0.007, $\dagger P < 0.05$ versus HS). Treatment of NS and HS with apamin increased the slope of the line almost identically, (0.25 ± 0.013 versus 0.28 ± 0.010) which were not statistically different. This data suggests that SK channels contribute to the regulation of neuronal excitability and that HS reduces SK channel function which contributes to increased PVN-RVLM neuronal excitability through an increase in sensitivity to a stimulus.

3.4. High Salt Intake and Role of SK Channels in Regulating Spike Frequency Adaptation. To test whether dysfunction of SK channels contributes to the increased neuronal excitability in rats with HS intake through the inhibition of spike frequency adaptation (SFA), PVN-RVLM neurons from NS and HS, with and without apamin, were analyzed for interspike interval time (ISI) on action potentials 2–12 at +200 pA current injection. We found that compared to NS control cells, blockade with apamin significantly reduced the ISI time (Figure 4(a), left). Furthermore, HS cells without apamin also exhibited a decreased ISI time compared to NS control cells (Figure 4(a), right). The ISI lines were fitted with a linear regression and the slopes were analyzed to give an understanding of the overall SFA. Compared to NS control cells, NS with apamin had a significantly reduced slope of the line (Figure 4(b), 2.07 ± 0.186 versus 0.242 ± 0.058, $^*P < 0.05$ versus NS). Similarly, HS control cells compared to HS with apamin had a significantly reduced slope, although not as

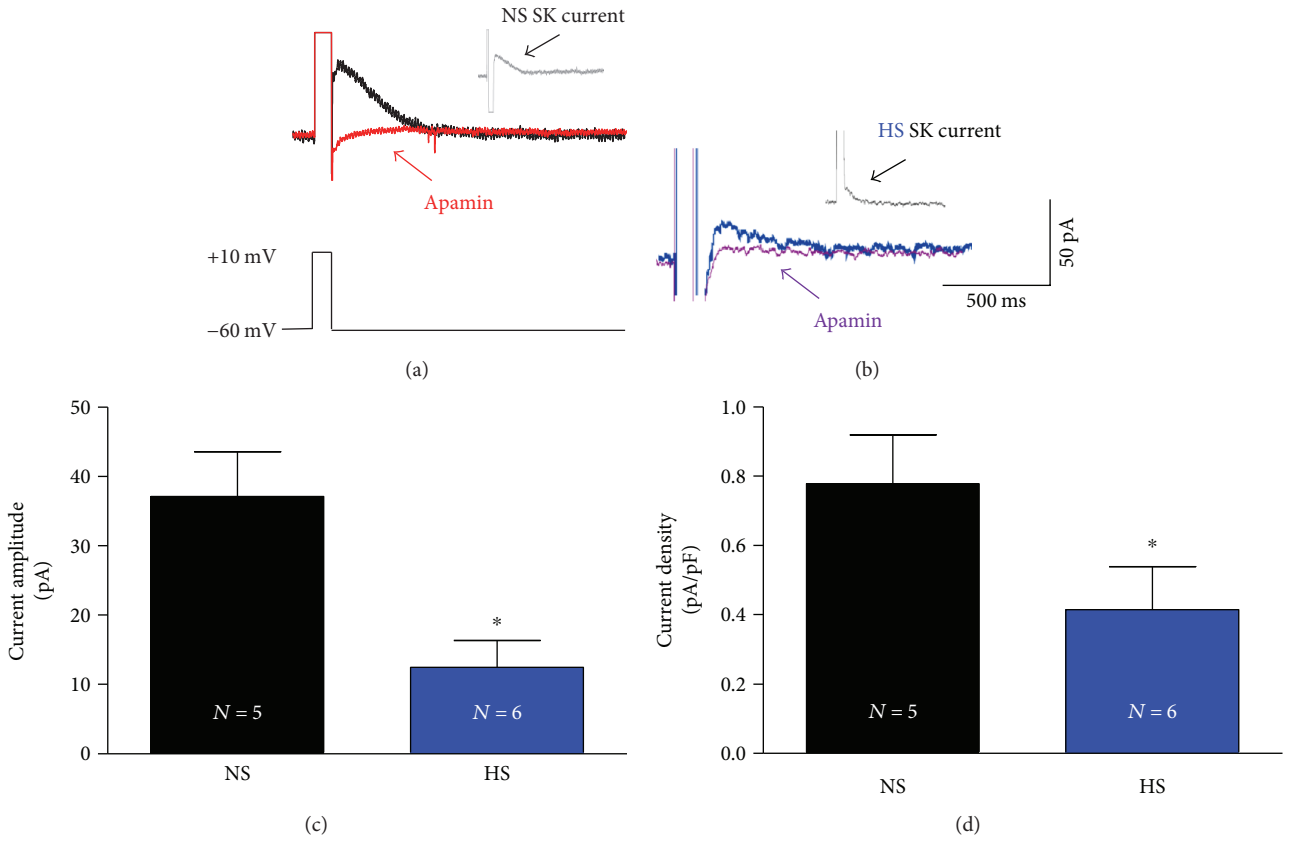

Figure 2: HS intake reduces SK currents in PVN-RVLM neurons. (a) The representative voltage-clamp recording traces from NS PVN-RVLM neuron. An outward tail current (black) prior to apamin and the outward tail current (red) after apamin with the total SK current (inset) from the subtraction of the apamin trace (red) from the nonapamin trace (black). (b) The representative voltage-clamp recording traces from HS PVN-RVLM neuron. An outward tail current (blue) prior to apamin and the outward tail current (purple) after apamin with the total SK current (inset) from the subtraction of the apamin trace (purple) from the nonapamin trace (blue). (c) Summary data for apamin-sensitive SK currents between NS controls and the HS group. (d) Summary data for SK current density between NS controls and the HS group showed a significant reduction in SK current density ($^*P < 0.05$ versus NS controls, unpaired t-test).

drastic as in the NS cells (Figure 4(b), 1.23 ± 0.055 versus 0.485 ± 0.033, $\dagger P < 0.05$ versus HS). HS control cells compared to NS control cells showed a significant decrease in the slope of the line (1.23 ± 0.055 versus 2.07 ± 0.186, $^*P < 0.05$ versus NS). NS and HS cells treated with apamin had very similar slopes for ISI, (0.242 ± 0.058 versus 0.485 ± 0.033) which were drastically reduced compared to cells without apamin. This data suggests reduced SK channel function in PVN-RVLM neurons contributes to the increased excitability in rats with HS intake through the mechanism of inhibition of spike frequency adaptation (SFA).

4. Discussion

The present study explored the effects of high salt (HS) intake on SK currents and the role of SK channels in regulating excitability among presympathetic PVN neurons. The major findings of this study were (1) the amplitude of whole-cell SK current was reduced and neuronal excitability was increased in the HS group compared with NS controls. SK channel blockade with apamin induced a greater increase in excitability in NS controls compared to that in the HS group; (2) A shorter interspike interval (ISI) was observed in the HS group compared to NS controls. Apamin significantly shortened the ISI in NS controls but had less effect in the HS group. This data suggests that HS diet reduces SK currents, which contributes to increased PVN-RVLM neuronal excitability at least in part through an increased sensitivity to a stimulus and a decrease in spike frequency adaptation (SFA).

We have previously demonstrated that rats with ang II-salt hypertension have reduced SK currents and increased PVN-RVLM neuronal excitability [1, 27, 28]. The effect of HS intake alone on the properties and function of SK channels in these neurons have not been well studied yet. What is clear is that chronic HS intake is capable of altering many neuronal properties. Previous publications regarding chronic HS intake have implicated a number of ion channels and neuronal signaling mechanisms which are affected, including downregulation of the potassium/chloride cotransporter 2 in vasopressin neurons [29], increased proinflammatory cytokine production [26, 30], increased NOX [31–34], reduced GABA [35–37] levels, and reduction in glutamate decarboxylase-67 in the PVN [33]. These studies provide direct evidence that chronic HS intake does have a dramatic effect on neuronal signaling molecules and on neuronal excitability. Despite this fact, very little is

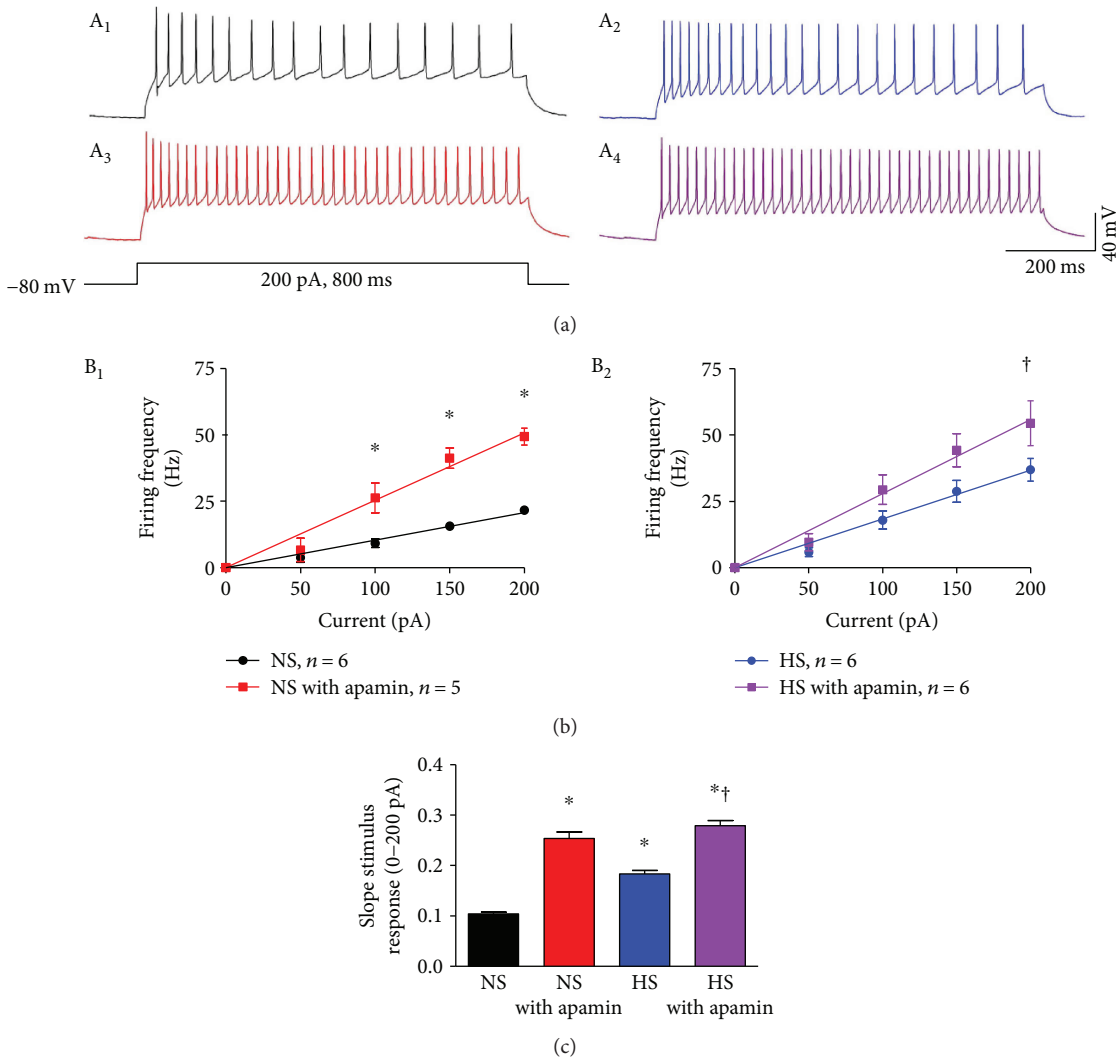

FIGURE 3: HS intake increases PVN-RVLM neuronal excitability. (a, black) A representative trace of NS control neuronal firing at +200 pA current injection. (a, blue) A representative trace of HS control neuronal firing at +200 pA current injection. (a, red) A representative trace of neuronal firing at +200 pA current injection in NS with apamin. (a, purple) A representative trace of neuronal firing at +200 pA current injection in HS with apamin. (b, left) A current injection stimulus-response curve for NS controls (black) and NS with apamin (red) to graded current injections ($^*P < 0.05$ versus NS controls without apamin, two-way ANOVA). (b, right) A current injection stimulus-response curve for the HS group (blue) and HS with apamin (purple) to graded current injections ($\dagger P < 0.05$ versus the HS group without apamin, two-way ANOVA). (c) Summary data for the slope of the linear regression line from the current injection response. The HS group showed a significant increase in the slope compared to NS controls. Treatment with apamin significantly increased the slope in both NS controls and the HS group, but less effect on the slope of the HS group compared to NS controls. ($^*P < 0.05$ versus NS controls; $\dagger P < 0.05$ versus the HS group, one-way ANOVA).

known regarding the effects of HS intake on PVN-RVLM neuronal excitability and SK currents in normotensive rats. That is to say, we were interested in whether SK channel dysfunction is secondary to hypertension or whether SK channel dysfunction precedes the development of hypertension.

How SK currents are reduced in rats with a HS diet is a bit unclear at this point. It is unlikely that the alterations are due to increases in sodium concentrations in the cerebral spinal fluid (CSF). Nakamura and colleagues have demonstrated that SD rats on a HS diet have no observable changes in sodium concentration in CSF compared to animals with NS control [38]. Furthermore, the PVN is encapsulated by a complete blood-brain barrier (BBB) indicating that influx of peripheral hormones is less likely [39]. We cannot however rule out upstream circumventricular organs (CVO) such as the subfornical organ (SFO), which have an incomplete BBB and are sensitive to changes in osmolality and circulating peripheral hormones such as Ang II [11, 27, 40, 41]. The SFO does have a projection to the PVN, and it has been postulated that alterations in SFO-PVN-RVLM neurons may contribute to the development of hypertension [11, 41]. Whether this presynaptic input of CVOs is capable of altering SK channel function through changes

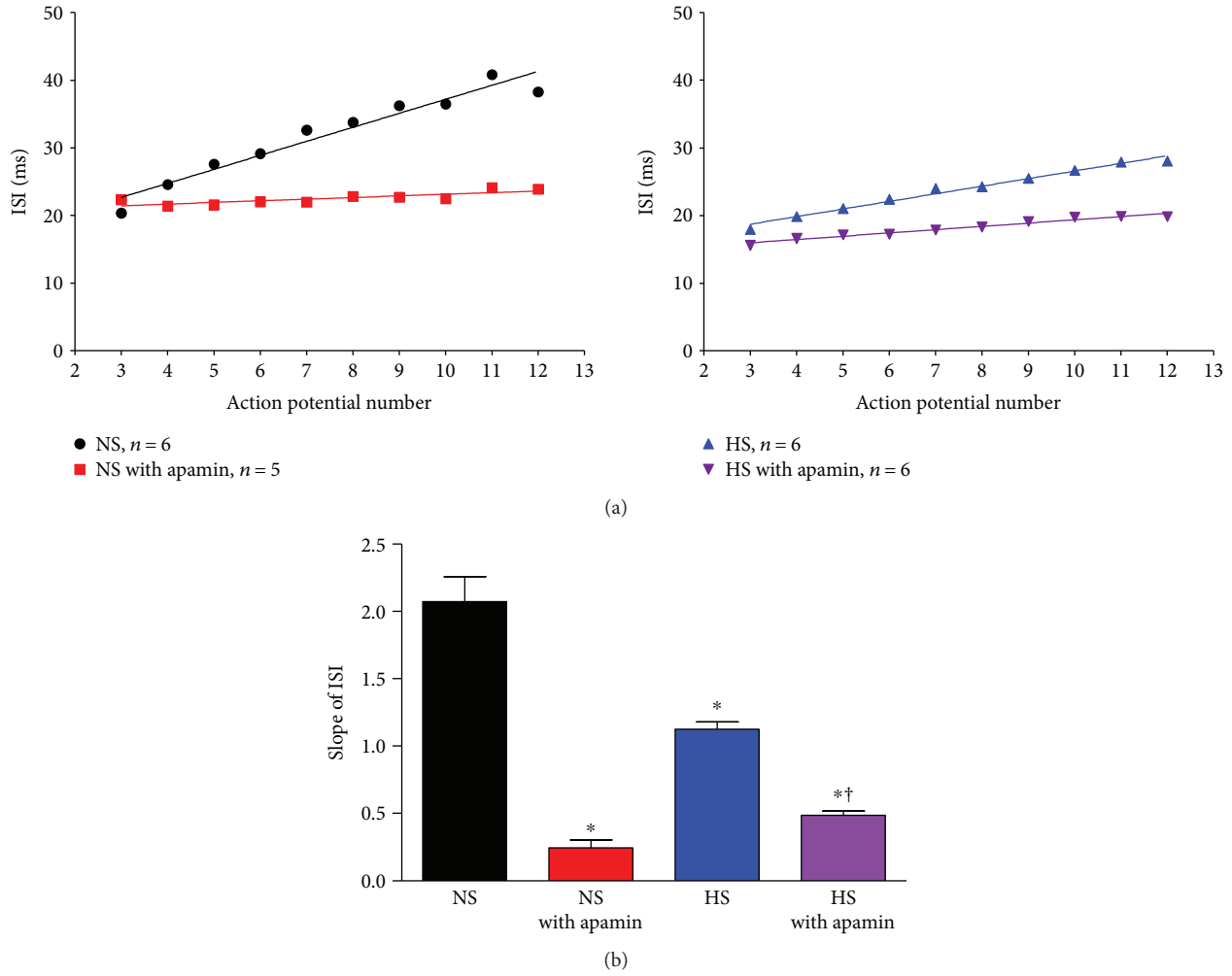

FIGURE 4: HS intake decreases interspike interval (ISI) in PVN-RVLM neurons. (a, left) ISI time for NS controls (black) and NS with apamin (red) PVN-RVLM neurons. (a, right) ISI time for the HS group (blue) and HS with apamin (purple) PVN-RVLM neurons. (b) Summary data for the slope of the linear regression line for the ISI in NS controls and NS with apamin, ISI in the HS group and HS with apamin ($^*P < 0.05$ versus NS; $\dagger P < 0.05$, versus HS, one-way ANOVA).

in presynaptic neurotransmitter release or gene expression remains to be elucidated.

Contrary to the unknown mechanisms of HS intake-induced increases in the excitability of presympathetic PVN neurons, the contributions of SK channels in regulating neuronal excitability in other areas of the brain have been consistently documented in the literature. In nonhypertensive studies, SK channels have been shown to modulate the excitability of neurons in the infralimbic cortex, contributing to fear extinction memory [42]. Similar to our studies in PVN-RVLM neurons, Criado-Marrero and colleagues showed an increase in neuronal excitability following blockade of SK channels with apamin, a decrease in ISI time and an increase in depolarizing R_{input} in the infralimbic cortex [42]. In a separate study, Yang found that SK channels in the dorsal horn of the spinal cord also controlled neuronal excitability and mAHP, with potential therapeutic value for treatment of pain [22]. In cardiac motor neurons, Lin and colleagues also established SK channel blockade with apamin-increased neuronal firing frequency, decreased mAHP, and abolished spike frequency adaptation (SFA) compared to neurons treated without apamin [43]. These groups contribute to the well-established concept that SK channels significantly regulate neuronal excitability, both in autonomic sympathetic neurons, parasympathetic neurons, and cortical neurons. Our conclusions from autonomic PVN-RVLM neurons are also consistent with these previous findings. It must also be mentioned that there is some regional specificity regarding SK channel activity and neuronal excitability. Gu and colleagues have reported differences in SK channel regulation of neuronal excitability between CA1 neurons and bursting pyramidal neurons [44]. CA1 neurons displayed no alterations in mAHP following apamin treatment, whereas bursting pyramidal neurons in the subiculum showed reductions in Na^+ driven, mAHP following apamin [44].

The mode of action of SK channels in regulating neuronal excitability is the production of an outward K^+ current

in response to a depolarizing stimulus, thus contributing to returning the neuron to a more hyperpolarized membrane potential. The SK currents in the HS group are reduced compared to NS and as such, the accumulation of intracellular K^+ in the HS group results in a reduction in the ability to reduce excitability. When examining the stimulus-response slope, NS averages ~0.1, which is significantly increased to ~0.25 in NS with apamin. HS treatment drastically increased the baseline slope to ~0.2 compared to NS ~0.1 and HS with apamin to ~0.28. Since SK currents are significantly reduced in HS versus NS, ~12 pA versus ~40 pA, respectively, we attribute the increased sensitivity to a stimulus response in HS is at least in part due to reduction in SK currents. NS with apamin versus HS with apamin had no statistical difference in their slopes to graded increases in current injection. This finding is supportive of our interpretation of loss of SK channel function in PVN neurons in rats with HS intake increases neuronal sensitivity to a depolarizing stimulus, as blockade of SK channels in NS or HS groups with apamin has nearly identical slopes (Figure 3(c)).

SFA is defined as when stimulated with depolarizing square pulse, neurons show a reduction in the firing frequency following an initial increase. This loss of SFA is usually at least in part as a result of decreased ISI [20]. When examining the raw traces to a +200 pA current injection in NS control cells, SFA is clearly visible as the interval between action potentials gradually lengthens (Figure 3(a), black). This ability is less pronounced in HS control cells (Figure 3(a), blue) and is completely absent in NS (Figure 3(a), red) and HS (Figure 3(a), purple) neurons treated with apamin. When examining the slope of the ISI (Figure 4(b)), one can note a reduction in the slope between NS and HS, ~2.0 versus ~1.1, respectively. We interpret the reduced slope of the ISI in the HS group compared to NS control as at least partially due to the loss in SK channel function. Supportive of this interpretation is that blockade of SK channels significantly reduced the slope of the ISI in both NS controls and the HS group and almost abolished the difference of the ISI between NS controls and the HS group. This suggests that the reduced SK channel function contributes at least partially to decreased ISI and loss of SFA in PVN-RVLM neurons in rats with HS intake.

4.1. Perspective. HS intake is a major risk factor which can contribute to the development of cardiovascular disease. While HS alone may not lead to the clinical manifestations of hypertension, it is capable of altering intrinsic properties of neurons especially those with regulation of sympatoexcitation. The present study evaluated the effects of HS intake on SK currents and neuronal excitability among PVN-RVLM neurons and revealed a reduction in SK channel function and increased PVN-RVLM neuronal excitability in HS diet-fed animals. We could expect that some factors including exercise training upregulate SK channel function expressed in the PVN, in turn, reduce sympathetic outflow and arterial blood pressure in SSH or spontaneous hypertension. SK channels could be a future target for treating salt-retaining cardiovascular disease including SSH, and congestive heart failure remains a topic that needs to be explored.

Disclosure

A portion of these results has been previously reported in abstract form (hypertension; 2012; 60: A506).

Conflicts of Interest

No conflicts of interest, financial or otherwise, are declared by the authors.

Authors' Contributions

Andrew D. Chapp performed the experiments. Andrew D. Chapp and Qing-Hui Chen analyzed the data; Andrew D. Chapp and Qing-Hui Chen prepared the figures. Andrew D. Chapp and Qing-Hui Chen drafted the manuscript; Andrew D. Chapp, Renjun Wang, Zixi (Jack) Cheng, Zhiying Shan, and Qing-Hui Chen edited and revised the manuscript; Andrew D. Chapp, Renjun Wang, Zixi (Jack) Cheng, Zhiying Shan, and Qing-Hui Chen approved the final version of the manuscript; Andrew D. Chapp and Qing-Hui Chen conceptualized and designed the research.

Acknowledgments

This study was supported by NIHR 15HL129213 (Zhiying Shan) and NIHR 15HL122952 (Qing-Hui Chen).

References

[1] Q. H. Chen, M. A. Andrade, A. S. Calderon, and G. M. Toney, "Hypertension induced by angiotensin II and a high salt diet involves reduced SK current and increased excitability of RVLM projecting PVN neurons," *Journal of Neurophysiology*, vol. 104, pp. 2329–2337, 2010.

[2] Q. H. Chen and G. M. Toney, "AT_1-receptor blockade in the hypothalamic PVN reduces central hyperosmolality-induced renal sympathoexcitation," *American Journal of Physiology - Regulatory, Integrative and Comparative Physiology*, vol. 281, pp. R1844–R1853, 2001.

[3] Q. H. Chen and G. M. Toney, "Excitability of paraventricular nucleus neurones that project to the rostral ventrolateral medulla is regulated by small-conductance Ca^{2+}-activated K^+ channels," *The Journal of Physiology*, vol. 587, pp. 4235–4247, 2009.

[4] Q. H. Chen and G. M. Toney, "In vivo discharge properties of hypothalamic paraventricular nucleus neurons with axonal projections to the rostral ventrolateral medulla," *Journal of Neurophysiology*, vol. 103, pp. 4–15, 2010.

[5] R. A. Dampney, J. Horiuchi, S. Killinger, M. J. Sheriff, P. S. Tan, and L. M. McDowall, "Long-term regulation of arterial blood pressure by hypothalamic nuclei: some critical questions," *Clinical and Experimental Pharmacology and Physiology*, vol. 32, pp. 419–425, 2005.

[6] G. D. Fink, "Long-term sympatho-excitatory effect of angiotensin II: a mechanism of spontaneous and renovascular hypertension," *Clinical and Experimental Pharmacology and Physiology*, vol. 24, pp. 91–95, 1997.

[7] J. W. Osborn, D. M. Olson, P. Guzman, G. M. Toney, and G. D. Fink, "The neurogenic phase of angiotensin II–salt hypertension is prevented by chronic intracerebroventricular

administration of benzamil," *Physiological Reports*, vol. 2, article e00245, 2014.

[8] S. S. Simmonds, J. Lay, and S. D. Stocker, "Dietary salt intake exaggerates sympathetic reflexes and increases blood pressure variability in normotensive rats," *Hypertension*, vol. 64, pp. 583–589, 2014.

[9] J. M. Adams, M. E. Bardgett, and S. D. Stocker, "Ventral lamina terminalis mediates enhanced cardiovascular responses of rostral ventrolateral medulla neurons during increased dietary salt," *Hypertension*, vol. 54, pp. 308–314, 2009.

[10] V. L. Brooks and J. W. Osborn, "Hormonal-sympathetic interactions in long-term regulation of arterial pressure: an hypothesis," *The American Journal of Physiology*, vol. 268, pp. R1343–R1358, 1995.

[11] J. W. Osborn, G. D. Fink, A. F. Sved, G. M. Toney, and M. K. Raizada, "Circulating angiotensin II and dietary salt: converging signals for neurogenic hypertension," *Current Hypertension Reports*, vol. 9, pp. 228–235, 2007.

[12] K. E. Scrogin, E. T. Grygielko, and V. L. Brooks, "Osmolality: a physiological long-term regulator of lumbar sympathetic nerve activity and arterial pressure," *American Journal of Physiology - Regulatory, Integrative and Comparative Physiology*, vol. 276, pp. R1579–R1586, 1999.

[13] R. D. Bunag and E. Miyajima, "Sympathetic hyperactivity elevates blood pressure during acute cerebroventricular infusions of hypertonic sait in rats," *Journal of Cardiovascular Pharmacology*, vol. 6, pp. 844–851, 1984.

[14] H. Schad and H. Seller, "Influence of intracranial osmotic stimuli on renal nerve activity in anaesthetized cats," *Pflugers Archiv*, vol. 353, pp. 107–121, 1975.

[15] D. R. Ziegler and J. P. Herman, "Neurocircuitry of stress integration: anatomical pathways regulating the hypothalamo-pituitary-adrenocortical axis of the rat," *Integrative and Comparative Biology*, vol. 42, pp. 541–551, 2002.

[16] Q. H. Chen and G. M. Toney, "Identification and characterization of two functionally distinct groups of spinal cord-projecting paraventricular nucleus neurons with sympathetic-related activity," *Neuroscience*, vol. 118, pp. 797–807, 2003.

[17] A. D. Shafton, A. Ryan, and E. Badoer, "Neurons in the hypothalamic paraventricular nucleus send collaterals to the spinal cord and to the rostral ventrolateral medulla in the rat," *Brain Research*, vol. 801, pp. 239–243, 1998.

[18] C. J. Yue, L. Feng, and Q. Huang, "RVLM-IML pathway may implicate controlling peripheral airways by melanocortinergic-sympathetic signaling: a transneuronal labeling study using pseudorabies virus," *International Journal of Clinical and Experimental Pathology*, vol. 7, pp. 7962–7966, 2014.

[19] G. J. Obermair, W. A. Kaufmann, H. G. Knaus, and B. E. Flucher, "The small conductance Ca^{2+}-activated K^+ channel SK3 is localized in nerve terminals of excitatory synapses of cultured mouse hippocampal neurons," *European Journal of Neuroscience*, vol. 17, pp. 721–731, 2003.

[20] M. Stocker, M. Krause, and P. Pedarzani, "An apamin-sensitive Ca^{2+}-activated K^+ current in hippocampal pyramidal neurons," *Proceedings of the National Academy of Sciences of the United States of America*, vol. 96, pp. 4662–4667, 1999.

[21] S. Yamada, H. Takechi, I. Kanchiku, T. Kita, and N. Kato, "Small-conductance Ca^{2+}-dependent K^+ channels are the target of spike-induced Ca^{2+} release in a feedback regulation of pyramidal cell excitability," *Journal of Neurophysiology*, vol. 91, pp. 2322–2329, 2004.

[22] K. Yang, "Regulation of excitability in tonic firing substantia gelatinosa neurons of the spinal cord by small-conductance Ca^{2+}-activated K^+ channels," *Neuropharmacology*, vol. 105, pp. 15–24, 2016.

[23] L. Gui, L. P. LaGrange, R. A. Larson, M. Gu, J. Zhu, and Q. H. Chen, "Role of small conductance calcium-activated potassium channels expressed in PVN in regulating sympathetic nerve activity and arterial blood pressure in rats," *American Journal of Physiology - Regulatory, Integrative and Comparative Physiology*, vol. 303, pp. R301–R310, 2012.

[24] R. A. Larson, A. D. Chapp, L. Gui et al., "High salt intake augments excitability of PVN neurons in rats: role of the endoplasmic reticulum Ca^{2+} store," *Frontiers in Neuroscience*, vol. 11, p. 182, 2017.

[25] P. Sah, "Ca^{2+}-activated K^+ currents in neurones: types, physiological roles and modulation," *Trends in Neurosciences*, vol. 19, pp. 150–154, 1996.

[26] M. Kleinewietfeld, A. Manzel, J. Titze et al., "Sodium chloride drives autoimmune disease by the induction of pathogenic T_H17 cells," *Nature*, vol. 496, pp. 518–522, 2013.

[27] J. S. Bains, A. Potyok, and A. V. Ferguson, "Angiotensin II actions in paraventricular nucleus: functional evidence for neurotransmitter role in efferents originating in subfornical organ," *Brain Research*, vol. 599, pp. 223–229, 1992.

[28] M. E. Bardgett, W. W. Holbein, M. Herrera-Rosales, and G. M. Toney, "Ang II–salt hypertension depends on neuronal activity in the hypothalamic paraventricular nucleus but not on local actions of tumor necrosis factor-α," *Hypertension*, vol. 63, pp. 527–534, 2014.

[29] K. Y. Choe, S. Y. Han, P. Gaub et al., "High salt intake increases blood pressure via BDNF-mediated downregulation of KCC2 and impaired baroreflex inhibition of vasopressin neurons," *Neuron*, vol. 85, pp. 549–560, 2015.

[30] E. Yamamoto, N. Tamamaki, T. Nakamura et al., "Excess salt causes cerebral neuronal apoptosis and inflammation in stroke-prone hypertensive rats through angiotensin II-induced NADPH oxidase activation," *Stroke*, vol. 39, pp. 3049–3056, 2008.

[31] J. N. Bech, C. B. Nielsen, P. Ivarsen, K. T. Jensen, and E. B. Pedersen, "Dietary sodium affects systemic and renal hemodynamic response to NO inhibition in healthy humans," *The American Journal of Physiology*, vol. 274, pp. F914–F923, 1998.

[32] X. Deng, W. J. Welch, and C. S. Wilcox, "Renal vasoconstriction during inhibition of NO synthase: effects of dietary salt," *Kidney International*, vol. 46, pp. 639–646, 1994.

[33] H. L. Gao, X. J. Yu, J. Qi et al., "Oral CoQ10 attenuates high salt-induced hypertension by restoring neurotransmitters and cytokines in the hypothalamic paraventricular nucleus," *Scientific Reports*, vol. 6, article 30301, 2016.

[34] P. J. Shultz and J. P. Tolins, "Adaptation to increased dietary salt intake in the rat. Role of endogenous nitric oxide," *The Journal of Clinical Investigation*, vol. 91, pp. 642–650, 1993.

[35] Q. H. Chen and G. M. Toney, "Responses to GABA-A receptor blockade in the hypothalamic PVN are attenuated by local AT_1 receptor antagonism," *American Journal of Physiology - Regulatory, Integrative and Comparative Physiology*, vol. 285, pp. R1231–R1239, 2003.

[36] D. P. Li and H. L. Pan, "Plasticity of GABAergic control of hypothalamic presympathetic neurons in hypertension," *American Journal of Physiology - Heart and Circulatory Physiology*, vol. 290, pp. H1110–H1119, 2006.

[37] D. P. Li and H. L. Pan, "Role of γ-aminobutyric acid $(GABA)_A$ and $GABA_B$ receptors in paraventricular nucleus in control of sympathetic vasomotor tone in hypertension," *The Journal of Pharmacology and Experimental Therapeutics*, vol. 320, pp. 615–626, 2007.

[38] K. Nakamura and A. W. Cowley Jr., "Sequential changes of cerebrospinal fluid sodium during the development of hypertension in Dahl rats," *Hypertension*, vol. 13, pp. 243–249, 1989.

[39] K. A. Frahm and S. A. Tobet, "Development of the blood–brain barrier within the paraventricular nucleus of the hypothalamus: influence of fetal glucocorticoid excess," *Brain Structure and Function*, vol. 220, pp. 2225–2234, 2015.

[40] M. B. Gutman, J. Ciriello, and G. J. Mogenson, "Effects of plasma angiotensin II and hypernatremia on subfornical organ neurons," *The American Journal of Physiology*, vol. 254, pp. R746–R754, 1988.

[41] H. Kawano and S. Masuko, "Region-specific projections from the subfornical organ to the paraventricular hypothalamic nucleus in the rat," *Neuroscience*, vol. 169, pp. 1227–1234, 2010.

[42] M. Criado-Marrero, E. Santini, and J. T. Porter, "Modulating fear extinction memory by manipulating SK potassium channels in the infralimbic cortex," *Frontiers in Behavioral Neuroscience*, vol. 8, p. 96, 2014.

[43] M. Lin, J. T. Hatcher, Q. H. Chen, R. D. Wurster, and Z. J. Cheng, "Small conductance Ca^{2+}-activated K^+ channels regulate firing properties and excitability in parasympathetic cardiac motoneurons in the nucleus ambiguus," *American Journal of Physiology Cell Physiology*, vol. 299, pp. C1285–C1298, 2010.

[44] N. Gu, H. Hu, K. Vervaeke, and J. F. Storm, "SK ($K_{Ca}2$) channels do not control somatic excitability in CA1 pyramidal neurons but can be activated by dendritic excitatory synapses and regulate their impact," *Journal of Neurophysiology*, vol. 100, pp. 2589–2604, 2008.

Hindawi
Neural Plasticity
Volume 2017, Article ID 4526417, 11 pages
https://doi.org/10.1155/2017/4526417

Research Article

Brain-Specific SNAP-25 Deletion Leads to Elevated Extracellular Glutamate Level and Schizophrenia-Like Behavior in Mice

Hua Yang,[1] Mengjie Zhang,[1] Jiahao Shi,[1] Yunhe Zhou,[1] Zhipeng Wan,[1] Yicheng Wang,[2] Yinghan Wan,[2] Jun Li,[2] Zhugang Wang,[2] and Jian Fei[1,2]

[1]*School of Life Science and Technology, Tongji University, Shanghai 200092, China*
[2]*Shanghai Engineering Research Center of Model Organisms (SRCMO/SMOC), Shanghai 201203, China*

Correspondence should be addressed to Jian Fei; jfei@tongji.edu.cn

Received 29 June 2017; Revised 31 August 2017; Accepted 15 October 2017; Published 28 November 2017

Academic Editor: Depei Li

Several studies have associated reduced expression of synaptosomal-associated protein of 25 kDa (SNAP-25) with schizophrenia, yet little is known about its role in the illness. In this paper, a forebrain glutamatergic neuron-specific SNAP-25 knockout mouse model was constructed and studied to explore the possible pathogenetic role of SNAP-25 in schizophrenia. We showed that SNAP-25 conditional knockout (cKO) mice exhibited typical schizophrenia-like phenotype. A significantly elevated extracellular glutamate level was detected in the cerebral cortex of the mouse model. Compared with Ctrls, SNAP-25 was dramatically reduced by about 60% both in cytoplasm and in membrane fractions of cerebral cortex of cKOs, while the other two core members of SNARE complex: Syntaxin-1 (increased ~80%) and Vamp2 (increased ~96%) were significantly increased in cell membrane part. Riluzole, a glutamate release inhibitor, significantly attenuated the locomotor hyperactivity deficits in cKO mice. Our findings provide *in vivo* functional evidence showing a critical role of SNAP-25 dysfunction on synaptic transmission, which contributes to the developmental of schizophrenia. It is suggested that a SNAP-25 cKO mouse, a valuable model for schizophrenia, could address questions regarding presynaptic alterations that contribute to the etiopathophysiology of SZ and help to consummate the pre- and postsynaptic glutamatergic pathogenesis of the illness.

1. Introduction

Schizophrenia (SZ), a complicated psychiatric disorder, affects almost 1 percent of the general population in the world [1, 2]. While the etiology and pathophysiology of SZ remain elusive, genetic risk factors are recognized as an important contributing factor to the pathogenesis of this neuropsychiatric disorder [3]. It has been documented that the synaptosomal-associated protein of 25 kDa (SNAP-25) is a candidate risk gene for SZ, as supported by the following lines of evidence: (1) Genetic association and linkage studies have revealed that chromosome region 20p12.2 which SNAP-25 locates in has significant linkage with SZ [4, 5]. (2) Large-scale genome-associated case-control studies have revealed that several single nucleotide polymorphisms (SNPs) of SNAP-25 are significantly associated with SZ [6]. (3) Various postmortem analyses have found that the expression of SNAP-25 is reduced in prefrontal cortex (PFC) and hippocampus in brain of patients with SZ [7–9]. However, how the reduction of SNAP-25 level is involved in the pathological phenotype remains unknown.

In the brain, SNAP-25 proteins are abundantly expressed in glutamatergic terminals, while relatively lower amounts of the protein are detectable in GABAergic terminals [10]. The primary role of SNAP-25 is a fundamental component of soluble N-ethylmaleimide-sensitive factor attachment protein receptor (SNARE). Together with cell membrane protein syntaxin and vesicle-associated membrane protein (VAMP), SNAP-25 mediates presynaptic vesicle docking and exocytosis [11]. In addition to regulation of synaptic transmission, SNAP-25 is also believed to regulate intracellular calcium dynamics through negative modulation of voltage-gated calcium channels. It also plays a role in other neuronal processes, including spine morphogenesis, postsynaptic receptor

trafficking, and neuronal plasticity [12]. But the underlying cellular mechanisms still need to be explored.

Over the past few decades, several mouse models have been constructed to elucidate the physiological role of SNAP-25 *in vivo*. Complete knockout of SNAP-25 in mice leads to no evoked exocytosis and death of the animal at birth. However, heterozygous mice are able to survive and exhibit locomotor hyperactivity and learning deficiencies. SNAP-25 knock-in mice, which have a single amino acid substitution of Ala for Ser187, have been shown to display epilepsy and anxiety-related behavior. The blind-drunk (Bdr) mouse expresses a dominant point mutant SNAP-25b protein, resulting in impaired sensorimotor gating and ataxia, while SNAP-25b-deficient model has developmental defects, seizures, and impaired synaptic plasticity. Conclusively, SNAP-25 mouse mutants occupied a series of psychophenotypes. However, the results derived from different models were inconsistent or conflicting, and no convincing evidence has supported an association between SNAP-25 and SZ. Therefore, additional investigations are necessary to demonstrate the possible role of SNAP-25 in SZ.

Taking into account that the cerebral cortex and hippocampus are the critical brain areas associated with SZ, brain-specific SNAP-25 knockout mice are most suitable to explore the relationship between SNAP-25 and SZ. Furthermore, SNAP-25 has been highly expressed both in neuron and endocrine cells, so brain-targeted SNAP-25 modification is capable of excluding interference signals from the surrounding system. In this study, we designed a brain-specific SNAP-25 knockout mouse, through behavioral phenotyping, molecular detection, and drug treatment within this model, to explore the possible pathogenetic role of SNAP-25 in SZ.

2. Materials and Methods

2.1. Animals. Mice were maintained in a specific pathogen-free (SPF) facility under a 12 h light/dark cycles. All animal protocols were approved by the Institutional Animal Care and Use Committee at Shanghai Research Center for Model Organisms (number 2015-0005). Mice were sacrificed with carbon dioxide when experiments were completed.

2.2. Generation of SNAP-25 cKO Mice. Genomic DNA of SCR012 ES cells isolated from 129S6/SvEv mouse strain was utilized to amplify SNAP-25 homologous fragments. The targeting strategy is flanking exon 4 of the mouse SNAP-25 gene with two loxP cassettes. Chimera mice were constructed by injecting recombination-positive ES cells into blastocyst and backcrossed to C57BL/6J mice. SNAP-25$^{L2/L2}$: CaMKIIα-Cre$^{+/wt}$ mice were obtained by regular breeding procedure between SNAP-25$^{L2/L2}$ mice and CaMKIIα-Cre strain (The Jackson Laboratory, stock number 005359) in which Cre-recombinase is extensively expressed in forebrain excitatory neurons by p20 [13, 14]. PCR genotyping was performed with genomic DNA isolated from mouse tail tissue. The primers used for genotyping were designed for identifying loxP (forward: 5′-CACTGCAGAGATTGCA GTATCACTA-3′, reverse: 5′- CAATGCACAGTTATTG TATTGAAGG-3′), and Cre sequences (forward: 5′- AGCG ATGGATTTCCGTCTCTGG-3′, reverse: 5′- AGCTTGCAT GATCTCCGGTATTGAA -3′).

2.3. Western Blot Analysis. Cell cytosolic or membrane protein lysates of mouse brain tissues were prepared using Mem-PER Plus Membrane Protein Extraction Kit (Thermo Scientific, 89842). Then, the lysates were separated by SDS–PAGE and probed with specific antibodies: SNAP-25 (Abcam, ab66066), SNAP-23 (Abcam, ab3340), syntaxin (Santa Cruz, sc-12736), Vamp2 (Abcam, ab6276), Munc-18 (SYSY, 116002), Phospho-Synaptotagmin (R&D Systems, PPS085), β-ACTIN (Abcam, ab6276), TUBULIN (Abcam, ab15246), and Na/K ATPase (Millipore, 05-369). For quantification, the densitometry measurement of each band was first normalized to that of β-ACTIN, TUBULIN, or Na/K ATPase (used as loading control) and then averaged from at least three independent samples.

2.4. Immunofluorescence Staining. Sagittal brain sections (15 μm in thickness) were prepared from a fixed brain with 4% paraformaldehyde, and immunostaining was performed as described [15]. Antibodies used for the immunostaining were SNAP-25 (Abcam, ab66066) and VGLUT1 (SYSY, 135304). Fluorescence was analyzed on a Nikon A1R confocal microscope (Nikon Instruments, Shanghai, CN).

2.5. Behavioral Testing. Behavioral phenotyping was performed on age-paired adult male mice (8 to 12 weeks for both cKO and Ctrl littermates). Prior to testing, mice were habituated to the testing room for 2 h.

2.5.1. Open-Field Test. The open field is a square arena (40 × 42 × 30 cm). 8 cm width elongated area along the wall is defined as the "peripheral zone," approximately 66% of the total area. We place the mouse in the center of the box and enable it to move freely for 15 mins, and an infrared tracking system (Kinder Scientific, Julian, USA) was borrowed to record the movement.

2.5.2. Prepulse Inhibition of the Startle Response. The Acoustic Startle Reflex Starter Package and Startle Reflex 5 software system (Med Associates Inc., St. Albans, VT) was used to assess prepulse inhibition (PPI). The test began with placing the mouse in the chamber's cylinder to acclimate for 5 mins. The remainder of the test consisted of two blocks of trials. A 65 dB background sound was presented throughout the session. The first block consisted of twenty trials of 20 ms and 105 dB sound served as startle stimuli and presented with different intertrial intervals (10–30 s). The second block consisted of 50 trials, with five varying trial types: startle only, or a 10 ms prepulse sound at 70, 75, 80, and 85 dB appeared 50 ms before the startle stimulus. The trial types were presented in random order with intertrial interval range from 10 to 30 s. Percent PPI of the startle response was calculated as the following formula: [1 − (startle response to prepulse + startle/startle response to startle only)] × 100.

2.5.3. Social Approach-Avoidance. The test was carried out as previously described [16]. Approach-avoidance behaviors toward an unfamiliar social partner were recorded by an infrared tracking system. The arena was a plastic open field (42 × 42 cm) containing an empty wire mesh cage (10 × 8 cm) located at one side of the field. During the first session ("no target"), the experimental mouse was introduced into the field and its trajectory was tracked for 5 mins. During the second session ("target 1"), the conditions were identical except that a social target animal (an unfamiliar C57BL/6J male mouse) had been introduced into the cage, and for the third session ("target 2"), the social target mouse was an unfamiliar C57BL/6J female. The tracking data from both the "no target" and "target" conditions were used to determine the time spent by the experimental mouse in the "interaction zone" (an 8 cm wide corridor surrounding the cage) and in the "corners" of the open field opposite to the location of the cage.

2.5.4. Hole-Board Test. The apparatus was a white wooden board (25 × 25 cm) with 16 evenly spaced holes. The number of head-dips was recorded by KS motor infrared monitor system over a 30-minute period.

2.5.5. Nest Building Assay. The nest building test was performed as previously described [17]. Briefly, one square piece of material made of cotton fibre (5 × 5 cm) was put in a cage with an individual mouse. Pictures of the nests were taken 16 h later. The quality of the nest was assessed using the following score: 1, nest not noticeably touched; 2, nest partially torn up; 3, mostly shredded but not identifiable nest site; 4, an identifiable but flat nest; 5, a well-defined nest with walls.

2.5.6. Passive Avoidance Task. The apparatus employed in the passive avoidance task is composed of compartment shuttle chambers, one dark with shock generator and other illuminated compartments. In acquisition trials (2 days), the mouse was allowed to explore the apparatus freely for 5 mins. It would encounter an electric shock (0.5 mA, 2 s duration) once it was inside of the dark chamber with all four paws. On the third day of the trial, the mouse was positioned in the illuminated compartment. Its latency to enter the dark compartment (step-through latency) was recorded automatically.

2.6. In Vivo Brain Microdialysis. In vivo brain microdialysis was carried out to measure glutamate content in the extracellular fluid in the cerebral cortex as previously described [18]. After mice had been anesthetized with inhaled isofluorane (3%), the cerebral cortex was surgically exposed and a microdialysis probe (MAB6.14.2) was inserted into the following coordinates relative to the bregma in mm: −2 to the anterior/posterior axis, ±2.0 to the lateral/medial axis, and −2.5 to the dorsal/ventral axis. Microdialysis was performed by perfusing of the probe with artificial cerebrospinal fluid at a flow rate of 2 μL/min via a microinfusing pump. The total volume of each dialysate sample (20 mins) was 40 μL. Samples were stored at −80°C until use.

2.7. Preparation of Tissue Samples for HPLC. Cerebral cortex and hippocampus tissues were isolated from the brains of *SNAP-25* cKO mice and their age- and sex-paired control littermates. After weighing, the samples were homogenized in ice-cold 0.4 M $HClO_4$ and centrifuged at 10,000g for 15 mins at 4°C. Then, 1 μL of supernatant was mixed with 750 μL of 2 M $KHCO_3$ and centrifuged at 3,000g for 5 mins. Supernatant was gathered and stored at −80°C until use.

2.8. High-Performance Liquid Chromatography (HPLC). HPLC analyses were performed in the State Key Laboratory of Medical Neurobiology of Fudan University as previously described [19]. The Agilent 1260 series neurotransmitter analyzer (Agilent Technologies, Santa Clara, CA) was utilized to detect the concentrations of amino acid neurotransmitters. Peaks and relative concentrations were identified by comparison to known external standards (Sigma-Aldrich).

2.9. Drug Treatments. Clozapine and LY354740 were purchased from Sigma-Aldrich (St. Louis, MO, USA), and lamotrigine was the product of Glaxosmithkline (Brentford, Middlesex, UK). For stock solutions, clozapine was dissolved in 0.1 M HCl and buffered with NaOH to achieve a final pH of 6.5–7.5. Riluzole was suspended in 10 *w*/*v*% cyclodextrin/saline, and LY354740 or lamotrigine was dissolved in saline. Vehicle was developed in an identical manner without the addition of drug, respectively. Concentrated aliquots of both drugs and vehicles were stored at −20°C. On the day of dosing, aliquots were thawed and diluted to their final concentration in sterile saline. Vehicles or clozapine (2.5 mg/kg), riluzole (10 mg/kg), and LY354740 (15 mg/kg) were injected intraperitoneally into age-matched male mice (8–12 weeks old), respectively, and submitted to the open-field test 30 mins later. Lamotrigine was administered to mice by gavage at a dose of 60 mg/kg per day for 2 weeks, followed by behavior testing.

The dose of drug was selected according to previously used doses in mouse behavioral studies [20–23] and our preliminary tests.

2.10. Statistical Analysis. Results are shown as the mean ± SEM. Student's *t*-test was utilized to compare two means and two-way ANOVA followed by Bonferroni test to compare multiple means. The nest building scores were treated as nonparametric data, and statistical analysis was performed using Kruskal-Wallis one-way analysis on ranks followed by multiple comparison using Dunn's method. All statistical analyses were performed using Excel 2010 (Microsoft) or GraphPad Prism 5.0. $P < 0.05$ was examined statistically significant.

3. Results

3.1. Generation of SNAP-25 Forebrain-Specific KO Mice. We generated the SNAP-25-floxed mouse strain SNAP-$25^{L2/L2}$ through inserting of loxP cassettes in the flank sequence of exon4 loci, which caused a frame shifting by Cre-loxP recombinant mechanism (Figure 1(a)). The mouse strain was crossed with CaMKIIα-Cre transgenic mice to generate forebrain-specific SNAP-25 cKO (SNAP-$25^{L2/L2}$:

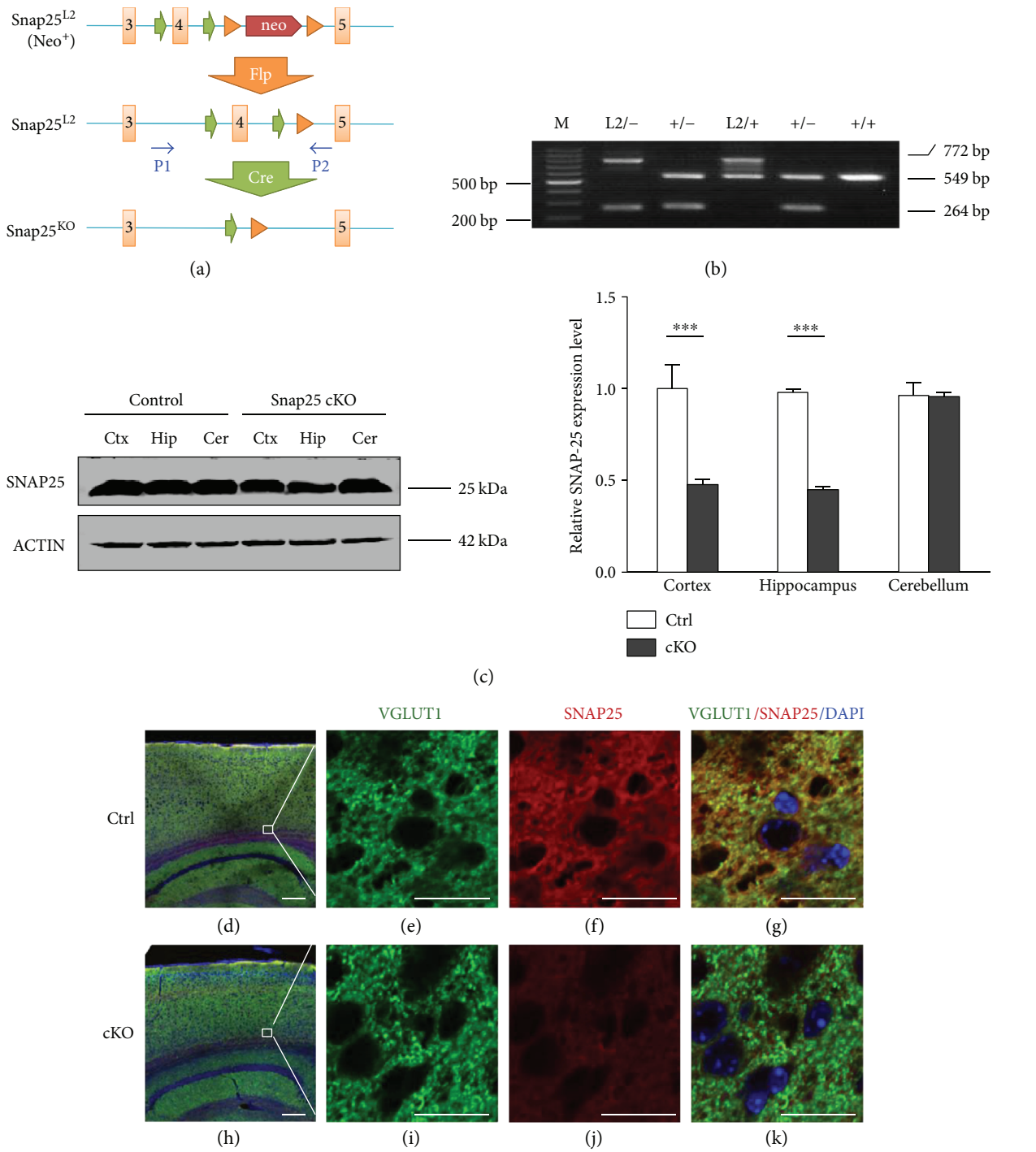

FIGURE 1: Generation of SNAP-25 forebrain-specific KO mice. (a) Targeting strategy used for the deletion of the SNAP-25 exon 4. P1-2 referred to PCR primers for genotyping, which is located on intron flank exon 4 separately. (b) PCR genotyping of recombinant SNAP-25 locus. (c) Western blot analysis of brain extracts of Ctrl and mutant mice. Right panel: quantitative analysis of western blot images. $n = 3$ per group. $^{***}P < 0.001$ compared with control littermates. (d–k) Immunostaining with anti-SNAP-25 (red) and anti-VGLUT1 (green) of cortex of sagittal sections from adult mice brains. Scale bars are 20 μm in (d) and 200 μm in (e).

CaMKIIα-Cre$^{+/wt}$) model. As we expected, the PCR product of wild-type SNAP-25 allele was 549 bp, whereas the floxed SNAP-25 allele (L2) was 772 bp and the knockout one (L-) was 264 bp. The accuracy of fragments was verified by sequencing (Figure 1(b)). SNAP-25 deletion in different brain areas was confirmed at protein levels. Dramatic reduction of SNAP-25 expression was observed in the cortex and hippocampus but no obvious change in the cerebellum of cKO mice (Figure 1(c)). Furthermore, we executed immunofluorescence examination with anti-SNAP-25 and anti-VGLUT1 (glutamatergic neuron marker) staining. It was found that abundant SNAP-25-positive glutamatergic

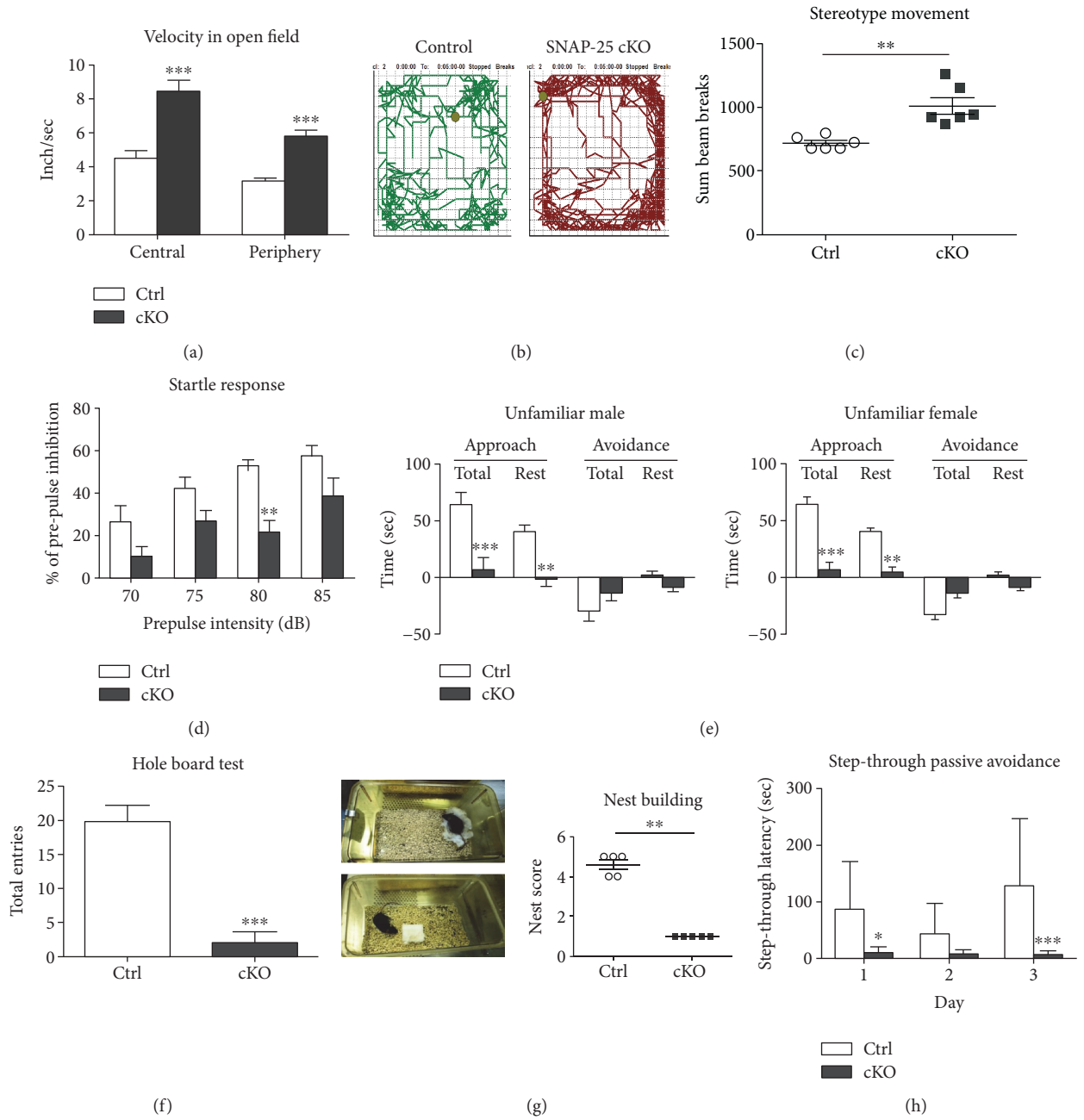

Figure 2: SNAP-25 cKO mice exhibit schizophrenia-like phenotype. (a–d) Summary plots of velocity, movement trajectory, stereotype movement in the open-field test ($n = 6$), and reduced prepulse inhibition ($n = 5$). (e) cKOs display deficient social skills as shown by social approach-avoidance test ($n = 10$). (f) cKOs occupy an impaired tendency to explore novel environment in hole-board test ($n = 6$). (g) Nest building. Left panel: pictures show the results of nesting of different genotypic mice. Right panel: statistical results of nesting scores ($n = 5$). (h) cKOs display impaired learning and memory in the step-through passive avoidance task ($n = 10$). $^{*}P < 0.05$, $^{**}P < 0.01$, and $^{***}P < 0.001$ compared with control littermates.

neurons were detected in the cerebral cortex of Ctrl mice, whereas little staining was found in those of cKOs, confirming that SNAP-25 was inactivated in forebrain glutamatergic neurons (Figures 1(d), 1(e), 1(f), 1(g), 1(h), 1(i), 1(j), and 1(k)).

3.2. SNAP-25 cKO Mice Exhibit SZ-Like Phenotype. To determine whether SNAP-25 cKO mice occupy behavioral impairments, we subjected these animals to a battery of behavioral tests. First, in the open-field test, cKO mice showed a significant increased locomotion (3.326 ± 0.160 versus 5.879 ± 0.334 inch/sec, $P < 0.0001$, $n = 6$) and remarkably enhanced stereotype movements (718.50 ± 20.74 versus 1012.00 ± 64.42 breaks, $P < 0.05$, $n = 6$) compared with their control littermates (SNAP-25$^{L2/L2}$, Ctrl, hereafter), demonstrating the abnormal hyperactivity and stereotypical behavior of cKOs (Figures 2(a), 2(b), and 2(c)). Acoustic startle test revealed that prepulse inhibition (PPI) was

Table 1: Mating and nursing test of SNAP-25 cKO females (crossed with C57BL/6 J male).

Genotype	Total pairs	Pregnant females	Born pups	Mean ± SEM	Survival pups	Mean ± SEM
Ctrl	10	9	57	5.70 ± 0.76	57	5.70 ± 0.76
cKO	10	4	25	2.50 ± 1.05*	13	1.30 ± 0.87**

*$P < 0.05$ and **$P < 0.01$ compared with Ctrl.

significantly decreased in the group of cKOs compared to Ctrls [F (1, 8) = 24.37, $P < 0.0001$, $n = 5$], and Bonferroni's post hoc comparison showed a significant disruption of PPI at the prepulse level of 80 dB ($P < 0.01$) (Figure 2(d)). There was no significant difference in the startle response between cKOs and Ctrls, suggesting no apparent hearing deficit (data not shown). Thus, hyperactivity, enhanced stereotypical movements and reduced PPI of SNAP-25 cKO mice fit into the positive symptoms of SZ.

For social behavior judgement, first, we used the social approach-avoidance test to probe animals for their voluntary initiation of social interaction. When presented with an unfamiliar partner, Ctrls had the tendency to spend more time interacting socially, but cKOs displayed intense aversive responses and spent less time in close proximity to the stranger (Figure 2(e)). Also, the significantly reduced head dipping times of cKOs in the hole-board test (19.83 ± 2.39 versus 1.67 ± 1.31 entries, $P < 0.0001$, $n = 6$) also reflected an impaired tendency to explore a novel environment (Figure 2(f)). By mating two genotypic females with wild-type C57BL/6J males, paired for a 4-month period, we observed that both the pregnancy rate and survival pups of cKO females were significantly lower than Ctrls, but the litter size per pregnant mother showed no difference between two groups (6.33 ± 0.47 versus 6.25 ± 0.63 pups/mother, $P = 0.92$, Ctrls $n = 9$, and cKOs $n = 4$), which indicates that both mating and maternal nursing behaviors were defective in cKOs (Table 1). While Ctrls could build clean and typical nests after 16 h with the nesting material, the nests of cKO mice were poorly formed. Substantially decreased nesting score of cKO mice demonstrated their impaired self-care ability (Figure 2(g)). Collectively, the results of the above behavioral tests showed that impaired social skills, exploratory tendency, self-care, and nursing abilities have occurred in cKOs. The cKO mice thus fit the criteria established for negative symptoms of SZ.

To determine whether cKOs have deficits in hippocampus-dependent learning and memory processes, we subjected mice to the step-through passive avoidance task. During the 3-day experiment, cKOs stepped faster into the darker-shock chamber than Ctrls. After subjected to electric shock, the step-through latencies of cKOs were more statistically pronounced compared with Ctrls, which indicated impaired learning and memory of cKOs (Figure 2(h)).

3.3. Elevated Glutamate Level in the Cortex of SNAP-25 cKO Mice. We measured the content of glutamate in cerebral cortex and hippocampus of two mice groups by combining *in vivo* microdialysis and HPLC. As indicated in Figure 3(a), a significant increase in glutamate concentration was detected in the microdialysis fluid of the cerebral cortex (0.27 ± 0.02 versus 0.72 ± 0.14 μg/mL, $P < 0.05$, Ctrls $n = 5$, and cKOs $n = 6$), while unchanged level were inspected in hippocampus area (0.48 ± 0.12 versus 0.58 ± 0.17 μg/mL, $P = 0.63$, Ctrls $n = 5$, and cKOs $n = 6$) in cKOs compared with Ctrl mice. However, there was no observable alteration between the concentration of amino acid neurotransmitters of homogenates freshly prepared from the same brain subregions of the cKO and Ctrl mice (Figure 3(b)).

Subsequently, by using TUBULIN and Na/K ATPase as loading controls, respectively, we examined the expression level of all three SNARE members in the cytoplasm and cell membrane fraction of the cerebral cortex. Compared with Ctrls, SNAP-25 was dramatically reduced around 60% both in cytoplasm and membrane fractions of cKOs, while the other two core members of SNARE complex: Syntaxin-1 (increased ~80%) and Vamp2 (increased ~96%) were significantly increased in cell membrane part (Figure 4). There was no difference in expression of SNAP-25 homologous molecule—SNAP-23 or another important SNARE member—Munc-18 in the cell membrane of the cerebral cortex between cKOs and Ctrls. However, the expression of presynaptic calcium sensor protein—phosphorylated synaptotagmin-1—was significantly elevated about 93% in the cell membrane of the cerebral cortex of cKOs.

3.4. Antipsychotic Drugs Attenuated Locomotor Hyperactivity Deficits in cKO Mice. Antipsychotic drugs, clozapine (atypical schizophrenic drug), lamotrigine (broad-spectrum antiepileptic drug), LY354740 (metabotropic glutamate 2/3 receptor agonist), and riluzole (glutamate release inhibitor) were selected to examine their effects on the locomotor hyperactivities and stereotype behavior of cKO mice. Compared with controls, LY354740 treatment has no detectable effects on all four test index, while lamotrigine could reduce the stereotype movement of cKOs. Administration of either clozapine or riluzole was able to significantly attenuate the hyperactivity and stereotype movements of the SNAP-25 cKO mice (Figure 5).

4. Discussion

SNAP-25 is a key molecule involved in synaptic vesicle docking and neurotransmitter release. In line with its central role in neuronal function, it is thought that SNAP-25 is related to human neurological syndromes, especially SZ. In this study, we specifically deleted SNAP-25 gene in forebrain glutamatergic neurons with utilization of the Cre/LoxP strategy. The phenotypes observed in this model fit into SZ-like behaviors, which include positive symptoms (such as hyperlocomotion and reduced PPI), negative symptoms (decreased motivation and impaired social skills), and

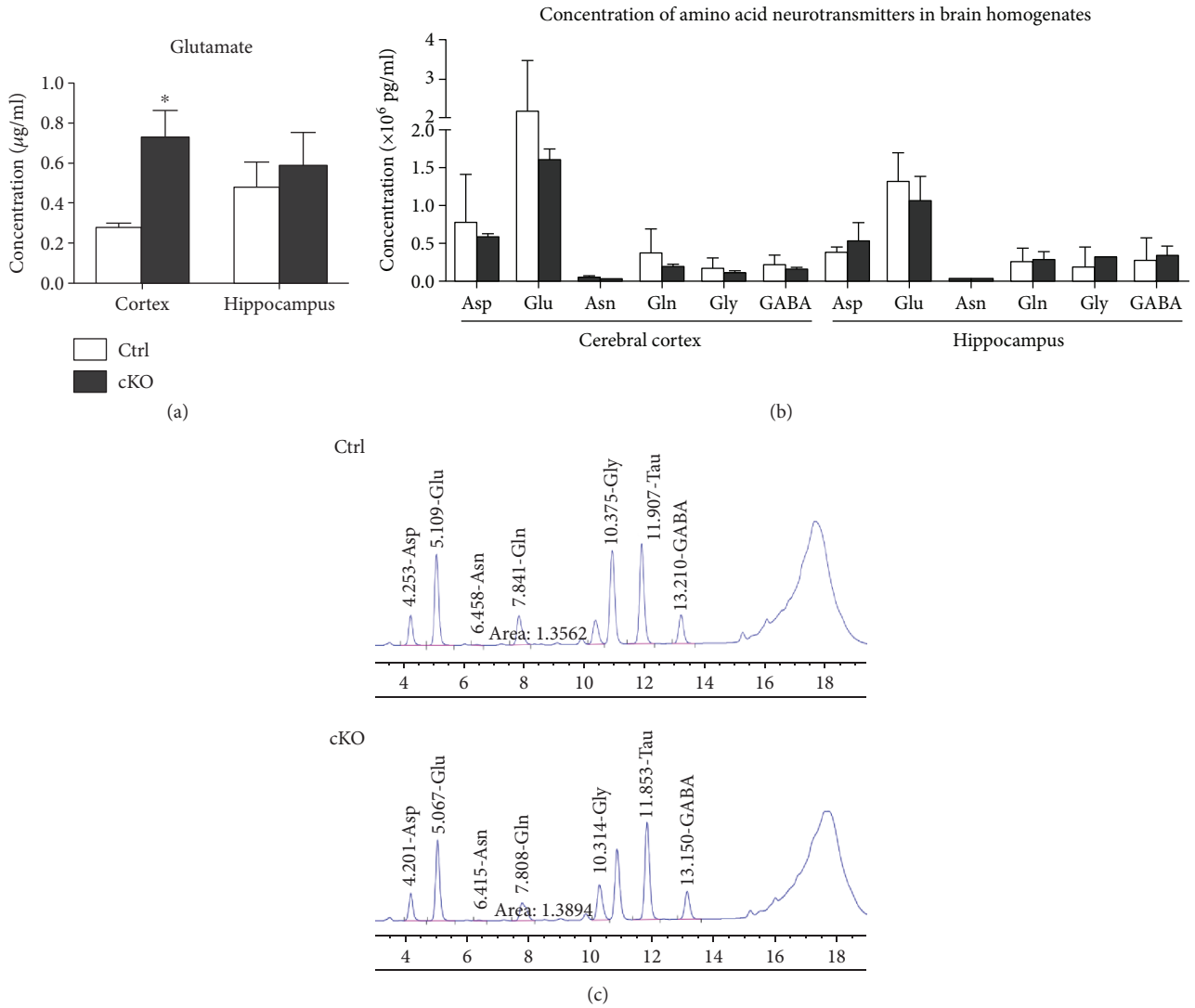

Figure 3: Elevated cortex glutamate level of SNAP-25 cKO mice. (a) The concentration of glutamate (μg/mL) in the microdialysis fluid (Ctrls, $n = 5$; cKOs, $n = 6$). (b) The concentration of amino acid neurotransmitters ($\times 10^6$ pg/mL) in brain homogenates ($n = 5$ per group). (c) The original representative HPLC figures of different genotypic mice. $^*P < 0.05$ compared with control littermates. Asp: aspartate; Glu: glutamate; Asn: asparaginate; Gln: glutamine; Gly: glycine; GABA: γ-aminobutyric acid.

memory deficit. Our results provided *in vivo* functional evidence to support that altered SNAP-25 expression in the forebrain glutamatergic neurons lead to a greater effect of the illness, confirming the strong association between SNAP-25 and SZ.

It is well known that SNAP-25 plays a key role in medicating neurotransmitter release. Previous studies provided evidence that botulinum neurotoxin type A (BoNT/A) could block synaptic vesicle neuroexocytosis by proteolytic cleavage of SNAP-25, indicating that SNAP-25-deficiency could inhibit neurotransmitter release [24]. However, by *in vivo* brain microdialysis, we found the remarkable elevation of extracellular glutamate levels in cerebral cortex of SNAP-25 cKO mice. No noticeable difference in the total content of amino acid neurotransmitters in the same brain subregions was found between the two groups. Subsequent western blot test revealed the elevated gathering of the SNARE proteins on the cell membrane, which indicated the possibility of increased synaptic vesicle assembly and release. SNAP-25 inactivation seemed not only to fail to block synaptic transmission but also to enhance glutamatergic neurotransmitter in the cortex of cKOs. Previously, Antonucci et al. reported that reduced SNAP-25 levels lead to enhanced evoked glutamatergic transmission in hippocampal cultures and identified that this consequence was not due to changes in a releasable pool of synaptic vesicles [25]. However, we did not detect a statistical difference in hippocampus microdialysis, and we do not know the exact reason yet. We noticed that there were several differences between our and their works: (1) the developmental state of animals (adult mice and E18 mice embryos); (2) the experimental condition (intact animal under physiological condition and *in vitro* cultured cell model); and (3) the detective method (*in vivo* brain microdialysis and whole-cell patch-clamp recording). All

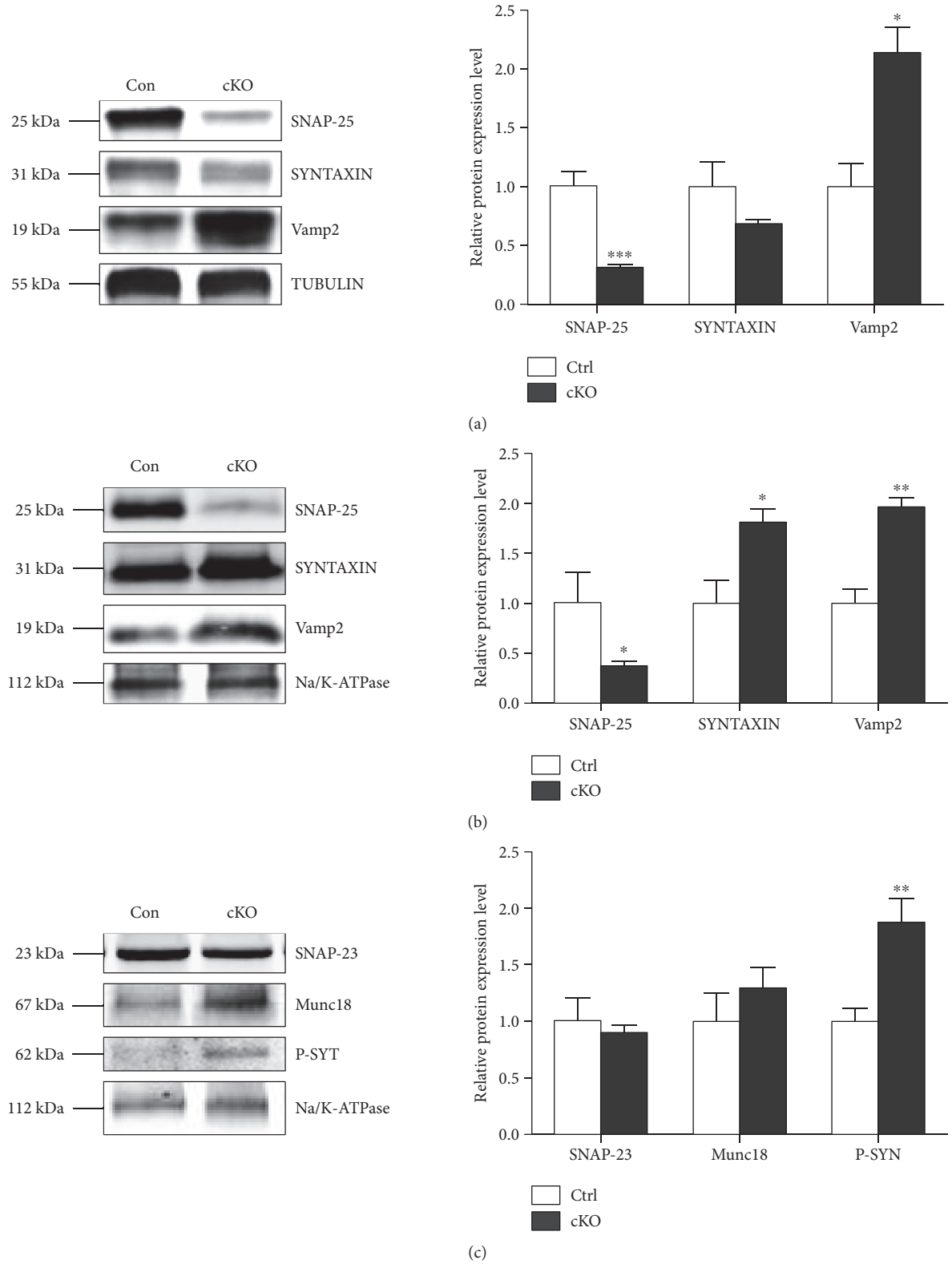

Figure 4: Alteration of expression pattern of SNARE-related proteins. Representative western blot (left) and densitometric analysis (right) of proteins in the cytosolic (a) and membrane (b and c) fractions prepared from mouse cerebral cortex ($n = 3$ per group). $^{*}P < 0.05$, $^{**}P < 0.01$, and $^{***}P < 0.001$ compared with control littermates. P-SYT: phosphorylated synaptotagmin-1.

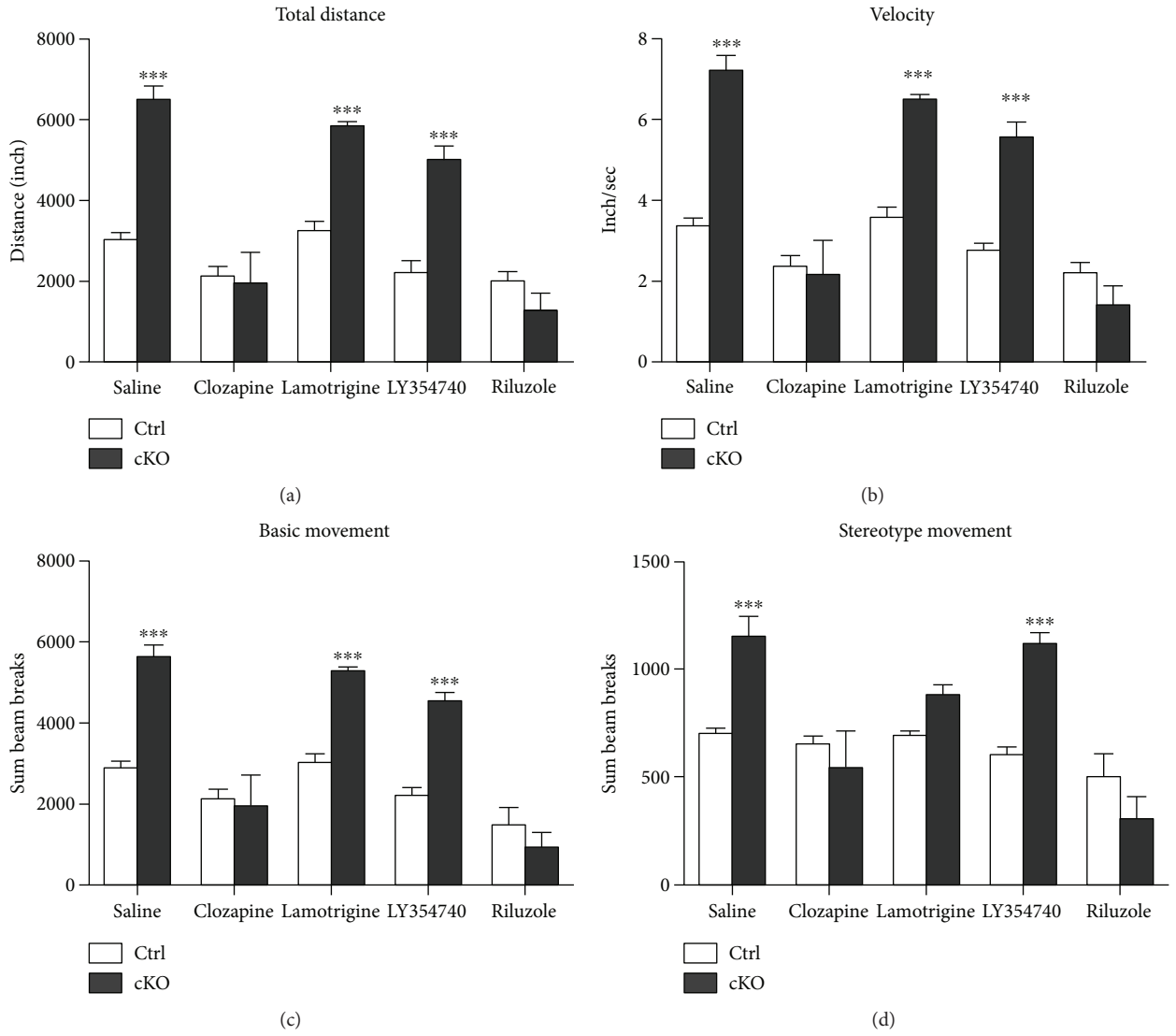

Figure 5: Antipsychotic drugs could attenuate the locomotor hyperactivity deficits in cKO mice. Summary plots of total distance (a), activity velocity (b), basic (c), and stereotype (d) movement in the open-field test. $^{***}P < 0.001$ compared with control littermates. Ctrls: $n = 5$; cKOs: $n = 8$.

above factors may contribute to the inconsistent results we have made.

Thus, the emerging question is how synaptic exocytosis could be enhanced without SNAP-25. To investigate the intrinsic mechanism of this phenomenon, we detected the expression level of three molecules, which are functionally related to SNAP-25 closely. These were (1) SNAP-23, the closest homolog of SNAP-25, which may be the substitution for SNAP-25 to mediate synaptic vesicle fusion [26]; (2) mammalian uncoordinated-18 (Munc-18), which has been found to have dual binding ability to syntaxin-1 and Vamp2, classified as the fourth crucial member of SNARE-pin assembly and may be another alternative for mediating neurotransmitter release [27, 28]; and (3) as the synaptic vesicle Ca^{2+} sensor, synaptotagmin-1 could be phosphorylated with calcium influx and trigger the synaptic release subsequently. Endogenous SNAP-25 negatively modulates neuronal voltage-gated calcium channels (VGCCs) [11, 29]. Therefore, SNAP-25 deficiency may release VGCC activity from SNAP-25-mediated inhibition, thus resulting in exaggerated calcium influx and triggering exocytic release of glutamate. Accordingly, our molecular detection results showed the phosphorylated synaptotagmin-1 was obviously elevated, which indicated the active of VGCCs and enhanced calcium influx that may lead to greater synaptic release at the presynaptic terminal.

Moreover, we assessed the effects of commonly used antipsychotic drugs on the locomotor hyperactivities and stereotype behavior of cKO mice. The atypical antipsychotic clozapine can bind to receptors of serotonin, dopaminergic, and glutamatergic system. Multitarget actions make clozapine one of the most efficacious antipsychotics. It is therefore considered the "gold standard" for the treatment of SZ [30]. In regard to the cortical hyperglutamatergic state within our model, we chose three drugs that aim to inhibit presynaptic glutamate release through different pathways. These

were (1) LY354740, a presynaptic metabotropic glutamate receptor 2/3 (mGlu2/3) receptor agonist, which helps suppress the release of neurotransmitters, including glutamate and GABA [31]; (2) lamotrigine, which acts primarily through inhibition of glutamate release via blockade of voltage-sensitive sodium channels and stabilization of neuronal membrane [32]; and (3) riluzole, which has diverse effects on multiple components of the glutamatergic system, such as inhibition of glutamate release by depression of voltage-gated ion channels (sodium, potassium, and calcium) and inhibition of autoreceptors. Riluzole also affects glial cells by increasing glutamate uptake, trafficks with AMPA receptors, and so on [33, 34]. Subsequent open-field test results showed that (1) clozapine could attenuate heightened locomotor activity of cKO mice. Its validity illustrated that SNAP-25 cKO mice could respond effectively to antipsychotics drug, which is the qualifying standard for an animal disease model; (2) glutamate release inhibitors occupied different efficacies on our mice and administration of riluzole has significantly corrected the hyperactivity of the SNAP-25 cKOs, whereas lamotrigine could only alleviate the stereotype movements of the mouse model, and LY354740 did not alter the activity at all. These results suggested that the hyperglutamatergic phenotype of our model may be associated closely with enhanced calcium influx rather than impaired mGlu2/3 receptor function, which corresponded with our previous observation. Further investigations are still required to provide more evidences to explore the detailed mechanisms of elevated extracellular glutamate tones in SNAP-25 cKO mice.

The involvement of glutamatergic mechanism in SZ has been hypothesized for many years. SZ-relative abnormalities have been well documented in mice with mutations in postsynaptic components of glutamatergic transmission, such as NMDAR [35, 36], glycine transporter [37], and metabotropic glutamate receptor [38]. The hypofunction of postsynaptic NMDAR on inhibitory neurons that leads to disinhibition of glutamate transmission and glutamate excitotoxicity has formed the bedrock of the glutamate hypothesis of SZ. However, influence of presynaptic glutamatergic deficits is less well understood. Being a key component of glutamatergic neurotransmission at presynaptic locus, SNAP-25 deficiency induced typical SZ-like behavior demonstrated the strong association between presynaptic dysfunction and the outbreak of SZ. SNAP-25 cKO mice would be a useful novel tool for investigating presynaptic alterations that contribute to the etiopathophysiology of SZ. This research helps to consummate the pre- and postsynaptic glutamatergic pathogenesis of SZ.

5. Conclusion

This study showed that the forebrain glutamatergic neuron-specific SNAP-25 cKO lead to a typical SZ-like phenotype. The deficiency of SNAP-25 may lead to enhanced calcium influx and exaggerated glutamatergic release and may result in the elevated extracellular glutamate level. Riluzole attenuates the locomotor hyperactivity deficits in cKO mice. Our results provided new insight that SNAP-25 dysfunction has direct consequences on synaptic transmission and contributes to developmental of SZ. SNAP-25 cKO mouse could be a valuable new model for SZ and could be used to address questions regarding pathophysiology and etiology of the illness.

Conflicts of Interest

The authors declare that there is no conflict of interests regarding the publication of this paper.

Acknowledgments

The authors gratefully acknowledge Professor Fang Huang (The State Key Laboratory of Medical Neurobiology, Fudan University) for the technical assistance and critically reading the manuscript. This work was supported by the grant from the National Natural Science Foundation of China (no. 81271483), the Funds of Science and Technology Commission of Shanghai Municipality (nos. 14140904300 and 16DZ2280800), and the Fundamental Research Funds for the Central Universities (no. 2000219140).

References

[1] T. R. Insel, "Rethinking schizophrenia," *Nature*, vol. 468, no. 7321, pp. 187–193, 2010.

[2] J. Van Os, G. Kenis, and B. P. Rutten, "The environment and schizophrenia," *Nature*, vol. 468, no. 7321, pp. 203–212, 2010.

[3] J. Van Os and S. Kapur, "Schizophrenia," *Lancet*, vol. 374, no. 9690, pp. 635–645, 2009.

[4] C. M. Lewis, D. F. Levinson, L. H. Wise et al., "Genome scan meta-analysis of schizophrenia and bipolar disorder, part II: schizophrenia," *American Journal of Human Genetics*, vol. 73, no. 1, pp. 34–48, 2003.

[5] A. H. Fanous, M. C. Neale, B. T. Webb et al., "Novel linkage to chromosome 20p using latent classes of psychotic illness in 270 Irish high-density families," *Biological Psychiatry*, vol. 64, no. 2, pp. 121–127, 2008.

[6] Q. Wang, Y. Wang, W. Ji et al., "SNAP25 is associated with schizophrenia and major depressive disorder in the Han Chinese population," *The Journal of Clinical Psychiatry*, vol. 76, no. 1, pp. e76–e82, 2015.

[7] V. E. Barakauskas, A. Moradian, A. M. Barr et al., "Quantitative mass spectrometry reveals changes in SNAP-25 isoforms in schizophrenia," *Schizophrenia Research*, vol. 177, no. 1-3, pp. 44–51, 2016.

[8] C. N. Karson, R. E. Mrak, K. O. Schluterman, W. Q. Sturner, J. G. Sheng, and W. S. T. Griffin, "Alterations in synaptic proteins and their encoding mRNAs in prefrontal cortex in schizophrenia: a possible neurochemical basis for 'hypofrontality'," *Molecular Psychiatry*, vol. 4, no. 1, pp. 39–45, 1999.

[9] S. H. Fatemi, J. A. Earle, J. M. Stary, S. Lee, and J. Sedgewick, "Altered levels of the synaptosomal associated protein SNAP-25 in hippocampus of subjects with mood disorders and schizophrenia," *Neuroreport*, vol. 12, no. 15, pp. 3257–3262, 2001.

[10] M. Matteoli, D. Pozzi, C. Grumelli et al., "The synaptic split of SNAP-25: different roles in glutamatergic and GABAergic neurons?," *Neuroscience*, vol. 158, no. 1, pp. 223–230, 2009.

[11] S. B. Condliffe, I. Corradini, D. Pozzi, C. Verderio, and M. Matteoli, "Endogenous SNAP-25 regulates native voltage-gated calcium channels in glutamatergic neurons," *The Journal of Biological Chemistry*, vol. 285, no. 32, pp. 24968–24976, 2010.

[12] F. Antonucci, I. Corradini, G. Fossati, R. Tomasoni, E. Menna, and M. Matteoli, "SNAP-25, a known presynaptic protein with emerging postsynaptic functions," *Frontiers in Synaptic Neuroscience*, vol. 8, p. 7, 2016.

[13] J. Z. Tsien, D. F. Chen, D. Gerber et al., "Subregion- and cell type-restricted gene knockout in mouse brain," *Cell*, vol. 87, no. 7, pp. 1317–1326, 1996.

[14] M. He, Y. Liu, X. Wang, M. Q. Zhang, G. J. Hannon, and Z. J. Huang, "Cell-type-based analysis of microRNA profiles in the mouse brain," *Neuron*, vol. 73, no. 1, pp. 35–48, 2012.

[15] I. H. Kim, S. K. Park, S. T. Hong et al., "Inositol 1,4,5-trisphosphate 3-kinase a functions as a scaffold for synaptic Rac signaling," *The Journal of Neuroscience*, vol. 29, no. 44, pp. 14039–14049, 2009.

[16] O. Berton, C. A. Mcclung, R. J. Dileone et al., "Essential role of BDNF in the mesolimbic dopamine pathway in social defeat stress," *Science*, vol. 311, no. 5762, pp. 864–868, 2006.

[17] H. Zhang, E. Kang, Y. Wang et al., "Brain-specific Crmp2 deletion leads to neuronal development deficits and behavioural impairments in mice," *Nature Communications*, vol. 7, 2016.

[18] Y. K. Wang, D. Shen, Q. Hao et al., "Overexpression of angiotensin-converting enzyme 2 attenuates tonically active glutamatergic input to the rostral ventrolateral medulla in hypertensive rats," *American Journal of Physiology. Heart and Circulatory Physiology*, vol. 307, no. 2, pp. H182–H190, 2014.

[19] M. Han, X. Xiao, Y. Yang et al., "SIP30 is required for neuropathic pain-evoked aversion in rats," *The Journal of Neuroscience*, vol. 34, no. 2, pp. 346–355, 2014.

[20] C. L. Schmid, J. M. Streicher, H. Y. Meltzer, and L. M. Bohn, "Clozapine acts as an agonist at serotonin 2A receptors to counter MK-801-induced behaviors through a βarrestin2-independent activation of Akt," *Neuropsychopharmacology*, vol. 39, no. 8, pp. 1902–1913, 2014.

[21] C. Procaccini, M. Maksimovic, T. Aitta-Aho, E. R. Korpi, and A. M. Linden, "Reversal of novelty-induced hyperlocomotion and hippocampal c-Fos expression in GluA1 knockout male mice by the mGluR2/3 agonist LY354740," *Neuroscience*, vol. 250, pp. 189–200, 2013.

[22] M. Y. Zhang, C. Y. Zheng, M. M. Zou et al., "Lamotrigine attenuates deficits in synaptic plasticity and accumulation of amyloid plaques in APP/PS1 transgenic mice," *Neurobiology of Aging*, vol. 35, no. 12, pp. 2713–2725, 2014.

[23] N. Egashira, R. Okuno, S. Harada et al., "Effects of glutamate-related drugs on marble-burying behavior in mice: implications for obsessive-compulsive disorder," *European Journal of Pharmacology*, vol. 586, no. 1-3, pp. 164–170, 2008.

[24] I. Matak and Z. Lackovic, "Botulinum neurotoxin type a: actions beyond SNAP-25?," *Toxicology*, vol. 335, pp. 79–84, 2015.

[25] F. Antonucci, I. Corradini, R. Morini et al., "Reduced SNAP-25 alters short-term plasticity at developing glutamatergic synapses," *EMBO Reports*, vol. 14, no. 7, pp. 645–651, 2013.

[26] S. Arora, I. Saarloos, R. Kooistra, R. van de Bospoort, M. Verhage, and R. F. Toonen, "SNAP-25 gene family members differentially support secretory vesicle fusion," *Journal of Cell Science*, vol. 130, no. 11, pp. 1877–1889, 2017.

[27] A. Pertsinidis, K. Mukherjee, M. Sharma et al., "Ultrahigh-resolution imaging reveals formation of neuronal SNARE/Munc18 complexes in situ," *Proceedings of the National Academy of Sciences of the United States of America*, vol. 110, no. 30, pp. E2812–E2820, 2013.

[28] D. Parisotto, J. Malsam, A. Scheutzow, J. M. Krause, and T. H. Sollner, "SNAREpin assembly by Munc18-1 requires previous vesicle docking by synaptotagmin 1," *The Journal of Biological Chemistry*, vol. 287, no. 37, pp. 31041–31049, 2012.

[29] S. B. Condliffe and M. Matteoli, "Inactivation kinetics of voltage-gated calcium channels in glutamatergic neurons are influenced by SNAP-25," *Channels*, vol. 5, no. 4, pp. 304–307, 2011.

[30] H. Y. Meltzer, "Update on typical and atypical antipsychotic drugs," *Annual Review of Medicine*, vol. 64, no. 1, pp. 393–406, 2013.

[31] R. Farazifard and S. H. Wu, "Metabotropic glutamate receptors modulate glutamatergic and GABAergic synaptic transmission in the central nucleus of the inferior colliculus," *Brain Research*, vol. 1325, pp. 28–40, 2010.

[32] A. L. Meehan, X. Yang, B. D. McAdams, L. Yuan, and S. M. Rothman, "A new mechanism for antiepileptic drug action: vesicular entry may mediate the effects of levetiracetam," *Journal of Neurophysiology*, vol. 106, no. 3, pp. 1227–1239, 2011.

[33] N. Lamanauskas and A. Nistri, "Riluzole blocks persistent Na^+ and $Ca2^+$ currents and modulates release of glutamate via presynaptic NMDA receptors on neonatal rat hypoglossal motoneurons *in vitro*," *The European Journal of Neuroscience*, vol. 27, no. 10, pp. 2501–2514, 2008.

[34] R. Machado-Vieira, G. Salvadore, L. A. Ibrahim, N. Diaz-Granados, and C. A. Zarate Jr, "Targeting glutamatergic signaling for the development of novel therapeutics for mood disorders," *Current Pharmaceutical Design*, vol. 15, no. 14, pp. 1595–1611, 2009.

[35] K. Nakazawa, V. Jeevakumar, and K. Nakao, "Spatial and temporal boundaries of NMDA receptor hypofunction leading to schizophrenia," *NPJ Schizophrenia*, vol. 3, no. 1, p. 7, 2017.

[36] D. Timucin, O. Ozdemir, and M. Parlak, "The role of NMDAR antibody in the etiopathogenesis of schizophrenia," *Neuropsychiatric Disease and Treatment*, vol. 12, pp. 2327–2332, 2016.

[37] E. Dunayevich, R. W. Buchanan, C. Y. Chen et al., "Efficacy and safety of the glycine transporter type-1 inhibitor AMG 747 for the treatment of negative symptoms associated with schizophrenia," *Schizophrenia Research*, vol. 182, pp. 90–97, 2017.

[38] J. Maksymetz, S. P. Moran, and P. J. Conn, "Targeting metabotropic glutamate receptors for novel treatments of schizophrenia," *Molecular Brain*, vol. 10, no. 1, p. 15, 2017.

Hindawi
Neural Plasticity
Volume 2017, Article ID 6589424, 7 pages
https://doi.org/10.1155/2017/6589424

Research Article

Glucose Intake Alters Expression of Neuropeptides Derived from Proopiomelanocortin in the Lateral Hypothalamus and the Nucleus Accumbens in Fructose Preference Rats

Guangfa Jiao,[1,2] Guozhong Zhang,[3] Haiying Wang,[2] Weilin Zhao,[2] Yanwei Cui,[2] Yongjing Liu,[2] Feng Gao,[4] Fang Yuan,[1] and Yi Zhang[1,5]

[1]*Department of Physiology, Hebei Medical University, Shijiazhuang 050017, China*
[2]*Department of Human Sport Science, Hebei Institute of Physical Education, Shijiazhuang 050000, China*
[3]*Hebei Key Laboratory of Forensic Medicine, Institute of Forensic Medicine of Hebei Medical University, Shijiazhuang 050017, China*
[4]*Sports Institute, Hebei Normal University, Shijiazhuang 050040, China*
[5]*Hebei Collaborative Innovation Center for Cardio-cerebrovascular Disease, Shijiazhuang 050000, China*

Correspondence should be addressed to Yi Zhang; zhyhenry@hotmail.com

Received 25 June 2017; Revised 21 August 2017; Accepted 7 September 2017; Published 8 November 2017

Academic Editor: Yulong Li

To study the neuroendocrine mechanism of sugar preference, we investigated the role of glucose feeding in the regulation of expression levels of neuropeptides derived from proopiomelanocortin (POMC) in the lateral hypothalamus (LH) and nucleus accumbens (NAc) in fructose preference rats. Fructose preference rats were induced by using the lithium chloride backward conditioning procedure. The fructose preference was confirmed by the two-bottle test. The drinking behavior of rats was assessed by the fructose concentration gradient test. The preference of 10% glucose or 0.1% saccharine was assessed, and the expression levels of neuropeptides derived from POMC in the LH and the NAc in fructose preference rats were measured by Western blot analysis. Fructose preference rats displayed a greater fructose preference than control rats. Furthermore, fructose preference rats preferred glucose solution rather than saccharine solution, while control rats preferred saccharine solution rather than glucose solution. The expression levels of neuropeptides derived from POMC in the LH and the NAc were changed by glucose but not saccharine intake. In summary, the data suggests that glucose intake increases the expression of neuropeptides derived from POMC in the LH and the NAc in fructose preference rats.

1. Introduction

Obesity is prevalent in a large portion of the world's population, as a result of the abundance of palatable hypercaloric foods [1]. Food addiction, manifested by food preference and binge eating disorder (BED), is one of the causes of this global health problem [2]. In modern society, individuals with obesity are more likely to be addicted to hypercaloric food containing carbohydrates. High-calorie sugar and non-calorie artificial sweeteners are different addictive substances [3]. It remains unclear if the sweet taste or the calories in sugar induces the hedonic overeating that produces a reward in sugar preference.

A previous study has shown that reward and motivation of feeding is controlled by neural circuits and neuroendocrine signals [4]. The hypothalamus is a brain region that controls satiation and starvation [5] and maintains energy homeostasis. The regulatory pathway from the arcuate nucleus (ARC) to the lateral hypothalamus (LH) may be involved in severe hyperphagia and short-term control of feeding behavior [6]. The nucleus of the solitary tract (NTS), nucleus accumbens (NAc), and ventral tegmental area

(VTA) in the nonhypothalamic system also play critical roles in the regulation of food intake and reward-related eating [7].

Proopiomelanocortin (POMC) is mainly expressed in the ARC and the NTS of the brainstem [8] and can be cleaved into multiple neuropeptides, such as α-melanocyte stimulating hormone (α-MSH), β-MSH, adrenocorticotropin (ACTH), β-endorphin (β-END), and β-lipotropin (β-LPH) [9]. POMC neurons in the ARC project and release α-MSH into many hypothalamic nuclei including LH [10]. Also, the POMC gene is expressed in the NAc reward system [11]. However, the function of POMC and the neuropeptides derived from POMC in the NAc, as well as the LH, is not well-understood in food addiction.

Melanocortin derived from POMC neurons is a well-characterized neuronal signal involved in the regulation of energy homeostasis. POMC neurons play an important role in the regulation of food intake [12] and are involved in cannabinoid-induced promotion of feeding [13]. POMC neurons are a key driver of ignition or cessation of feeding behavior. The dysregulation of the POMC system including POMC neurons and POMC-related neuropeptides plays a pivotal role in food addiction. We hypothesize that the POMC system in the NAc and LH is important in regulating sugar preference.

We used a rat model of fructose preference (conditioned stimulus) based on the theory of the backward conditioning procedure using lithium chloride (unconditioned stimulus) [14]. Fructose is the sweetest sugar among all naturally produced carbohydrates [15]. Preference for food or sugar solutions is due to the sweet flavor taste and postoral effect of sugar that may lead to food addiction [16]. In this study, we assessed the responses of fructose preference rats to different concentrations of fructose solution and to calorie (glucose) and noncalorie (saccharine) sweet solutions. We also determined the expression of neuropeptides derived from POMC in the LH and NAc in fructose preference rats.

2. Materials and Methods

2.1. Experimental Animals and Drugs. Male Sprague-Dawley rats (12-weeks-old, 200–220 g) were housed individually in plastic cages under controlled temperature (21–23°C), humidity (50%), and a 12 h/12 h light/dark cycle (light on at 0800) with access to chow and water ad libitum. The rats were purchased from the Laboratory Animal Center of Hebei Medical University. The experimental procedures followed the Guide for the Care and Use of Laboratory Animals (National Research Council, 1996) and were approved by the Animal Care and Use Committee of Hebei Medical University. All rats were randomly divided into the control ($n = 36$) and fructose preference groups ($n = 36$).

Rats were habituated to a limited period of access to water before the experiment. They were allowed to drink water from 0930 to 1130 and from 1600 to 1700 to assure that the rats obtained a daily physiological requirement of water during later experiments when they accessed the testing solution at the given time.

The solutions of lithium chloride (MP Biomedicals, Shanghai Co., 0.15 M/L), fructose (Biotopped, 10% W/W), saccharine (Fluka Chemie, Germany, 0.1% W/W), and glucose (Beichen Fangzheng, Tianjin Co., 10% W/W) were prepared in deionized water, and the test solution preference was conducted in the rat's home cage [17].

2.2. Fructose Preference Test. The conditioned and unconditioned procedures were similar to the procedure in a previous study with minor modifications [18]. The rats began fasting daily from 0800 h and were simultaneously administered with lithium chloride (0.15 M at 1.0 mL/100 g body weight, intraperitoneal injection). One and a half-hour later, the rats were allowed to access 10% (w/v) fructose solution for 2 h (0930–1130 h), with the total intake of the solution measured. The rats fasted in a 3.5 h induction period. During the other 20.5 h in the day, food was provided ad libitum. This procedure was performed daily for 10 consecutive days.

2.3. Preference Tests. Before each of the following tests, rats were deprived of water for 12 h.

2.3.1. Fructose Preference Test. Prior to the fructose preference test, all rats were exposed to 10% fructose solution for 15 min to prevent neophobia [19]. All rats were allowed to adapt to drinking water in the two bottles (1600–1700 h) for two days. In the two-bottle test, rats were provided one bottle with 10% fructose solution and simultaneously another bottle with tap water for 30 min [20]. The fructose solution preference ratio was calculated as follows [21]: fructose solution preference ratio = [fructose solution intake/(fructose solution intake + water intake)] × 100%.

2.3.2. Fructose Concentration Gradient Test. The rats in the fructose preference and control groups were given 10%, 8%, 6%, 4%, and 2% concentration fructose solutions, respectively. The tests were performed in the morning (0930) for 2 h every day for 5 successive days.

2.3.3. Saccharine and Glucose Choice Tests. The one-bottle test was conducted in all rats. In this test, rats received one bottle of 0.1% saccharine solution for 2 h in the morning, then the next day a 10% glucose solution with all volumes of intake was recorded.

The two-bottle test for saccharine or glucose preference was conducted in fructose preference rats. Rats received one bottle of 0.1% saccharine solution and one bottle of 10% glucose solution at the same time. To avoid the interference of the flavor tastes of saccharine and glucose, this test was repeated by using these solutions with an addition of 0.1% grape flavor to ensure they have the same flavor.

2.4. Tissue Preparation and Neuropeptide Western Blotting. The intake volumes of water, 0.1% saccharine, and 10% glucose solutions were controlled in the metabolic monitoring system (CLAMS; Columbus, OH, USA) at 0900. The solution volumes were given as 2 ml/100 g body weight [22, 23]. After 30 min of solution intake, rats were sacrificed by an overdose of pentobarbital sodium (60 mg/kg). The whole brain was immediately removed and placed on a cold rat brain matrix. The LH and NAc were microdissected [24, 25] according to the rat brain atlas [26]. A 1.0 mm coronal slice was taken

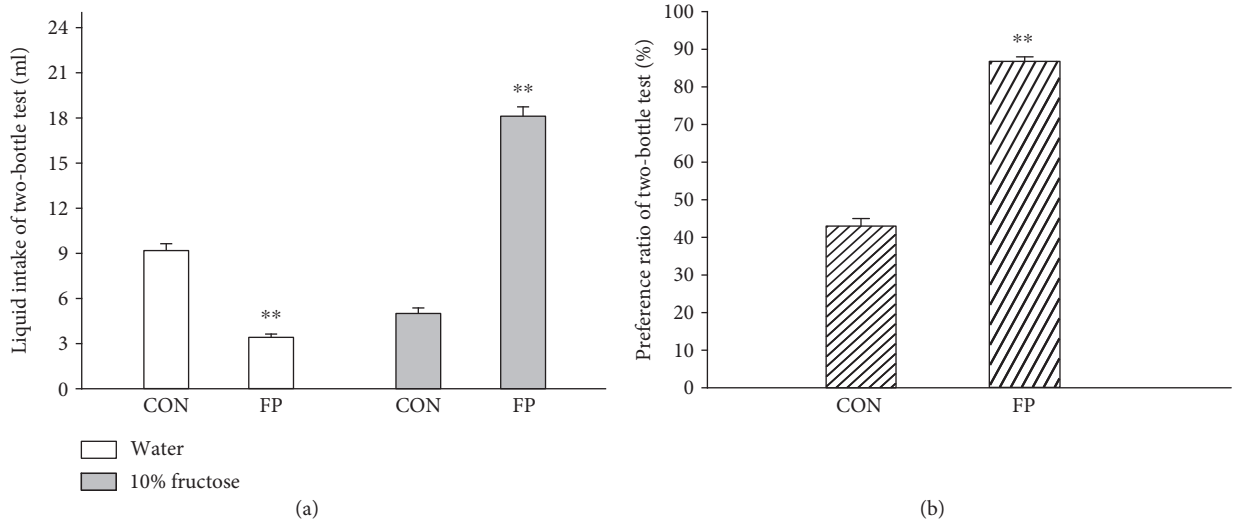

Figure 1: Two-bottle test for fructose preference (liquid intake (a) and preference ratio (b)). Data are represented as mean ± SEM, $n = 15$ in each group. $^{**}p < 0.01$ control rats (CON) versus fructose preference rats (FP).

from a bregma of 1.70 mm to 0.60 mm for the NAc and a bregma of −1.80 mm to −3.80 mm for the LH [27, 28]. Tissue samples were obtained bilaterally for the LH or NAc, respectively. The tissue was finally snap frozen in liquid nitrogen and stored at −80°C for Western blot analysis. The POMC polyclonal antibody (1 : 1000, Bioworld BS7477) was used to detect endogenous levels of the POMC protein and its cleavage products in the NAc and LH, according to standard operating procedures, as described previously [29].

2.5. Data Presentation and Statistical Analysis. Data are presented as mean ± SEM. Statistical analyses were performed by using an SPSS version 19 (IBM Institute Inc., Armonk, NY, USA). Data obtained from the tests in the study were analyzed using Student *t*-test or one-way ANOVA with a post hoc Tukey's test to compare the data from multiple groups. Statistical significance was set at $p < 0.05$.

3. Results

3.1. Fructose Preference Rats Displayed Greater Preference for Glucose or Fructose Solutions than Control Rats. Two-bottle tests were used to measure the preference for fructose solution on fructose preference and control rats (Figure 1). The body weights of the fructose preference rats did not significantly differ from the control rats (data not shown). There were significant differences in the intake of the glucose solution ($p < 0.01$) and the fructose solution preference ratio between the two groups ($p < 0.01$).

In the fructose concentration gradient test, 10%, 8%, 6%, 4%, and 2% fructose solutions were given for 2 h (Figure 2). The intake volumes of each concentration of solution did not differ in the fructose preference rats at low concentrations (even at 2% concentration). The fructose solution intake at 6% concentration was significantly lower than that of 10% ($p < 0.01$) and 8% in control rats ($p < 0.01$). The intake volumes for each concentration from 10% to 2% of fructose solution were higher in fructose preference rats than

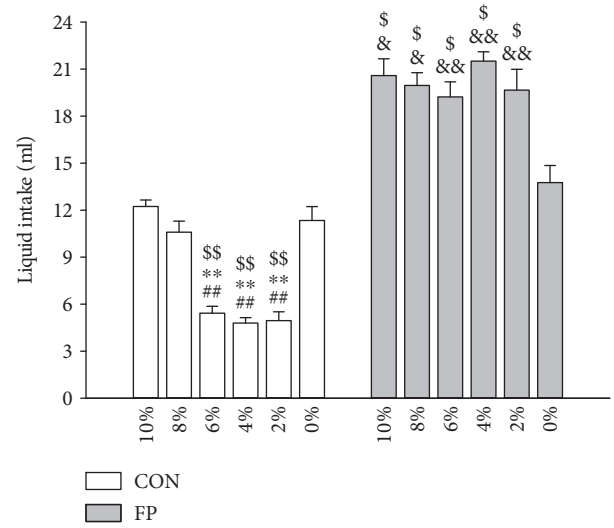

Figure 2: Fructose concentration gradient test. Data are represented as mean ± SEM, $n = 8$ in each group. $^{**}p < 0.01$ versus 10% fructose solution, $^{\#\#}p < 0.01$ versus 8% fructose solution, $^{\$}p < 0.05$, and $^{\$\$}p < 0.01$ versus 0% fructose solution intragroup and $^{\&}p < 0.05$ and $^{\&\&}p < 0.01$ control rats (CON) versus fructose preference rats (FP) for corresponding concentration of fructose solution.

the respective concentrations of fructose solutions in control rats (Figure 2). These results suggest that fructose preference rats have a higher preference for fructose solution than control rats.

3.2. Saccharine and Glucose Choice Tests. To determine the elements (sweet taste or calories) in fructose that are involved in glucose preference in fructose preference rats, one-bottle choice test was conducted with 0.1% saccharine solution and 10% glucose solution (Figure 3). Fructose preference rats preferred glucose solution ($p < 0.01$), while control rats preferred saccharine solution ($p < 0.01$). The two-bottle

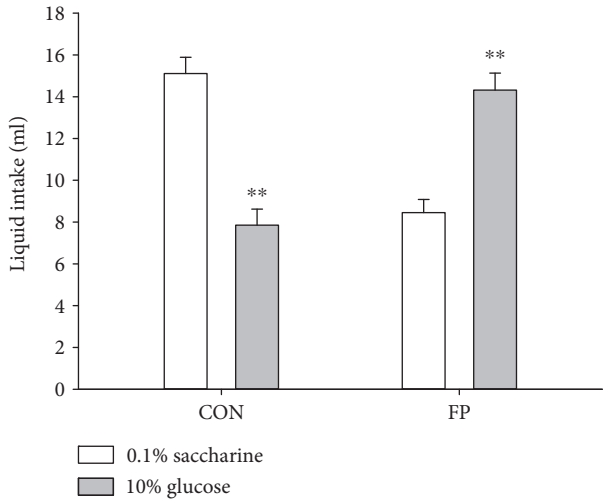

Figure 3: One-bottle test for saccharine and glucose choice. Data are represented as mean ± SEM, $n = 13$ in each group. $^{**}p < 0.01$ versus corresponding 0.1% saccharine.

choice test revealed that the intake volume of glucose solution was higher than saccharine solution in fructose preference rats ($p < 0.01$) (Figure 4(a)). To avoid the possible interference of flavor taste on the preference to these two solutions, a new spicy flavor (grape flavor) was added into the solutions to normalize the flavor taste of saccharine and glucose solutions. Fructose preference rats showed higher intake volumes for glucose than saccharine solution ($p < 0.01$, Figure 4(b)). These findings suggest that the fructose preference rats prefer calories with sweet taste than noncalories with sweet taste.

3.3. Expression of Neuropeptides in the LH and NAc. The Western blot results showed that there were no significant differences in the expression of neuropeptides derived from POMC in the NAc of control rats exposed to three kinds of solution stimuli. The expression of neuropeptides in the NAc of fructose preference rats with glucose solution was increased than that of water and 0.1% saccharine solutions ($p < 0.01$ and $p < 0.05$). Also, the 0.1% saccharine solution increased the expression of the neuropeptides compared with water ($p < 0.05$) (Figure 5(a)). Compared with control rats in the corresponding solution, the expression of neuropeptides in the NAc of fructose preference rats decreased in water ($p < 0.01$) and 0.1% saccharine solutions ($p < 0.01$).

The expression of neuropeptides derived from POMC was decreased in the LH in fructose preference rats fed by 10% glucose compared with rats fed by water or 0.1% saccharine solutions ($p < 0.05$). The expression of neuropeptides derived from POMC showed no difference in control rats fed by 10% glucose, water, or 0.1% saccharine solutions (Figure 5(b)).

4. Discussion

In this study, fructose preference rats were established by using the backward conditioning procedure, in which fructose solution was given following lithium chloride injection. This unconditioned solution-conditioned solution pairing tends to endow the conditioned solution (fructose) to promote the preference learning of rats [14]. Further tests observed that fructose preference rats drunk more low-concentration (2%) fructose solution than control rats, suggesting that fructose preference rats prefer nonsweet glucose solution [30]. We found that the expression level of neuropeptides derived from POMC in the LH and NAc of fructose preference rats was changed by glucose feeding, but not by saccharine intake. The POMC protein and the neuropeptides derived from POMC include α-MSH, β-MSH, ACTH, β-END, and β-LPH. These data suggest that neuroplasticity that occurs in the LH and NAc may be involved in the preference of calorie-containing sweet solution in fructose preference rats. In addition, the expression levels of neuropeptides derived from POMC are significantly decreased in fructose preference rats than in the control rat group. It is possible that POMC and the neuropeptides derived from POMC had distinct functions or sensitivities to glucose in different nuclei.

These fructose preference rats strongly prefer fructose solution and binge drinking a large amount of fructose solution in a short period of time in the two-bottle test, revealing some features of binge eating and preference [31, 32]. Rats are not only attracted to the sweet taste of sugar but they also acquire a preference for flavors associated with calories of sugar. Saccharine is a classic artificial sweetener that contains no calories. Rats may develop conditioned flavor preferences due to the sweet taste of saccharine [16]. On the other hand, fructose contains calories, has postoral actions, and causes flavor preference in rats. Similarly, glucose is a monosaccharide and is very effective in supporting postoral flavor conditioning [16]. It has been shown that mice lacking the sweet taste receptors are initially not able to recognize diluted glucose solution and strongly prefer concentrated solutions [33]. The sweet taste receptor knockout mice develop a preference for high concentrations of sugar solution demonstrating that they prefer sugar calorie more than sweet taste. Consistently, we found in this study that fructose preference rats prefer 10% glucose to 0.1% saccharine. Taken together, the results demonstrate that rats have a preference for calorie-containing sugar. This preference may be due to complex neuroplasticity of neuronal circuits involving the POMC system in the LH and NAc.

Previous studies have found that glucose levels in the rat brain increase 30 min after food intake [34]. Furthermore, a small amount of preloaded sucrose for 30 min in rats markedly changes the expression level of neuropeptides in the ARC [35]. We found that in fructose preference rats, glucose solution intake increased the expression of neuropeptides derived from POMC in the NAc, whereas it decreased the expression of these neuropeptides in the LH. However, saccharine solution intake had little effect on the expression of these neuropeptides. The data suggests that glucose preference is associated with neuroplasticity in the brain reward system. Previous studies have shown that the NAc to the LH pathway that is involved in food reward contributes to hedonic feeding or overconsumption of palatable calorie-

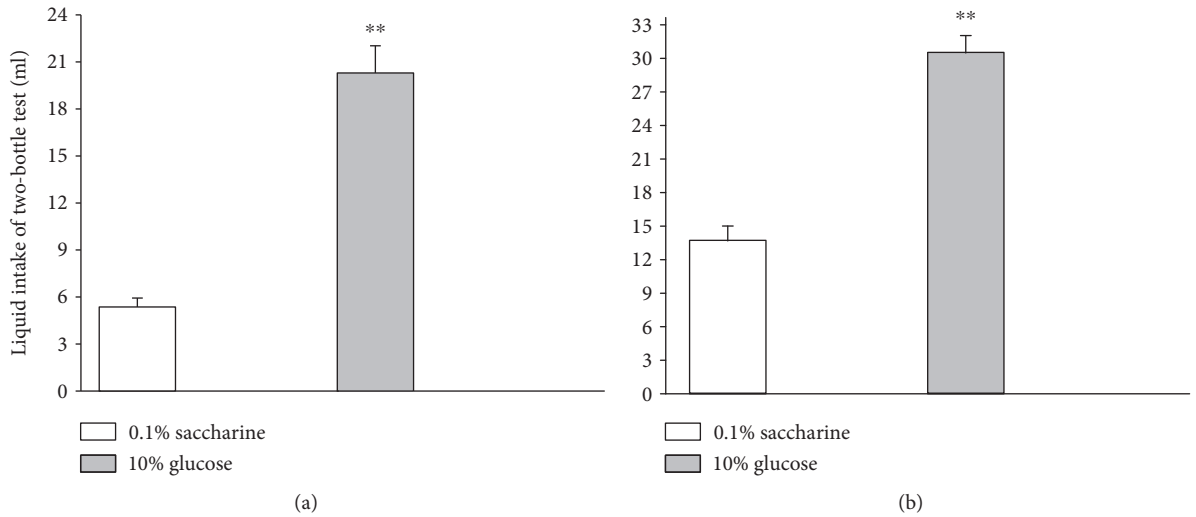

Figure 4: Two-bottle test for saccharine and glucose choice (2 h intake test (a) and flavor solution test (b) of fructose preference rats). Data are represented as mean ± SEM, $n = 15$ in each group. $^{**}p < 0.01$ 10% glucose versus 0.1% saccharine.

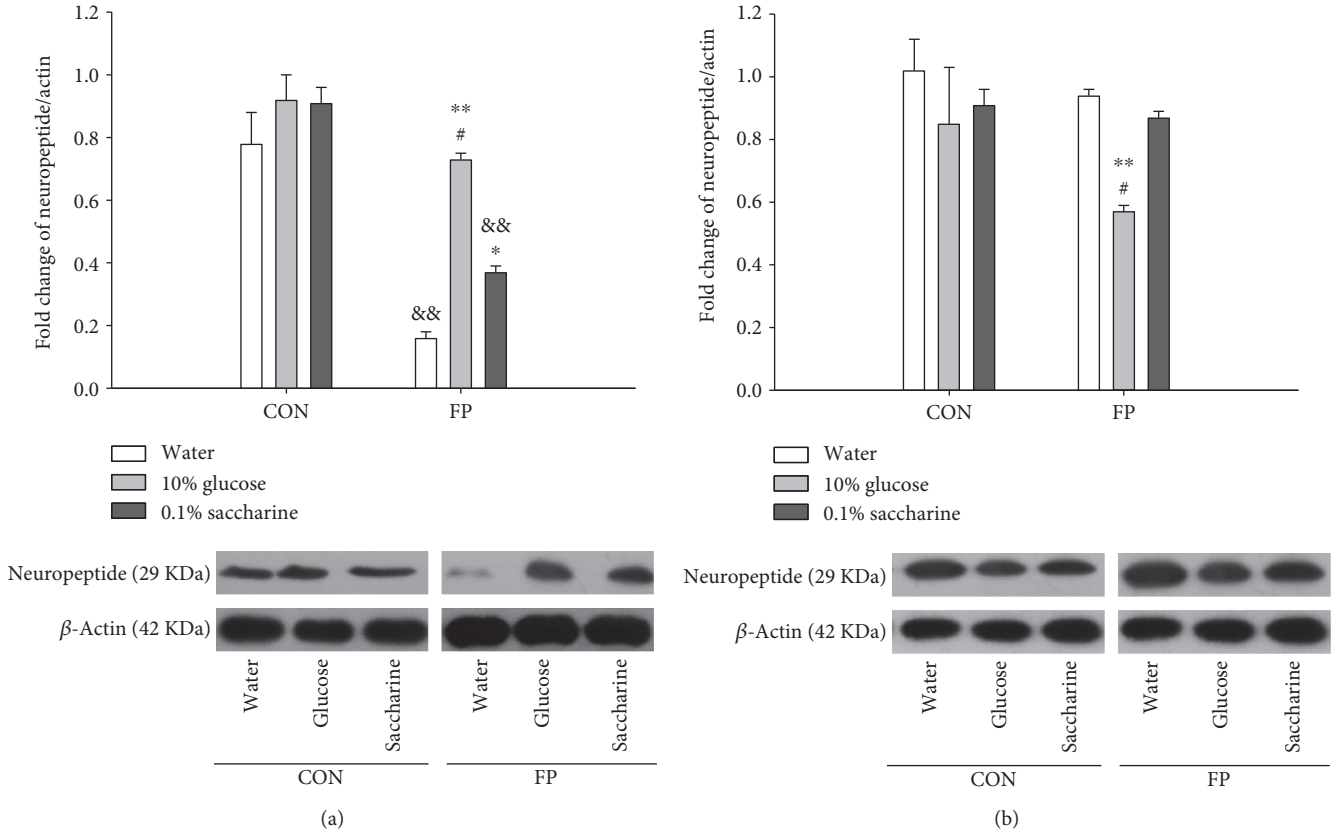

Figure 5: Expression of the POMC protein in the NAc (a) and LH (b) of rats intervened with water, 0.1% saccharine, and 10% glucose. Data are represented as mean ± SEM, $n = 3$ in each group. $^{*}p < 0.05$ and $^{**}p < 0.01$ versus water intragroup, $^{\#}p < 0.05$ versus 0.1% saccharine intragroup, and $^{\&\&}p < 0.01$ control rats (CON) versus fructose preference rats (FP) for corresponding solution.

dense food [36]. The neuroanatomical circuits from the NTS to the NAc and from the ARC to the LH indicate that the POMC system forms a complex neural circuit to regulate feeding behavior [6, 37]. On the other hand, findings from this study suggest that glucose preference leads to an alteration of POMC neural circuits (at least a change of the expression levels of neuropeptides derived from POMC).

POMC is synthesized from precursor pre-proopiomelanocortin (pre-POMC) and can be cleaved to generate multiple neuropeptides, which are involved in many neurological

functions including food addiction [38]. We realized that a limitation exists in this study. The antibody used to detect multiple peptides derived from POMC was generated using full-length human POMC as an immunogen (according to the manufacturer's instruction). Therefore, this antibody should detect ACTH and β-LPH, which typically originate from adenohypophysis (anterior pituitary gland). In fact, POMC neurons in the ARC of the hypothalamus and the NTS express prohormone convertase 2, which cleaves ACTH and β-LPH to generate α-MSH/CLIP and γ-LPH/β-MSH/β-endorphin, respectively [9]. It is possible that these "POMC-derived" peptides found in the NAc and the LH may have originated from brain regions that produce POMC precursor protein. Thus, changes in homeostasis and food addiction as well as changes in the neuroendocrine system such as the hypothalamus-pituitary-adrenal gland neuroendocrine axis may be involved in this fructose preference phenotype. It is possible that POMC functions as a "switch" to control the choice of caloric-containing foods. Further studies may be needed to clarify the role of POMC and its products in different brain nuclei in feeding behavior.

In summary, we found in this study that fructose preference rats prefer glucose solution, but not saccharine solution. Glucose intake changed the expression of neuropeptides derived from POMC in the LH and NAc. The data indicates that the POMC system in the LH of the hypothalamus and the NAc of the central reward system might be involved in food preference development.

Conflicts of Interest

The authors declare that there is no conflict of interest for this study.

Authors' Contributions

Guangfa Jiao and Guozhong Zhang contributed equally to this work.

Acknowledgments

This study is supported by the research grant from the General Administration of Sport of China (2014B039) and Natural Science Foundation of Hebei Province (C2016205238). The authors also are grateful for Professor Wenzhong Bai for his valuable advice on this study.

References

[1] J. P. Morin, L. F. Rodríguez-Durán, K. Guzmán-Ramos et al., "Palatable hyper-caloric foods impact on neuronal plasticity," *Frontiers in Behavioral Neuroscience*, vol. 11, p. 19, 2017.

[2] E. Attia, A. E. Becker, R. Bryant-Waugh et al., "Feeding and eating disorders in DSM-5," *The American Journal of Psychiatry*, vol. 170, no. 11, pp. 1237–1239, 2013.

[3] A. S. Levine, C. M. Kotz, and B. A. Gosnell, "Sugars and fats: the neurobiology of preference," *The Journal of Nutrition*, vol. 133, no. 3, pp. 831S–834S, 2003.

[4] C. Sánchez-Lasheras, A. C. Könner, and J. C. Brüning, "Integrative neurobiology of energy homeostasis-neurocircuits, signals and mediators," *Frontiers in Neuroendocrinology*, vol. 31, no. 1, pp. 4–15, 2010.

[5] M. O. Dietrich and T. L. Horvath, "Hypothalamic control of energy balance: insights into the role of synaptic plasticity," *Trends in Neurosciences*, vol. 36, no. 2, pp. 65–73, 2013.

[6] G. Williams, C. Bing, X. J. Cai, J. A. Harrold, P. J. King, and X. H. Liu, "The hypothalamus and the control of energy homeostasis: different circuits, different purposes," *Physiology & Behavior*, vol. 74, no. 4-5, pp. 683–701, 2001.

[7] S. Tabe-Bordbar and T. J. Anastasio, "Computational analysis of the hypothalamic control of food intake," *Frontiers in Computational Neuroscience*, vol. 10, p. 27, 2016.

[8] D. Wang, X. He, Z. Zhao et al., "Whole-brain mapping of the direct inputs and axonal projections of POMC and AgRP neurons," *Frontiers in Neuroanatomy*, vol. 9, p. 40, 2015.

[9] N. X. Cawley, Z. Li, and Y. P. Loh, "60 years of POMC: biosynthesis, trafficking, and secretion of pro-opiomelanocortin-derived peptides," *Journal of Molecular Endocrinology*, vol. 56, no. 4, pp. T77–T97, 2016.

[10] E. J. P. Anderson, I. Çakir, S. J. Carrington et al., "60 years of POMC: regulation of feeding and energy homeostasis by α-MSH," *Journal of Molecular Endocrinology*, vol. 56, no. 4, pp. T157–T174, 2016.

[11] M. Valenza, R. Picetti, V. Yuferov, E. R. Butelman, and M. J. Kreek, "Strain and cocaine-induced differential opioid gene expression may predispose Lewis but not Fischer rats to escalate cocaine self-administration," *Neuropharmacology*, vol. 105, pp. 639–650, 2016.

[12] R. D. Cone, "Anatomy and regulation of the central melanocortin system," *Nature Neuroscience*, vol. 8, no. 5, pp. 571–578, 2005.

[13] M. Koch, L. Varela, J. G. Kim et al., "Hypothalamic POMC neurons promote cannabinoid-induced feeding," *Nature*, vol. 519, no. 7541, pp. 45–50, 2015.

[14] R. C. Chang, A. P. Blaisdell, and R. R. Miller, "Backward conditioning: mediation by the context," *Journal of Experimental Psychology: Animal Behavior Processes*, vol. 29, no. 3, pp. 171–183, 2003.

[15] L. M. Hanover and J. S. White, "Manufacturing, composition, and applications of fructose," *The American Society for Clinical Nutrition*, vol. 58, no. 5, pp. 724S–732S, 1993.

[16] K. Touzani, R. J. Bodnar, and A. Sclafani, "Neuropharmacology of learned flavor preferences," *Pharmacology, Biochemistry, and Behavior*, vol. 97, no. 1, pp. 55–62, 2010.

[17] S. Zukerman, J. I. Glendinning, R. F. Margolskee, and A. Sclafani, "T1R3 taste receptor is critical for sucrose but not Polycose taste," *American Journal of Physiology - Regulatory, Integrative and Comparative Physiology*, vol. 296, no. 4, pp. R866–R876, 2009.

[18] K. Touzani and A. Sclafani, "Lateral hypothalamic lesions impair flavour-nutrient and flavour-toxin trace learning in rats," *European Journal of Neuroscience*, vol. 16, no. 12, pp. 2425–2433, 2002.

[19] M. Domjan, "Determinants of the enhancement of flavored-water intake by prior exposure," *Journal of Experimental Psychology: Animal Behavior Processes*, vol. 2, no. 1, pp. 17–27, 1976.

[20] P. Sun, S. Wei, X. Wei et al., "Anger emotional stress influences VEGF/VEGFR2 and its induced PI3K/AKT/mTOR signaling

pathway," *Neural Plasticity*, vol. 2016, Article ID 4129015, 12 pages, 2016.

[21] J. R. Criado and C. L. Ehlers, "Effects of adolescent onset voluntary drinking followed by ethanol vapor exposure on subsequent ethanol consumption during protracted withdrawal in adult Wistar rats," *Pharmacology Biochemistry and Behavior*, vol. 103, no. 3, pp. 622–630, 2013.

[22] A. Sclafani and K. Ackroff, "Operant licking for intragastric sugar infusions: differential reinforcing actions of glucose, sucrose and fructose in mice," *Physiology & Behavior*, vol. 153, pp. 115–124, 2016.

[23] B. B. Rui, H. Chen, L. Jang et al., "Melatonin upregulates the activity of AMPK and attenuates lipid accumulation in alcohol-induced rats," *Alcohol and Alcoholism*, vol. 51, no. 1, pp. 11–19, 2016.

[24] S. M. MohanKumar, C. L. Smith, and P. S. MohanKumar, "Central adaptation to chronic administration of interleukin-1β (IL-1β) in rats," *Brain Research Bulletin*, vol. 62, no. 1, pp. 71–76, 2003.

[25] M. Palkovits, L. Záborszky, M. J. Brownstein, M. I. Fekete, J. P. Herman, and B. Kanyicska, "Distribution of norepinephrine and dopamine in cerebral cortical areas of the rat," *Brain Research Bulletin*, vol. 4, no. 5, pp. 593–601, 1979.

[26] G. Paxinos and C. Watson, *The Rat Brain in Stereotaxic Co-Ordinates*, Academic Press, San Diego, 1998.

[27] W. F. Mathes, D. L. Nehrenberg, R. Gordon, K. Hua, T. Garland Jr., and D. Pomp, "Dopaminergic dysregulation in mice selectively bred for excessive exercise or obesity," *Behavioural Brain Research*, vol. 210, no. 2, pp. 155–163, 2010.

[28] E. A. Nillni, A. Lee, G. Legradi, and R. M. Lechan, "Effect of precipitated morphine withdrawal on post-translational processing of prothyrotropin releasing hormone (proTRH) in the ventrolateral column of the midbrain periaqueductal gray," *Journal of Neurochemistry*, vol. 80, no. 5, pp. 874–884, 2002.

[29] J. Cui, Y. Ding, S. Chen et al., "Disruption of *Gpr45* causes reduced hypothalamic POMC expression and obesity," *The Journal of Clinical Investigation*, vol. 126, no. 9, pp. 3192–3206, 2016.

[30] A. Sclafani and K. Ackroff, "Glucose- and fructose-conditioned flavor preferences in rats: taste versus postingestive conditioning," *Physiology & Behavior*, vol. 56, no. 2, pp. 399–405, 1994.

[31] M. Perello, S. Valdivia, G. G. Romero, and J. Raingo, "Considerations about rodent models of binge eating episodes," *Frontiers in Psychology*, vol. 5, p. 372, 2014.

[32] K. B. Bonacchi, K. Ackroff, K. Touzani, R. J. Bodnar, and A. Sclafani, "Opioid mediation of starch and sugar preference in the rat," *Pharmacology Biochemistry and Behavior*, vol. 96, no. 4, pp. 507–514, 2010.

[33] S. Zukerman, J. I. Glendinning, R. F. Margolskee, and A. Sclafani, "Impact of T1r3 and Trpm5 on carbohydrate preference and acceptance in C57BL/6 mice," *Chemical Senses*, vol. 38, no. 5, pp. 421–437, 2013.

[34] I. F. de Sousa, A. P. de Souza, I. S. Andrade et al., "Effect of fish oil intake on glucose levels in rat prefrontal cortex, as measured by microdialysis," *Lipids in Health and Disease*, vol. 12, no. 1, p. 188, 2013.

[35] V. A. Gaysinskaya, O. Karatayev, J. Shuluk, and S. F. Leibowitz, "Hyperphagia induced by sucrose: relation to circulating and CSF glucose and corticosterone and orexigenic peptides in the arcuate nucleus," *Pharmacology Biochemistry and Behavior*, vol. 97, no. 3, pp. 521–530, 2011.

[36] P. J. Kenny, "Reward mechanisms in obesity: new insights and future directions," *Neuron*, vol. 69, no. 4, pp. 664–679, 2011.

[37] A. L. Alhadeff, L. E. Rupprecht, and M. R. Hayes, "GLP-1 neurons in the nucleus of the solitary tract project directly to the ventral tegmental area and nucleus accumbens to control for food intake," *Endocrinology*, vol. 153, no. 2, pp. 647–658, 2012.

[38] M. Chrétien and M. Mbikay, "60 years of POMC: from the prohormone theory to pro-opiomelanocortin and to proprotein convertases (PCSK1 to PCSK9)," *Journal of Molecular Endocrinology*, vol. 56, no. 4, pp. T49–T62, 2016.

Hindawi
Neural Plasticity
Volume 2017, Article ID 4174010, 10 pages
https://doi.org/10.1155/2017/4174010

Research Article

Enhancement in Tonically Active Glutamatergic Inputs to the Rostral Ventrolateral Medulla Contributes to Neuropathic Pain-Induced High Blood Pressure

Wei Wang,[1] Zui Zou,[2] Xing Tan,[3] Ru-Wen Zhang,[3] Chang-Zhen Ren,[3] Xue-Ya Yao,[4] Cheng-Bao Li,[4] Wei-Zhong Wang,[3] and Xue-Yin Shi[1]

[1]*Department of Anesthesiology and SICU, XinHua Hospital, Shanghai JiaoTong University School of Medicine, Shanghai 200092, China*
[2]*Department of Anesthesiology, Changzheng Hospital, Second Military Medical University, Shanghai 200433, China*
[3]*Department of Physiology, Second Military Medical University, Shanghai 200433, China*
[4]*Hebei North University, Zhangjiakou, Hebei Province 075000, China*

Correspondence should be addressed to Wei-Zhong Wang; wangwz68@hotmail.com and Xue-Yin Shi; shixueyin1128@163.com

Received 1 April 2017; Revised 19 June 2017; Accepted 10 July 2017; Published 12 October 2017

Academic Editor: Depei Li

Neuropathic pain increases the risk of cardiovascular diseases including hypertension with the characteristic of sympathetic overactivity. The enhanced tonically active glutamatergic input to the rostral ventrolateral medulla (RVLM) contributes to sympathetic overactivity and blood pressure (BP) in cardiovascular diseases. We hypothesize that neuropathic pain enhances tonically active glutamatergic inputs to the RVLM, which contributes to high level of BP and sympathetic outflow. Animal model with the trigeminal neuropathic pain was induced by the infraorbital nerve-chronic constriction injury (ION-CCI). A significant increase in BP and renal sympathetic nerve activity (RSNA) was found in rats with ION-CCI (BP, $n = 5$, RSNA, $n = 7$, $p < 0.05$). The concentration of glutamate in the RVLM was significantly increased in the ION-CCI group ($n = 4$, $p < 0.05$). Blockade of glutamate receptors by injection of kynurenic acid into the RVLM significantly decreased BP and RSNA in the ION-CCI group ($n = 5$, $p < 0.05$). In two major sources (the paraventricular nucleus and periaqueductal gray) for glutamatergic inputs to the RVLM, the ION-CCI group ($n = 5$, $p < 0.05$) showed an increase in glutamate content and expression of glutaminase 2, vesicular glutamate transporter 2 proteins, and c-fos. Our results suggest that enhancement in tonically active glutamatergic inputs to the RVLM contributes to neuropathic pain-induced high blood pressure.

1. Introduction

Neuropathic pain is widely recognized as one of the most difficult pain syndromes to manage, and its outcomes are often unsatisfactory. Neuropathic pain is a risk factor for cardiovascular diseases, such as hypertension, diabetes, and stroke, seriously affects the quality of patients' life, and results in the higher anxiety/depression scores [1–6]. Neuropathic pain is capable of increasing blood pressure (BP) and heart rate (HR) [3, 4, 7]. However, the mechanism by which neuropathic pain induces cardiovascular dysfunction is not fully understood.

A major characteristic of cardiovascular diseases including hypertension and heart failure is overactivity of the sympathetic nervous system (SNS). Increasing clinical evidence indicates a key role for sympathoactivation in the development of these cardiovascular diseases [8, 9]. Interestingly, neuropathic pain is suggested to be a stressor for stimulating the SNS [10]. The rostral ventrolateral medulla (RVLM) is a key region involved in the central control of sympathetic outflow and plays an important role in maintaining resting BP and sympathetic tone [8]. Abnormalities in the function and structure of the RVLM are closely relative to pathophysiological precession of hypertension [11].

Notably, neuropathic pain also has an effect on neuronal activity in the RVLM. Jung et al. [12] reported that tooth pulpal pain elicited c-fos expression in cardiovascular centers, such as the nucleus tractus solitarius (NTS) and RVLM, and further moderated cardiovascular reflex function.

It is well known that glutamate, a major excitatory neurotransmitter, plays an important role in mediating cardiovascular regulation in the RVLM. Glutamate receptors including NMDA and AMPA receptors in the RVLM have been demonstrated to be involved in control of BP and cardiovascular reflexes [8, 11]. Interestingly, an enhancement in tonically active glutamatergic inputs to the RVLM is reported to be responsible to hyperactivity of RVLM vasomotor neurons, high BP and sympathoexcitation in hypertension and heart failure [13, 14]. Based on our [15, 16] and other's studies [17], the release of glutamate in the RVLM is increased in the spontaneous hypertensive rats (SHR). On the one hand, microinjection of the glutamate receptor (GluR) antagonist kynurenic acid (KYN) into the RVLM induces a significant decrease in resting BP in hypertensive rats but not in normotensive rats [18, 19]. On the other hand, enhanced tonic glutamatergic input to the RVLM contributes to the hyperactivity of RVLM vasomotor neurons and sympathetic tone in rats with chronic heart failure [20]. Interestingly, neuropathic pain also enhances the release of the excitatory neurotransmitter glutamate in several brain regions including the thalamus, insular cortex, and periaqueductal gray (PAG) [21–23], which also send the fibers to connect with the RVLM. However, it is not clear whether high level of BP and sympathetic outflow induced by neuropathic pain is associated with an enhancement in tonically active glutamatergic inputs to the RVLM. Therefore, the hypothesis of the present study is that neuropathic pain enhances tonically active glutamatergic inputs to the RVLM, which contributes to high level of BP and sympathetic outflow. In order to test this hypothesis, we investigated the effects of neuropathic pain on the release of glutamate in the RVLM, expression of glutamate receptor NMDA, and the response of cardiovascular activity to RVLM injection of glutamate receptor antagonist.

2. Materials and Methods

2.1. Animals. Male Sprague-Dawley rats (220–260 g) were purchased from Sino-British SIPPR/BK Lab Animal Ltd. (Shanghai, China). Experimental protocols were approved by the Institutional Animal Care and Use Committees at Second Military Medical University and Shanghai JiaoTong University School of Medicine. All methods were performed in accordance with the relevant guidelines and regulations.

2.2. Production of Animal Model with Neuropathic Pain. The rat model with neuropathic pain was produced according to the previous study [24]. Briefly, rats were anesthetized with 10% chloral hydrate (35 mg/kg, ip). The skin below the bilateral eyes was shaved, and the position of the rat head was fixed. Below the eyes, a small, approximately 5 mm, incision was made at the junction between the zygomatic arch and the nasal bone. Nerves were separated from the surrounding connective tissues carefully, and then the infraorbital nerve (ION), which is the secondary branch of the trigeminal nerve, was exposed clearly. Two absorbable threads (4–0 chromic catgut) were appropriately tied around the ION. The two ligatures were spaced approximately 2 mm apart from each other. After the surgery, the rats were fed in comfortable cages. The sham operation was performed by exposing the infraorbital nerve without ligatures.

2.3. Assessing Mechanical Sensitivity. To relieve stress during the study, the animals were trained to adapt to the environment and specific procedures one week before surgery. The behavioral tests were carried out with Von Frey filaments [24, 25]. The baseline pain thresholds were measured 3 days prior to surgery and then measured again on postsurgery days 5, 10, 15, 20, 25, and 30. The mechanical stimulus intensities from low to high were 0.07 g, 0.16 g, 0.4 g, 0.6 g, 1.0 g, 1.4 g, 2.0 g, 4.0 g, 6.0 g, 8.0 g, 10.0 g, 15.0 g, and 26.0 g. Each stimulus intensity was tested five times on the bilateral whisker pads of rats. The threshold value for mechanical pain was determined according to the corresponding stimulation strength to the rats presented with one or more of the following items: (1) Dodge actions, such as backward movement, turning around, or shaking the head; to avoid the stimuli, the rats curled their body, moved closer to the cage walls, or hid their face and head under their body; (2) scratching their face; the animals scratched the stimulated region on the face more than three times; and (3) aggressive behaviors; the rats grasped and bit the stimulating device and exhibited attack actions.

2.4. Measurement of Resting BP and HR. To determine whether the ION injury has an influence on cardiovascular activity, levels of BP and HR in conscious rats were recorded using a computerized noninvasive tail-cuff system (ALC-NIBP, Shanghai Alcott Biotech) a week before and after the ION-CCI surgery. The measurement of BP and HR was carried out at days 5, 10, 15, 20, 25, and 30 after the surgery. The measurement of BP and HR by tail-cuff method was performed according to our previous methods [12, 16]. Briefly, the animals were placed in a specific holding device with a thermostatically controlled warming plate and then warmed to an ambient temperature of 32°C to keep the tail artery vasodilated. Approximately 20–30 min before recording the BP, the rats were put in chambers to acclimate to the measuring chambers. Pressure was applied to the tail to occlude blood flow and was slowly released until the first pulse of arterial flow was detected. Then, the cuff was connected to a transducer, which could amplify the signal and record by a data acquisition system. At least six consecutive cycles were measured, and the averaged values were recorded.

2.5. In Vivo Experiments. The surgical procedures and recording of BP, HR, and renal sympathetic nerve activity (RSNA) under anesthetized condition were based on our previous studies [20, 26]. Briefly, rats were anesthetized by urethane (800 mg/kg, ip) and achloralose (40 mg/kg, ip). A catheter was inserted into the right femoral artery to measure BP, and the femoral vein was catheterized for supplemental

drugs. Rats were placed on a stereotaxic frame, and head fixed horizontally, and dorsal surface of the medulla was surgically exposed. The renal sympathetic nerve was separated and recorded with a pair of recording electrodes. In order to avoid afferent activity, the distal terminus of the renal nerve was cut. Then, the RSNA signal was amplified and monitored together with BP and HR by the PowerLab system. The baseline RSNA was taken as 100% from the absolute value after the noise level was subtracted. The maximum RSNA was measured during euthanasia, as described previously [26]. Usually, the maximum nerve activity (Max) occurred 5 min after the rat was euthanized with an overdose of pentobarbital sodium (200 mg/kg). Background noise levels for sympathetic nerve activity were recorded 15–20 min after the rat was euthanized. According to the unit conversion of Powerlab Chart (AD Instruments) system, the Max value was set to 100%, and the noise level was set to 0%. Baseline nerve activity was taken as the percentage of Max. The body temperature was maintained at 37°C with a temperature controller.

2.6. RVLM Microinjection. As reported in our previous study [27], RVLM microinjection was performed with a three-barrel micropipette. The RVLM coordinates were 1.5–2.5 mm rostral to the obex, 1.8–2.0 mm lateral to the midline, and 3.0–3.2 mm deep to the dorsal surface of the brainstem. The microinjections were completed within 5–10 s by a pressure injector, and the microinjection volume was 100 nl. The functional location of the RVLM was identified by a pressor response to microinjection of L-glutamate (1 nmol). The interval between bilateral injections was within 2 min. The BP, HR, and RSNA were then recorded continuously for at least 60 min after the bilateral injection of KYN (2.7 nmol) into the RVLM. At the end of each experiment, a histological identification was conducted to verify microinjection site marked by dye blue.

2.7. Microdialysis. Brain microdialysis *in vivo* was carried out as previously described [28]. The rats were anesthetized with inhaled isoflurane (3%), and the RVLM was surgically exposed as described above. A microdialysis probe (MAB.6.14.2) was inserted into the RVLM. Brain microdialysis was carried out by perfusing the probe with artificial cerebrospinal fluid at a rate of 2 μl/min. The volume of each dialysate sample (10 min) was 20 μl, and the samples were obtained after at least 60 min of rest following the surgical operation.

2.8. Western Blot Analysis. Ten days after the ION-CCI surgery, the rat brains were obtained and stored at −80°C. The RVLM, PAG, and paraventricular nucleus (PVN) tissues were punched in accordance with the rat brain atlas [29]. In this study, the Obex point was suggested to a landmark to identify the RVLM, which is based on the brain alignment map, and then measured the location of each nucleus from this map. The freezing microtome was set the slice thickness of 50 μm, and the number of slices was counted to locate the longitudinal distance. The distance from RVLM to Obex is 2 mm. To identify PVN, we located the anterior commissure based on the brain alignment map. The distance from the PVN to the disappearing point of anterior commissure is 1.2 mm. PAG is the area around the aqueduct of the brain, which was recognized in the transverse section of the brain. The lateral distance was measured according to the brain localization map, and the location of the nucleus from the midline of the brain was measured. Protein concentrations were measured using a BCA protein assay kit (Beyotime, Shanghai). The Western blot procedures were based on the previous study [25]. Equal amounts of protein (40 μg) were separated by SDS-PAGE (10% acrylamide) and then transferred to a polyvinylidene fluoride membrane. The membrane was blocked with 5% nonfat milk dissolved in Tris-buffered saline solution containing 0.1% Tween 20 for 2 h at room temperature. Membranes were probed with primary antibody overnight at 4°C. The primary antibodies included anti-vGLUT2 (1 : 2000, antivesicular glutamate transporter 2, MAB5504, EMD Millipore), anti-GLS2 (1 : 1000, antiglutaminase 2, AV43562; Sigma-Aldrich), and anti-NMDAR1(1 : 1000, ab2824–1, Abcam). β-Actin was used as a loading control. After washing the membranes three times for 5 min each, the membranes were incubated with a secondary antibody for 2 h at room temperature. After immunoblotting, the bands were visually detected and analyzed by the Syngene Bio Imaging system (number 55000, Gene Company).

2.9. High-Performance Liquid Chromatography (HPLC). The concentrations of glutamate in dialysis samples and the brain nuclei (PAG, PVN) were measured by HPLC as described previously [12]. After the PAG and PVN tissues were punched from the brain and weighed, 0.05 mM HClO4 was placed into the tube, and the tissues were homogenized and centrifuged for 10 min, and the supernatant was collected for further analysis. There was no pretreatment for the dialysate samples from the RVLM. All the samples were analyzed by HPLC (model 582 pump, ESA) with electrochemical detection (model 5300, ESA). o-Phthalaldehyde (OPA)/2-mercaptoethanol (b-ME) was used for derivatization for the amino acid analysis. Supernatant sample (20 μl) was mixed with 50 μl of OPA/b-ME solution. However, 50 μl of the supernatant from the brain nuclei tissue samples was mixed with 20 μl of OPA/b-ME solution and derivatized approximately 2 min before analysis, and then 50 μl of the derivatized sample was injected for subsequent amino acid analysis. The HPLC analysis was carried out on a reverse-phase C18 column (Shiseido Capcell Pak 75 × 3 mm, 3 μm C18, P/N 88-90816, Shiseido Co. Ltd., Tokyo, Japan). The mobile phase consisted of 100 mM anhydrous disodium hydrogen phosphate, 22% methanol, and 3.5% acetonitrile at pH 6.75, and the flow rate was 0.5 ml/min. The detection channel potentials were set at +150 mV and +550 mV.

Content of norepinephrine (NE) in 24 h urine was also detected by HPLC. Twenty-four-hour urinary samples were collected from metabolism cages in which the rats were placed for 24 h. To reduce the degradation of NE, the samples were acidified with glacial acetic acid in 15 ml centrifuge tubes, which were embedded in crushed ice. Dihydroxybenzylamine (Sigma) was used as the internal standard. Before the experiment, the samples were dissociated carefully

according to the detailed procedure referenced in our previous report [16]. The flow rate was 0.5 ml/min. The HPLC data were acquired, processed, and analyzed using Coulochem software.

2.10. Immunohistochemistry. The immunohistochemistry procedures were carried out according to our previous study [30]. The rats were killed with an overdose of sodium pentobarbital (200 mg/kg, ip) and perfused with 0.9% saline followed by 4% paraformaldehyde. The brains were dissected, postfixed with 4% paraformaldehyde for approximately 24 h, and then cryoprotected in 20% sucrose for at least 24 h. Brain sections were made with a freezing microtome (Leica, CM1850), and the thickness of sections was 10 μm. The free-floating sections were rinsed 3 times with 0.1 M PBS and blocked with 5% BSA for 1 h at 37°C immediately prior to the incubation with primary antibody. The sections were incubated with the primary antibodies overnight at 4°C. The primary antibody was rabbit anti-fos (1 : 100; Phoenix Pharmaceuticals Inc., Burlingame, CA, USA). For direct staining, the sections were washed in 0.1 M PBS 3 times at 5 min intervals and incubated with secondary antibody for 2 h at room temperature. Finally, the diaminobenzidine (DAB) coloration method was used to determine the expression of c-fos protein.

2.11. Data Analysis. Values are presented as the means ± SD. Statistical analyses were carried out using SPSS software (version 15.0). To assess the effect of the ION-CCI surgery on mechanical hypersensitivity, a repeated measures analysis of variance (ANOVA) followed by a post hoc Bonferroni test was applied to evaluate the mechanical threshold before and after surgery. The values of BP obtained by tail-cuff method were also analyzed and compared using a repeated measures ANOVA. The extent of the glutamate in the RVLM and BP during different time courses was compared using a Factorial design ANOVA followed by a post-LSD test. Other data were analyzed using unpaired t tests. Differences were considered to be significant at $p < 0.05$.

3. Results

3.1. Effects of ION-CCI on Hyperalgesia and Resting BP. The mechanical thresholds after ION-CCI were measured repeatedly to confirm that the pain influence was continuous. We found that the basal mechanical thresholds (before surgery) between the sham and ION-CCI groups were not significantly different (9.64 ± 1.58 versus 9.68 ± 0.79 g, $p > 0.05$). However, mechanical threshold of the ION-CCI group was decreased significantly 10 days after the ION-CCI surgery and persisted to 30 days after operation (Figure 1). As shown in Figure 2(a), levels of mean arterial pressure (MAP) from 5-day postoperation (PO5) (158 ± 9 mmHg) to PO20 (140 ± 8 mmHg) were significantly higher in the ION-CCI rats than in the sham rats. However, a maximal increase in MAP reached on PO10 in the ION-CCI rats (169 ± 10 mmHg). Ten days after the surgery, these two groups were anesthetized and MAP was measured through the arterial cannula. It was found that MAP was also

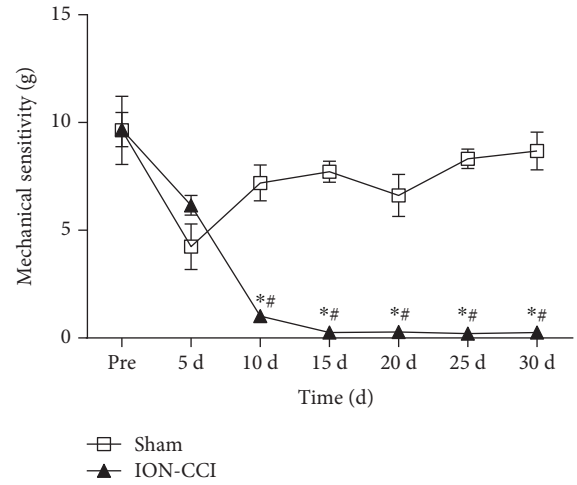

Figure 1: Time courses of the mechanical sensitivity in sham and ION-CCI rats. The data of PRE indicates an average of mechanical sensitivity at 1 and 2 days before surgery. $n = 5$/group. $^{*}p < 0.05$ compared with PRE value, $^{\#}p < 0.05$ compared with sham.

significantly higher (146 ± 8 versus 109 ± 7 mmHg) in the ION-CCI rats than in the sham rats (Figure 2(b)).

3.2. Effects of ION-CCI on 24 h Urinary Excretion of NE and RSNA. To identify whether trigeminal neuropathic pain increases sympathetic nerve activity, the 24 h urinary excretion of NE and RSNA was measured 10 days after the ION-CCI and sham operation. As illustrated in Figures 3(a) and 3(b), the 24 h urinary excretion of NE was increased significantly in the ION-CCI group compared with the sham group (0.32 ± 0.08 versus 0.15 ± 0.04 μg, $n = 5$, $p < 0.05$). Similar to the NE result, the baseline RSNA (of Max) in the ION-CCI group was predominantly higher than that in the sham group (29.5 ± 3.7 versus 13.2 ± 2.2%, $n = 5$, $p < 0.05$).

3.3. Effects of ION-CCI on the Release of Glutamate in the RVLM. Figure 4 shows glutamate concentration in the microdialysis fluid of the RVLM. The glutamate content was significantly higher in the ION-CCI group compared with the sham rats on 10 days (1636 ± 169 versus 347 ± 24 μg/l), 15 days (1147 ± 149 versus 309 ± 31 μg/l), 20 days (757 ± 53 versus 405 ± 79 μg/l), and 25 days (470 ± 43 versus 367 ± 58 μg/l) after ION-CCI operation. The glutamate content began to increase at 5 days, reached the peak value on 10 days, and persisted on 30 days postoperation. However, the glutamate concentration in the RVLM of the sham group was no different at the different time points. Moreover, the level of NMDAR1 protein expression on RVLM in the ION-CCI group was higher than that in the sham group (Figure 4(b)).

3.4. Cardiovascular Effects of Bilateral Microinjections of KYN into the RVLM. Figure 5(a) represents original tracings of BP, HR, and RSNA in response to microinjection of KYN (2.7 nmol for each side) into the RVLM. Bilateral injection of KYN into the RVLM produced a significant decrease in MAP (−20.0 ± 5.4%), HR (−15.7 ± 5.5%), and

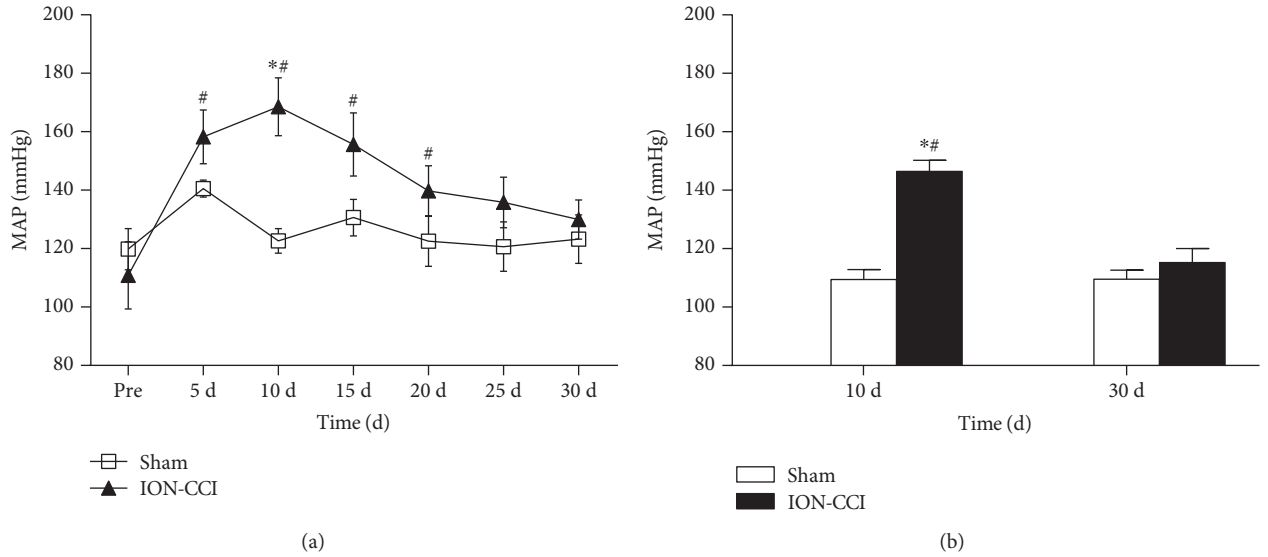

Figure 2: Effects of ION-CCI on blood pressure. (a) Time course of mean arterial pressure (MAP) consciously measured by tail-cuff method in awake rats. $n = 5$/group, $^{*}p < 0.05$ compared with PRE, $^{\#}p < 0.05$ compared with sham. (b) MAP measured through the arterial cannula in anesthetized rats. $n = 5$/group $^{*}p < 0.05$ compared with 10 d, $^{\#}p < 0.05$ compared with sham.

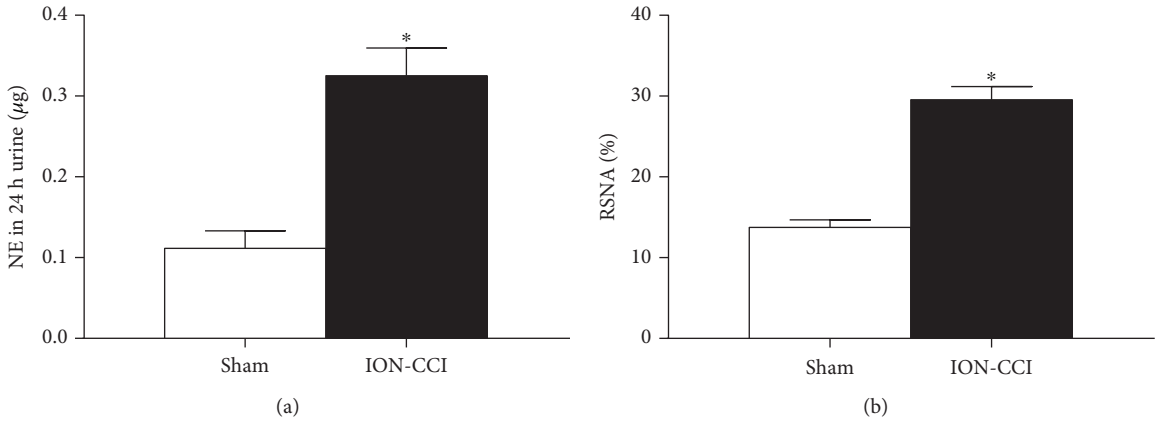

Figure 3: Effects of ION-CCI on basal renal sympathetic nerve activity (RSNA, (b)) and increased the 24 h urinary excretion of norepinephrine (NE, (a)). $n = 7$ in each group. $^{*}p < 0.05$ compared with sham.

RSNA ($-23.5 \pm 6.7\%$) in the ION-CCI rats but not in the sham rats (Figure 5(b)).

3.5. Effects of ION-CCI on the Glutamate Content and the Expression of vGLUT2 and Glutaminase 2 (GLS2) in the PAG and PVN. As depicted in Figure 6, the glutamate concentration in the PAG and PVN was significantly higher on 10 days after ION-CCI. The levels of GLS2 and vGLUT2 protein expressions in the PAG and PVN were also significantly increased in the ION-CCI rats compared with the sham rats.

3.6. Effects of ION-CCI on c-Fos Expression in the PAG, PVN, and RVLM. In this study, we used Fos-positive cells to examine the activity of neurons. The ION-CCI rats showed a significant increase in Fos expression in the PAG, PVN, and RVLM (Figure 7). The number of Fos-positive cells in the PAG and RVLM was increased by approximately 3-4 times in the ION-CCI group more than in the sham group. The number of Fos-positive neurons in the PVN of the ION-CCI rats was much greater than that in the PVN of the sham group.

4. Discussion

The major findings of our present experiments are the following: (1) ION-CCI effectively increased BP and sympathetic nerve activity; (2) ION-CCI significantly increased the tonic release of glutamate in the RVLM; and (3) the PAG and PVN may be important sources for enhanced tonic glutamatergic inputs to the RVLM in the ION-CCI. Based on these results, it is suggested that the enhancement of tonically active glutamatergic inputs to the RVLM plays an important role in the neuropathic pain associated with increase in BP and sympathetic nerve activity.

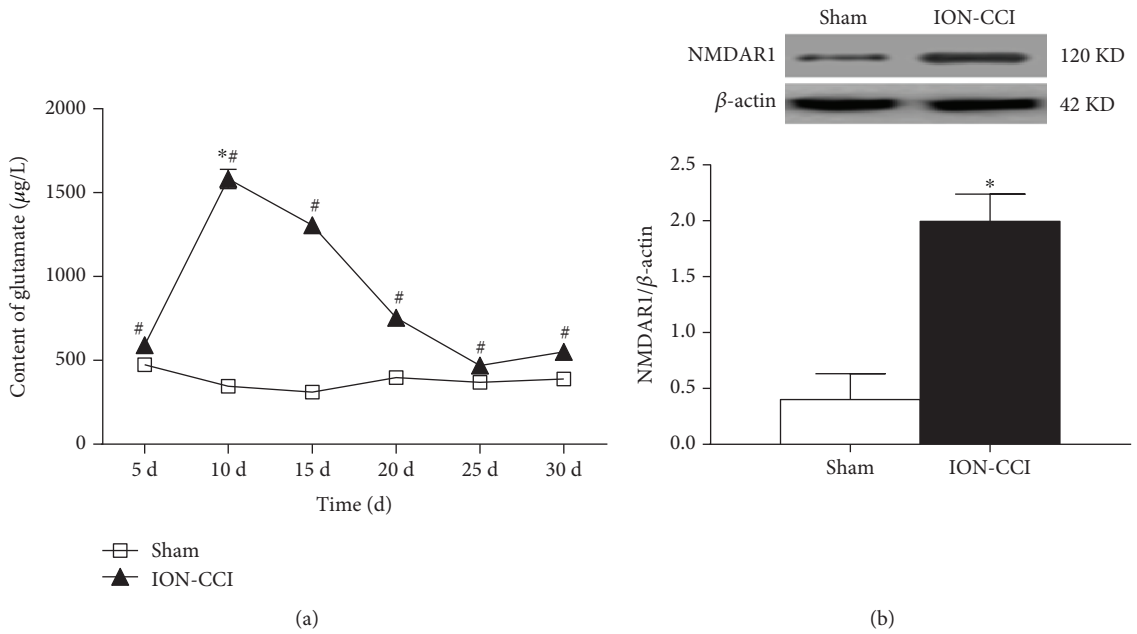

(a) (b)

Figure 4: Effects of ION-CCI on glutamate release and glutamate receptor expression in the RVLM. (a) Time course of content of glutamate in dialysis fluid from the RVLM in the ION-CCI group. $n = 4$/group. $^{*}p < 0.05$ compared with PO5, $^{\#}p < 0.05$ compared with sham. (b) NMDAR1 expression levels in the RVLM. $n = 5$/group. $^{*}p < 0.05$ compared with sham.

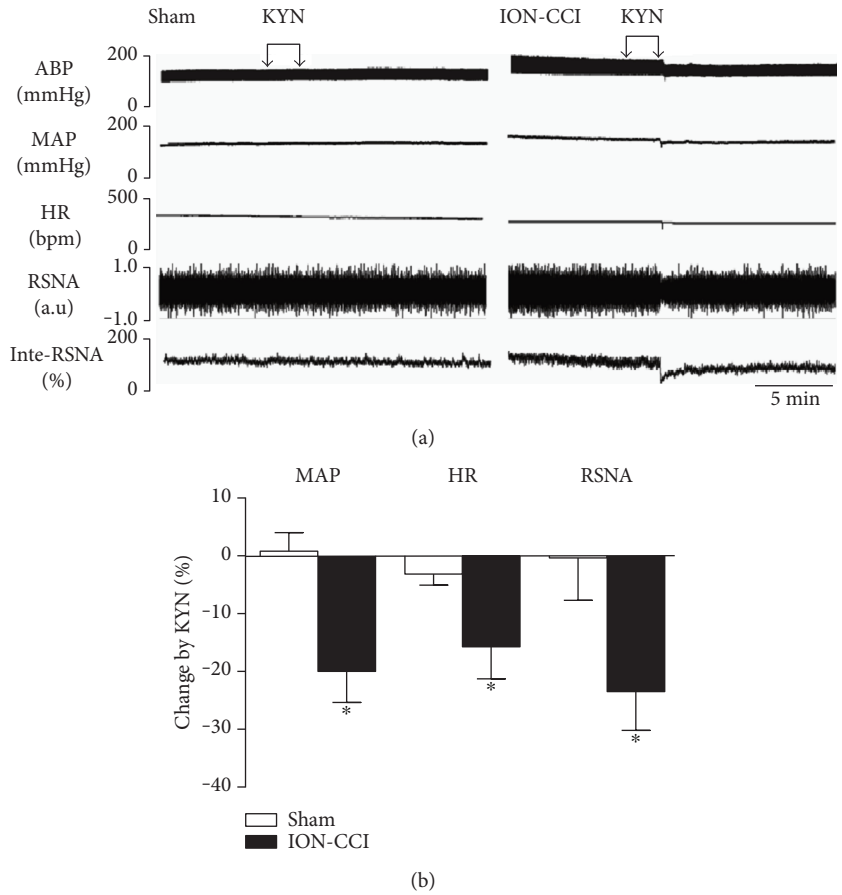

(a) (b)

Figure 5: Cardiovascular response to microinjection of KYN into the RVLM in the ION-CCI group. Representative tracings (a) and percent changes (b) of BP, HR, and RSNA in response to microinjection of KYN into the RVLM in the sham and ION-CCI groups. $n = 5$/group, $^{*}p < 0.05$ compared with sham.

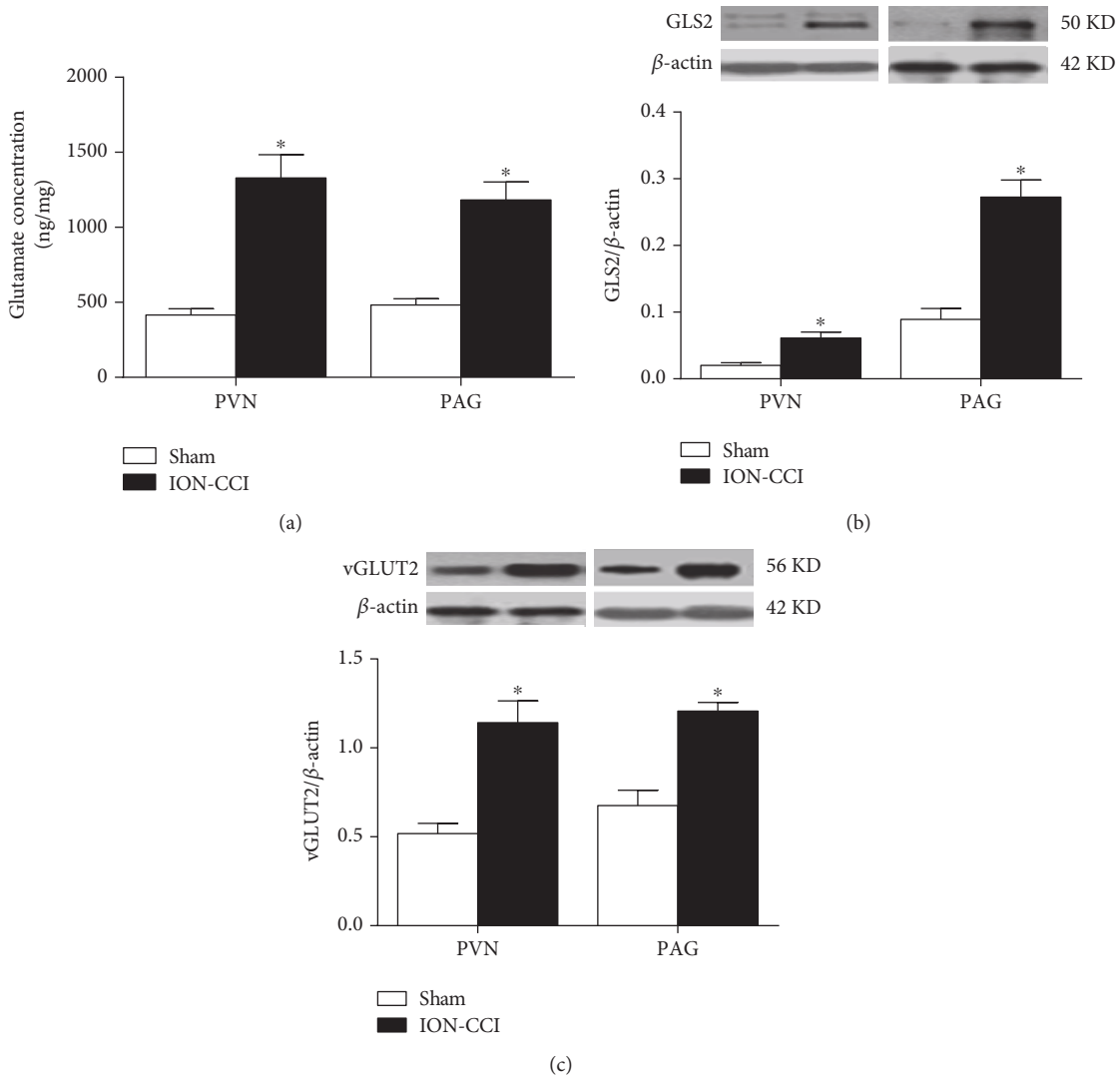

Figure 6: Effects of ION-CCI on the content of glutamate and the expression of vGLUT2 and GLS2 proteins in the PAG and PVN. (a) The concentration of glutamate and the protein levels of GLS2 and vGLUT2 in the PAG (a) and PVN (b), $n = 5$/group. $^*p < 0.05$ compared with sham.

In this study, VonFrey filaments were used to evaluate the CCI. It is confirmed that ION-CCI significantly decreases the mechanical pain threshold in the trigeminal nerve's innervating regions, which leads to neuropathic pain syndromes [31]. Additionally, we determined the mechanical pain threshold for 30 days and obtained the reduplicated value of the MAP in conscious rats, which was an abrupt increase of MAP 10 days after the ION-CCI surgery. These observations are similar to the previous evidence in sciatic nerve CCI, in which basal BP of the rats remains a high level during the first 2 weeks after the CCI [32]. It was also observed that the BP level measured by the femoral artery in anesthetized rats was significantly increased in the ION-CCI rats. We found that the level of BP measured by the tail-cuff method in awake rats was somewhat higher than the BP that was directly obtained from the femoral artery in anesthetized rats. This is possible that stress could result in a rise in BP. One of the most important mechanisms of hypertension is the overactivity of SNS. Partial nerve injury or tissue damage results in a change in peripheral nociceptors, which is associated with overactivity of the SNS [33]. In the present study, we measured the RSNA and 24 h urinary excretion of NE on PO10 and found that the RSNA and 24 h urinary excretion of NE were higher in the ION-CCI rats compared with the sham rats. These results indicate that the trigeminal neuropathic pain increases sympathetic nerve activity. Collectively, these data suggested that trigeminal neuropathic pain could substantially increase BP and sympathetic activity.

Pain, a type of noxious stimulation, has been demonstrated to result in an increase in the release of excitatory neurotransmitters (e.g., glutamate). Many studies have found that pain can lead to the increased release of glutamate in certain brain areas, such as the PAG [34], RVM [35], and insular cortex [21]. Our previous research [12, 27] has reported that tonically active glutamatergic input to the RVLM is significantly enhanced in SHRs and heart failure. In this study, we measured the glutamate concentration in the RVLM microdialysis samples over different time courses.

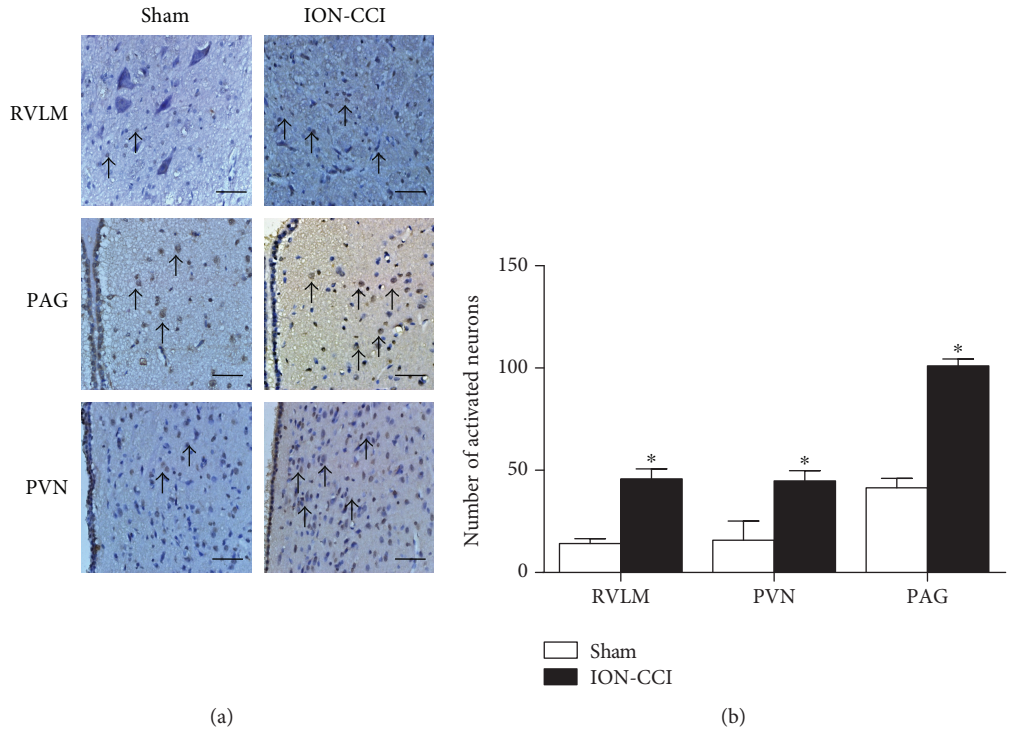

Figure 7: Effects of ION-CCI on the expressions of c-fos protein in the RVLM, PAG, and PVN. Immunostaining images (a) and group data (b) of fos-positive cells in the RVLM, PAG, and PVN in the sham and ION-CCI groups. The scale bar is 50 μm in (a). $n = 5$/group. $^*p < 0.05$ compared with sham.

The results indicate that the glutamate concentration in the ION-CCI group was obviously higher compared with the sham group. The glutamate concentration in the ION-CCI group reached a peak on PO10, which is consistent with change in BP. Furthermore, microinjection of the glutamate receptor antagonist KYN into the RVLM induced a significant reduction in BP, HR, and RSNA in the ION-CCI group but not in the sham rats. These data suggest that the trigeminal neuropathic pain enhances the tonically active glutamatergic inputs to the RVLM. It is suggested that KYN, a nonselective receptor antagonist, blocks both NMDA and AMPA receptors. NMDA and AMPA receptors are two subtypes of ionotropic glutamate receptors that play an important role in cardiovascular control and the occurrence of neuropathic pain [36, 37]. Our study focused on the presynaptic release of glutamate, which may activate both NMDA and AMPA receptors. So we selected KYN to block both NMDA and AMPA receptors. However, we do not exclude the possibility that NMDA and AMPA receptors may have different roles in mediating the effects of ION-CCI-induced release of glutamate. In addition, the present study was focused on the cardiovascular effects in response to neuropathic pain. KYN was injected acutely in the anesthetized state, and it may be difficult to measure the pain threshold again after injection. It is not clear whether blocking glutamatergic activity in RVLM is able to normalize the reduction of mechanical sensitivity (pain threshold).

Glutamate release is mainly dependent on synthesis of glutamate and nerve impulses in the presynaptic mechanism. The catalytic synthesis of glutamate-releasing glutaminase and neuronal excitability was subjected to determine the intensity level of glutamatergic input to the RVLM [38, 39]. It has been indicated that the glutamatergic inputs to the RVLM originate from various areas, such as the PAG and PVN [40, 41]. Functional changes in these areas have a direct effect on the RVLM sympathetic output and its control of cardiovascular function. The RVLM has some connections with the PAG and PVN, which has an effect on the regulation of cardiovascular activity [34, 42–44]. In this study, we found that the glutamate content in the PAG and PVN was also increased in the trigeminal neuropathic pain rats. Furthermore, we observed that trigeminal neuropathic pain led to a significant augmentation in the expression of GLS2, a key enzyme for glutamate synthesis, in the PAG and PVN. The protein level of vGLUT2, which can package the glutamate into presynaptic vesicles so that these vesicles can be released into the synapse, was also increased in the trigeminal neuropathic pain rats. A previous study from our laboratory suggested that exercise training resulted in a significant decrease in the expression level of GLS2 in the PVN of SHR [12]. Glutamatergic inputs to the RVLM may originate from multiple sources, including the above-mentioned regions within the brainstem and forebrain. The key mechanism of enhanced tonic glutamatergic inputs to RVLM is presynaptic release of glutamate, which is based on neurotransmitter synthesis and nerve impulse. A limitation of this study is that we do not further determine the changes of afferent nerve impulses to the RVLM by electrophysiological approach.

The RVLM plays an important role in maintaining resting BP and sympathetic tone, and sympathetic nerve

activity is regulated by the activities of RVLM neurons. The c-Fos protein is a product of the c-fos gene, which is commonly used as a marker of changes in neuronal activity [45]. Pain can cause a strong enhancement of c-Fos expression in several brain regions [46]. The presented data revealed that trigeminal neuropathic pain provoked c-Fos expression in the RVLM of the ION-CCI rats, suggesting that trigeminal neuropathic pain is an inducer or stressor of RVLM neurons. Trigeminal neuropathic pain causes the excitation of RVLM neurons and leads to the excitation of sympathetic nerves. Furthermore, we also confirmed that c-Fos expression in the PVN and PAG was also increased in the ION-CCI rats. PVN and RVLM have many kinds of neurons, all of which can express c-fos. In this work, we did not identify neurons for c-fos expression, which is a limitation of our study. A significant change in cardiovascular activity in response to injection of RVLM KYN was confirmed, suggesting that the autonomic/presympathetic neurons in the RVLM are involved in the processing of ION-CCI. In addition, neuropathic pain is a kind of chronic noxious stimulation. It is suggested that many nuclei in the brain may be affected in response to neuropathic pain. We do not rule out the involvement of other regions such as cortex and hippocampus.

Our present study has demonstrated that trigeminal neuropathic pain increased BP and sympathetic outflow, which is associated with enhancement in tonically active glutamatergic inputs to the RVLM. This mechanism may contribute to autonomic regulation of cardiovascular activity under the state of neuropathic pain.

Conflicts of Interest

The authors declare that they have no conflicts of interest.

Authors' Contributions

Wei Wang, Zui Zou, and Xing Tan contributed equally to this work.

Acknowledgments

The authors gratefully acknowledge the statistical assistance of Dr Jian Lu (from the Department of Statistical Analysis, SMMU). This work was supported by the National Natural Science Foundation of China (nos. 81370363, 81570385, and 81630012 to Wei-Zhong Wang; 81372013 to Xue-Yin Shi), the SMMU Creativity and Innovation Training Program (2014QN02 to Ru-Wen Zhang), and the 12th Five-Year Plan of the People's Liberation Army Key Project Grant (BWS12J027 to Xue-Yin Shi).

References

[1] N. Attal, A. Masselin-Dubois, V. Martinez et al., "Does cognitive functioning predict chronic pain? Results from a prospective surgical cohort," *Brain*, vol. 137, pp. 904–917, 2014.

[2] N. Attal, M. Lanteri-Minet, B. Laurent, J. Fermanian, and D. Bouhassira, "The specific disease burden of neuropathic pain: results of a French nationwide survey," *Pain*, vol. 152, no. 12, pp. 2836–2843, 2011.

[3] S. Bruehl, O. Y. Chung, J. N. Jirjis, and S. Biridepalli, "Prevalence of clinical hypertension in patients with chronic pain compared to nonpain general medical patients," *The Clinical Journal of Pain*, vol. 21, no. 2, pp. 147–153, 2005.

[4] R. B. Olsen, S. Bruehl, C. S. Nielsen, L. A. Rosseland, A. E. Eggen, and A. Stubhaug, "Hypertension prevalence and diminished blood pressure-related hypoalgesia in individuals reporting chronic pain in a general population. The Tromsø Study," *Pain*, vol. 154, no. 2, pp. 257–262, 2012.

[5] S.-L. Pan, L.-S. Chen, M.-F. Yen, Y.-H. Chiu, and H.-H. Chen, "Increased risk of stroke after trigeminal neuralgia—a population-based follow-up study," *Cephalalgia*, vol. 31, no. 8, pp. 937–942, 2011.

[6] N. J. Goodson, B. H. Smith, L. J. Hocking et al., "Cardiovascular risk factors associated with the metabolic syndrome are more prevalent in people reporting chronic pain: results from a cross-sectional general population study," *Pain*, vol. 154, no. 9, pp. 1595–1602, 2013.

[7] A. Teruel, S. Ram, S. K. Kumar, S. Hariri, and G. T. Clark, "Prevalence of hypertension in patients with trigeminal neuralgia," *Journal of Headache and Pain*, vol. 10, no. 3, pp. 199–201, 2009.

[8] S. C. Malpas, "Sympathetic nervous system overactivity and its role in the development of cardiovascular disease," *Physiological Reviews*, vol. 90, no. 2, pp. 513–557, 2010.

[9] P. G. Guyenet, "The sympathetic control of blood pressure," *Nature Reviews Neuroscience*, vol. 7, no. 5, pp. 335–346, 2006.

[10] T. Schlereth and F. Birklein, "The sympathetic nervous system and pain," *Neuromolecular Medicine*, vol. 10, no. 3, pp. 141–147, 2008.

[11] A. F. Sved, S. Ito, and J. C. Sved, "Brainstem mechanisms of hypertension: role of the rostral ventrolateral medulla," *Current Hypertension Reports*, vol. 5, no. 3, pp. 262–268, 2003.

[12] J.-Y. Jung, H.-R. Yang, Y.-J. Jeong et al., "Effects of acupuncture on c-Fos expression in brain after noxious tooth stimulation of the rat," *The American Journal of Chinese Medicine*, vol. 34, no. 06, pp. 989–1003, 2006.

[13] Z. Yang, D. Bertram, and J. H. Coote, "The role of glutamate and vasopressin in the excitation of RVL neurones by paraventricular neurones," *Brain Research*, vol. 908, no. 1, pp. 99–103, 2001.

[14] M. K. Sun and D. J. Reis, "NMDA receptor-mediated sympathetic chemoreflex excitation of RVL-spinal vasomotor neurones in rats," *Journal of Physiology*, vol. 482, Part 1, pp. 53–68, 1995.

[15] Y. P. Zha, Y. K. Wang, Y. Deng et al., "Exercise training lowers the enhanced tonically active glutamatergic input to the rostral ventrolateral medulla in hypertensive rats," *CNS Neuroscience & Therapeutics*, vol. 19, no. 4, pp. 244–251, 2013.

[16] Y. K. Wang, D. Shen, Q. Hao et al., "Overexpression of angiotensin-converting enzyme 2 attenuates tonically active glutamatergic input to the rostral ventrolateral medulla in hypertensive rats," *American Journal of Physiology-Heart and Circulatory Physiology*, vol. 307, no. 2, pp. H182–H190, 2014.

[17] T. Kubo, M. Kihara, and Y. Misu, "Genetically altered brain amino acid metabolism in spontaneously hypertensive rats: a study by using young spontaneously hypertensive rats and renal hypertensive rats," *Clinical and Experimental Hypertension*, vol. 12, no. 7, pp. 1191–1201, 1990.

[18] S. Ito, K. Komatsu, K. Tsukamoto, and A. F. Sved, "Excitatory amino acids in the rostral ventrolateral medulla support blood pressure in spontaneously hypertensive rats," *Hypertension*, vol. 35, no. 1, Part 2, pp. 413–417, 2000.

[19] S. Ito, K. Komatsu, K. Tsukamoto, and A. F. Sved, "Tonic excitatory input to the rostral ventrolateral medulla in Dahl salt-sensitive rats," *Hypertension*, vol. 37, no. 2, Part 2, pp. 687–691, 2001.

[20] W. Z. Wang, L. Gao, H. J. Wang, I. H. Zucker, and W. Wang, "Tonic glutamatergic input in the rostral ventrolateral medulla is increased in rats with chronic heart failure," *Hypertension*, vol. 53, no. 2, pp. 370–374, 2009.

[21] S. Qiu, T. Chen, K. Koga et al., "An increase in synaptic NMDA receptors in the insular cortex contributes to neuropathic pain," *Science Signaling*, vol. 6, no. 275, article ra34, 2013.

[22] L. F. Da Silva, J. M. Desantana, and K. A. Sluka, "Activation of NMDA receptors in the brainstem, rostral ventromedial medulla, and nucleus reticularis gigantocellularis mediates mechanical hyperalgesia produced by repeated intramuscular injections of acidic saline in rats," *The Journal of Pain*, vol. 11, no. 4, pp. 378–387, 2010.

[23] R. Radhakrishnan and K. A. Sluka, "Increased glutamate and decreased glycine release in the rostral ventromedial medulla during induction of a pre-clinical model of chronic widespread muscle pain," *Neuroscience Letters*, vol. 457, no. 3, pp. 141–145, 2009.

[24] M. Kernisant, R. W. Gear, L. Jasmin, J.-P. Vit, and P. T. Ohara, "Chronic constriction injury of the infraorbital nerve in the rat using modified syringe needle," *Journal of Neuroscience Methods*, vol. 172, no. 1, pp. 43–47, 2008.

[25] M. Cha, K. J. Kohan, X. Zuo, J. X. Ling, and J. G. Gu, "Assessment of chronic trigeminal neuropathic pain by the orofacial operant test in rats," *Behavioural Brain Research*, vol. 234, no. 1, pp. 82–90, 2012.

[26] J. Peng, Y.-K. Wang, L.-G. Wang et al., "Sympathoinhibitory mechanism of moxonidine: role of the inducible nitric oxide synthase in the rostral ventrolateral medulla," *Cardiovascular Research*, vol. 84, no. 2, pp. 283–291, 2009.

[27] Y. K. Wang, Q. Yu, X. Tan et al., "Centrally acting drug moxonidine decreases reactive oxygen species via inactivation of the phosphoinositide-3 kinase signaling in the rostral ventrolateral medulla in hypertensive rats," *Journal of Hypertension*, vol. 34, no. 5, pp. 993–1004, 2016.

[28] J. F. Peng, Z. T. Wu, Y. K. Wang et al., "GABAergic mechanism in the rostral ventrolateral medulla contributes to the hypotension of moxonidine," *Cardiovascular Research*, vol. 89, no. 2, pp. 473–483, 2010.

[29] G. Paxinos and C. Watson, *The Rat Brain in Stereotaxic Coordinates*, Academic, New York, 3rd edition, 1998.

[30] J. W. Maniscalco, H. Zheng, P. J. Gordon, and L. Rinaman, "Negative energy balance blocks neural and behavioral responses to acute stress by "silencing" Central glucagon-like peptide 1 signaling in rats," *Journal of Neuroscience*, vol. 35, no. 30, pp. 10701–10714, 2015.

[31] J. Gutierrez, S. Raju, J. P. Riley, and N. M. Boulis, "Introduction to neuropathic pain syndromes," *Neurosurgery Clinics of North America*, vol. 25, no. 4, pp. 639–662, 2014.

[32] Y. Jin, J. Sato, M. Yamazaki et al., "Changes in cardiovascular parameters and plasma norepinephrine level in rats after chronic constriction injury on the sciatic nerve," *Pain*, vol. 135, no. 3, pp. 221–231, 2008.

[33] T. Kawada, T. Akiyama, S. Shimizu et al., "Acute effects of arterial baroreflex on sympathetic nerve activity and plasma norepinephrine concentration," *Autonomic Neuroscience-Basic & Clinical*, vol. 186, pp. 62–68, 2014.

[34] M. Rodríguez-Muñoz, P. Sánchez-Blázquez, A. Vicente-Sánchez, E. Berrocoso, and J. Garzón, "The mu-opioid receptor and the NMDA receptor associate in PAG neurons: implications in pain control," *Neuropsychopharmacology*, vol. 37, no. 2, pp. 338–349, 2011.

[35] L. F. S. D. Silva, R. Y. Walder, B. L. Davidson, S. P. Wilson, and K. A. Sluka, "Changes in expression of NMDA-NR1 receptor subunits in the rostral ventromedial medulla modulate pain behaviors," *Pain*, vol. 151, no. 1, pp. 155–161, 2010.

[36] S. Y. Chen, W. C. Wu, C. J. Tseng, J. S. Kuo, and C. Y. Chai, "Involvement of non-NMDA and NMDA receptors in glutamate-induced pressor or depressor responses of the pons and medulla," *Clinical & Experimental Pharmacology & Physiology*, vol. 24, no. 1, pp. 46–56, 1997.

[37] E. Kondo, K. Iwata, A. Ogawa et al., "Involvement of glutamate receptors on hyperexcitability of wide dynamic range neurons in the gracile nucleus of the rats with experimental mononeuropathy," *Pain*, vol. 95, no. 1, pp. 153–163, 2002.

[38] A. F. Sved, "Tonic glutamatergic drive of RVLM vasomotor neurons?," *American Journal of Physiology-Regulatory Integrative and Comparative Physiology*, vol. 287, no. 6, pp. R1301–R1303, 2004.

[39] D. Soto, X. Altafaj, C. Sindreu, and A. Bayes, "Glutamate receptor mutations in psychiatric and neurodevelopmental disorders," *Communicative & Integrative Biology journal*, vol. 7, no. 1, article e27887, 2014.

[40] H. Ferreira-Neto, S. Yao, and V. Antunes, "Purinergic and glutamatergic interactions in the hypothalamic paraventricular nucleus modulate sympathetic outflow," *Purinergic Signalling*, vol. 9, no. 3, pp. 337–349, 2013.

[41] G. G. Pelosi, C. Busnardo, R. F. Tavares, and F. M. A. Corrêa, "Cardiovascular responses to glutamate microinjection in the dorsomedial periaqueductal gray of unanesthetized rats," *Journal of Neuroscience Research*, vol. 90, no. 11, pp. 2193–2200, 2012.

[42] S. Delatorre, G. Rojas-Piloni, G. Martinez-Lorenzana, J. Rodriguez-Jimenez, L. Villanueva, and M. Condes-Lara, "Paraventricular oxytocinergic hypothalamic prevention or interruption of long-term potentiation in dorsal horn nociceptive neurons: electrophysiological and behavioral evidence," *Pain*, vol. 144, no. 3, pp. 320–328, 2009.

[43] M. Condes-Lara, G. Rojas-Piloni, G. Martinez-Lorenzana, J. Rodriguez-Jimenez, M. Lopez Hidalgo, and M. J. Freund-Mercier, "Paraventricular hypothalamic influences on spinal nociceptive processing," *Brain Research*, vol. 1081, no. 1, pp. 126–137, 2006.

[44] J. Hu, Z. Wang, Y. Y. Guo et al., "A role of periaqueductal grey NR2B-containing NMDA receptor in mediating persistent inflammatory pain," *Molecular Pain*, vol. 5, pp. 71–81, 2009.

[45] J. A. Harris, "Using c-fos as a neural marker of pain," *Brain Research Bulletin*, vol. 45, no. 1, pp. 1–8, 1998.

[46] M. Lehner, E. Taracha, A. Skorzewska et al., "Sensitivity to pain and c-Fos expression in brain structures in rats," *Neuroscience Letters*, vol. 370, no. 1, pp. 74–79, 2004.

Hindawi
Neural Plasticity
Volume 2017, Article ID 9182748, 12 pages
https://doi.org/10.1155/2017/9182748

Research Article

Effects of Propofol Treatment in Neural Progenitors Derived from Human-Induced Pluripotent Stem Cells

Bo Long,[1,2,3] Shenglan Li,[1,3] Haipeng Xue,[1,3] Li Sun,[1,3,4] Dong H. Kim,[1,3] and Ying Liu[1,3,5]

[1]*Vivian L. Smith Department of Neurosurgery, McGovern Medical School, The University of Texas Health Science Center at Houston, Houston, TX, USA*
[2]*Department of Anesthesiology, Shengjing Hospital, China Medical University, Shenyang, China*
[3]*Center for Stem Cell and Regenerative Medicine, The University of Texas Health Science Center at Houston, Houston, TX, USA*
[4]*Department of Oncology, Renji Hospital, Shanghai Jiao Tong University School of Medicine, Shanghai, China*
[5]*Senator Lloyd and B.A. Bentsen Center for Stroke Research, The Brown Foundation Institute of Molecular Medicine, The University of Texas Health Science Center at Houston, Houston, TX, USA*

Correspondence should be addressed to Bo Long; longb@sj-hospital.org and Ying Liu; ying.liu@uth.tmc.edu

Received 6 June 2017; Revised 21 July 2017; Accepted 3 August 2017; Published 8 October 2017

Academic Editor: Yulong Li

Propofol is an intravenous anesthetic that has been widely used in clinics. Besides its anesthetic effects, propofol has also been reported to influence the regulation of the autonomic system. Controversies exist with regard to whether propofol exposure is safe for pregnant women and young children. In this work, human-induced pluripotent stem cell- (hiPSC-) derived neural progenitor cells (NPCs) were treated with propofol at 20, 50, 100, or 300 μM for 6 h or 24 h, and acute and subacute cell injury, cell proliferation, and apoptosis were evaluated. Comparison of genome-wide gene expression profiles was performed for treated and control iPSC-NPCs. Propofol treatment for 6 h at the clinically relevant concentration (20 or 50 μM) did not affect cell viability, apoptosis, or proliferation, while propofol at higher concentration (100 or 300 μM) decreased NPC viability and induced apoptosis. In addition, 20 μM propofol treatment for 6 h did not alter global gene expression. In summary, propofol treatment at commonly practiced clinical doses for 6 h did not have adverse effects on hiPSC-derived NPCs. In contrast, longer exposure and/or higher concentration could decrease NPC viability and induce apoptosis.

1. Introduction

Propofol (2,6-diisopropylphenol) is an anesthetic agent for induction and intravenous maintenance of anesthesia during surgery. It has also been used as a sedative agent in ICUs for diagnostic imaging tests such as MRIs and endoscopies. Besides its anesthetic effects, propofol has been reported to influence the regulation of the autonomic system [1–3]. Interestingly, although it has been widely used off-label for anesthesia maintenance in toddlers and pregnant women, propofol has not been approved by the FDA in either target population, probably partly due to safety concerns on the developing central nervous system [4, 5]. Some reports have linked general anesthetic use in rodent and nonhuman primate babies with induced widespread neuronal degeneration and/or apoptosis followed by long-term memory and learning deficiency in adults [6–14], while other reports have suggested that no such association exists [15]. These controversies could partly stem from the lack of recapitulative models that truly reflect the response of human brain cells to the treatment of general anesthetics agents including propofol.

Human neural progenitor cells (NPCs) have the potential to serve as an ideal in vitro system to evaluate the effect of propofol among other anesthetics agents [16–18]. However, human NPCs are usually derived from fetal brains, which are extremely difficult to obtain. In addition, human fetal brain-derived cells pose ethical concerns as well as exhibit interindividual variability due to the diverse genetic background of the sources and the age of the fetuses at the time

of cell derivation. Human-induced pluripotent stem cells (hiPSCs) have recently emerged as a promising and convenient cell source for obtaining pure NPCs. hiPSCs are reprogrammed from somatic cells such as dermal fibroblasts with a cocktail of transcription factors, OCT4, SOX2, KLF4, and C-MYC [19, 20]. iPSCs can then be induced toward the neural lineage to give rise to NPCs and mature neural cells including neuron subtypes and glia. The use of NPCs derived from human iPSCs could theoretically provide a stable and inexhaustible cell source for in vitro testing of anesthetics. The NPCs have also become a platform for personalized medicine which could help determine the effects of certain anesthetics precisely for each and every individual patient tested.

In the current work, we attempted to examine whether propofol was toxic to hiPSC-derived NPCs. We found that propofol treatment at commonly practiced clinical doses for 6 h did not have adverse effects on hiPSC-derived NPCs. By a genome-wide gene expression analysis, we proposed several pathways that may be involved in the cytotoxicity of propofol at higher concentrations on multiple human NPC cell lines derived from iPSCs.

2. Materials and Methods

2.1. Cell Culture. Three hiPSC lines were used in this work. NESTIN-GFP knockin reporter (NES-GFP) and ND2-0 hiPSC were obtained from the NIH Center for Regenerative Medicine. hiPSC line USCK7 was generated in-house from human urine-derived cells by Cytotune (Life Technologies) reprogramming kit [21]. All hiPSCs were cultured on Matrigel-coated dishes in TeSR-E8 medium (Stemcell Technologies).

2.2. Generation of NPCs. NPCs were differentiated from hiPSCs following a modified dual SMAD inhibition method [22]. Briefly, hiPSCs were digested into small clumps using 0.5 mM EDTA, transferred to 10 cm Petri dishes and suspended in medium containing DMEM : F12, 20% knockout serum replacement, 1% nonessential amino acids (NEAA), 1% GlutaMAX, and 55 μM 2-mercaptoethanol, supplemented with 10 μM SB-431542 and 1 μM dorsomorphin (Tocris). The medium was replaced on day 2 with neural induction (ND) medium containing DMEM : F12, 1% NEAA, 1% GlutaMAX, 1 mg/ml heparin, 1% N2, 1% B27, and 1% antibiotic-antimycotic solution, supplemented with 10 μM SB-431542 and 1 μM dorsomorphin. On day 6, the embryoid bodies were transferred to Matrigel-coated dishes and cultured in ND medium with 20 ng/ml basic fibroblast growth factor (bFGF). Within 3-4 days, typical neural rosettes were manually isolated under a dissection microscope and then treated with Accutase to form uniform NPCs. The NPCs were cultured and expanded in ND medium and passaged every 4-5 days with Accutase.

2.3. Propofol Treatment. Propofol (Sigma) was diluted with dimethyl sulfoxide (DMSO) to make a 500 mM stock solution. NPCs were treated at different concentrations (20, 50, 100, and 300 μM) for 6 or 24 h.

2.4. MTT Assay. To detect early cell damage, MTT assay was performed according to manufacturer's instructions (Life Technologies). Briefly, NPCs were seeded on 96-well plates (3000 cells/well) and grown overnight. Cells were treated with propofol for 6 or 24 h, or 6 h followed by a 20 h washout period. MTT was added to the medium and the reaction was incubated at 37°C for 4 h. The MTT formazan product was then dissolved in DMSO and quantified spectrophotometrically at 540 nm.

2.5. Lactate Dehydrogenase (LDH) Assay. To detect late-stage cell damage, LDH assay was performed using LDH cytotoxicity assay kit (Thermo Scientific). Briefly, NPCs were seeded on 96-well plates and were treated with propofol (20, 50, 100, and 300 μM) for 6 h. Fifty μl of culture supernatant was harvested, mixed with equal volume of reaction mixture, and incubated at room temperature for 30 min. All samples were quantified spectrophotometrically at 490 nm and 680 nm.

2.6. Immunocytochemistry. Immunocytochemistry was performed as previously described [23]. Briefly, cells grown on glass coverslips were fixed with 4% paraformaldehyde and incubated in blocking buffer containing 5% goat serum, 1% bovine serum albumin, and 0.1% Triton X-100 for 30 min. Cells were incubated in primary antibodies at 4°C overnight. Appropriate Alexa Fluor secondary antibodies were used. Primary antibodies include Nestin (1 : 200, R&D systems), Sox1 (1 : 250, Millipore), and Ki-67 (1 : 500, Abcam). Nuclei were identified with DAPI (Sigma). Images were captured using a Zeiss AxioVision microscope with a z-stack split view function. For quantification of Ki-67+ cells, at least 1000 cells were counted for each staining.

2.7. Quantification of Apoptotic Cells. After propofol treatment, NPCs were labelled with the Annexin V-FITC apoptosis detection kit (BD) following manufacturer's instructions. Propofol-treated NPCs were suspended in Annexin V binding buffer at a concentration of 1×10^6 cells/ml. Cell suspension (100 μl) was mixed with 5 μl of Annexin V-FITC and was incubated at room temperature for 15 min protected from light. Reaction was stopped with 400 μl of Annexin V binding buffer. Dead cells were labelled with DAPI. The apoptosis ratio was measured by flow cytometry.

2.8. Microarray and DEG Analysis. Total RNA was isolated with RNAeasy mini kit (Qiagen) and run on HumanHT-12 v4 expression BeadChip kit (Illumina). BeadArray data was annotated with GenomeStudio. After variance-stabilizing transformation and normalization with the robust spline normalization method in the package lumi of *R*, differential analysis was performed using package limma for the following groups: (1) 20 μM versus untreated control; (2) 300 μM versus untreated. To screen for differentially expressed genes (DEGs), cut-off criteria were set as fold change (FC) > 2 (|Log FC| > 1) and $p < 0.05$. The expression value of DEGs from the 300 μM treatment group and untreated was hierarchically clustered by package pheatmap of *R*. Raw and normalized data was submitted to Gene Expression Omnibus (GEO) under the accession number GSE101724.

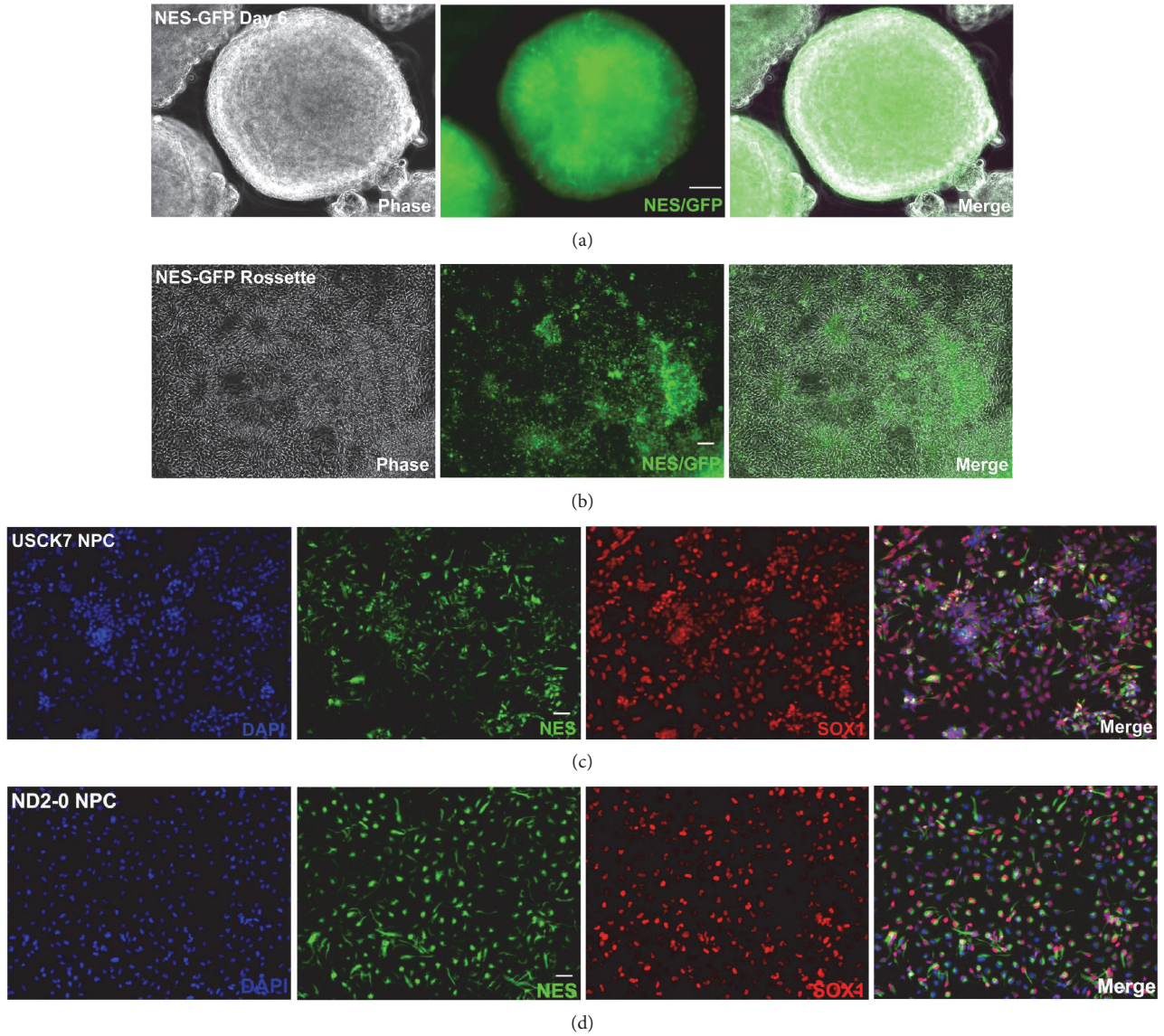

Figure 1: Generation of NPCs from hiPSCs. Representative images of neural tube structures generated from differentiating NES-GFP reporter hiPSC line via embryoid body formation method on day 6. GFP serves as a surrogate marker for NESTIN, a widely accepted NPC marker (a). The neural rosettes were attached to culture plates on day 10 as monolayer culture which continued to express GFP (NESTIN) (b). Similarly, NESTIN and another NPC marker SOX1 were both expressed robustly and uniformly in NPCs that were derived from two additional hiPSC lines, USCK7 (c) and ND2-0 (d), as revealed by immunocytochemistry staining of both NESTIN (green) and SOX1 (red). DAPI (blue) was used to reveal nuclei. Bar, 50 μm.

2.9. Functional Enrichment Analysis. Functional enrichment analysis of DEGs was performed with DAVID (Database for Annotation, Visualization and Integrated Discovery) to identify gene ontology (GO) categories in biological processes and KEGG (Kyoto Encyclopedia of Genes and Genomes) signaling pathways. The false discovery rate (FDR) < 0.05 was set as the cut-off criterion.

2.10. PPI Network Construction. The protein-protein interaction (PPI) of the DEGs was obtained using STRING (search tool for the retrieval of interacting genes, https://string-db.org/) and visualized by the Cytoscape 3 software (http://www.cytoscape.org/). Combined score > 0.4 was set as the cut-off criterion for PPI relationship. The connectivity degree of each node of the network was calculated. Molecular COmplex DEtection (MCODE) was then used to find clusters based on topology to locate densely connected regions.

2.11. qRT-PCR. Total RNAs were extracted using Quick-RNA MiniPrep Kit (Zymo Research). RNA was converted to cDNA using the iScript cDNA synthesis kit (Bio-Rad). qRT-PCR was performed to determine mRNA levels using the iQ SYBR green supermix (Bio-Rad). GAPDH was used as an internal control. The relative fold change in gene expression was evaluated using the comparative threshold cycle $\Delta\Delta$Ct method. The qRT-PCR primers are listed in Supplementary Table S2 available online at https://doi.org/10.1155/2017/9182748.

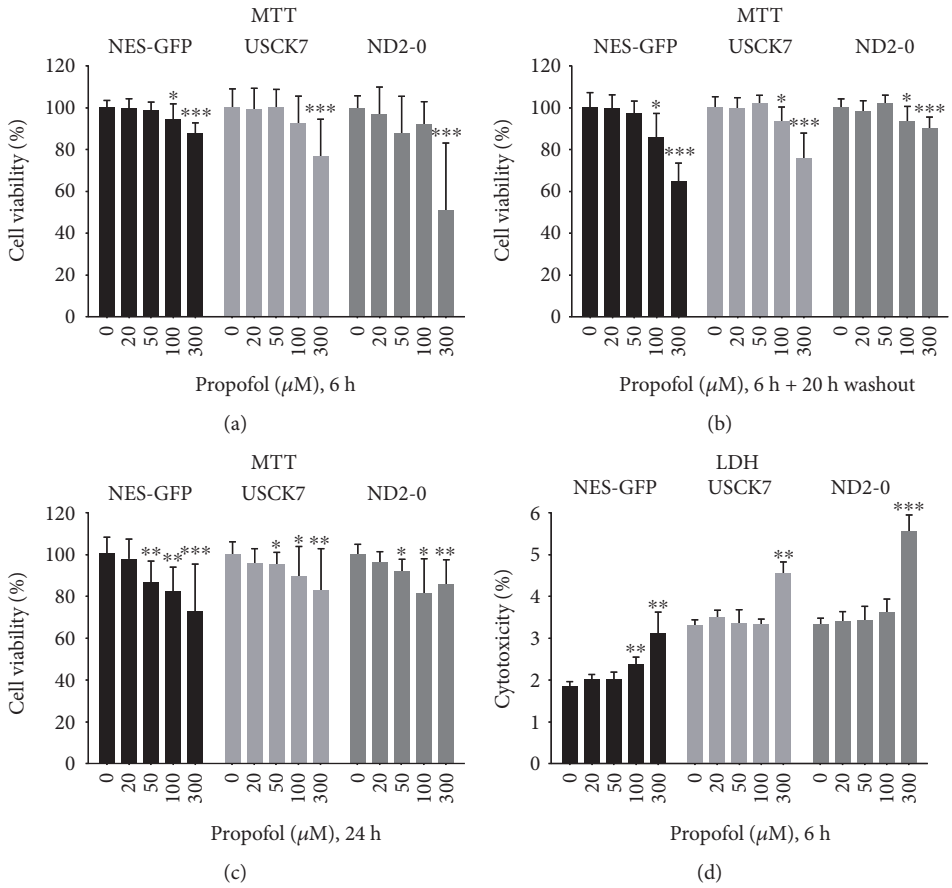

Figure 2: High-concentration propofol treatment exerts toxicity to NPCs. NPCs derived from three hiPSC lines were exposed to propofol at different concentrations (0, 20, 50, 100, and 300 μM). MTT assays showed high-concentration propofol-reduced NPCs viability after the 6 h (a) or 24 h (c) treatment, or 6 h treatment followed by 20 h washout (b). Data from LDH assays further showed that propofol at a high concentration reduced the number of NPCs (d). Data at each concentration were analyzed by unpaired *t*-tests. For MTT assays, data were expressed as a percentage of viable cells of the treatment compared to the untreated (0 μM propofol) group (mean ± SD). For LDH assays, data were expressed as a percentage of positive control (mean ± SD), compared to 0 μM propofol exposure group. For both assays, 5 wells per treatment condition were examined. Each experiment was repeated for at least three times. $^{*}p < 0.05$; $^{**}p < 0.01$; $^{***}p < 0.001$.

2.12. Statistical Analysis. All data were represented as mean ± SD. All assays were repeated at least three times and each experiment was performed in triplicate. Data were analyzed using Student's *t*-test, where two independent groups were compared. $p < 0.05$ was considered to be significant.

3. Results

3.1. Generation of NPCs from hiPSCs. The NPCs were generated with a modified dual SMAD inhibition method [22]. A good proportion of cells started to express Nestin as early as day 6 of differentiation, as indicated by GFP expression in the NES-GFP reporter (Figure 1(a)), and by NESTIN and SOX1 staining (Figures 1(c) and 1(d)). After manual isolation of neural rosettes (Figure 1(b)), pure NESTIN+/SOX1 + NPCs were obtained (Figures 1(c) and 1(d)).

3.2. Propofol Did Not Have Neurotoxicity to hiPSC-Derived NPCs at Clinically Relevant Concentrations. Previous reports indicated that the concentration of propofol in the brain during induction and maintenance of anesthesia is less than 10 μg/ml (50 μM) [24–26]. To determine the dosage of propofol treatment on NPCs, we chose 20, 50, 100, and 300 μM. NPCs treated with propofol at 20 or 50 μM for 6 h did not show any change in cell viability or late-stage cell injury as evaluated by MTT assay and LDH release (Figure 2), while NPCs treated with 300 μM propofol for 6 h showed significantly decreased cell viability ($p < 0.01$) and induced cytotoxicity in all three cell lines, especially in NPCs derived from ND2-0 hiPSC line (Figure 2). Although propofol at 20 or 50 μM did not show any toxicity at 6 h, after 24 h of treatment, the 50 μM group showed a decrease in NPC viability in all cell lines (Figure 2), indicating that sustained exposure of propofol could result in negative effects on cell viability.

3.3. Propofol Did Not Induce Apoptosis in Human NPCs. To investigate whether propofol could induce apoptosis in human NPCs, we treated NPCs with different concentrations of propofol for 6 h and quantified FITC-labeled Annexin V+

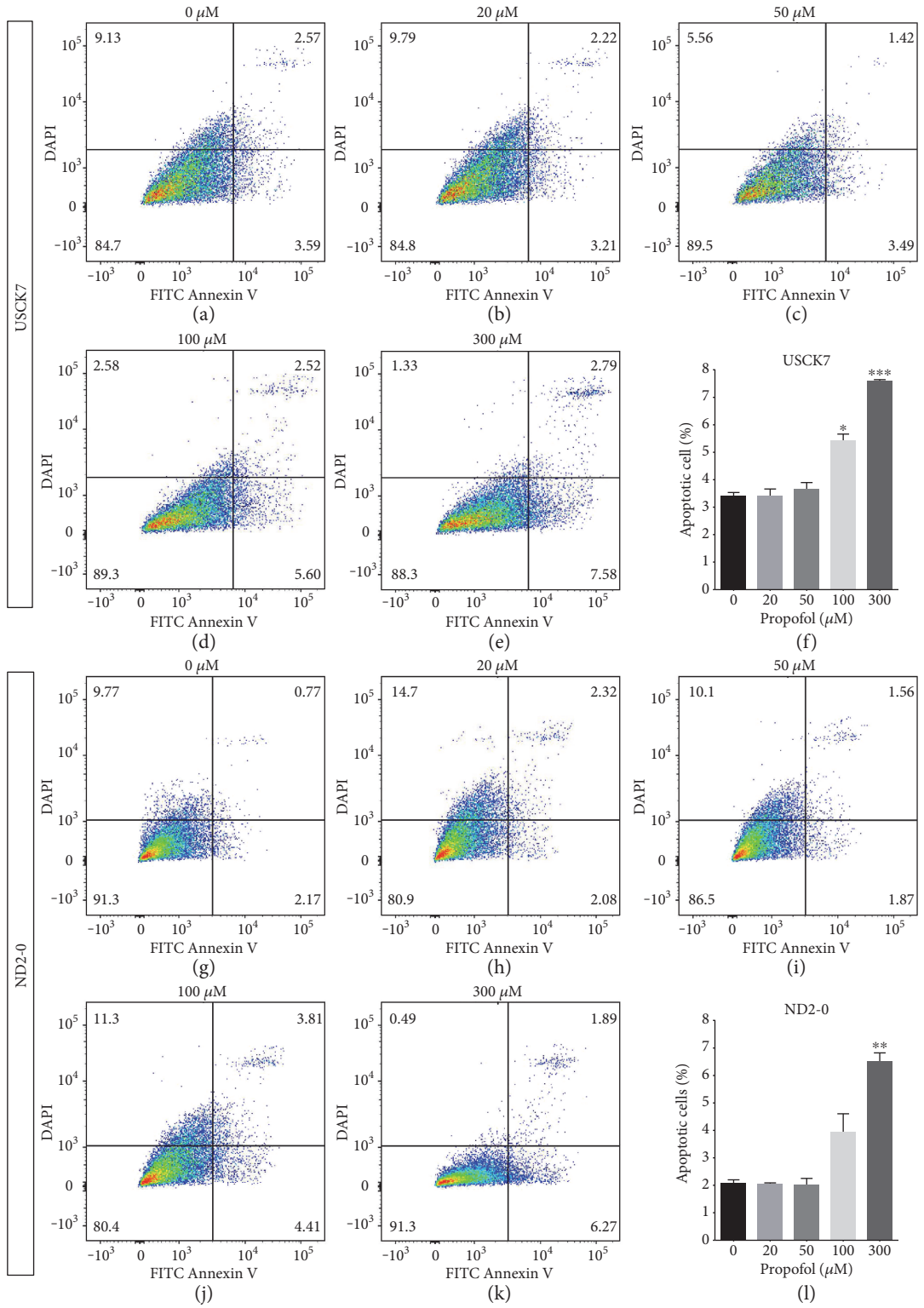

Figure 3: Propofol-induced apoptosis in NPCs. NPCs derived from USCK7 and ND2-0 were treated with propofol at 0, 20, 50, 100, and 300 μM for 6 h and apoptotic cells quantified by flow cytometry of FITC-labelled Annexin V. The percentage of different cell populations is shown in each of the four quadrants of the representative flow cytometry charts, and the statistical analyses are summarized in (USCK7) (f) and (ND2-0) (i). The percentage of apoptotic cells is shown at the left lower quadrant of each chart. For USCK7-NPCs, the 100 and 300 μM propofol treatment groups showed significantly higher percentage of apoptotic cells (a, b, c, d, e, f). For ND2-0 NPCs, only the 300 μM treatment group showed a significantly higher percentage of apoptotic cells (g, h, i, j, k, l). Data were expressed as a percentage of FITC+/DAPI− cells (mean ± SD) for $n = 3$ flow cytometry experiments per treatment condition. $^{*}p < 0.05$; $^{**}p < 0.01$; $^{***}p < 0.001$.

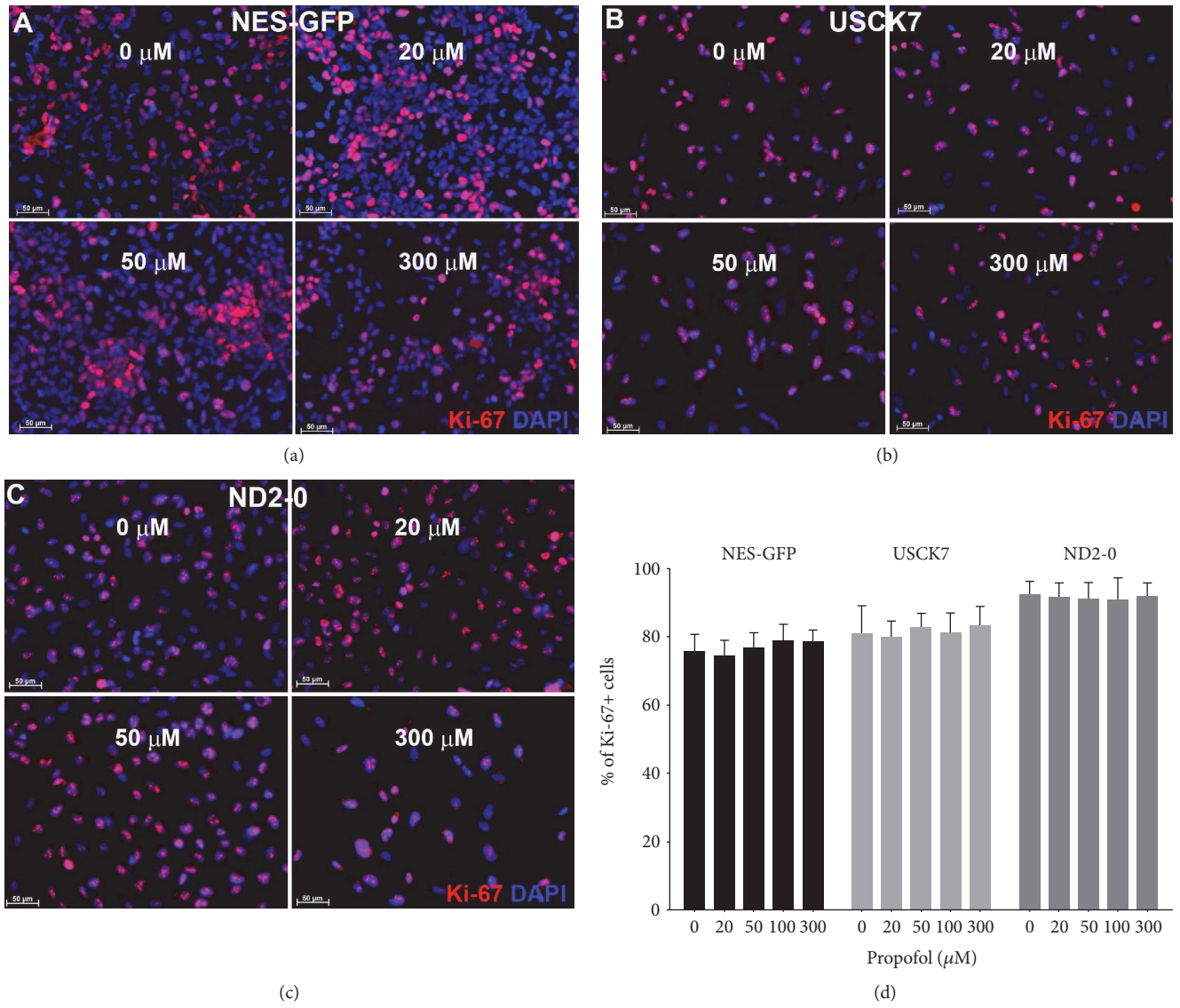

Figure 4: Propofol treatment for 6 h did not affect NPC proliferation. NPCs derived from three hiPSC lines were treated with propofol at different concentrations (0, 20, 50, 100, and 300 μM). Cell proliferation was assessed by Ki-67 (red) immunocytochemistry staining. Nuclei were revealed by DAPI (blue) (a, b, c). At least 1000 cells were counted for each experiment. Data were expressed as percentage of Ki-67+ cells (mean ± SD). $n = 3$ Ki-67 staining per treatment condition. Bar, 50 μm.

apoptotic cells by flow cytometry. Our results showed that exposure of NPCs to propofol at clinically relevant concentrations (20 or 50 μM) for 6 h did not cause apoptosis in USCK7 or ND2-0 NPCs (Figures 3(a), 3(b), 3(c), 3(f), 3(g), 3(h), 3(i), and 3(l)). However, the percentage of apoptotic cells in both cell lines increased significantly after treatment with 300 μM propofol (7.61 ± 0.03% versus 3.41 ± 0.1% in USCK7 and 6.5 ± 0.2% versus 2.1 ± 0.1% in ND2-0) (Figures 3(e), 3(f), 3(k), and 3(l)). The percentage of apoptotic cells also slightly increased in the 100 μM propofol treatment group in both cell lines, although statistical significance could be found in ND2-0 NPCs only (Figures 3(d), 3(f), 3(j), and 3(l)).

3.4. Propofol Treatment Did Not Affect NPC Proliferation. The percentage of Ki-67+ cells remained in the same range after treatment with different concentrations of propofol for 6 h in all three lines of NPCs (Figure 4).

3.5. Global Gene Expression Profiles of NPCs. Since propofol treatment at 300 μM for 6 h significantly decreased cell viability and increased cytotoxicity and apoptosis in NPCs, we further examined global gene expression profiles and signaling pathways potentially involved in the effects of propofol on NPCs. Twenty μM and 300 μM were chosen for further comparison and analysis. No differentially expressed genes (DEGs) that satisfy our cut-off criteria (FC > 2, $p < 0.05$) were found between the 20 μM and the untreated groups, indicating that propofol at 20 μM did not alter gene expression of NPCs, which was further confirmed by the heatmap generated by hierarchical clustering analysis (Figure 5(a)), in which duplicates of untreated (0 μM) and 20 μM groups

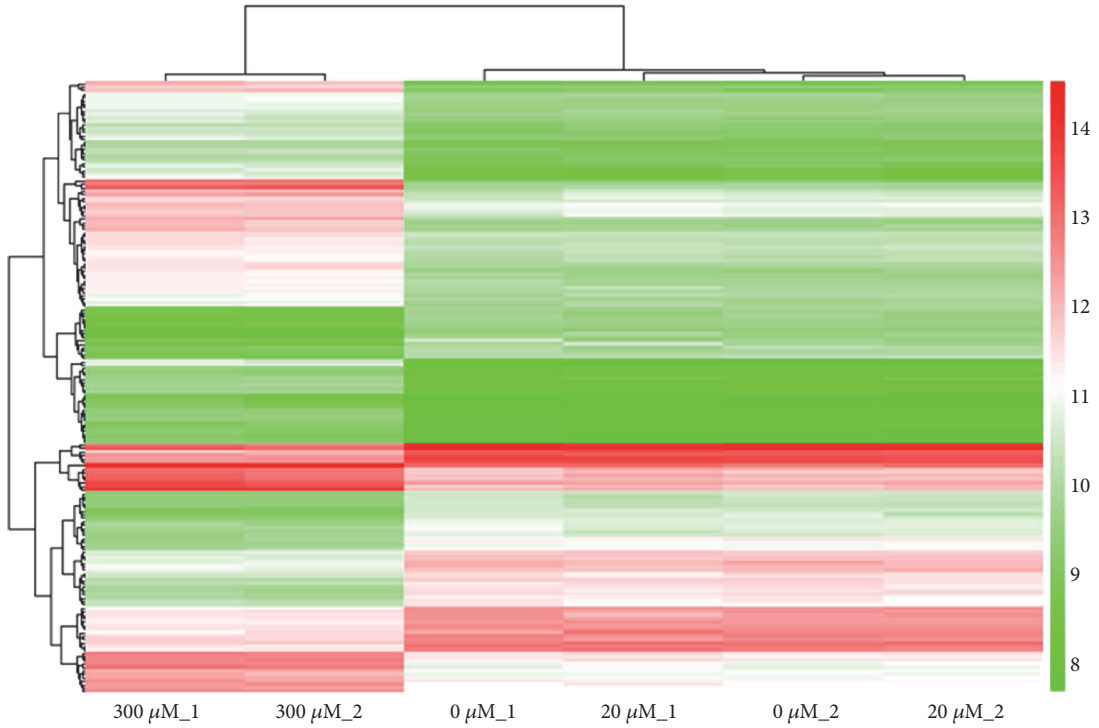

(a)

Top ten upregulated DEGs				Top ten downregulated DEGs			
Probe ID	Gene	logFC	adj.P.Val	Probe ID	Gene	logFC	adj.P.Val
ILMN_1787815	TRIB3	3.784048646	3.69E-07	ILMN_3209832	LOC100131801	−1.778332121	5.32E-05
ILMN_1693014	CEBPB	3.404448702	5.03E-06	ILMN_1720889	SC4MOL	−1.69535592	5.11E-05
ILMN_1703178	SCG2	3.284755302	2.96E-06	ILMN_1784641	NDUFA3	−1.682343183	3.48E-05
ILMN_1661599	DDIT4	3.046907659	2.96E-06	ILMN_3231944	LOC100130516	−1.639847181	0.0001887
ILMN_2188862	GDF15	2.920307983	1.74E-06	ILMN_1793474	INSIG1	−1.61482331	0.000163365
ILMN_1679041	SLC3A2	2.842323149	3.12E-06	ILMN_1657395	HMGCR	−1.607172444	7.31E-05
ILMN_1676984	DDIT3	2.465519383	8.34E-05	ILMN_1726603	ATP5I	−1.551925515	6.18E-06
ILMN_1757497	VGF	2.334556293	1.53E-05	ILMN_2078975	GRM3	−1.542667431	5.32E-05
ILMN_1656057	PLAU	2.243902072	1.53E-05	ILMN_1668629	LOC401115	−1.51042915	0.000173304
ILMN_1689004	TNFRSF12A	2.231613003	1.58E-05	ILMN_1732296	ID3	−1.496275357	5.09E-05

(b)

Figure 5: Gene expression profile of propofol-treated NPCs. NES-GFP iPSC-derived NPCs were treated with propofol (20 μM or 300 μM) for 6 h, and RNAs extracted immediately for Illumina BeadArray. Heatmap (a) of hierarchical clustering of differentially expressed genes (DEGs) shows that the 20 μM propofol-treated group clustered together with the untreated group, while the 300 μM propofol-treated group shows distinct gene expression profile. The top ten upregulated and downregulated DEGs are listed in (b).

clustered together with completely indistinguishable gene expression patterns. On the other hand, the 300 μM group showed a distinct gene expression pattern (Figure 5(a)) that clearly separated it from the untreated and the 20 μM cluster. Further analysis revealed a total of 176 DEGs between the 300 μM and the untreated control group, including 109 upregulated and 67 downregulated genes. The top 10 upregulated and downregulated DEGs are listed in Figure 5(b). Collectively, these analyses indicated that propofol at 20 μM, 6 h, does not interfere with the gene expression of human NPCs.

3.6. Functional Enrichment Analysis. To further dissect the molecular changes in gene expression that might be caused by the treatment of a high-concentration propofol (300 μM, 6 h), we performed functional annotation enrichment analysis of DEGs with bioinformatics tool DAVID (Database for Annotation, Visualization and Integrated Discovery, version

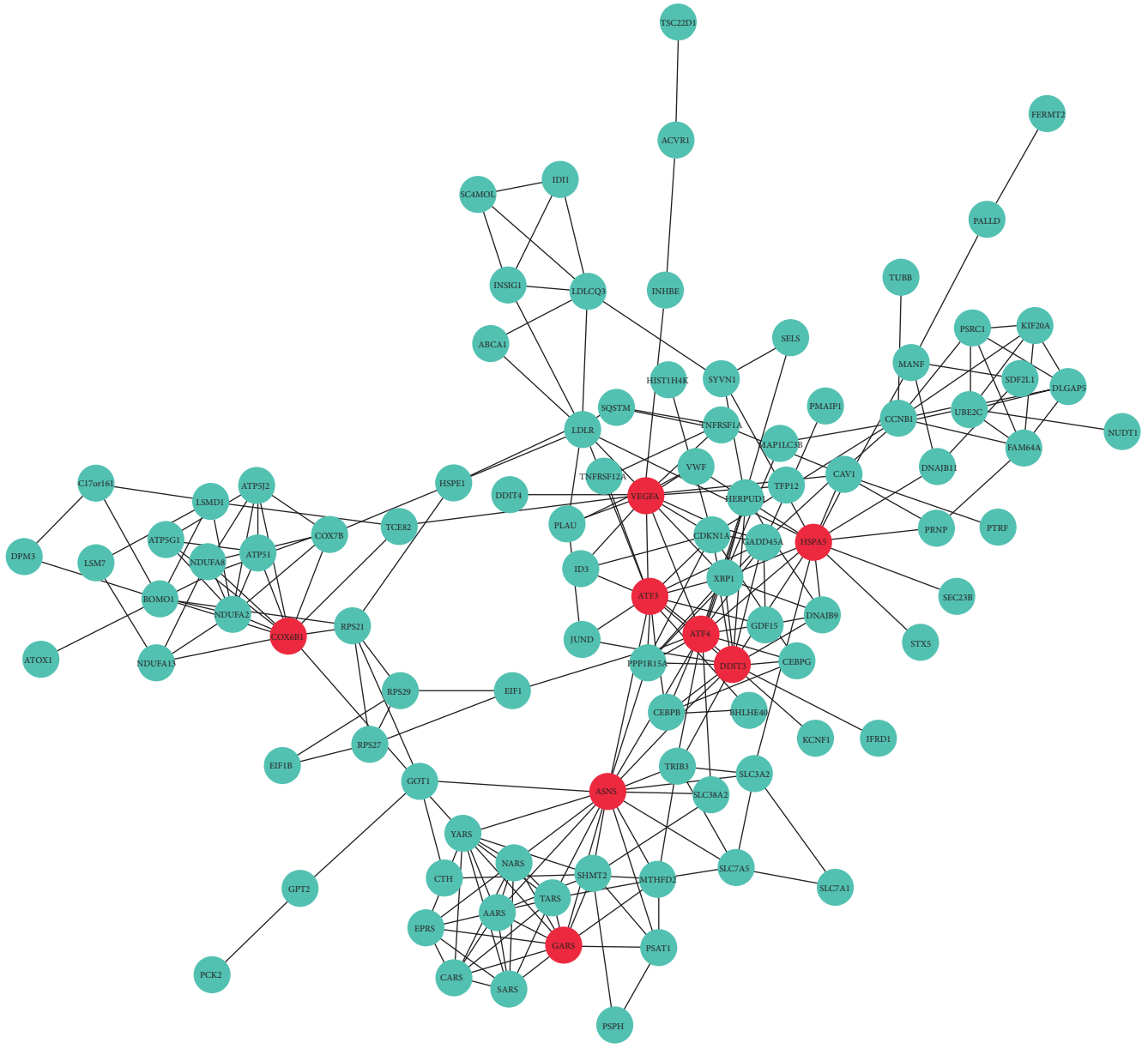

(a)

Gene symbol	Gene name	Degree
ASNS	Asparagine synthetase	17
ATF4	Activating transcription factor 4	17
HSPA5	Heat shock 70kDa protein 5	16
DDIT3	DNA-damage-inducible transcript 3	15
ATF3	Activating transcription factor 3	15
VEGFA	Vascular endothelial grownth factor A	15
GARS	Glycyl-tRNA synthetase	11
COX6B1	Cytochrome c oxidase subunit VIb polypeptide 1	11

(b)

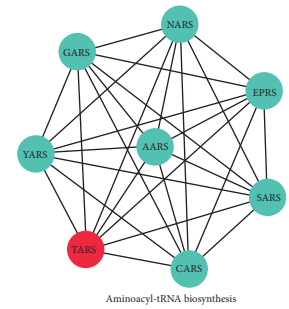

(c)

Figure 6: Continued.

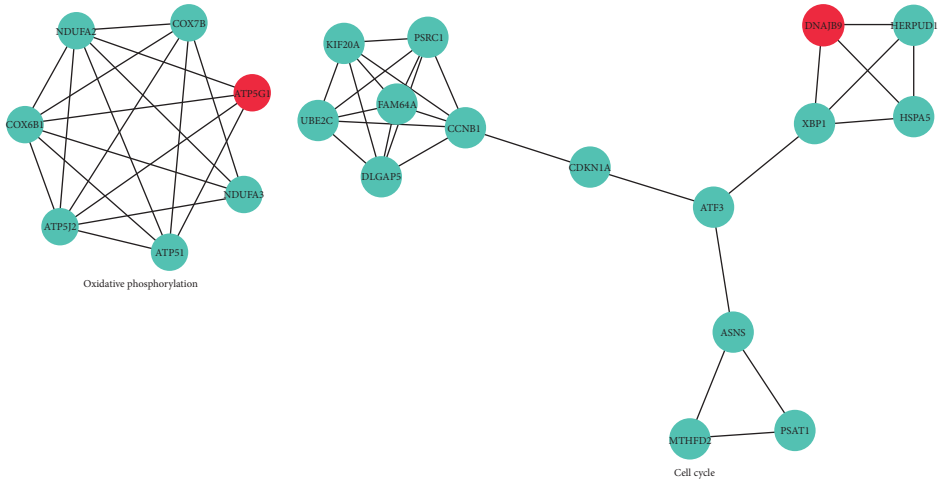

(d) (e)

Figure 6: PPI network construction of DEGs extracted from comparison of treated (300 μM) with untreated NPCs. The PPI relationships of the DEGs were obtained by using search tool for the retrieval of interacting genes (STRING) and visualized using the Cytoscape 3 software. After filtering out disconnected DEGs, a network with 101 nodes and 251 edges were obtained with the combined score > 0.4 (a). The connectivity degree of each node of the PPI network was calculated. Eight genes with connectivity degree > 10 were selected as hub genes (b). Clusters with densely connected regions based on topology were built with Molecular COmplex DEtection (MCODE). The top three subnetworks represent important cellular and molecular pathways including aminoacyl-tRNA biosynthesis (c), oxidative phosphorylation (d), and cell cycle (e).

6.8, https://david.ncifcrf.gov/) to identify Gene Ontology (GO) categories in biological processes and KEGG signaling pathways. The false discovery rate (FDR) < 0.05 was set as the cut-off criterion. Fourteen biological process (BP) terms and 5 molecular function (MF) terms were obtained from the upregulated DEGs, and 7 cellular component (CC) terms were found from the downregulated DEGs. One KEGG pathway was identified from the upregulated DEGs and the 1 KEGG pathway was found from the downregulated DEGs (Supplementary Table S1). The upregulated DEGs were significantly related to protein translation and apoptosis regulation, while the downregulated DEGs were significantly related to mitochondrial function and oxidative phosphorylation.

3.7. PPI Network Construction Reveals Interaction of Critical Genes. After filtering out disconnected DEGs, a PPI network with 101 nodes (genes) and 251 edges (connections) was obtained with a combined score of >0.4 (Figure 6(a)). The connectivity degree of each node of the network was calculated. Eight genes with a connectivity degree > 10 were selected as hub genes (Figure 6(b)), which included critical molecules in ER stress-UPR signaling pathway such as ATF3, ATF4, DDIT3, and HSPA5. To better identify the hierarchy of critically involved genes and to determine densely connected regions, we performed an analysis with MCODE algorithm, aiming to find gene clusters based on topology. Seven subnetworks formed within the general DEG network, of which genes responsible for aminoacyl-tRNA biosynthesis, oxidative phosphorylation, and cell cycle were identified (Figures 6(c), 6(d), and 6(e)). We also verified the mRNA expression level of related genes by qRT-PCR. Expression of ATF4, CEBPB, DDIT3, and TRIB3 was significantly upregulated in the high-concentration propofol-treated group (300 μM, 6 h), which is consistent with data extracted from microarray (Figure 7).

4. Discussion

In the current work, we assessed the effects of propofol at a clinically relevant and experimentally high dosage in hiPSC-derived NPCs for the first time. Our results showed that at clinical concentrations (20 and 50 μM) and durations (6 h), propofol had no negative effects on human NPCs, while at higher concentrations (300 μM) and durations (24 h), propofol induced apoptosis in NPCs. Our global gene expression analysis indicated that sustained endoplasmic reticulum (ER) stress and inhibition of mitochondrial oxidative phosphorylation are two major pathways that propofol might employ to execute its toxicity to hiPSC-derived NPCs. Aberration of both pathways would also lead to abnormal protein translation and energy metabolism in these cells.

Increasing concerns have recently arisen about the safe use of propofol in expecting mothers and young children, as the brain is thought to be vulnerable to anesthetics from the third trimester to the first 3 years of life [8, 11, 27, 28]. Animal models and cells derived from human fetal tissues have been used to mimic the developing brain. However, animal models do not always recapitulate human conditions especially in the case of CNS. Fetal tissues suffer from limited availability as well as interindividual genetic differences. These limitations have prompted us to search for alternative yet authentic human cell models, such as using the increasingly powerful hiPSCs and their various neural lineage derivatives.

Two types of human pluripotent stem cells, embryonic stem cells (hESCs) and induced pluripotent stem cells (hiPSCs), have been widely used. hESCs [29] are derived

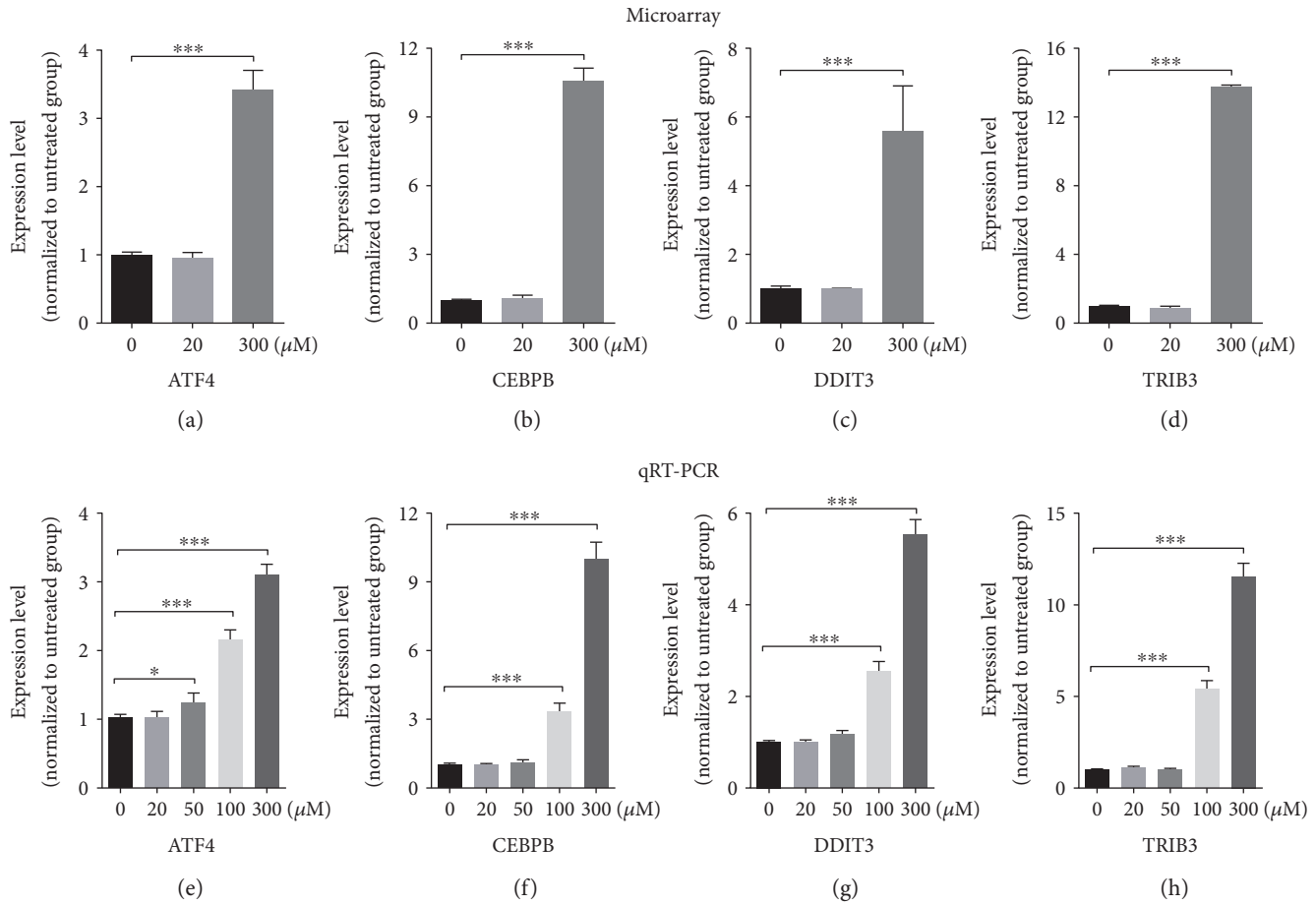

Figure 7: Verification of the expression level of genes related to UPR and ER press. NES-GFP iPSC-derived NPCs were treated with propofol (0, 20, 50, 100, or 300 μM) for 6 h. The mRNA expression level of ATF4, CEBPB, DDIT3, and TRIB3 was evaluated by microarray (a, b, c, d) and qRT-PCR (e, f, g, h). The qRT-PCR results were normalized to the GAPDH mRNA level. All data are presented as mean ± SD ($n = 3$; $^{*}p < 0.05$; $^{***}p < 0.001$, Student's t-test).

from the inner cell mass of blastocysts and theoretically have the potential to give rise to any lineage of the body. hiPSCs are reprogrammed from somatic cells and share a remarkable degree of similarity with hESCs on key cellular features, including genetic and epigenetic profiles, self-renewal capabilities, and differentiation potentials. Like hESCs, hiPSCs are able to generate cells of all three germ layers, including cells of the neuroectoderm. One of the most attractive advantages for hiPSCs over hESCs is that hiPSCs retain all genetic information of the individuals they are derived from and are therefore an autologous and personalized cell source. hiPSC-derived NPCs have the potential to faithfully represent the developing brain and could serve as an in vitro platform for drug screening and testing.

Here, we assessed the effects of propofol on multiple lines of hiPSC-NPCs. Our data are consistent with previous reports on propofol treatment on rat or human embryonic neural stem cells [9, 18, 30] and collectively suggested that short-term exposure (<6 h) of propofol within the commonly practiced clinical dose range is safe to human NPCs, while prolonged exposure could result in extensive toxic effects.

Multiple pathways have been reported to be involved in propofol neurotoxicity, including increasing calcium influx to trigger the caspase cascade in apoptosis and activating the GABAA receptor and the p75 neurotrophin receptor, leading to ATP depletion. Propofol could also downregulate miR-21, a microRNA proposed to be neuroprotective [30–33]. To comprehensively interrogate gene expression changes after propofol treatment, we performed microarray analysis, aiming to identify differentially regulated genes and protein-protein interactions (PPI) involved upon exposure to propofol. The upregulated genes indicated that propofol treatment could induce apoptosis and cell death in human NPCs through unfolded protein response- (UPR-) associated ER stress [34–36]. Previously identified UPR-related genes, such as DDIT3 (DNA damage-inducible transcript 3), TRB3 (tribbles-related protein 3), CEBP/β, GADD34, and ATF4, were all upregulated significantly in the 300 μM group, indicating that the UPR pathway might participate in propofol-induced toxicity (Supplementary Table S1). As ER stress and the UPR pathway are highly likely involved in propofol toxicity, efforts on identifying potential therapeutic candidates that reverse such process could be helpful to maintain cellular homeostasis under high concentrations of propofol. For example, O-demethyldemethoxycurcumin, a curcumin analogue, has been shown

to downregulate the expression of several ER stress signaling molecules, including PERK, IRE-1, and CHOP, and has neuroprotective effect against ER stress-induced cell death [37]. Among the downregulated genes, NDUFA3, NDUF2, ATP5I, ATP5J2, ATP5G1, and COX7B are related to mitochondrial oxidative phosphorylation. Molecules that boost mitochondrial oxidative phosphorylation could potentially alleviate propofol toxicity.

It is interesting to note that propofol treatment reduced cell viability in NPCs at high concentration (100 and 300 μm) as shown by the MTT assays (Figure 2). However, the proportion of cell viability reduction in the MTT assays was much larger than the proportion of increased apoptosis as detected by Annexin V in flow cytometry (Figure 3). This discrepancy suggested that propofol exposure may cause cell cycle arrest followed by attenuated proliferation. We examined genes involved in the cell cycle progression of NPCs in response to propofol treatment. Our data showed that several cell cycle related genes, such as DDIT3, PPP1R15A, and GADD45A, were upregulated in the propofol-treated group, while other genes that are involved in cell cycle progression, including CCNA2, CDKN3, CDC2, and CDC25B, were downregulated. Additional experiments to elucidate the mechanism that cell cycle molecules are affected by propofol treatment are warranted.

There are some weaknesses in our study. Our work is an in vitro study. Although we identified candidate genes and potential mechanisms that could contribute to propofol toxicity, whether these candidates play a role in the clinics still needs to be rigorously tested in in vivo settings. These in vivo tests can be carried out using transgenic mice with perturbed genes identified from our hiPSC-NPC work presented here or treating mice with candidate molecules (e.g., the aforementioned O-demethyldemethoxycurcumin) that might lead to reduced propofol toxicity. In addition, While NPCs to a certain extent represent the fetal developing brain, tests with additional cell types including more differentiated neural cells and neuron subtypes would provide a more comprehensive picture on the impact of propofol. The recently emerged technique of generating cerebral organoids from hiPSCs [38, 39] will be able to provide multiple brain cell types in a 3D mini brain scenario; hence, testing the effects of propofol on the cerebral organoids will likely yield data of more translational relevance and mechanistic insights. In addition, hiPSCs can be differentiated into cells of the peripheral nervous system and cardiomyocytes, among other cell types. Our platform of using hiPSCs to examine the effects of propofol can be extended to the field of autonomic dysregulation. These experiments are ongoing.

In conclusion, our work showed that propofol treatment at clinical concentrations had no adverse effects on multiple hiPSC line-derived NPCs. At supraclinical dose, its toxicity is possibly exerted through the ER stress pathway and the disturbance of mitochondrial energy metabolism.

Conflicts of Interest

The authors declare no conflict of interest.

Authors' Contributions

Bo Long and Shenglan Li contributed equally and are co-first author to this work.

Acknowledgments

The authors thank Dr. Joanna S. O'Leary for editing the manuscript. The authors thank the IMM FACS core facility and the Cancer Prevention and Research Institute of Texas (CPRIT) for the supported use of flow cytometry. The authors also wish to thank Quantitative Genomics & Microarray Core Lab at The University of Texas Health Science Center at Houston for running the microarrays for this work. This work was supported by the Vivian L. Smith Department of Neurosurgery, McGovern Medical School, The University of Texas Health Science Center at Houston. Microarray data was deposited to GEO under the Accession no. GSE101724.

References

[1] F. Heid, D. W. Kauff, H. Lang, and W. Kneist, "Impact of inhalation vs. intravenous anaesthesia on autonomic nerves and internal anal sphincter tone," *Acta Anaesthesiologica Scandinavica*, vol. 59, no. 9, pp. 1119–1125, 2015.

[2] S. Hidaka, M. Kawamoto, S. Kurita, and O. Yuge, "Comparison of the effects of propofol and midazolam on the cardiovascular autonomic nervous system during combined spinal and epidural anesthesia," *Journal of Clinical Anesthesia*, vol. 17, no. 1, pp. 36–43, 2005.

[3] C. H. Martini, M. Boon, S. J. Broens et al., "Ability of the nociception level, a multiparameter composite of autonomic signals, to detect noxious stimuli during propofol-remifentanil anesthesia," *Anesthesiology*, vol. 123, no. 3, pp. 524–534, 2015.

[4] V. Chidambaran, A. Costandi, and A. D'Mello, "Propofol: a review of its role in pediatric anesthesia and sedation," *CNS Drugs*, vol. 29, no. 7, pp. 543–563, 2015.

[5] K. M. Kuczkowski, "The safety of anaesthetics in pregnant women," *Expert Opinion on Drug Safety*, vol. 5, no. 2, pp. 251–264, 2006.

[6] A. M. Brambrink, A. S. Evers, M. S. Avidan et al., "Isoflurane-induced neuroapoptosis in the neonatal rhesus macaque brain," *Anesthesiology*, vol. 112, no. 4, pp. 834–841, 2010.

[7] V. Jevtovic-Todorovic, R. E. Hartman, Y. Izumi et al., "Early exposure to common anesthetic agents causes widespread neurodegeneration in the developing rat brain and persistent learning deficits," *The Journal of Neuroscience*, vol. 23, no. 3, pp. 876–882, 2003.

[8] C. Creeley, K. Dikranian, G. Dissen, L. Martin, J. Olney, and A. Brambrink, "Propofol-induced apoptosis of neurones and oligodendrocytes in fetal and neonatal rhesus macaque brain," *British Journal of Anaesthesia*, vol. 110, Supplement 1, pp. i29–i38, 2013.

[9] F. Liu, S. W. Rainosek, N. Sadovova et al., "Protective effect of acetyl-L-carnitine on propofol-induced toxicity in embryonic neural stem cells," *Neurotoxicology*, vol. 42, pp. 49–57, 2014.

[10] C. E. Creeley, K. T. Dikranian, G. A. Dissen, S. A. Back, J. W. Olney, and A. M. Brambrink, "Isoflurane-induced apoptosis of neurons and oligodendrocytes in the fetal rhesus macaque brain," *Anesthesiology*, vol. 120, no. 3, pp. 626–638, 2014.

[11] M. Xiong, J. Li, H. M. Alhashem et al., "Propofol exposure in pregnant rats induces neurotoxicity and persistent learning deficit in the offspring," *Brain Sciences*, vol. 4, no. 2, pp. 356–375, 2014.

[12] R. T. Wilder, R. P. Flick, J. Sprung et al., "Early exposure to anesthesia and learning disabilities in a population-based birth cohort," *Anesthesiology*, vol. 110, no. 4, pp. 796–804, 2009.

[13] C. Ing, C. DiMaggio, A. Whitehouse et al., "Long-term differences in language and cognitive function after childhood exposure to anesthesia," *Pediatrics*, vol. 130, no. 3, pp. e476–e485, 2012.

[14] R. P. Flick, S. K. Katusic, R. C. Colligan et al., "Cognitive and behavioral outcomes after early exposure to anesthesia and surgery," *Pediatrics*, vol. 128, no. 5, pp. e1053–e1061, 2011.

[15] M. Bartels, R. R. Althoff, and D. I. Boomsma, "Anesthesia and cognitive performance in children: no evidence for a causal relationship," *Twin Research and Human Genetics*, vol. 12, no. 3, pp. 246–253, 2009.

[16] C. Wang, F. Liu, T. A. Patterson, M. G. Paule, and W. Slikker Jr., "Utilization of neural stem cell-derived models to study anesthesia-related toxicity and preventative approaches," *Molecular Neurobiology*, vol. 48, no. 2, pp. 302–307, 2013.

[17] X. Bai, Y. Yan, S. Canfield et al., "Ketamine enhances human neural stem cell proliferation and induces neuronal apoptosis via reactive oxygen species-mediated mitochondrial pathway," *Anesthesia and Analgesia*, vol. 116, no. 4, pp. 869–880, 2013.

[18] D. M. Twaroski, Y. Yan, I. Zaja, E. Clark, Z. J. Bosnjak, and X. Bai, "Altered mitochondrial dynamics contributes to propofol-induced cell death in human stem cell-derived neurons," *Anesthesiology*, vol. 123, no. 5, pp. 1067–1083, 2015.

[19] K. Takahashi, K. Tanabe, M. Ohnuki et al., "Induction of pluripotent stem cells from adult human fibroblasts by defined factors," *Cell*, vol. 131, no. 5, pp. 861–872, 2007.

[20] J. Yu, M. A. Vodyanik, K. Smuga-Otto et al., "Induced pluripotent stem cell lines derived from human somatic cells," *Science*, vol. 318, no. 5858, pp. 1917–1920, 2007.

[21] Y. Liu, Y. Zheng, S. Li et al., "Human neural progenitors derived from integration-free iPSCs for SCI therapy," *Stem Cell Research*, vol. 19, pp. 55–64, 2017.

[22] S. M. Chambers, C. A. Fasano, E. P. Papapetrou, M. Tomishima, M. Sadelain, and L. Studer, "Highly efficient neural conversion of human ES and iPS cells by dual inhibition of SMAD signaling," *Nature Biotechnology*, vol. 27, no. 3, pp. 275–280, 2009.

[23] H. Xue, S. Wu, S. T. Papadeas et al., "A targeted neuroglial reporter line generated by homologous recombination in human embryonic stem cells," *Stem Cells*, vol. 27, no. 8, pp. 1836–1846, 2009.

[24] X. Viviand, L. Berdugo, C. A. De La Noe, A. Lando, and C. Martin, "Target concentration of propofol required to insert the laryngeal mask airway in children," *Paediatric Anaesthesia*, vol. 13, no. 3, pp. 217–222, 2003.

[25] K. Allegaert, M. Y. Peeters, R. Verbesselt et al., "Inter-individual variability in propofol pharmacokinetics in preterm and term neonates," *British Journal of Anaesthesia*, vol. 99, no. 6, pp. 864–870, 2007.

[26] J. W. Sall, G. Stratmann, J. Leong, E. Woodward, and P. E. Bickler, "Propofol at clinically relevant concentrations increases neuronal differentiation but is not toxic to hippocampal neural precursor cells in vitro," *Anesthesiology*, vol. 117, no. 5, pp. 1080–1090, 2012.

[27] J. Dobbing and J. Sands, "Comparative aspects of the brain growth spurt," *Early Human Development*, vol. 3, no. 1, pp. 79–83, 1979.

[28] A. J. Davidson, "Anesthesia and neurotoxicity to the developing brain: the clinical relevance," *Paediatric Anaesthesia*, vol. 21, no. 7, pp. 716–721, 2011.

[29] J. A. Thomson, J. Itskovitz-Eldor, S. S. Shapiro et al., "Embryonic stem cell lines derived from human blastocysts," *Science*, vol. 282, no. 5391, pp. 1145–1147, 1998.

[30] W. W. Zou, H. P. Xiao, M. N. Gu, K. X. Liu, and Z. Q. Liu, "Propofol induces rat embryonic neural stem cell apoptosis by activating both extrinsic and intrinsic pathways," *Molecular Medicine Reports*, vol. 7, no. 4, pp. 1123–1128, 2013.

[31] S. Kahraman, S. L. Zup, M. M. McCarthy, and G. Fiskum, "GABAergic mechanism of propofol toxicity in immature neurons," *Journal of Neurosurgical Anesthesiology*, vol. 20, no. 4, pp. 233–240, 2008.

[32] D. M. Twaroski, Y. Yan, J. M. Olson, Z. J. Bosnjak, and X. Bai, "Down-regulation of microRNA-21 is involved in the propofol-induced neurotoxicity observed in human stem cell-derived neurons," *Anesthesiology*, vol. 121, no. 4, pp. 786–800, 2014.

[33] M. L. Pearn, Y. Hu, I. R. Niesman et al., "Propofol neurotoxicity is mediated by p75 neurotrophin receptor activation," *Anesthesiology*, vol. 116, no. 2, pp. 352–361, 2012.

[34] D. T. Rutkowski and R. J. Kaufman, "A trip to the ER: coping with stress," *Trends in Cell Biology*, vol. 14, no. 1, pp. 20–28, 2004.

[35] M. Schroder and R. J. Kaufman, "ER stress and the unfolded protein response," *Mutation Research*, vol. 569, no. 1-2, pp. 29–63, 2005.

[36] R. Kim, M. Emi, K. Tanabe, and S. Murakami, "Role of the unfolded protein response in cell death," *Apoptosis*, vol. 11, no. 1, pp. 5–13, 2006.

[37] A. Janyou, C. Changtam, A. Suksamrarn, C. Tocharus, and J. Tocharus, "Suppression effects of O-demethyldemethoxycurcumin on thapsigargin triggered on endoplasmic reticulum stress in SK-N-SH cells," *Neurotoxicology*, vol. 50, pp. 92–100, 2015.

[38] M. A. Lancaster, M. Renner, C. A. Martin et al., "Cerebral organoids model human brain development and microcephaly," *Nature*, vol. 501, no. 7467, pp. 373–379, 2013.

[39] X. Qian, H. N. Nguyen, M. M. Song et al., "Brain-region-specific organoids using mini-bioreactors for modeling ZIKV exposure," *Cell*, vol. 165, no. 5, pp. 1238–1254, 2016.

Hindawi
Neural Plasticity
Volume 2017, Article ID 3256325, 7 pages
https://doi.org/10.1155/2017/3256325

Research Article

The Cardiovascular Effect of Systemic Homocysteine Is Associated with Oxidative Stress in the Rostral Ventrolateral Medulla

Mei-Fang Zhong,[1] Yu-Hong Zhao,[2] Hua Xu,[3] Xing Tan,[4] Yang-Kai Wang,[4] and Wei-Zhong Wang[4]

[1]*Medical Training Center of Songjiang District, Shanghai 201620, China*
[2]*Department of Medicine, Sijing Hospital, Shanghai 201601, China*
[3]*Department of Nursing, Wuxi Higher Health Vocational Technology School, Wuxi 214028, China*
[4]*Department of Physiology and Center of Polar Medical Research, Second Military Medical University, Shanghai 200433, China*

Correspondence should be addressed to Wei-Zhong Wang; wangwz68@hotmail.com

Received 30 June 2017; Accepted 15 August 2017; Published 29 September 2017

Academic Editor: Sheng Wang

It has been demonstrated that homocysteine (HCY) is a significant risk factor of hypertension, which is characterized by overactivity of sympathetic tone. Excessive oxidative stress in the rostral ventrolateral medulla (RVLM), a key region for control of sympathetic outflow, contributes to sympathetic hyperactivity in hypertension. Therefore, the goal of the present study is to determine the effect of systemic HCY on production of reactive oxygen species (ROS) in the RVLM. In the rat model of the diet-induced hyperhomocysteinemia (L-methionine, 1 g/kg/day, 8 weeks), we found that the HCY resulted in a significant increase (≈3.7-fold, $P < 0.05$) in ROS production in the RVLM, which was paralleled with enhanced sympathetic tone and blood pressure (BP). Compared to the vehicle group, levels of BP and basal renal sympathetic nerve activity in the HCY group were significantly ($P < 0.05$, $n = 5$) increased by an average of 27 mmHg and 31%, respectively. Furthermore, the rats treated with L-methionine (1 g/kg/day, 8 weeks) showed an upregulation of NADPHase (NOX4) protein expression and a downregulation of superoxide dismutase protein expression in the RVLM. The current data suggest that central oxidative stress induced by systemic HCY plays an important role in hypertension-associated sympathetic overactivity.

1. Introduction

Cardiovascular disease is a worldwide leading cause of morbidity and mortality in patients with heart failure, atherosclerosis, and hypertension. Individuals that suffered cardiovascular diseases usually possess an unhealthy food and dietary intake, which is closely associated with health-related conditions (e.g., hypertension) [1, 2]. It has been well estimated that homocysteine (HCY), derived from the dietary amino acid, is a causal agent for cardiovascular diseases [3]. In addition to being indisputably regarded as a biomarker of coronary artery disease and atherosclerosis changes [4, 5], hyperhomocysteinemia is also relative to the processing of demyelinization in the central nervous system (CNS) [6], and clinical studies suggest that the excess HCY level frequently parallels with neurodegenerative and acute disorders of CNS [7]. It has been widely established that the rostral ventrolateral medulla (RVLM), containing the sympathetic promoter neurons, is responsible for the central control of sympathetic vasomotor tone and blood pressure (BP) [8, 9]. Moreover, the elevated sympathetic tone is a pathophysiologic hallmark of hypertension and other cardiovascular dysfunctions [10]. There is accumulating evidences proving that oxidative stress plays an important role in the activation of the sympathetic nervous system and consequently hypertension [11]. Enhancement in oxidative stress in the RVLM contributes to the neural mechanisms of cardiovascular dysfunction in spontaneously hypertensive rats

(SHRs) [12]. Oxidative stress mainly results from an imbalance between the production of reactive oxygen species (ROS), especially superoxide and the capacity of its scavenger such as superoxide dismutase (SOD). Activation of NADPH oxidase (NADPHase) is an important mechanism for ROS production and has been demonstrated to contribute to sympathetic overactivity in the RVLM of SHR [13, 14]. Thus, NADPHase and SOD are two crucial factors in maintaining the level of ROS production. It is reported that HCY increases ROS production in the intracellular levels, leading to atherosclerosis in vascular smooth muscle cells and neurotoxicity in neural stem cells [15, 16]. Coupled with oxidative stress, HCY is closely relative to the presence of hypertension [17]. However, the role of HCY in the activation of oxidative stress and sympathetic activity in the RVLM needs to be determined. Herein, we investigated the effects of systemic HCY on oxidative stress in the RVLM and further determined its underlying mechanism.

2. Materials and Methods

2.1. Animals and Experimental Treatments. Male Sprague-Dawley rats (12 weeks old) were purchased from Sino-British SIPPR/BK Laboratory Animal Ltd. (Shanghai, China) in the whole study. All of the procedures were guided and approved by the Animal Care and Use Committee of the Second Military Medical University and conducted specifically to the principles of the Institutional Animal Care.

Animals were divided into two groups. The HCY group at the age of 12 weeks was given by L-methionine (1 g/kg body weight per day) in tap water for a period of 8 weeks, as previously described [18]. The amount of water drank by animals every day was divided into two parts. The first part was mixed with L-methionine according to body weight of the individual, while the second one was the normal potable water without L-methionine. The control group was given equal volume of water. Eight weeks after HCY treatment, plasma HCY levels in rats were measured. Blood samples were taken from rats and were centrifuged for 10 min at 1500 rpm at 4°C, followed by collection of plasma for the evaluation of HCY. HCY reagent (Beijing Strong Biotechnologies Inc., Beijing, China) was used to detect the levels of HCY by an enzymatic cycling method with Beckman AU 5800 automatic biochemical analyzer (Beckman, USA).

2.2. Measurements of Cardiovascular Parameters. Using a noninvasive computerized tail-cuff system (ALC-NIBP; Shanghai Alcott Biotech Inc., Shanghai, China), as previously depicted [19], BP in conscious rats was measured at baseline (12 weeks of age) and then every 4 days until the end of the study period. After completion of 8-week L-methionine treatment, levels of BP, HR, and basal renal sympathetic nerve activity (RSNA) were measured in an anesthetized state (urethane 800 mg/kg and α-chloralose 40 mg/kg i.p.). Briefly, the right femoral artery was cannulated to collect the data of mean arterial pressure (MAP) and heart rate (HR) by the PowerLab system. The left renal sympathetic nerve was dissected retroperitoneally and put on a pair of silver recording electrodes to measure RSNA. The RSNA signal was amplified, filtered, integrated, sampled, and converted to a digital signal by the PowerLab system (AD Instruments). The basal RSNA was taken by the percent of the maximum value, as previously described [20]. Usually, the maximum (Max) RSNA was obtained 5 min after the rat was euthanized (pentobarbital sodium, 200 mg/kg). Background noise levels for RSNA were measured 15–20 min after the rat was euthanized. Using the unit conversion of the PowerLab Chart system, the Max was set to 100%, and the noise level was set to 0%. Baseline nerve activity was taken as the percent of the Max.

2.3. Detection of ROS Production in the RVLM. ROS production in the RVLM was detected by fluorescence, as previously delineated [21, 22]. Briefly, the rats were killed by an overdose of pentobarbital sodium (200 mg/kg). After being fixed and dehydrated in 4% paraformaldehyde and 20% sucrose, the brain of the rat was dissected into sections of 15 μm and then incubated with dihydroethidium (DHE, 5 μmol/L) at 37°C for 30 min. Brain sections were washed in cold PBS (0.1 M) 1 min for three times and finally examined using confocal laser scanning microscope. The excitation wavelength was 535 nm and the emission wavelength was 610 nm. The original images were acquired at red fluorescence microscope in the RVLM and were calculated by LAS-AF-Lite software.

2.4. Western Blot Analysis. Protein expression in the RVLM was detected by Western blot, as described previously [23]. After the RVLM tissues were punched from 100 μm coronal sections of brainstem according to the rat atlas, they were immersed in cell lysate and centrifuged at 4°C for 20 min. The supernatant was left to determine the protein concentration and then applied to a 10% SDS-PAGE gel. Thereafter, transferring the protein sample to the PVDF membrane was performed and then, the membrane was blocked and incubated with NOX4 antibody (1 : 2000, Epitomics, America) or SOD1 antibody (1 : 2000, Epitomics, America) at 4°C overnight [23]. One day later, the membrane was combined with secondary antibody goat anti-rabbit IgG (H + L) for 2 h at room temperature, and the binds of protein were examined by the Syngene Bio Imaging system (Gene Company). Tubulin was severed as the loading control.

2.5. Statistical Analysis. Data are presented as mean ± SEM. The changes in BP by the tail-cuff system and the body weight between the vehicle and HHC groups were analyzed by two-way ANOVA with repeated measures, followed by Tukey' post hoc tests. The difference in the rest of this study between the two groups was calculated using unpaired t-test. The level of significance was set at $P < 0.05$ statistically.

3. Results

3.1. Establishment of the Diet-Induced HHC Rat Model. As shown in Figure 1, the rat model of diet-induced hyperhomocysteinemia was identified by the assessment of plasma HCY concentration 8 weeks after L-methionine treatment (Figure 1(a)). It was found that a consistent elevation of mean arterial pressure (MAP) was induced by systemic treatment with L-methionine compared with vehicle treatment. In

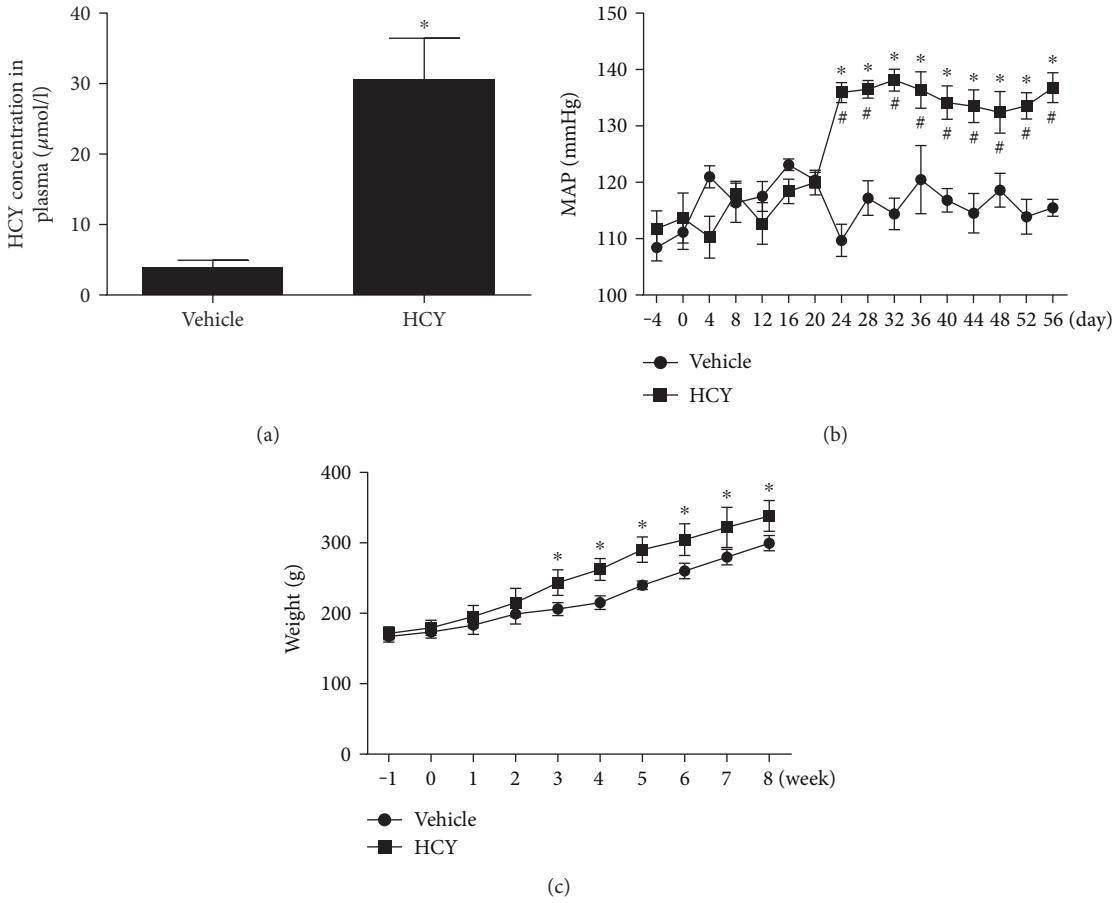

Figure 1: The concentration of HCY in plasma and changes in blood pressure and body weight in vehicle- and L-methionine-treated rats. Plasma HCY concentration (a), BP (b) obtained in conscious rats, and body weight (c) were significantly increased in the HCY group compared to the vehicle group. $n = 5$/group. $^{*}P < 0.05$ versus the vehicle group, $^{\#}P < 0.05$ versus 0 day.

addition, the HCY rats showed a significance in body weight (Figure 1(b) and 1(c)). Compared with the control group, however, L-methionine treatment had no effect on heart rate.

3.2. Effects of HCY on BP, HR, and Basal RSNA Detected in Anesthetized Rats. Eight weeks after the L-methionine treatment, the rats were anesthetized to examine the value of BP, HR, and basal RSNA. Compared to the vehicle group, levels of MAP and basal RSNA in the HCY group were ($P < 0.05$, $n = 5$) increased by an average of 27 mmHg and 31%, respectively. There was no significance in HR between the HCY and control groups (Figure 2).

3.3. Detection of ROS Production in the RVLM. In order to detect the change in ROS production in the RVLM by HCY, we performed the fluorescent labeling (DHE) to examine ROS production in the RVLM. As presented in Figure 3, L-methionine treatment caused a significant ($P < 0.05$, $n = 5$) increase in ROS production in the RVLM compared with vehicle treatment.

3.4. Protein Levels of NOX4 and SOD1 in the RVLM. As indicated in Figure 4, the protein expression of NOX4 in the RVLM was significantly ($P < 0.05$, $n = 5$) increased in rats treated L-methionine compared with vehicle. However, HCY significantly ($P < 0.05$, $n = 5$) reduced the expression of SOD1 protein.

4. Discussion

The main purpose of this study is to elucidate the effects of systemic HCY on ROS production in the RVLM. Our data shows that the diet-induced hyperhomocysteinemia leads to accelerated oxidative stress in the RVLM, which is associated with high levels in BP and sympathetic overactivity.

It is well known that the RVLM plays a key role in regulation of sympathetic out flow [24, 25]. The abnormalities of the RVLM in the regulation of sympathetic nerve activity contribute to cardiovascular dysfunction like chronic heart failure and hypertension [25, 26]. Previous studies have suggested that HCY plays a role as a neurotransmitter or neuromodulator in the medullary autonomic nuclei [27]. Therefore, our present study was designed to determine the relationship between hyperhomocysteinemia and increased sympathetic activity and BP at the level of the RVLM. It is suggested that hyperhomocysteinemia is an important contributor to high levels of sympathetic overactivity and BP in the RVLM. It has been demonstrated that there are multiple centers involved in cardiovascular regulation. The function of the other areas

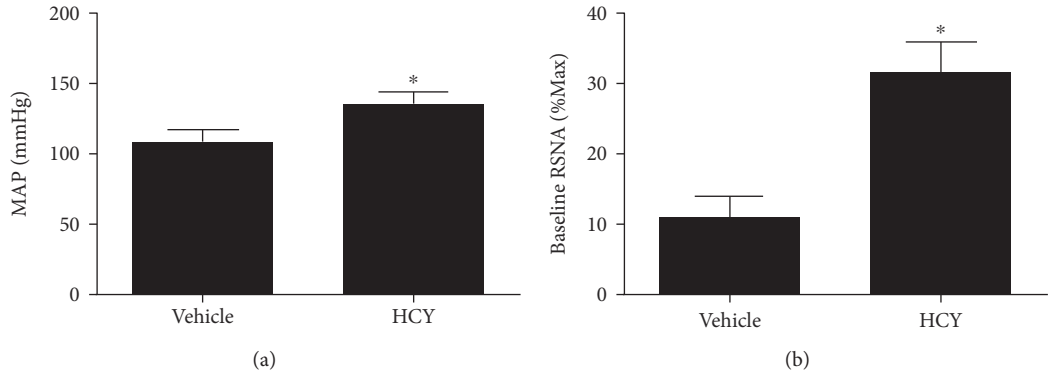

Figure 2: Levels of BP (a) and basal RSNA (b) obtained in anesthetized rats with L-methionine treatment. $n = 5$/group. $^*P < 0.05$ versus the vehicle group.

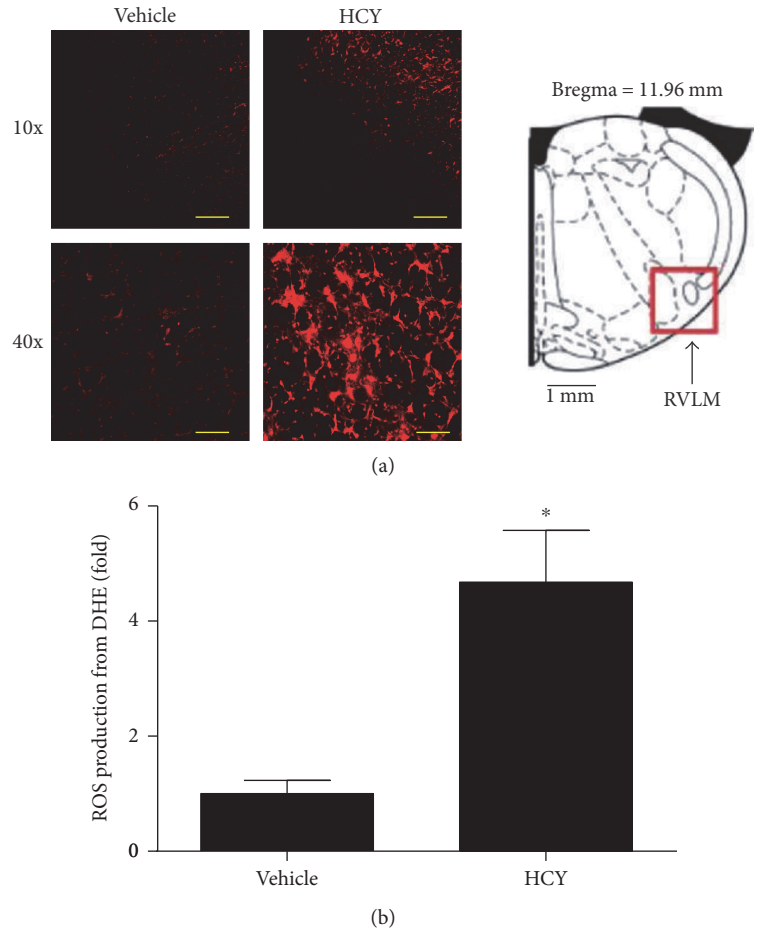

Figure 3: The ROS production in the RVLM in response to systemic HCY. (a) Representative images of ROS (red) by the DHE method in the RVLM region (right). Scale bars = 200 μm in 10x magnification and 50 μm in 40x magnification. (b) Quantification of ROS production in the RVLM. $n = 5$/group. $^*P < 0.05$ versus the vehicle group.

can also be influenced through systemic drug administration. We do not completely rule out the possibility that the effects of HCY on BP and the sympathetic nervous system are associated with the other areas. In this study, however, RVLM tissue was punched to analyze the changes in oxidative stress and confirmed that systemic HCY produced the oxidative stress at the level of the RVLM. So, oxidative stress at the level of the RVLM is at least involved in the central effect of HCY on BP.

Abundant evidences suggest that HCY acts as a risk factor for cardiovascular diseases such as chronic heart and renal failure, type II diabetes, and hypertension [4, 28, 29]. HCY, a sulfur amino acid which is synthesized from dietary methionine by a process of demethylation [30], has been

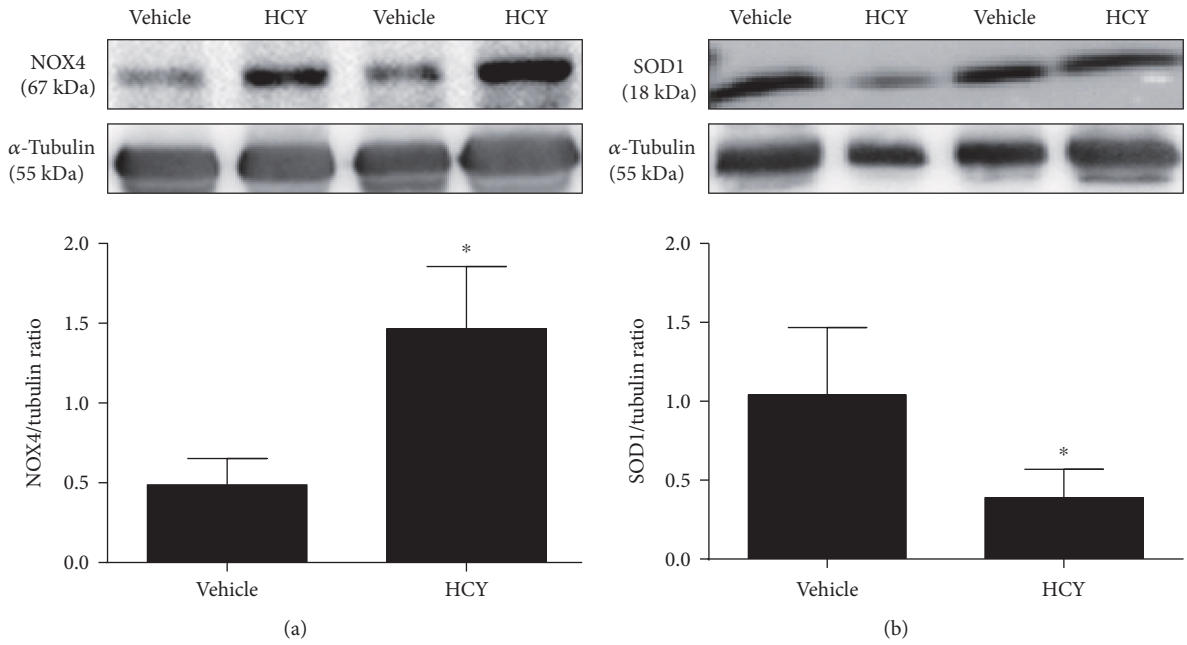

Figure 4: Protein levels of NOX4 and SOD1 in the RVLM in response to systemic HCY. As shown, NOX4 was dramatically increased within the HCY group (a) while SOD1 represented the opposite (b). $n = 4$-5/group. $^*P < 0.05$ versus the vehicle group.

demonstrated to be closely involved in the abnormal cardiovascular autonomic control and increased arterial pressure [31]. Increase in resting BP caused by hyperhomocysteinemia was totally reversed by interference with β1-adrenoceptor antagonist atenolol, indicating that the HCY-relative hypertension is associated with the increase in sympathetic activity [32]. It has been well established that ROS has a pivotal role in the activation of the central and peripheral sympathetic nerve system [12, 33]. Increased ROS production in the RVLM disrupts the balance of excitatory and inhibitory inputs by enhancing glutamatergic while attenuating GABAergic inputs to the RVLM, thereby leading to sympathoexcitation [34]. High salt intake has been reported to accelerate the progress of hypertension via oxidative stress in the RVLM [35]. Similarly, recent evidence shows that high fructose intake also results in hypertension by increasing ROS production in the RVLM via angiotensin II receptor 1 (AT1R) [36]. With respect to HCY mainly obtained from dietary amino conversion, accumulating evidence has demonstrated that HCY is able to positively trigger ROS production in rat vascular smooth muscle cells and aggravates ROS-induced impairment of transmitter release in neurodegenerative diseases [37, 38]. However, whether HCY is associated with deleterious ROS production in the RVLM remains unclear. In this study, we exactly authenticate that high HCY intake contributes to the augmented ROS production in the RVLM. Moreover, we find that the expression of NOX4 (a subtype of NADPHase) is significantly increased, whereas SOD1 was decreased in hyperhomocysteinemia rats compared to vehicle groups. ROS generated by NOX4 has been shown to initiate plenty of cardiovascular disorders such as myofibroblast and hypertension [39, 40]. Importantly, NOX4, a homolog of NOX2/gp91, has been confirmed to be expressed in the brain. Conversely, overexpression of the antioxidant SOD1 in microglia cells completely altered ROS production and the corresponding neurotoxic signaling [41]. On the basis of our study and previous findings, we put forward a hypothesis that hyperhomocysteinemia causes increased ROS production by modulating NOX4 and SOD1 activity in the RVLM.

Although HCY is highly associated with increased ROS production in the RVLM, the exact mechanisms by which HCY changes the expression of NADPHase and SOD are not further determined. HCY-induced imbalance of oxidative stress and redox state could be mediated by many intracellular signaling molecules, such as PI3K and P38/ERK [15]. In terms of this, we truly need to take further deep investigation to find a correlative signaling pathway to better illustrate the pro-ROS effect of HCY in the RVLM. Oxidative stress is often linked to inflammation; HCY is as well a proinflammatory factor that is able to stimulate C-reactive protein production in vascular smooth muscle cells, accelerating the pathogenesis of atherosclerosis [15, 37]. Interestingly, it is inclined to be a hotspot of the negative role of inflammation in the RVLM in the contribution to neurogenic hypertension [42, 43]. Nevertheless, whether HCY takes part in the progress of inflammation in the RVLM still remains unknown. In this study, a limitation was that we did not further investigate the effect of feeding folate on changes induced by HCY. It is reported that folic acid treatment reduces plasma HCY level and the angiotensin II-induced high blood pressure [44]. Furthermore, folic acid treatment is also capable of reducing oxidative stress in a rat model of pregnancy-induced hypertension [45]. Therefore, it is possible that feeding folate to rats reverses oxidative stress in the RVLM

induced by systemic HCY. These questions need to be investigated in our future study.

In conclusion, the present study suggests that high HCY diet-induced hyperhomocysteinemia acts as a risk factor for oxidative stress in the RVLM, leading to sympathoexcitation and hypertension. It consolidates the theories of treating neurogenic hypertension by targeting HCY and reinforces the importance of taking a healthy diet.

Conflicts of Interest

The authors declare that they have no conflicts of interest.

Authors' Contributions

Mei-Fang Zhong, Yu-Hong Zhao, and Hua Xu contributed equally to this work.

Acknowledgments

This work was supported by the Leading Medical Cooperation Project of Songjiang District (2012028 and 2014LX04) and the National Natural Science Foundation of China (nos. 81370363, 81570385, and 81630012).

References

[1] S. Yamini and P. R. Trumbo, "Qualified health claim for whole-grain intake and risk of type 2 diabetes: an evidence-based review by the US Food and Drug Administration," *Nutrition Reviews*, vol. 74, pp. 601–611, 2016.

[2] M. Talaei, A. Pan, J. M. Yuan, and W. P. Koh, "Dairy food intake is inversely associated with risk of hypertension: the Singapore Chinese Health Study," *The Journal of Nutrition*, vol. 147, pp. 235–241, 2016.

[3] B. Fowler, "Homocystein–an independent risk factor for cardiovascular and thrombotic diseases," *Therapeutische Umschau Revue therapeutique*, vol. 62, pp. 641–646, 2005.

[4] B. Glowinska, M. Urban, J. Peczynska, B. Florys, and E. Szydlowska, "Elevated concentrations of homocysteine in children and adolescents with arterial hypertension accompanying type 1 diabetes," *Medical Science Monitor*, vol. 7, pp. 1242–1249, 2001.

[5] A. Mirdamadi, H. Farzamnia, P. Varzandeh, N. Almasi, and M. Arasteh, "Association between serum homocysteine concentration with coronary artery disease in Iranian patients," *ARYA Atherosclerosis*, vol. 7, pp. 63–67, 2011.

[6] E. A. Shirokov and S. F. Leonova, "Neurological syndromes associated with homocystein dismetabolism," *Klinicheskaia Meditsina*, vol. 84, pp. 39–42, 2006.

[7] N. Dionisio, I. Jardin, G. M. Salido, and J. A. Rosado, "Homocysteine, intracellular signaling and thrombotic disorders," *Current Medicinal Chemistry*, vol. 17, pp. 3109–3119, 2010.

[8] K. Nakamura, K. Matsumura, S. Kobayashi, and T. Kaneko, "Sympathetic premotor neurons mediating thermoregulatory functions," *Neuroscience Research*, vol. 51, pp. 1–8, 2005.

[9] E. E. Nishi, B. S. Martins, M. I. Milanez et al., "Stimulation of renal afferent fibers leads to activation of catecholaminergic and non-catecholaminergic neurons in the medulla oblongata," *Autonomic Neuroscience*, vol. 204, pp. 48–56, 2017.

[10] P. R. Pellegrino, A. M. Schiller, K. K. Haack, and I. H. Zucker, "Central angiotensin-II increases blood pressure and sympathetic outflow via rho kinase activation in conscious rabbits," *Hypertension*, vol. 68, pp. 1271–1280, 2016.

[11] A. M. Briones and R. M. Touyz, "Oxidative stress and hypertension: current concepts," *Current Hypertension Reports*, vol. 12, pp. 135–142, 2010.

[12] Y. Hirooka, "Oxidative stress in the cardiovascular center has a pivotal role in the sympathetic activation in hypertension," *Hypertension Research*, vol. 34, pp. 407–412, 2011.

[13] M. Nozoe, Y. Hirooka, Y. Koga et al., "Mitochondria-derived reactive oxygen species mediate sympathoexcitation induced by angiotensin ii in the rostral ventrolateral medulla," *Journal of Hypertension*, vol. 26, pp. 2176–2184, 2008.

[14] C. Z. Ren, Y. H. Yang, J. C. Sun et al., "Exercise training improves the altered renin-angiotensin system in the rostral ventrolateral medulla of hypertensive rats," *Oxidative Medicine and Cellular Longevity*, vol. 2016, Article ID 7413963, 11 pages, 2016.

[15] X. Pang, J. Si, S. Xu, Y. Li, and J. Liu, "Simvastatin inhibits homocysteine-induced CRP generation via interfering with the ROS-p38/ERK1/2 signal pathway in rat vascular smooth muscle cells," *Vascular Pharmacology*, vol. 88, pp. 42–47, 2017.

[16] X. M. Zhang, Y. Q. Zhao, H. Yan, H. Liu, and G. W. Huang, "Inhibitory effect of homocysteine on rat neural stem cell growth in vitro is associated with reduced protein levels and enzymatic activities of aconitase and respiratory complex III," *Journal of Bioenergetics and Biomembranes*, vol. 49, no. 2, pp. 131–138, 2016.

[17] L. J. Dominguez, A. Galioto, A. Pineo et al., "Age, homocysteine, and oxidative stress: relation to hypertension and type 2 diabetes mellitus," *Journal of the American College of Nutrition*, vol. 29, pp. 1–6, 2010.

[18] C. H. Yen and Y. T. Lau, "Vascular responses in male and female hypertensive rats with hyperhomocysteinemia," *Hypertension*, vol. 40, pp. 322–328, 2002.

[19] Y. P. Zha, Y. K. Wang, Y. Deng et al., "Exercise training lowers the enhanced tonically active glutamatergic input to the rostral ventrolateral medulla in hypertensive rats," *CNS Neuroscience & Therapeutics*, vol. 19, pp. 244–251, 2013.

[20] H. J. Wang, Y. X. Pan, W. Z. Wang et al., "Exercise training prevents the exaggerated exercise pressor reflex in rats with chronic heart failure," *Journal of Applied Physiology*, vol. 108, pp. 1365–1375, 2010.

[21] Y. K. Wang, D. Shen, Q. Hao et al., "Overexpression of angiotensin-converting enzyme 2 attenuates tonically active glutamatergic input to the rostral ventrolateral medulla in hypertensive rats," *American Journal of Physiology: Heart and Circulatory Physiology*, vol. 307, pp. H182–H190, 2014.

[22] Y. K. Wang, Q. Yu, X. Tan et al., "Centrally acting drug moxonidine decreases reactive oxygen species via inactivation of the phosphoinositide-3 kinase signaling in the rostral ventrolateral medulla in hypertensive rats," *Journal of Hypertension*, vol. 34, pp. 993–1004, 2016.

[23] F. Hao, Y. Gu, X. Tan et al., "Estrogen replacement reduces oxidative stress in the rostral ventrolateral medulla of ovariectomized rats," *Oxidative Medicine and Cellular Longevity*, vol. 2016, Article ID 2158971, 8 pages, 2016.

[24] T. S. Moreira, A. C. Takakura, E. Colombari, and P. G. Guyenet, "Central chemoreceptors and sympathetic vasomotor outflow," *The Journal of Physiology*, vol. 577, pp. 369–386, 2006.

[25] I. S. Pinto, A. A. Mourao, E. F. da Silva et al., "Blockade of rostral ventrolateral medulla (RVLM) bombesin receptor type 1 decreases blood pressure and sympathetic activity in anesthetized spontaneously hypertensive rats," *Frontiers in Physiology*, vol. 7, p. 205, 2016.

[26] T. Kishi and Y. Hirooka, "Central mechanisms of abnormal sympathoexcitation in chronic heart failure," *Cardiology Research and Practice*, vol. 2012, Article ID 847172, 7 pages, 2012.

[27] Y. Takemoto, "Functional cardiovascular action of l-cysteine microinjected into pressor sites of the rostral ventrolateral medulla of the rat," *Amino Acids*, vol. 46, pp. 863–872, 2014.

[28] B. Jakovljevic, B. Gasic, P. Kovacevic, Z. Rajkovaca, and T. Kovacevic, "Homocystein as a risk factor for developing complications in chronic renal failure," *Materia Socio-Medica*, vol. 27, pp. 95–98, 2015.

[29] S. Korkmaz, A. Yilmaz, G. Yildiz, F. Kilicli, and S. Icagasioglu, "Relationship between homocysteine and non-dipper pattern in patients with type 2 diabetes mellitus," *Arquivos Brasileiros de Endocrinologia e Metabologia*, vol. 56, pp. 285–290, 2012.

[30] S. Veeranki and S. C. Tyagi, "Defective homocysteine metabolism: potential implications for skeletal muscle malfunction," *International Journal of Molecular Sciences*, vol. 14, pp. 15074–15091, 2013.

[31] R. H. Mendes, C. Mostarda, G. O. Candido et al., "Moderate hyperhomocysteinemia provokes dysfunction of cardiovascular autonomic system and liver oxidative stress in rats," *Autonomic Neuroscience*, vol. 180, pp. 43–47, 2014.

[32] L. B. Resstel, C. R. de Andrade, R. Haddad, M. N. Eberlin, A. M. de Oliveira, and F. M. Correa, "Hyperhomocysteinaemia-induced cardiovascular changes in rats," *Clinical and Experimental Pharmacology & Physiology*, vol. 35, pp. 949–956, 2008.

[33] V. M. Campese, S. Ye, H. Zhong, V. Yanamadala, Z. Ye, and J. Chiu, "Reactive oxygen species stimulate central and peripheral sympathetic nervous system activity," *American Journal of Physiology - Heart and Circulatory Physiology*, vol. 287, pp. H695–H703, 2004.

[34] M. Nishihara, Y. Hirooka, R. Matsukawa, T. Kishi, and K. Sunagawa, "Oxidative stress in the rostral ventrolateral medulla modulates excitatory and inhibitory inputs in spontaneously hypertensive rats," *Journal of Hypertension*, vol. 30, pp. 97–106, 2012.

[35] Y. Koga, Y. Hirooka, S. Araki, M. Nozoe, T. Kishi, and K. Sunagawa, "High salt intake enhances blood pressure increase during development of hypertension via oxidative stress in rostral ventrolateral medulla of spontaneously hypertensive rats," *Hypertension Research*, vol. 31, pp. 2075–2083, 2008.

[36] K. L. Wu, C. W. Wu, Y. L. Tain et al., "Effects of high fructose intake on the development of hypertension in the spontaneously hypertensive rats: the role of $AT_1R/gp91^{PHOX}$ signaling in the rostral ventrolateral medulla," *The Journal of Nutritional Biochemistry*, vol. 41, pp. 73–83, 2017.

[37] X. Pang, J. Liu, J. Zhao et al., "Homocysteine induces the expression of C-reactive protein via NMDAr-ROS-MAPK-NF-κB signal pathway in rat vascular smooth muscle cells," *Atherosclerosis*, vol. 236, pp. 73–81, 2014.

[38] E. Bukharaeva, A. Shakirzyanova, V. Khuzakhmetova, G. Sitdikova, and R. Giniatullin, "Homocysteine aggravates ROS-induced depression of transmitter release from motor nerve terminals: potential mechanism of peripheral impairment in motor neuron diseases associated with hyperhomocysteinemia," *Frontiers in Cellular Neuroscience*, vol. 9, p. 391, 2015.

[39] N. Sampson, R. Koziel, C. Zenzmaier et al., "ROS signaling by NOX4 drives fibroblast-to-myofibroblast differentiation in the diseased prostatic stroma," *Molecular Endocrinology*, vol. 25, pp. 503–515, 2011.

[40] N. N. Zheleznova, C. Yang, and A. W. Cowley Jr., "Role of Nox4 and p67phox subunit of nox2 in ROS production in response to increased tubular flow in the mTAL of Dahl salt-sensitive rats," *American Journal of Physiology Renal Physiology*, vol. 311, pp. F450–F458, 2016.

[41] F. O. Dimayuga, C. Wang, J. M. Clark, E. R. Dimayuga, V. M. Dimayuga, and A. J. Bruce-Keller, "SOD1 overexpression alters ROS production and reduces neurotoxic inflammatory signaling in microglial cells," *Journal of Neuroimmunology*, vol. 182, pp. 89–99, 2007.

[42] K. L. Wu, S. H. Chan, and J. Y. Chan, "Neuroinflammation and oxidative stress in rostral ventrolateral medulla contribute to neurogenic hypertension induced by systemic inflammation," *Journal of Neuroinflammation*, vol. 9, p. 212, 2012.

[43] K. Kapoor, A. M. Bhandare, P. E. Nedoboy, S. Mohammed, M. M. Farnham, and P. M. Pilowsky, "Dynamic changes in the relationship of microglia to cardiovascular neurons in response to increases and decreases in blood pressure," *Neuroscience*, vol. 329, pp. 12–29, 2016.

[44] S. B. Pushpakumar, S. Kundu, N. Metreveli, and U. Sen, "Folic acid mitigates angiotensin-II-induced blood pressure and renal remodeling," *PLoS One*, vol. 8, article e83813, 2013.

[45] F. Cheng, J. Lan, W. Xia et al., "Folic acid attenuates vascular endothelial cell injury caused by hypoxia via the inhibition of ERK1/2/NOX4/ROS pathway," *Cell Biochemistry and Biophysics*, vol. 74, pp. 205–211, 2016.

Hindawi
Neural Plasticity
Volume 2017, Article ID 5819514, 12 pages
https://doi.org/10.1155/2017/5819514

Review Article

Neural Vascular Mechanism for the Cerebral Blood Flow Autoregulation after Hemorrhagic Stroke

Ming Xiao,[1] Qiang Li,[2] Hua Feng,[2] Le Zhang,[3] and Yujie Chen[2]

[1]*College of Computer and Information Science, Southwest University, Chongqing, China*
[2]*Department of Neurosurgery, Southwest Hospital, Third Military Medical University, Chongqing, China*
[3]*College of Computer Science, Sichuan University, Chengdu, China*

Correspondence should be addressed to Le Zhang; zhanglcq@swu.edu.cn and Yujie Chen; yujiechen6886@foxmail.com

Received 30 June 2017; Accepted 11 September 2017; Published 26 September 2017

Academic Editor: Sheng Wang

During the initial stages of hemorrhagic stroke, including intracerebral hemorrhage and subarachnoid hemorrhage, the reflex mechanisms are activated to protect cerebral perfusion, but secondary dysfunction of cerebral flow autoregulation will eventually reduce global cerebral blood flow and the delivery of metabolic substrates, leading to generalized cerebral ischemia, hypoxia, and ultimately, neuronal cell death. Cerebral blood flow is controlled by various regulatory mechanisms, including prevailing arterial pressure, intracranial pressure, arterial blood gases, neural activity, and metabolic demand. Evoked by the concept of vascular neural network, the unveiled neural vascular mechanism gains more and more attentions. Astrocyte, neuron, pericyte, endothelium, and so forth are formed as a communicate network to regulate with each other as well as the cerebral blood flow. However, the signaling molecules responsible for this communication between these new players and blood vessels are yet to be definitively confirmed. Recent evidence suggested the pivotal role of transcriptional mechanism, including but not limited to miRNA, lncRNA, exosome, and so forth, for the cerebral blood flow autoregulation. In the present review, we sought to summarize the hemodynamic changes and underline neural vascular mechanism for cerebral blood flow autoregulation in stroke-prone state and after hemorrhagic stroke and hopefully provide more systematic and innovative research interests for the pathophysiology and therapeutic strategies of hemorrhagic stroke.

1. Introduction

Human brain receives almost 20% of body's oxygen and glucose of cardiac output. Both oxygen and glucose are delivered to the central nervous system by cerebral blood flow (CBF) and then transported across blood-brain barrier for the brain consumption. Therefore, brain functions depend on the proper CBF due to the normal autoregulation of healthy blood vessels and cardiovascular system. If CBF stops, brain functions will shut down in seconds and neurons will be irreversibly damaged in minutes.

CBF is maintained by a coordinated action of interconnected blood vessels, which in the human brain form a 400-mile long vascular network. Within this network, cerebral arteries, arterioles, and capillaries supply the brain with oxygen, energy metabolites, and nutrients. The cerebral venous return removes carbon dioxide and metabolic waste products from the brain and into the systemic circulation for clearance. During the initial stages of hemorrhagic stroke, including intracerebral hemorrhage (ICH) and subarachnoid hemorrhage (SAH), the reflex mechanisms are activated to protect cerebral perfusion, but secondary dysfunction of cerebral flow autoregulation will eventually reduce global CBF and the delivery of metabolic substrates, leading to generalized cerebral ischemia, hypoxia, and ultimately, neuronal cell death.

CBF is controlled by various regulatory mechanisms, including prevailing arterial pressure, intracranial pressure, arterial blood gases, neural activity, and metabolic demand. Evoked by the concept of vascular neural network, the unveiled neural vascular mechanism gains more and more attentions. This mechanism ensures a rapid increase in the rate of CBF to activated brain structures. Under physiological conditions, the capacity of increased CBF and oxygen

delivery exceeds metabolic demand and oxygen consumption by activated brain sites, thus providing a large gradient for oxygen diffusion to brain cells furthest from capillaries. And different cell types, such as astrocyte, neuron, pericyte, endothelium, and so forth, are formed as a communicate network to regulate with each other as well as the cerebral blood flow. However, the signaling molecules responsible for this communication between these new players and blood vessels are yet to be definitively confirmed. Recent evidence suggested the pivotal role of transcriptional mechanism, including but not limited to miRNA, lncRNA, exosome, and so forth, for the CBF autoregulation. In the present review, we sought to summarize the hemodynamic changes and underline neural vascular mechanism for CBF autoregulation (Figure 1) in stroke-prone state and after hemorrhagic stroke and hopefully provide more systematic and innovative research interests for the pathophysiology and therapeutic strategies of hemorrhagic stroke.

2. Hemodynamic Changes in Stroke-Prone State and Hemorrhagic Stroke State

2.1. Intracerebral Hemorrhage. ICH is the second most common cause of stroke, which initiates with brain parenchyma bleeding and hematoma growth, despite of the direct incentives [1]. Because ICH was thought to be an arterial hemorrhagic brain injury, there is little attention to the role of cerebral vein or venule in ICH pathophysiology [1, 2]. However, in the acute phase of ICH, a rapid increase of intracranial pressure due to hematoma formation could cause failure of autoregulation and reduce cerebral perfusion pressure [3]. That is why the guidelines suggest controlled lowering blood pressure treatment instead of aggressive lowering blood pressure, which intends to maintain the cerebral blood flow [4]. Moreover, recent studies found that there are new ischemic lesions coexisting with acute ICH [5–9], suggesting possible involvement of small vessel pathogenesis [5, 6].

The main secondary brain injury after ICH is thought to be three intertwined degenerative cascades adjacent to hematoma [10], including inflammation [11], red cell lysis and iron deposition [1, 12], and thrombin production [1, 12]. Moreover, besides the ischemic lesions near hematoma, there also are some remote ischemic lesions been found [3]. Similar to ischemic brain injury we reviewed above, all of these pathophysiological factors could directly and indirectly cause cerebral venule endothelial dysfunction, microthrombus, and eventually outflow reduction. Combined with other pathophysiological mechanisms, such as oxidative stress, apoptosis, and others, these factors could also lead to blood-brain barrier disruption, brain edema, and hydrocephalus, which makes further increased intracranial pressure and a vicious cycle [10]. On the other hand, most of intracranial hemorrhage occurs in hypertension patient, and the hypertensive vasculopathy, including arteries/arterioles and veins/venules, could cause "stroke-prone state" to lower the threshold of ischemic [3] and outflow dysfunction [13].

2.2. Subarachnoid Hemorrhage. Subarachnoid hemorrhage is a special subtype of intracranial hemorrhage, which caused by bleeding into subarachnoid hemorrhage. For a long time, cerebral vasospasm is the classic cause of delayed neurological deterioration after aneurysmal subarachnoid hemorrhage, leading to cerebral ischemia and infarction and thus to poor outcome and occasionally death [14]. However, recent clinical trials have demonstrated marked prevention of vasospasm with the endothelin receptor antagonist clazosentan, yet patient outcome was not improved [15, 16]. These disappointing results reminded researchers switching interests into early brain injury [17, 18], but this concept is merely limited in neurons and overlooks the functions of other cell types. Fortunately, recent evolving concepts, such as neurovascular unit [19], vascular neural network [20], and then vasculo-neuronal-glia triad model [21], noticed the contributions of cerebral microcirculation. However, they all keep cerebral veins and venules at an arm's length.

Rethinking of the failed clazosentan clinical trials, there might be a missing factor that, compare to arteries, endothelin only has less potent as a constrictor in cerebral veins [22], which means powerful endothelin receptor antagonist clazonsentan may not alleviate the "vasospasm" in cerebral venous system after subarachnoid hemorrhage. Moreover, clazosentan did not prevent the formation of microthrombi [23]. Recent studies found that there is also vasospasm in deep cerebral veins after subarachnoid hemorrhage [24], and the diameter significantly decreased 1 day and peaked at 5–7 days after subarachnoid hemorrhage [25]. In the meantime, whether there has diameter reducing in cerebral venules after SAH is still controversial [26–29]. In addition, SAH elicited time- and size-dependent increases in rolling and adherent platelets and leukocytes in cerebral venules [30], which lead to microthrombus and microvascular stasis [29, 31]. Similar to other brain injuries, subarachnoid hemorrhage can also cause brain edema [21, 32, 33], hydrocephalus [34, 35], and then cerebral hypoperfusion [36] just like we reviewed above.

In another way, cerebral venous thrombosis [37–40] or stenosis [41] is also an uncommon etiology of subarachnoid hemorrhage, mostly perimesencephalic subarachnoid hemorrhage [42–44]. Potential cause may be elevated intracranial venous pressure or mechanical swelling of the intracranial venous system, leading to variant of cerebral venous drainage [45–49], arteriovenous malformation [50], and eventually veins or venule breakdown [36, 38, 51].

2.3. Hypertension. Hypertension is one of the most important risk factors of brain injuries. Sustained high blood pressure could cause smooth muscle cell hypertrophy and then vessel remodeling [52], eventually leading to vessel lumen stenosis and decreased venous distensibility [53, 54]. In the meantime, hypertension could increase the collagen biosynthesis and deposition in perivascular spaces [55], which could have similar effect to the perivenous cuffs in MS patients [56]. However, the major vascular complication under hypertension condition is endothelial dysfunction [57], which will lead to BBB disruption [58–61] and impairment of vascular tone modulation [57]. In addition, hypertension could also cause adherent leukocytes and platelets in cerebral venules [62]. All these pathophysiological effects could increase

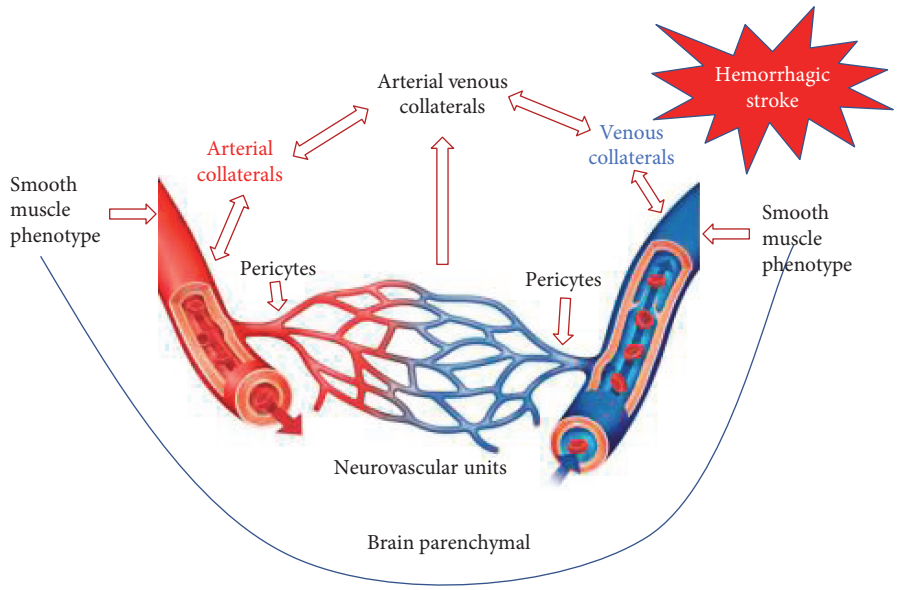

Figure 1: Neural vascular mechanisms for the cerebral blood flow autoregulation in the present review.

cerebral venous pressure, impair cerebral venous outflow [63–65], and eventually rCBF reduction [66].

2.4. Diabetes. Diabetes is another major risk factor of stroke. Diabetes develops because of inadequate pancreas islet β-cell and adipose-tissue responses to chronic fuel excess, which results in nutrition excess, insulin resistance, and metabolic stress [67]. Among these, metabolic stress leads to endothelial dysfunction, including cerebral venous system, which is considered to be the initial process in vascular manifestations of diabetes [68, 69]. Following vascular related alterations involves platelet adhesiveness and coagulation cascade, vasoconstriction, and inflammation [69, 70]. Similar to other brain injuries, these pathophysiological changes ultimately lead to cerebral venous thrombus [71, 72], venous hyperaemia, and brain edema [73].

3. Neurovascular Networks as Future Therapeutic Targets

3.1. Pericytes as a Potential Interventional Target. Pericytes cover venules of superficial cerebral veins in the central nervous system as well as arterioles, which determine the contraction and dilation of these vessels. Recent evidence has suggested that pericytes secrete matrix metalloproteinase-9 to degrade the endothelial matrix and blood-brain barrier around their somatic bodies. In addition to mechanic stress caused by hyperperfusion after recanalization [74], pericytes may have a fundamental role in the disruption of the blood-brain barrier in poststroke venules but not arterioles and capillaries. This detrimental function may have been induced by cyclophilin A and its downstream signaling pathways.

However, pericytes have multipotential functions that could underlie blood-brain barrier development and repair. First, pericytes can form intercellular tight junctions in the blood-brain barrier [75]. Additionally, pericytes also contribute to the formation of the basal lamina by synthesizing type IV collagen, glycosaminoglycans, and laminin (Allt and Lawrenson, 2001). Large efforts have been undertaken to induce angiogenesis and protect the blood-brain barrier [76–79], but it is still far from clinical application. Recently, we successfully stimulated tight junction and adherens junction proteins by activating Frizzled-4 receptor, a canonical Wnt signaling receptor that is also expressed on pericytes [80], suggesting that pericytes may be a promising target to maintain blood-brain barrier integrity and functions during subarachnoid hemorrhage treatment [21].

Furthermore, previous evidence suggests that the occurrence of global ischemia after subarachnoid hemorrhage significantly constricts pericytes and reduces blood flow in the microcirculation. However, in contrast to intuition, dilated pericytes may not reverse blood flow, which we called a "no-reflow phenomenon" [81, 82]. Second, during subarachnoid hemorrhage and other brain injury pathophysiologies, pericyte contraction, usually together with pericyte-programmed cell death, caused a reduced capillary density and maintained an inactive microcirculation [27, 83, 84]. Our recent studies indicated that pericytes are induced to contract in response to hemoglobin and nitric oxide/cGMP pathway, forming pearl string-like contractions in microvessels to deteriorate the microcirculation [85].

In addition, pericytes could modulate the proliferation, migration, and differentiation of endothelial cells; pericytes cocultured with endothelial cells and astrocytes could establish a stable capillary-like structure [86, 87]. In their efforts to orchestrate initiation, sprout connection, and termination in angiogenesis, pericytes secrete vascular endothelial growth factor and interleukin-6 to facilitate endothelial cell maturation and microvessel sprouting, contributing a pivotal role in the initial stage of angiogenesis [88]. Transforming growth factor-β binds to its receptor on endothelial cells and pericytes to self-regulate and induce perivascular mesenchymal cell differentiation into pericytes and smooth muscle cells [89]. Moreover, the platelet-derived growth factor (PDGF)

pathway is the crucial factor for sprouting capillary recruitment of pericytes. Angiopoietin-1 from pericytes binds to Tie-2 on the endothelial cell to enhance pericyte surrounding of the new blood spout, increasing the vessel stability [90].

Due to their specific spatial distribution along microvessels and their broad cellular properties, pericytes could be an ideal target for the development of novel preventive and therapeutic strategies by modulating and controlling the neural vascular network, consequently improving neuroprotection [91]. For example, targeting pericytes during the development of microvascular dysfunction and elucidating the molecular pathways involved in the regulation of pericyte activities for attenuating chronic rejection intervention have been demonstrated [92]. A recent review also targeted pericytes as clinical endpoints and therapeutic interventions in diabetic retinopathy [93]. Interestingly, maintaining high levels of estrogen E2 are critical for the control of PDGF-mediated crosstalk between endothelial cells and pericytes, which governs the microvessel stability and is essential for preserving intracranial homeostasis, consequently reducing the risk of intracranial hemorrhage and decreasing the incidence of stroke and cerebral aneurysm [94]. Future studies should further determine the role of pericytes before and after hemorrhage to illustrate the mechanism underlying the occurrence and development of this critical disorder. Additional drugs and trials targeting pericytes and their effectiveness are also required to develop new strategies for the prevention and treatment of hemorrhagic stroke.

3.2. Smooth Muscle Phenotype for Autoregulation. In addition to pericytes, smooth muscle cells also contribute to regulation of the cerebral blood supply with much greater strength. In fact, some researchers consider the smooth muscle cells as the dominator for microvessel autoregulation. In 1993, Contard et al. demonstrated that smooth muscle phenotypes in stroke-prone spontaneously hypertensive rats had no effect on blood pressure or associations with thickness [95]. Most importantly, the changes in the smooth muscle cell phenotype may be beneficial for ischemic tissue lesions in the heart [95]. After traumatic brain injury, mechanical stress can also induce subarachnoid hemorrhage, similar to vasospasm in response to smooth muscle cell hypercontractility and phenotype switching for prolonged vessel remodeling and lumen occlusion. Our recent experiments also propose a potential role for the maintenance of the cerebral smooth muscle phenotype in early brain injury after subarachnoid hemorrhage [96].

Regarding its internal mechanism, the smooth muscle phenotype was mainly regulated by platelet-derived growth factor-BB (PDGF-BB), which has been reported to stimulate smooth muscle cell differentiation, proliferation, and phenotypic transformation [97]. Additionally, PDGF-BB induces the differentiation of the bone marrow endothelial progenitor cell-derived cell line TR-BME2 into mural cells/pericytes and alters the smooth muscle cell phenotype [98]. Other studies have suggested that the ACTA2 gene, calcium signals, cadherin 6B, and integrin receptor may also participate in this pathophysiological process [96, 99–101]. Due to limited evidence in this field, especially in the central nervous system, additional efforts are still needed to elucidate the pivotal role of the smooth muscle phenotype in autoregulation after stroke and other central nervous system disorders.

3.3. Collaterals for Recirculation. Due to the great contributions of the collateral circulation to stroke outcomes, we wondered how to manipulate this important and neglected factor in previous stroke pathophysiologies and therapies. Current strategies include the following. (1) Statins may open collaterals after stroke, preserve penumbra, and expand the time window of thrombolysis [102, 103]. Ovbiagele et al. evaluated the relationship between prestroke statin use and pretreatment angiographic collateral grade among patients with acute ischemic stroke, and they found that the statin-treated group had significantly higher collateral scores than the nonstatin users, suggesting an association between statin use and improved collateralization during acute stroke [104]. (2) Intracellular chloride channel 4 is a determinant of native collateral formation in the brain [105]. Chalothorn et al. observed reduced collateral formation in mice that were deficient in chloride intracellular channel 4, which displayed greater ischemia and worse perfusion [106] and recovery [106]. (3) Vascular endothelial growth factor (VEGF) may be specific for collateral development. Harrigan et al. treated MCAO rats with chronic intraventricular infusions of VEGF, which increased the vascular density in a dose-dependent manner and minimized the associated brain edema after ischemic stroke [107, 108]. (4) Pioglitazone reduces the no-flow phenomenon in microvessels. Shimazu et al. found that the peroxisome proliferator-activated receptor-gamma (PPARγ) agonist reduces the infarction size in transient but not permanent MCAO, suggesting that the role of PPARγ is specific to events that occur during reperfusion, possibly the collateral circulation [109]. During the postischemic, reperfusion phase, pioglitazone, a synthetic agonist for PPARγ, also improves recovery from ischemic stroke [110]. Nevertheless, due to the outlook for collateral circulation, especially the venous collaterals, in translational stroke research over the past decades, limited strategies have been discovered and developed. In future studies, an improved understanding of collateral hemostasis after stroke and of precision therapeutic therapies is highly encouraged. And the pathophysiological therapeutic time window, depending on the collateral circulation of the patient, might replace the current suggested time window for the endovascular treatment after stroke.

4. Transcriptional Signals for the Autoregulation

4.1. Classical Molecule Signals. As we summarized above, cerebral autoregulation, an inherent ability to maintain a relatively steady-state CBF despite fluctuation in arterial blood pressure, is attributed to an intrinsic ability of smooth muscle cells and pericytes to constrict or relax to minimize variation in CBF. The signaling event underlying myogenic response consists of an activation of stretch-activated Ca^{2+} channels by an increase in intravascular pressure [111]. This results in an elevation in intracellular Ca^{2+} and subsequent

stimulation of phospholipase A2, leading to the release of arachidonic acid from membrane phospholipids. Arachidonic acid metabolites, 20-HETEs, inhibit Ca^{2+}-dependent K channels resulting in depolarization of smooth muscles and vasoconstriction. Functional hyperemia implies an increase in CBF induced by neural activity to meet the local metabolic demand. This is a well-coordinated event involving neurons, astrocytes, and vascular cells.

It is widely assumed that calcium-dependent release of vasoactive substances by astrocytes results in arteriole dilation and the increased blood flow which accompanies neuronal activity. Howarth [112] summarized the evidence which has convincingly demonstrated that astrocytes are able to modify the diameter of cerebral arterioles. Howarth discussed the prevalence, presence, and timing of stimulus-induced astrocyte calcium transients and described the evidence for and against the role of calcium-dependent formation and release of vasoactive substances by astrocytes.

4.2. Transcriptional Modulators. Nuclear factor-kappa B (NF-kappaB) is a multisubunit transcription factor that when activated induces the expression of genes encoding acute-phase proteins, cell adhesion molecules, cell surface receptors, and cytokines. Stephenson et al. [113] demonstrate that transient focal cerebral ischemia results in activation of NF-kappaB in neurons and supports previous observations that neuroprotective antioxidants may inhibit neuronal death by preventing the activation of NF-kappaB. Samraj et al. [114], using system biology tools and experimental SAH models, have identified signal transducer and activator of transcription 3 (STAT3) transcription factor as a possible major regulatory molecule in late cerebral ischemia after subarachnoid hemorrhage.

4.3. Genomic Targets for Autoregulation. miRNAs play important regulatory roles in a variety of cellular functions as well as in several diseases, including stroke. Jeyaseelan et al. [115] showed miR-103 and rno-miR-107 related to transient focal ischemia by middle cerebral artery occlusion. Wang et al. [116] concluded that miR-29b could potentially predict stroke outcomes as a novel circulating biomarker and miR-29b overexpression reduced BBB disruption after ischemic stroke. MicroRNA-210 (miR-210), a master and pleiotropic hypoxia-microRNA, plays multiple roles in brain ischemia. Zeng et al. [117] valuate the correlation of blood miR-210 with clinical findings in acute ischemic stroke and found blood miR-210 is a novel sensitive biomarker for clinical diagnosis and prognosis in acute cerebral ischemia. Yin et al. [118] suggest that miR-497 promotes ischemic neuronal death by negatively regulating antiapoptotic proteins, bcl-2 and bcl-w. We raise the possibility that this pathway may contribute to the pathogenesis of the ischemic brain injury in stroke. Gan et al. [119] demonstrated that hemostatic mechanisms are affected by ischemic stroke and concluded that circulating microRNA-145 has potential as a biomarker for ischemic stroke.

4.4. Big Data Analysis for the CBF Autoregulation. Many data mining methods are used in the field of CBF regulation, such as nonlinear analysis [1], which is often used to analyze the relationship between CBF regulation and other factors. For example, Saleem et al. [120] determine the consistency of dynamic cerebral autoregulation by characterizing the pressure-flow relationships. Mitsis et al. [121] build a nonlinear model of the dynamic effects of arterial pressure and blood gas variations on cerebral blood flow in healthy humans. Tan [122] defined the characteristic relationship between arterial pressure and cerebral flow. Mitsis et al. [123] assessed by examining the dynamic relationship between spontaneous fluctuations of cerebral blood flow and arterial blood pressure under various levels of lower body negative pressure in healthy humans. Other data mining methods are used in the field too. Chiu et al. [124] use time domain cross-correlation analysis of prefiltered mean arterial blood pressure and mean cerebral blood flow velocity which were applied to assess the cerebral autoregulation. Liau et al. [125] use time domain cross-correlation function which was applied to evaluate the relationship between blood pressure and cerebral blood flow velocity signals acquiring from healthy subjects and stroke patients both in supine and head-up tilt positions to evaluate the effect of posture change. Chacón et al. [126] posit a nonlinear model of the CBF autoregulation system through the evaluation of various types of neural networks [127] that have been used in the field of system identification. Chiu et al. [128] use support vector machine to [129] build a classification of dynamic cerebral autoregulation in diabetics with autonomic neuropathy. Liau et al. [130] used chaotic analysis [131] in diabetic autonomic neuropathy and assessed dynamic cerebral autoregulation and suggested that impaired autoregulation would be more chaotic and less predictable.

Although many data mining techniques have been applied to the field, but in some researches, the amount of data is small, which has a great impact on the accuracy of the algorithm or model. At present, big data [132] are very broadly used, and we can use big data technology to improve this problem. There are a lot of big data applications on the field of stroke therapy [133–135], but there is little reference to big data in the cerebral blood flow autoregulation research. There are numerous imaging techniques such as SPECT, CT, MRI, and PET used in the cerebral blood flow research field [136], and as we know, the amount of image data is far more than the other data, and we can use big data technology and its 3V (velocity, volumes, and variety) [132] feature to improve the algorithm or model. Big data can also be used for genetic data analysis to find genomic targets for autoregulation. Also, the computer industry has transitioned into multicore and many-core parallel systems [137] and GPU programming like CUDA [138] are wildly used in speeding up algorithms. We can also employ high performance computing and related data mining algorithm [139–145] to speed up the algorithms of the cerebral blood flow research.

5. Hemodynamic Changes for Therapeutic Strategies of Hemorrhagic Stroke

The central spirit of summarizing CBF autoregulation mechanism is to help reperfusing the ischemic brain region after

hemorrhagic stroke. Compared to the progressive stage of shock, when the compensatory mechanisms begin to fail, blood remains in the capillaries, leading to tissue anoxia, and there are somehow similarity with cerebral congestion under cerebral venous dysfunction. We might get benefit to diagnose the prevalence of cerebral venous dysfunction by monitoring rCBF [146, 147] due to autoregulation failure and blood congestion, $SjvO_2$ [148, 149] due to significantly reduced brain energy consumption, and lactate [150, 151] of internal jugular vein due to sustained anaerobic metabolism in related brain regions. Moreover, carefully monitoring cerebral venous drainage could be applied to prognostic evaluation after brain injury [152].

Current reperfusion treatment barely involves cerebral venous system, including surgical interventions such as aneurysm clipping or coiling [153], which can be used to prevent rebleeding after subarachnoid hemorrhage. Mechanical clot-retrieving devices [154] or chemical agents such as rtPA [155] are used to reopen occluded arteries. However, these treatments might not effectively restore the blood flow in capillary and downstream venous system. Existing data support the use of systemic anticoagulation as an initial therapy in all patients [156], even in the presence of hemorrhage. Interestingly, Simard et al. recently demonstrated that low-dose intravenous heparin infusion after surgery in patients with aneurysmal subarachnoid hemorrhage is safe and beneficial [157]. Furthermore, while controversial, surgical interventions are being used to reverse the possible pathogenesis chronic cerebrospinal venous insufficiency [158]. And improved decompressive craniotomy could alleviate intervention toward cerebral venous system and less brain damage [36, 159]. In sum, carefully monitoring and treating the cerebral venous dysfunction are critical, therefore, to effectively restore optimal cerebrovascular function.

6. Perspective and Conclusion

During the initial stages of hemorrhagic stroke, including intracerebral hemorrhage and subarachnoid hemorrhage, the reflex mechanisms are activated to protect cerebral perfusion, but secondary dysfunction of cerebral flow autoregulation will eventually reduce global cerebral blood flow and the delivery of metabolic substrates, leading to generalized cerebral ischemia, hypoxia, and ultimately, neuronal cell death. Evoked by the concept of vascular neural network, the unveiled neural vascular mechanism gains more and more attentions. Different cell types and molecular and transcriptional modulators may be involved in the neural vascular mechanism for CBF autoregulation. However, current understandings could not explain all the clinical phenomenon and strategies for autoregulation after hemorrhagic stroke.

Recently, application of the cerebral venous dysfunction for hemorrhagic stroke pathophysiology presents an opportunity to identify how cerebral venous system is involved in the prone vulnerability of brain injury and the control of reperfusion. This strategy expands the vascular neural network by improved understanding of cerebral venous system playing a key role in the mechanism of brain injury. However, more research is needed to figure out the time course of cerebral venous changes after hemorrhagic stroke and their implications for the CBF autoregulation. And studies are also needed to investigate the interactions between different kinds of cell types in the CBF autoregulation before and after hemorrhagic stroke. Communications among venous endothelial cells, pericytes, astrocytes, smooth muscle cells, and perivascular neurons should be studied systematically to elucidate how and when these happen. More precised animal models and detective method toward CBF autoregulation are also needed. Ultimately, these efforts should facilitate the development of therapeutic strategies, no matter surgeries or pharmacological agents target the sewerage system of the brain and all kinds of plumbers that serve to build, maintain, and regulate it.

Conflicts of Interest

The authors declare no conflict of interests.

Acknowledgments

This study was funded by the National Natural Science Foundation of China (no. 81501002 to Yujie Chen and no. 81220108009 to Hua Feng), the Major Innovation Project of Southwest Hospital (no. SWH2016ZDCX1011 to Hua Feng), the National Basic Research Program of China (973 Program, no. 2014CB541600 to Hua Feng), and the Basic Science and Advanced Technology Research Project of Chongqing (no. cstc2016jcyjA1730 to Yujie Chen).

References

[1] G. Xi, R. F. Keep, and J. T. Hoff, "Mechanisms of brain injury after intracerebral haemorrhage," *Lancet Neurology*, vol. 5, no. 1, pp. 53–63, 2006.

[2] M. N. Diringer, "Intracerebral hemorrhage: pathophysiology and management," *Critical Care Medicine*, vol. 21, no. 10, pp. 1591–1603, 1993.

[3] S. Prabhakaran and A. M. Naidech, "Ischemic brain injury after intracerebral hemorrhage: a critical review," *Stroke*, vol. 43, no. 8, pp. 2258–2263, 2012.

[4] L. B. Morgenstern, J. C. Hemphill, C. Anderson et al., "Guidelines for the management of spontaneous intracerebral hemorrhage: a guideline for healthcare professionals from the American Heart Association/American Stroke Association," *Stroke*, vol. 41, no. 9, pp. 2108–2129, 2010.

[5] D. W. Kang, M. K. Han, H. J. Kim et al., "New ischemic lesions coexisting with acute intracerebral hemorrhage," *Neurology*, vol. 79, no. 9, pp. 848–855, 2012.

[6] S. M. Gregoire, A. Charidimou, N. Gadapa et al., "Acute ischaemic brain lesions in intracerebral haemorrhage: multicentre cross-sectional magnetic resonance imaging study," *Brain*, vol. 134, Part 8, pp. 2376–2386, 2011.

[7] R. S. Menon, R. E. Burgess, J. J. Wing et al., "Predictors of highly prevalent brain ischemia in intracerebral hemorrhage," *Annals of Neurology*, vol. 71, no. 2, pp. 199–205, 2012.

[8] S. Prabhakaran, R. Gupta, B. Ouyang et al., "Acute brain infarcts after spontaneous intracerebral hemorrhage: a

diffusion-weighted imaging study," *Stroke*, vol. 41, no. 1, pp. 89–94, 2010.

[9] W. T. Kimberly, A. Gilson, N. S. Rost et al., "Silent ischemic infarcts are associated with hemorrhage burden in cerebral amyloid angiopathy," *Neurology*, vol. 72, no. 14, pp. 1230–1235, 2009.

[10] W. C. Ziai, "Hematology and inflammatory signaling of intracerebral hemorrhage," *Stroke*, vol. 44, no. 6, Supplement 1, pp. S74–S78, 2013.

[11] J. Wang, "Preclinical and clinical research on inflammation after intracerebral hemorrhage," *Progress in Neurobiology*, vol. 92, no. 4, pp. 463–477, 2010.

[12] Y. Hua, R. F. Keep, J. T. Hoff, and G. Xi, "Brain injury after intracerebral hemorrhage: the role of thrombin and iron," *Stroke*, vol. 38, no. 2, pp. 759–762, 2007.

[13] G. A. Bateman, "Association between arterial inflow and venous outflow in idiopathic and secondary intracranial hypertension," *Journal of Clinical Neuroscience*, vol. 13, no. 5, pp. 550–556, 2006, discussion 557.

[14] R. L. Macdonald, R. M. Pluta, and J. H. Zhang, "Cerebral vasospasm after subarachnoid hemorrhage: the emerging revolution," *Nature Clinical Practice Neurology*, vol. 3, no. 5, pp. 256–263, 2007.

[15] R. L. Macdonald, N. F. Kassell, S. Mayer et al., "Clazosentan to overcome neurological ischemia and infarction occurring after subarachnoid hemorrhage (CONSCIOUS-1): randomized, double-blind, placebo-controlled phase 2 dose-finding trial," *Stroke*, vol. 39, no. 11, pp. 3015–3021, 2008.

[16] R. L. Macdonald, R. T. Higashida, E. Keller et al., "Clazosentan, an endothelin receptor antagonist, in patients with aneurysmal subarachnoid haemorrhage undergoing surgical clipping: a randomised, double-blind, placebo-controlled phase 3 trial (CONSCIOUS-2)," *Lancet Neurology*, vol. 10, no. 7, pp. 618–625, 2011.

[17] J. Cahill and J. H. Zhang, "Subarachnoid hemorrhage: is it time for a new direction?," *Stroke*, vol. 40, no. 3, Supplement 1, pp. S86–S87, 2009.

[18] F. A. Sehba, R. M. Pluta, and J. H. Zhang, "Metamorphosis of subarachnoid hemorrhage research: from delayed vasospasm to early brain injury," *Molecular Neurobiology*, vol. 43, no. 1, pp. 27–40, 2011.

[19] E. H. Lo and G. A. Rosenberg, "The neurovascular unit in health and disease: introduction," *Stroke*, vol. 40, no. 3, Supplement 1, pp. S2–S3, 2009.

[20] J. H. Zhang, J. Badaut, J. Tang, A. Obenaus, R. Hartman, and W. J. Pearce, "The vascular neural network—a new paradigm in stroke pathophysiology," *Nature Reviews Neurology*, vol. 8, no. 12, pp. 711–716, 2012.

[21] S. Chen, H. Feng, P. Sherchan et al., "Controversies and evolving new mechanisms in subarachnoid hemorrhage," *Progress in Neurobiology*, vol. 115, pp. 64–91, 2014.

[22] J. E. Hardebo, J. Kåhrström, C. Owman, and L. G. Salford, "Endothelin is a potent constrictor of human intracranial arteries and veins," *Blood Vessels*, vol. 26, no. 5, pp. 249–253, 1989.

[23] G. Chen, A. Tariq, J. Ai et al., "Different effects of clazosentan on consequences of subarachnoid hemorrhage in rats," *Brain Research*, vol. 1392, pp. 132–139, 2011.

[24] Z. Dai, X. Deng, Z. Zhang et al., "MRI study of deep cerebral veins after subarachniod hemorrhage in rabbits," *Chinese Journal of Clinical Anatomy*, vol. 30, no. 2, pp. 176–180, 2012.

[25] Z. Zhang, X. Deng, Z. Dai et al., "MRI image of the internal cerebral vein and basilar artery of rabbit following subarachnoid hemorrhage," *Chinese Journal of Clinical Anatomy*, vol. 35, no. 2, pp. 137–140, 2012.

[26] B. L. Sun, C. B. Zheng, M. F. Yang, H. Yuan, S. M. Zhang, and L. X. Wang, "Dynamic alterations of cerebral pial microcirculation during experimental subarachnoid hemorrhage," *Cellular and Molecular Neurobiology*, vol. 29, no. 2, pp. 235–241, 2009.

[27] E. Uhl, J. Lehmberg, H. J. Steiger, and K. Messmer, "Intraoperative detection of early microvasospasm in patients with subarachnoid hemorrhage by using orthogonal polarization spectral imaging," *Neurosurgery*, vol. 52, no. 6, pp. 1307–1315, 2003, disacussion 1315-7.

[28] E. Perkins, H. Kimura, A. D. Parent, and J. H. Zhang, "Evaluation of the microvasculature and cerebral ischemia after experimental subarachnoid hemorrhage in dogs," *Journal of Neurosurgery*, vol. 97, no. 4, pp. 896–904, 2002.

[29] B. Friedrich, F. Müller, S. Feiler, K. Schöller, and N. Plesnila, "Experimental subarachnoid hemorrhage causes early and long-lasting microarterial constriction and microthrombosis: an *in-vivo* microscopy study," *Journal of Cerebral Blood Flow and Metabolism*, vol. 32, no. 3, pp. 447–455, 2012.

[30] M. Ishikawa, G. Kusaka, N. Yamaguchi et al., "Platelet and leukocyte adhesion in the microvasculature at the cerebral surface immediately after subarachnoid hemorrhage," *Neurosurgery*, vol. 64, no. 3, pp. 546–553, 2009, discussion 553-4.

[31] L. K. Bittencourt, F. Palma-Filho, R. C. Domingues, and E. L. Gasparetto, "Subarachnoid hemorrhage in isolated cortical vein thrombosis: are presentation of an unusual condition," *Arquivos de Neuro-Psiquiatria*, vol. 67, no. 4, pp. 1106–1108, 2009.

[32] F. A. Sehba, J. Hou, R. M. Pluta, and J. H. Zhang, "The importance of early brain injury after subarachnoid hemorrhage," *Progress in Neurobiology*, vol. 97, no. 1, pp. 14–37, 2012.

[33] J. Cahill, J. W. Calvert, and J. H. Zhang, "Mechanisms of early brain injury after subarachnoid hemorrhage," *Journal of Cerebral Blood Flow and Metabolism*, vol. 26, no. 11, pp. 1341–1353, 2006.

[34] A. H. Shah and R. J. Komotar, "Pathophysiology of acute hydrocephalus following subarachnoid hemorrhage," *World Neurosurgery*, vol. 80, no. 3-4, pp. 304–306, 2013.

[35] S. Okubo, J. Strahle, R. F. Keep, Y. Hua, and G. Xi, "Subarachnoid hemorrhage-induced hydrocephalus in rats," *Stroke*, vol. 44, no. 2, pp. 547–550, 2013.

[36] A. Csókay, G. Pataki, L. Nagy, and K. Belán, "Vascular tunnel construction in the treatment of severe brain swelling caused by trauma and SAH. (evidence based on intra-operative blood flow measure)," *Neurological Research*, vol. 24, no. 2, pp. 157–160, 2002.

[37] H. El Otmani, F. Moutaouakil, H. Fadel, and I. Slassi, "Subarachnoid hemorrhage induced by cerebral venous thrombosis," *Journal des Maladies Vasculaires*, vol. 37, no. 6, pp. 323–325, 2012.

[38] Y. Kato, H. Takeda, D. Furuya et al., "Subarachnoid hemorrhage as the initial presentation of cerebral venous thrombosis," *Internal Medicine*, vol. 49, no. 5, pp. 467–470, 2010.

[39] Y. Benabu, L. Mark, S. Daniel, and R. Glikstein, "Cerebral venous thrombosis presenting with subarachnoid

hemorrhage: case report and review," *The American Journal of Emergency Medicine*, vol. 27, no. 1, pp. 96–106, 2009.

[40] R. Shukla, P. Vinod, S. Prakash, R. V. Phadke, and R. K. Gupta, "Subarachnoid haemorrhage as a presentation of cerebral venous sinus thrombosis," *The Journal of the Association of Physicians of India*, vol. 54, pp. 42–44, 2006.

[41] A. Shad, T. J. Rourke, A. Hamidian Jahromi, and A. L. Green, "Straight sinus stenosis as a proposed cause of perimesencephalic non-aneurysmal haemorrhage," *Journal of Clinical Neuroscience*, vol. 15, no. 7, pp. 839–841, 2008.

[42] J. Lee, E. M. Koh, C. S. Chung et al., "Underlying venous pathology causing perimesencephalic subarachnoid hemorrhage," *The Canadian Journal of Neurological Sciences*, vol. 36, no. 5, pp. 638–642, 2009.

[43] M. S. Sangra, E. Teasdale, M. A. Siddiqui, and K. W. Lindsay, "Perimesencephalic nonaneurysmal subarachnoid hemorrhage caused by jugular venous occlusion: case report," *Neurosurgery*, vol. 63, no. 6, pp. E1202–E1203, 2008, discussion E1203.

[44] M. S. Mathews, D. Brown, and M. Brant-Zawadzki, "Perimesencephalic nonaneurysmal hemorrhage associated with vein of Galen stenosis," *Neurology*, vol. 70, 24 Part 2, pp. 2410-2411, 2008.

[45] J. N. Song, H. Chen, M. Zhang, Y. L. Zhao, and X. D. Ma, "Dynamic change in cerebral microcirculation and focal cerebral metabolism in experimental subarachnoid hemorrhage in rabbits," *Metabolic Brain Disease*, vol. 28, no. 1, pp. 33–43, 2013.

[46] Y. Kawamura, O. Narumi, M. Chin, and S. Yamagata, "Variant deep cerebral venous drainage in idiopathic subarachnoid hemorrhage," *Neurologia Medico-Chirurgica (Tokyo)*, vol. 51, no. 2, pp. 97–100, 2011.

[47] H. Yamakawa, N. Ohe, H. Yano, S. Yoshimura, and T. Iwama, "Venous drainage patterns in perimesencephalic nonaneurysmal subarachnoid hemorrhage," *Clinical Neurology and Neurosurgery*, vol. 110, no. 6, pp. 587–591, 2008.

[48] J. F. Alén, A. Lagares, J. Campollo et al., "Idiopathic subarachnoid hemorrhage and venous drainage: are they related?," *Neurosurgery*, vol. 63, no. 6, pp. 1106–1111, 2008, discussion 1111-2.

[49] I. C. van der Schaaf, B. K. Velthuis, A. Gouw, and G. J. Rinkel, "Venous drainage in perimesencephalic hemorrhage," *Stroke*, vol. 35, no. 7, pp. 1614–1618, 2004.

[50] A. Hashiguchi, C. Mimata, H. Ichimura, M. Morioka, and J. Kuratsu, "Venous aneurysm development associated with a dural arteriovenous fistula of the anterior cranial fossa with devastating hemorrhage—case report," *Neurologia Medico-Chirurgica (Tokyo)*, vol. 47, no. 2, pp. 70–73, 2007.

[51] T. Matsuyama, K. Okuchi, T. Seki, T. Higuchi, and Y. Murao, "Perimesencephalic nonaneurysmal subarachnoid hemorrhage caused by physical exertion," *Neurologia Medico-Chirurgica (Tokyo)*, vol. 46, no. 6, pp. 277–281, 2006, discussion 281-2.

[52] G. Faraco and C. Iadecola, "Hypertension: a harbinger of stroke and dementia," *Hypertension*, vol. 62, no. 5, pp. 810–817, 2013.

[53] M. A. Fitzpatrick, A. L. Hinderliter, B. M. Egan, and S. Julius, "Decreased venous distensibility and reduced renin responsiveness in hypertension," *Hypertension*, vol. 8, 6 Part 2, pp. II36–II43, 1986.

[54] N. Ito, A. Takeshita, S. Higuchi, and M. Nakamura, "Venous abnormality in normotensive young men with a family history of hypertension," *Hypertension*, vol. 8, no. 2, pp. 142–146, 1986.

[55] S. Spector, A. Ooshima, K. Iwatsuki, G. Fuller, G. Cardinale, and S. Udenfriend, "Increased vascular collagen biosynthesis by hypertension and reversal by antihypertensive drugs," *Blood Vessels*, vol. 15, no. 1–3, pp. 176–182, 1978.

[56] W. R. Brown and C. R. Thore, "Perivascular fibrosis in multiple sclerosis lesions," *Brain Pathology*, vol. 21, no. 3, p. 355, 2011.

[57] D. D. Heistad and G. L. Baumbach, "Cerebral vascular changes during chronic hypertension: good guys and bad guys," *Journal of Hypertension Supplement*, vol. 10, no. 7, pp. S71–S75, 1992.

[58] H. Al-Sarraf and L. Philip, "Effect of hypertension on the integrity of blood brain and blood CSF barriers, cerebral blood flow and CSF secretion in the rat," *Brain Research*, vol. 975, no. 1-2, pp. 179–188, 2003.

[59] W. G. Mayhan, "Role of activation of bradykinin B_2 receptors in disruption of the blood-brain barrier during acute hypertension," *Brain Research*, vol. 738, no. 2, pp. 337–341, 1996.

[60] A. H. Werber and M. C. Fitch-Burke, "Pial venous pressure and acute hypertensive disruption of the blood-brain barrier in spontaneous and renal hypertension," *Brain Research*, vol. 515, no. 1-2, pp. 235–240, 1990.

[61] W. G. Mayhan, F. M. Faraci, J. L. Siems, and D. D. Heistad, "Role of molecular charge in disruption of the blood-brain barrier during acute hypertension," *Circulation Research*, vol. 64, no. 4, pp. 658–664, 1989.

[62] S. F. Rodrigues, S. A. Vital, and D. N. Granger, "Mild hypercholesterolemia blunts the proinflammatory and prothrombotic effects of hypertension on the cerebral microcirculation," *Journal of Cerebral Blood Flow and Metabolism*, vol. 33, no. 4, pp. 483–489, 2013.

[63] T. J. Roberts, A. C. Chapman, and M. J. Cipolla, "PPAR-γ agonist rosiglitazone reverses increased cerebral venous hydraulic conductivity during hypertension," *American Journal of Physiology Heart and Circulatory Physiology*, vol. 297, no. 4, pp. H1347–H1353, 2009.

[64] T. M. Ripp, I. A. Astanina, I. N. Vorozhtsova, V. F. Mordovin, and R. S. Karpov, "Function of the brain venous system and a 24-h profile of arterial pressure in hypertensive patients," *Terapevticheskiĭ Arkhiv*, vol. 77, no. 12, pp. 22–25, 2005.

[65] D. J. Langer, T. M. Lasner, R. W. Hurst, E. S. Flamm, E. L. Zager, and J. T. King Jr, "Hypertension, small size, and deep venous drainage are associated with risk of hemorrhagic presentation of cerebral arteriovenous malformations," *Neurosurgery*, vol. 42, no. 3, pp. 481–489, 1998.

[66] O. Z. Chi, H. M. Wei, J. Tse, S. L. Klein, and H. R. Weiss, "Cerebral microregional oxygen balance during chronic versus acute hypertension in middle cerebral artery occluded rats," *Anesthesia and Analgesia*, vol. 82, no. 3, pp. 587–592, 1996.

[67] C. J. Nolan, P. Damm, and M. Prentki, "Type 2 diabetes across generations: from pathophysiology to prevention and management," *Lancet*, vol. 378, no. 9786, pp. 169–181, 2011.

[68] P. C. Deedwania, "Diabetes is a vascular disease: the role of endothelial dysfunction in pathophysiology of cardiovascular disease in diabetes," *Cardiology Clinics*, vol. 22, no. 4, pp. 505–509, 2004.

[69] M. A. Creager, T. F. Lüscher, F. Cosentino, and J. A. Beckman, "Diabetes and vascular disease: pathophysiology, clinical consequences, and medical therapy: part I," *Circulation*, vol. 108, no. 12, pp. 1527–1532, 2003.

[70] A. Mafrici and R. Proietti, "Atherothrombosis in patients with type 2 diabetes mellitus: an overview of pathophysiology," *Giornale Italiano di Cardiologia (Rome)*, vol. 11, no. 6, pp. 467–477, 2010.

[71] L. S. Usdan, K. W. Choong, and M. E. McDonnell, "Type 2 diabetes mellitus manifesting with a cerebral vein thrombosis and ketoacidosis," *Endocrine Practice*, vol. 13, no. 6, pp. 687–690, 2007.

[72] M. J. Sasiadek, D. Sosnowska-Pacuszko, M. Zielinska, and T. Turek, "Cerebral venous thrombosis as a first presentation of diabetes," *Pediatric Neurology*, vol. 35, no. 2, pp. 135–138, 2006.

[73] A. P. Carlotti, C. St George-Hyslop, A. M. Guerguerian, D. Bohn, K. S. Kamel, and M. Halperin, "Occult risk factor for the development of cerebral edema in children with diabetic ketoacidosis: possible role for stomach emptying," *Pediatric Diabetes*, vol. 10, no. 8, pp. 522–533, 2009.

[74] I. Linfante and M. J. Cipolla, "Improving reperfusion therapies in the era of mechanical thrombectomy," *Translational Stroke Research*, vol. 7, no. 4, pp. 294–302, 2016.

[75] F. Shimizu, Y. Sano, T. Maeda et al., "Peripheral nerve pericytes originating from the blood-nerve barrier expresses tight junctional molecules and transporters as barrier-forming cells," *Journal of Cellular Physiology*, vol. 217, no. 2, pp. 388–399, 2008.

[76] Y. Zhan, P. R. Krafft, T. Lekic et al., "Imatinib preserves blood-brain barrier integrity following experimental subarachnoid hemorrhage in rats," *Journal of Neuroscience Research*, vol. 93, no. 1, pp. 94–103, 2015.

[77] J. Yan, A. Manaenko, S. Chen et al., "Role of SCH79797 in maintaining vascular integrity in rat model of subarachnoid hemorrhage," *Stroke*, vol. 44, no. 5, pp. 1410–1417, 2013.

[78] O. Altay, H. Suzuki, Y. Hasegawa et al., "Isoflurane attenuates blood-brain barrier disruption in ipsilateral hemisphere after subarachnoid hemorrhage in mice," *Stroke*, vol. 43, no. 9, pp. 2513–2516, 2012.

[79] H. Suzuki, Y. Hasegawa, K. Kanamaru, and J. H. Zhang, "Mechanisms of osteopontin-induced stabilization of blood-brain barrier disruption after subarachnoid hemorrhage in rats," *Stroke*, vol. 41, no. 8, pp. 1783–1790, 2010.

[80] Y. Chen, Y. Zhang, J. Tang et al., "Norrin protected blood-brain barrier via frizzled-4/β-catenin pathway after subarachnoid hemorrhage in rats," *Stroke*, vol. 46, no. 2, pp. 529–536, 2015.

[81] F. M. O'Farrell and D. Attwell, "A role for pericytes in coronary no-reflow," *Nature Reviews. Cardiology*, vol. 11, no. 7, pp. 427–432, 2014.

[82] D. M. Greif and A. Eichmann, "Vascular biology: brain vessels squeezed to death," *Nature*, vol. 508, no. 7494, pp. 50-51, 2014.

[83] H. Ohkuma, K. Itoh, S. Shibata, and S. Suzuki, "Morphological changes of intraparenchymal arterioles after experimental subarachnoid hemorrhage in dogs," *Neurosurgery*, vol. 41, no. 1, pp. 230–235, 1997, discussion 235-6.

[84] H. Johshita, N. F. Kassell, T. Sasaki, and H. Ogawa, "Impaired capillary perfusion and brain edema following experimental subarachnoid hemorrhage: a morphometric study," *Journal of Neurosurgery*, vol. 73, no. 3, pp. 410–417, 1990.

[85] Q. Li, Y. Chen, B. Li et al., "Hemoglobin induced NO/cGMP suppression deteriorate microcirculation via pericyte phenotype transformation after subarachnoid hemorrhage in rats," *Scientific Reports*, vol. 6, article 22070, 2016.

[86] I. Spokoyny, R. Raman, K. Ernstrom et al., "Pooled assessment of computed tomography interpretation by vascular neurologists in the STRokE DOC telestroke network," *Journal of Stroke and Cerebrovascular Diseases*, vol. 23, no. 3, pp. 511–515, 2014.

[87] B. Obermeier, R. Daneman, and R. M. Ransohoff, "Development, maintenance and disruption of the blood-brain barrier," *Nature Medicine*, vol. 19, no. 12, pp. 1584–1596, 2013.

[88] M. Hagedorn, M. Balke, A. Schmidt et al., "VEGF coordinates interaction of pericytes and endothelial cells during vasculogenesis and experimental angiogenesis," *Developmental Dynamics*, vol. 230, no. 1, pp. 23–33, 2004.

[89] S. Sinha, M. H. Hoofnagle, P. A. Kingston, M. E. McCanna, and G. K. Owens, "Transforming growth factor-β1 signaling contributes to development of smooth muscle cells from embryonic stem cells," *American Journal of Physiology. Cell Physiology*, vol. 287, no. 6, pp. C1560–C1568, 2004.

[90] K. Gaengel, G. Genové, A. Armulik, and C. Betsholtz, "Endothelial-mural cell signaling in vascular development and angiogenesis," *Arteriosclerosis, Thrombosis, and Vascular Biology*, vol. 29, no. 5, pp. 630–638, 2009.

[91] W. Cai, H. Liu, J. Zhao et al., "Pericytes in brain injury and repair after ischemic stroke," *Translational Stroke Research*, vol. 8, no. 2, pp. 107–121, 2016.

[92] M. Kloc, J. Z. Kubiak, X. C. Li, and R. M. Ghobrial, "Pericytes, microvasular dysfunction, and chronic rejection," *Transplantation*, vol. 99, no. 4, pp. 658–667, 2015.

[93] J. F. Arboleda-Velasquez, C. N. Valdez, C. K. Marko, and P. A. D'Amore, "From pathobiology to the targeting of pericytes for the treatment of diabetic retinopathy," *Current Diabetes Reports*, vol. 15, no. 2, p. 573, 2015.

[94] O. V. Glinskii, V. H. Huxley, V. V. Glinskii, L. J. Rubin, and V. V. Glinsky, "Pulsed estrogen therapy prevents post-OVX porcine dura mater microvascular network weakening via a PDGF-BB-dependent mechanism," *PLoS One*, vol. 8, no. 12, article e82900, 2013.

[95] F. Contard, A. Sabri, M. Glukhova et al., "Arterial smooth muscle cell phenotype in stroke-prone spontaneously hypertensive rats," *Hypertension*, vol. 22, no. 5, pp. 665–676, 1993.

[96] J. Wu, Y. Zhang, P. Yang et al., "Recombinant osteopontin stabilizes smooth muscle cell phenotype via integrin receptor/integrin-linked kinase/Rac-1 pathway after subarachnoid hemorrhage in rats," *Stroke*, vol. 47, no. 5, pp. 1319–1327, 2016.

[97] M. H. Lee, B. J. Kwon, H. J. Seo et al., "Resveratrol inhibits phenotype modulation by platelet derived growth factor-bb in rat aortic smooth muscle cells," *Oxidative Medicine and Cellular Longevity*, vol. 2014, Article ID 572430, 9 pages, 2014.

[98] T. Miyata, H. Iizasa, Y. Sai, J. Fujii, T. Terasaki, and E. Nakashima, "Platelet-derived growth factor-BB (PDGF-BB) induces differentiation of bone marrow endothelial progenitor cell-derived cell line TR-BME2 into mural cells, and changes the phenotype," *Journal of Cellular Physiology*, vol. 204, no. 3, pp. 948–955, 2005.

[99] P. Munot, D. E. Saunders, D. M. Milewicz et al., "A novel distinctive cerebrovascular phenotype is associated with heterozygous Arg179 *ACTA2* mutations," *Brain*, vol. 135, no. Pt 8, pp. 2506–2514, 2012.

[100] C. K. Griswold, "A model of the physiological basis of a multivariate phenotype that is mediated by Ca^{2+} signaling and controlled by ryanodine receptor composition," *Journal of Theoretical Biology*, vol. 282, no. 1, pp. 14–22, 2011.

[101] Y. Chimori, K. Hayashi, K. Kimura et al., "Phenotype-dependent expression of cadherin 6B in vascular and visceral smooth muscle cells," *FEBS Letters*, vol. 469, no. 1, pp. 67–71, 2000.

[102] N. Henninger and M. Fisher, "Extending the time window for endovascular and pharmacological reperfusion," *Translational Stroke Research*, vol. 7, no. 4, pp. 284–293, 2016.

[103] L. Chazalviel, B. Haelewyn, M. Degoulet et al., "Hyperbaric oxygen increases tissue-plasminogen activator-induced thrombolysis *in vitro*, and reduces ischemic brain damage and edema in rats subjected to thromboembolic brain ischemia," *Medical Gas Research*, vol. 6, no. 2, pp. 64–69, 2016.

[104] B. Ovbiagele, J. L. Saver, S. Starkman et al., "Statin enhancement of collateralization in acute stroke," *Neurology*, vol. 68, no. 24, pp. 2129–2131, 2007.

[105] J. L. Lucitti, N. J. Tarte, and J. E. Faber, "Chloride intracellular channel 4 is required for maturation of the cerebral collateral circulation," *American Journal of Physiology Heart and Circulatory Physiology*, vol. 309, no. 7, pp. H1141–H1150, 2015.

[106] D. Chalothorn, H. Zhang, J. E. Smith, J. C. Edwards, and J. E. Faber, "Chloride intracellular channel-4 is a determinant of native collateral formation in skeletal muscle and brain," *Circulation Research*, vol. 105, no. 1, pp. 89–98, 2009.

[107] M. R. Harrigan, S. R. Ennis, S. E. Sullivan, and R. F. Keep, "Effects of intraventricular infusion of vascular endothelial growth factor on cerebral blood flow, edema, and infarct volume," *Acta Neurochirurgica*, vol. 145, no. 1, pp. 49–53, 2003.

[108] M. R. Harrigan, S. R. Ennis, T. Masada, and R. F. Keep, "Intraventricular infusion of vascular endothelial growth factor promotes cerebral angiogenesis with minimal brain edema," *Neurosurgery*, vol. 50, no. 3, pp. 589–598, 2002.

[109] T. Shimazu, I. Inoue, N. Araki et al., "A peroxisome proliferator-activated receptor-γ agonist reduces infarct size in transient but not in permanent ischemia," *Stroke*, vol. 36, no. 2, pp. 353–359, 2005.

[110] J. Culman, M. Nguyen-Ngoc, T. Glatz, P. Gohlke, T. Herdegen, and Y. Zhao, "Treatment of rats with pioglitazone in the reperfusion phase of focal cerebral ischemia: a preclinical stroke trial," *Experimental Neurology*, vol. 238, no. 2, pp. 243–253, 2012.

[111] M. A. Hill, Z. Sun, L. Martinez-Lemus, and G. A. Meininger, "New technologies for dissecting the arteriolar myogenic response," *Trends in Pharmacological Sciences*, vol. 28, no. 7, pp. 308–315, 2007.

[112] C. Howarth, "The contribution of astrocytes to the regulation of cerebral blood flow," *Frontiers in Neuroscience*, vol. 8, no. 8, p. 103, 2014.

[113] D. Stephenson, T. Yin, E. B. Smalstig et al., "Transcription factor nuclear factor-kappa B is activated in neurons after focal cerebral ischemia," *Journal of Cerebral Blood Flow & Metabolism*, vol. 20, no. 3, pp. 592–603, 2000.

[114] A. K. Samraj, A. H. Müller, A. S. Grell, and L. Edvinsson, "Role of unphosphorylated transcription factor STAT3 in late cerebral ischemia after subarachnoid hemorrhage," *Journal of Cerebral Blood Flow & Metabolism*, vol. 34, no. 5, pp. 759–763, 2014.

[115] K. Jeyaseelan, K. Y. Lim, and A. Armugam, "MicroRNA expression in the blood and brain of rats subjected to transient focal ischemia by middle cerebral artery occlusion," *Stroke*, vol. 39, no. 3, pp. 959–966, 2008.

[116] Y. Wang, J. Huang, Y. Ma et al., "MicroRNA-29b is a therapeutic target in cerebral ischemia associated with aquaporin 4," *Journal of Cerebral Blood Flow & Metabolism*, vol. 35, no. 12, 2015.

[117] L. Zeng, J. Liu, Y. Wang et al., "MicroRNA-210 as a novel blood biomarker in acute cerebral ischemia," *Frontiers in Bioscience*, vol. 3, no. 4, p. 1265, 2011.

[118] K. J. Yin, Z. Deng, H. Huang et al., "miR-497 regulates neuronal death in mouse brain after transient focal cerebral ischemia," *Neurobiology of Disease*, vol. 38, no. 1, p. 17, 2010.

[119] C. S. Gan, C. W. Wang, and K. S. Tan, "Circulatory microRNA-145 expression is increased in cerebral ischemia," *Genetics & Molecular Research*, vol. 11, no. 1, p. 147, 2012.

[120] S. Saleem, P. D. Teal, W. B. Kleijn, T. O'Donnell, T. Witter, and Y. C. Tzeng, "Non-linear characterisation of cerebral pressure-flow dynamics in humans," *PLoS One*, vol. 10, no. 9, article e0139470, 2015.

[121] G. D. Mitsis, P. N. Ainslie, M. J. Poulin, P. A. Robbins, and V. Z. Marmarelis, *Nonlinear Modeling of the Dynamic Effects of Arterial Pressure and Blood Gas Variations on Cerebral Blood Flow in Healthy Humans*, Springer, United States of America, 2004.

[122] C. O. Tan, "Defining the characteristic relationship between arterial pressure and cerebral flow," *Journal of Applied Physiology*, vol. 113, no. 8, pp. 1194–1200, 2012.

[123] G. D. Mitsis, A. Mahalingam, R. Zhang, B. D. Levine, and V. Z. Marmarelis, "Nonlinear analysis of dynamic cerebral autoregulation in humans under orthostatic stress," in *Engineering in Medicine and Biology Society, 2003. Proceedings of the 25th Annual International Conference of the IEEE*, Cancun, Mexico, 2003.

[124] C. C. Chiu and S. J. Yeh, "Assessment of cerebral autoregulation using time-domain cross-correlation analysis," *Computers in Biology & Medicine*, vol. 31, no. 6, p. 471, 2001.

[125] B. Y. Liau, S. J. Yeh, and C. C. Chiu, "Using cross-correlation function to assess dynamic cerebral autoregulation in response to posture changes for stroke patients," *Computing in Cardiology*, vol. 37, no. 23, pp. 605–608, 2011.

[126] M. Chacón, C. Blanco, R. Panerai, and D. Evans, "Nonlinear modeling of dynamic cerebral autoregulation using recurrent neural networks," in *10th Iberoamerican Congress on Pattern Recognition, CIARP 2005*, Havana, Cuba, November 15–18, 2005.

[127] H. Lu, R. Setiono, and H. Liu, "Effective data mining using neural networks," *IEEE Transactions on Knowledge & Data Engineering*, vol. 8, no. 6, pp. 957–961, 1996.

[128] C. C. Chiu, Y. H. Hu, S. J. Yeh, and D. Y. Chou, "Classification of dynamic cerebral autoregulation in diabetics with autonomic neuropathy using support vector machine," in *International Conference on Bioinformatics & Computational*

Biology, BIOCOMP 2009, vol. 2, Las Vegas Nevada, United States of America, July 13–16, 2009.

[129] G. M. Fung, *Machine Learning and Data Mining Via Mathematical Programming-Based Support Vector Machines*, The University of Wisconsin-Madison, Madison, WI, USA, 2003.

[130] B. Y. Liau, S. J. Yeh, C. C. Chiu, and Y. C. Tsai, "Dynamic cerebral autoregulation assessment using chaotic analysis in diabetic autonomic neuropathy," *Medical & Biological Engineering & Computing*, vol. 46, no. 1, pp. 1–9, 2008.

[131] G. Qi, G. Chen, S. Du, Z. Chen, and Z. Yuan, "Analysis of a new chaotic system," *Physica A Statistical Mechanics & Its Applications*, vol. 352, no. 2–4, pp. 295–308, 2005.

[132] A. Mcafee and E. Brynjolfsson, "Big data: the management revolution," *Harvard Business Review*, vol. 90, no. 10, p. 60, 2012.

[133] D. S. Liebeskind, "Big and bigger data in endovascular stroke therapy," *Expert Review of Neurotherapeutics*, vol. 15, pp. 335–337, 2015.

[134] K. Nishimura, "Big data visualization of acute stroke care practices using a nationwide neurosurgeon survey," *Japanese Journal of Neurosurgery*, vol. 24, no. 10, pp. 676–683, 2015.

[135] A. Nishimura, K. Nishimura, A. Kada, K. Iihara, and J-ASPECT Study GROUP, "Status and future perspectives of utilizing big data in neurosurgical and stroke research," *Neurologia Medico-Chirurgica*, vol. 56, no. 11, pp. 655–663, 2016.

[136] N. P. Saeed, N. Pater, and T. G. Robinson, "Comparative overview of imaging techniques in stroke; measuring cerebral blood flow and estimating cerebral autoregulation," *International Journal of Stroke*, vol. 7, pp. 61–61, 2012.

[137] M. Modat, G. R. Ridgway, Z. A. Taylor et al., "Fast free-form deformation using graphics processing units," *Computer Methods & Programs in Biomedicine*, vol. 98, no. 3, pp. 278–284, 2010.

[138] S. Z. Ueng, M. Lathara, S. S. Baghsorkhi, and W. H. Wen-mei, "CUDA-lite: reducing GPU programming complexity," *Lecture Notes in Computer Science*, vol. 8, pp. 1–15, 2008.

[139] B. Jiang, W. Dai, A. Khaliq, M. Carey, X. Zhou, and L. Zhang, "Novel 3D GPU based numerical parallel diffusion algorithms in cylindrical coordinates for health care simulation," *Mathematics and Computers in Simulation*, vol. 109, pp. 1–19, 2015.

[140] B. Jiang, A. Struthers, Z. Sun et al., "Employing graphics processing unit technology, alternating direction implicit method and domain decomposition to speed up the numerical diffusion solver for the biomedical engineering research," *International Journal for Numerical Methods in Biomedical Engineering*, vol. 27, no. 11, pp. 1829–1849, 2011.

[141] H. Peng, T. Peng, J. Wen et al., "Characterization of p38 MAPK isoforms for drug resistance study using systems biology approach," *Bioinformatics*, vol. 30, no. 13, pp. 1899–1907, 2014.

[142] L. Zhang, B. Jiang, Y. Wu et al., "Developing a multiscale, multi-resolution agent-based brain tumor model by graphics processing units," *Theoretical Biology & Medical Modelling*, vol. 8, p. 46, 2011.

[143] L. Zhang, M. Qiao, H. Gao et al., "Investigation of mechanism of bone regeneration in a porous biodegradable calcium phosphate (CaP) scaffold by a combination of a multi-scale agent-based model and experimental optimization/validation," *Nanoscale*, vol. 8, no. 31, p. 14877, 2016.

[144] L. Zhang, Y. Xue, B. Jiang et al., "Multiscale agent-based modelling of ovarian cancer progression under the stimulation of the STAT 3 pathway," *International Journal of Data Mining and Bioinformatics*, vol. 9, no. 3, pp. 235–253, 2014.

[145] L. Zhang and S. Zhang, "Using game theory to investigate the epigenetic control mechanisms of embryo development: comment on: "epigenetic game theory: how to compute the epigenetic control of maternal-to-zygotic transition" by Qian Wang et al," *Physics of Life Reviews*, vol. 20, pp. 140–142, 2017.

[146] M. Jaeger, M. Soehle, M. U. Schuhmann, D. Winkler, and J. Meixensberger, "Correlation of continuously monitored regional cerebral blood flow and brain tissue oxygen," *Acta Neurochirurgica*, vol. 147, no. 1, pp. 51–56, 2005, discussion 56.

[147] P. J. Sioutos, J. A. Orozco, L. P. Carter, M. E. Weinand, A. J. Hamilton, and F. C. Williams, "Continuous regional cerebral cortical blood flow monitoring in head-injured patients," *Neurosurgery*, vol. 36, no. 5, pp. 943–949, 1995, discussion 949-50.

[148] C. S. Robertson, S. P. Gopinath, J. C. Goodman, C. F. Contant, A. B. Valadka, and R. K. Narayan, "SjvO2 monitoring in head-injured patients," *Journal of Neurotrauma*, vol. 12, no. 5, pp. 891–896, 1995.

[149] M. Sheinberg, M. J. Kanter, C. S. Robertson, C. F. Contant, R. K. Narayan, and R. G. Grossman, "Continuous monitoring of jugular venous oxygen saturation in head-injured patients," *Journal of Neurosurgery*, vol. 76, no. 2, pp. 212–217, 1992.

[150] G. K. Barcelos, Y. Tholance, S. Grousson et al., "Outcome of poor-grade subarachnoid hemorrhage as determined by biomarkers of glucose cerebral metabolism," *Neurocritical Care*, vol. 18, no. 2, pp. 234–244, 2013.

[151] K. Ide and N. H. Secher, "Cerebral blood flow and metabolism during exercise," *Progress in Neurobiology*, vol. 61, no. 4, pp. 397–414, 2000.

[152] R. Parthasarathy, M. Kate, J. L. Rempel et al., "Prognostic evaluation based on cortical vein score difference in stroke," *Stroke*, vol. 44, no. 10, pp. 2748–2754, 2013.

[153] E. S. Connolly Jr, A. A. Rabinstein, J. R. Carhuapoma et al., "Guidelines for the management of aneurysmal subarachnoid hemorrhage: a guideline for healthcare professionals from the American Heart Association/American Stroke Association," *Stroke*, vol. 43, no. 6, pp. 1711–1737, 2012.

[154] W. S. Smith, "Technology insight: recanalization with drugs and devices during acute ischemic stroke," *Nature Clinical Practice Neurology*, vol. 3, no. 1, pp. 45–53, 2007.

[155] P. A. Ringleb, P. D. Schellinger, C. Schranz, and W. Hacke, "Thrombolytic therapy within 3 to 6 hours after onset of ischemic stroke: useful or harmful?," *Stroke*, vol. 33, no. 5, pp. 1437–1441, 2002.

[156] R. Medel, S. J. Monteith, R. W. Crowley, and A. S. Dumont, "A review of therapeutic strategies for the management of cerebral venous sinus thrombosis," *Neurosurgical Focus*, vol. 27, no. 5, article E6, 2009.

[157] J. M. Simard, E. F. Aldrich, D. Schreibman, R. F. James, A. Polifka, and N. Beaty, "Low-dose intravenous heparin infusion in patients with aneurysmal subarachnoid

hemorrhage: a preliminary assessment," *Journal of Neurosurgery*, vol. 119, no. 6, pp. 1611–1619, 2013.

[158] P. Zamboni, A. Bertolotto, P. Boldrini et al., "Efficacy and safety of venous angioplasty of the extracranial veins for multiple sclerosis. Brave dreams study (brain venous drainage exploited against multiple sclerosis): study protocol for a randomized controlled trial," *Trials*, vol. 13, p. 183, 2012.

[159] R. Burger, D. Duncker, N. Uzma, and V. Rohde, "Decompressive craniotomy: durotomy instead of duroplasty to reduce prolonged ICP elevation," *Acta Neurochirurgica Supplement*, vol. 102, pp. 93–97, 2008.

Hindawi
Neural Plasticity
Volume 2017, Article ID 2361675, 11 pages
https://doi.org/10.1155/2017/2361675

Research Article

A Hypothalamic Leptin-Glutamate Interaction in the Regulation of Sympathetic Nerve Activity

Hong Zheng,[1] Xuefei Liu,[1] Yulong Li,[2] and Kaushik P. Patel[1]

[1]*Department of Cellular and Integrative Physiology, University of Nebraska Medical Center, Omaha, NE 68198-5850, USA*
[2]*Department of Emergency Medicine, University of Nebraska Medical Center, Omaha, NE 68198-5850, USA*

Correspondence should be addressed to Hong Zheng; hzheng@unmc.edu

Received 16 March 2017; Revised 24 May 2017; Accepted 30 May 2017; Published 3 August 2017

Academic Editor: J. Michael Wyss

Accumulated evidence indicates that obesity-induced type 2 diabetes (T2D) is associated with enhanced sympathetic activation. The present study was conducted to investigate the role for leptin-glutamate signaling within the hypothalamus in regulating sympathetic nerve activity. In anesthetized rats, microinjections of leptin (5 ng ~ 100 ng) into the arcuate nucleus (ARCN) and paraventricular nucleus (PVN) induced increases in renal sympathetic nerve activity (RSNA), blood pressure (BP), and heart rate (HR). Prior microinjections of NMDA receptor antagonist AP5 (16 pmol) into the ARCN or PVN reduced leptin-induced increases in RSNA, BP, and HR in both ARCN and PVN. Knockdown of a leptin receptor with siRNA inhibited NMDA-induced increases in RSNA, BP, and HR in the ARCN but not in the PVN. Confocal calcium imaging in the neuronal NG108 and astrocytic C6 cells demonstrated that preincubation with leptin induced an increase in intracellular calcium green fluorescence when the cells were challenged with glutamate. In high-fat diet and low-dose streptozotocin-induced T2D rats, we found that leptin receptor and NMDA NR_1 receptor expressions in the ARCN and PVN were significantly increased. In conclusion, these studies provide evidence that within the hypothalamic nuclei, leptin-glutamate signaling regulates the sympathetic activation. This may contribute to the sympathoexcitation commonly observed in obesity-related T2D.

1. Introduction

Overweight and obesity are a growing "worldwide epidemic problem." The prevalence of type 2 diabetes (T2D) has significantly increased with the prevalence of obesity. Obesity accompanying T2D is known to be closely linked with insulin resistance and elevated sympathetic nervous system activity [1, 2]. Increased sympathetic nerve activity contributes to the onset and maintenance of cardiovascular complications such as hypertension and heart failure in T2D [3]. Various types of autonomic abnormalities in relation to the cardiovascular system have been observed in diabetic patients as well as in animal models of diabetes [4, 5]. The myriad of mechanisms linking diabetes with sympathetic overactivation is complex, multifaceted, and not clearly understood. The central nervous system plays a very important role in regulating sympathetic activation and contributing to the altered neurohumoral drive during diabetes [6–9]. The activation of the sympathetic nervous system through the central action of the adipokine leptin has been suggested as a possible major mechanism that contributes to the development of hypertension and heart failure leading to cardiovascular morbidity and mortality in T2D [8, 9].

The factors that cause the elevation in sympathetic drive are the critical keys to understanding the etiology of obesity-related diabetes. Among them, leptin is an adipocyte-derived hormone that promotes weight loss by reducing appetite and by increasing energy expenditure through sympathetic stimulation of thermogenic tissue [10]. Leptin is a 16 kDa protein released by fat cells into the blood, is able to cross the blood brain barrier to interact with its receptors in various hypothalamic nuclei to affect feeding and thermogenesis, and also induces sympathetic activation to kidneys, hindlimb vasculature, and the adrenal glands [3]. Central administration of leptin has been shown to increase renal sympathetic nerve activity (RSNA), mean arterial pressure (MAP), and heart

rate (HR) in conscious rabbits [11]. Elevated levels of circulating leptin associated with obesity may contribute to the development of enhanced sympathetic outflow in T2D.

The leptin receptor is expressed in several hypothalamic nuclei including the arcuate nucleus (ARCN), paraventricular nucleus (PVN), and ventromedial hypothalamus [12]. Several neurotransmitters and neuropeptides, such as glutamate, GABA, and neuropeptide Y, have emerged as principal mediators of leptin-induced action within the hypothalamus [12]. These neurotransmitters and neuropeptides exert varying effects by different pathways. However, the specific hypothalamic pathways that can mediate the effects of leptin have not been fully elucidated. As a major excitatory neurotransmitter, glutamate has been found to modulate sympathetic nerve activity in several brain areas, including the ARCN and the PVN [13, 14]. In diabetic rats, glutamatergic tone is increased in the PVN via an upregulation of the N-methyl-D-aspartate (NMDA) type 1 (NR_1) receptor [15]. In the hippocampus, leptin has been shown to facilitate NMDA receptor function and modulate synaptic plasticity [16]. Despite this evidence, the precise central mechanisms by which leptin-glutamate signaling contributes to altered neurohumoral drive during T2D remain unknown. The present study was conducted to investigate the role for leptin-glutamate signaling within the hypothalamus in regulating sympathetic nerve activity under normal conditions and in T2D rats.

2. Materials and Methods

2.1. Animals. Normal rats: Male Sprague-Dawley rats weighing between 325 and 350 g (age 10-11 weeks) were obtained from SASCO Breeding Laboratories (Omaha, NE). This study was approved by the Institutional Animal Care and Use Committee of the University of Nebraska and was carried out under the guidelines of the American Physiological Society and the National Institutes of Health Guide for the Care and Use of Laboratory Animals.

Type II diabetic rats: Male Sprague-Dawley rats (150–180 g, age 6-7 weeks, SASCO) were maintained in a vivarium with a 12 h light/12 h dark cycle and placed on a high-fat diet (HFD, 42% of calories are from fat, Harlan). After 4 weeks, the rats were injected with low-dose streptozotocin (STZ, 30 mg/kg in citric acid, i.p.) to induce partial insulin deficiency. The rats were then fed with HFD for additional 8 weeks [17]. The "normal diet-" fed rats with vehicle injection were used as nondiabetic controls. Postprandial plasma glucose, body weight, and food consumption were monitored weekly. Glucose levels were measured from tail bleeds with a glucometer weekly. The experiments were performed after 12 weeks of HFD-STZ induction.

2.2. General Surgery for Recording of Renal Sympathetic Nerve Activity and Arterial Pressure. Rats were anesthetized with α-chloralose (140 mg/kg, i.p.) and urethane (0.75–1.5 g/kg, i.p.). The femoral artery was cannulated for monitoring mean arterial pressure (MAP) and heart rate (HR). The femoral vein was cannulated for administration of supplemental anesthesia and 0.9% saline. The left renal nerve was isolated, and the electrical signal was recorded with the PowerLab (ADInstruments, Colorado Spring, CO) as described before [18, 19]. Basal RSNA was recorded at the beginning of the experiment. Background noise was determined by nerve activity recorded at the end of the experiment after the rat was euthanized. The RSNA was calculated by subtracting the background noise from the recorded value. The changes in integrated RSNA were expressed as a percentage from the basal value. The changes in MAP and HR were expressed as the absolute difference between the basal value and the value after injection of a drug.

2.3. Microinjections into the ARCN and the PVN. Rats were anesthetized with α-chloralose (140 mg/kg, i.p.) and urethane (0.75–1.5 g/kg, i.p.). Rats were placed in a stereotaxic apparatus. An incision was made on the midline of the scalp to expose the bregma. The coordinates of the right ARCN with reference to the bregma were calculated as being 2.3 mm posterior, 0.5 mm lateral, and 9.6–9.9 mm ventral to the dura [20, 21]. The coordinates of the right side of the PVN with reference to the bregma were calculated as being 1.5 mm posterior, 0.4 mm lateral, and 7.8 mm ventral to the dura [18, 19]. 30 minutes after the surgery, a needle (0.2 mm OD) that was connected to a microsyringe (0.5 μL) was lowered into the ARCN or PVN. At the end of the experiment, monastral blue dye (2% Chicago blue, 30 nL) was injected into the brain for histological verification.

The brain was carefully removed and fixed in 4% formaldehyde. The brain was then frozen, and serial transverse sections (30 μm) were cut using a cryostat. The sections were thaw-mounted on slides. The sections were stained using 1% aqueous neutral red. Presence of blue dye within the ARCN or PVN was determined using a light microscope. The results of these injections are shown in Figure 1.

2.4. Knockdown of the Leptin Receptor with siRNA. In a separated group, rats were anesthetized with ketamine (48 mg/kg, i.p.) and xylazine (12 mg/kg, i.p.). siRNA-targeting leptin receptors were purchased from Santa Cruz Biotechnology (Santa Cruz, CA). Transfection was performed using Lipofectamine 2000 (Invitrogen, Carlsbad, CA) and microinjection into the ARCN or PVN. siRNA for leptin receptors (50 nL) was delivered into the ARCN or PVN by bilateral microinjections. The coordinates of the ARCN and the PVN were described above. The skin was sutured after injection, and the rats were returned to their cages for the next 48 hours. The rats were given analgesic Buprenex injection after surgery to prevent pain.

2.5. Experimental Protocols

2.5.1. Experiment 1. In normal rats, leptin (RD Systems, Minneapolis, MN) was microinjected (5, 25, and 100 ng in 50 nL) into the ARCN or PVN ($n = 8$ rats/group). The responses of RSNA, MAP, and HR over the following 30 minutes were recorded.

2.5.2. Experiment 2. In normal rats, NMDA receptor antagonist AP5 (16 pmol in 50 nL) was microinjected into the ARCN or PVN, 10 minutes prior to microinjection of leptin

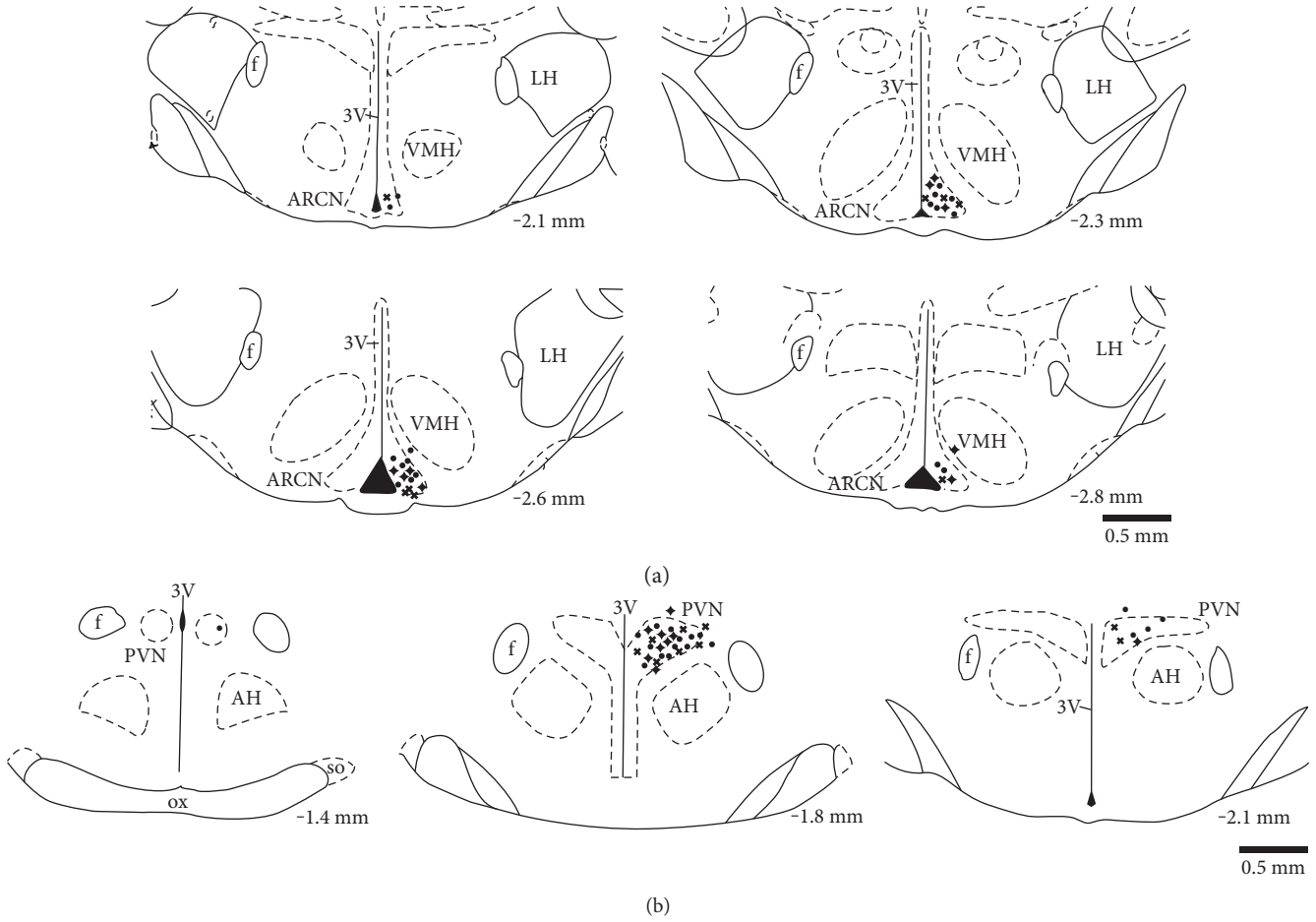

Figure 1: (a) Schematic representations of injection sites in serial sections from the rostral (−2.1) to the caudal (−2.8) extent of the region of the ARCN. (b) Schematic representations of injection sites in serial sections from the rostral (−1.4) to the caudal (−2.1) extent of the region of the PVN. The distance, in millimeters, posterior to the bregma is shown for each section according to Paxinos and Watson. "•" represents the center of microinjection sites from normal rats. "+" represents the center of microinjection sites from control rats. "X" represents the center of microinjection sites from T2D rats. LH: lateral hypothalamus; VMH: ventromedial hypothalamus; AH: anterior hypothalamus; f: fornix; 3V: third ventricle; OX: optic tract.

(100 ng in 50 nL; $n = 8$ rats/group). The responses of RSNA, MAP, and HR over the next 30 minutes were recorded.

2.5.3. Experiment 3. In a separate group of control and T2D rats, leptin receptor siRNA was microinjected into the ARCN or PVN. 48 hours after microinjection of leptin receptor siRNA, NMDA (100 pmol in 50 nL) was microinjected into the ARCN or PVN ($n = 8$ rats/group). The responses of RSNA, MAP, and HR were recorded. Negative controls (scrambled siRNA) were used in order to verify the nonspecific effects of siRNA.

2.6. Confocal Ca^{2+} Imaging. Cultured neuronal NG108 cells and astrocytic C6 cells (ATCC, Manassas, VA) were preincubated with leptin (5 μM) for 24 hours at 37°C in a Petri dish containing laminin-coated glass cover slips. After incubation, cells were then loaded with Fluo-3 (5 μM) for 30 minutes at 37°C. At the end of the incubation, cells were washed with DME medium to remove extracellular Fluo-3 and placed in a chamber on the stage of a laser confocal microscope (Zeiss Confocal LSM 510 META). The confocal calcium image with green fluorescence was taken when the neurons were challenged with glutamate (1 μM). Fluo-3 was excited by light at 488 nm, and fluorescence was measured at wavelengths of >515 nm, using a 100x objective. Raw data were imported into Excel file for analysis.

2.7. Micropunch of the PVN for Western Blot Measurements. In a separate group of control ($n = 6$) and T2D ($n = 6$) rats, the rats were sacrificed with pentobarbital (150 mg/kg, i.p.). Then, brains were removed and frozen on dry ice. Frozen serial coronal sections (100 μm/section) of the ARCN (15 sections) and PVN (6 sections) were cut with a cryostat according to a stereotaxic atlas and bilaterally punched with an 18-gauge needle using the Palkovits and Brownstein technique [22]. The punches for each brain were combined and placed in 100 μL of protein extraction buffer (10 mM Tris, 1 mM ethylenediaminetetraacetic acid, 1% sodium dodecyl sulfate, 0.1% Triton X-100, and 1 mM phenylmethylsulfonyl fluoride) to extract the protein.

Table 1: General characteristics of control and T2D rats.

	Control ($n = 16$)	T2D ($n = 16$)		Control ($n = 16$)	T2D ($n = 16$)
Body weight (g)	427 ± 24	485 ± 29*	Plasma glucose (mmol/L)	5.3 ± 0.3	17.2 ± 1.5*
Retroperitoneal fat pad (g)	5.1 ± 0.3	8.7 ± 1.6*	Plasma insulin (mU/L)	13.7 ± 1.3	13.9 ± 1.1
Epydidimal fat pad (g)	8.2 ± 1.2	9.5 ± 1.4	Insulin sensitivity index	−4.28 ± 0.14	−5.47 ± 0.28*
Brown adipose tissue (g)	1.2 ± 0.2	0.3 ± 0.1*	Plasma leptin (ng/mL)	304 ± 26	479 ± 39*
Basal MAP (mmHg)	90 ± 4	93 ± 5	Basal heart rate (beat/min)	350 ± 16	362 ± 20
Basal int. RSNA (μV·s)	3.2 ± 0.3	4.7 ± 0.4*	24 hrs urine NE (μg)	183 ± 36	403 ± 50*

Values are mean ± SE. *$P < 0.05$ versus control group. MAP: mean arterial pressure; int. RSNA: integrated renal sympathetic activity; NE: norepinephrine.

2.8. Western Blot Measurement of the Leptin Receptor and NMDA NR_1 Receptor Protein. The total protein concentrations in the punched ARCN and PVN samples were measured with a bicinchoninic acid assay kit (Pierce, Rockford, IL). Samples were adjusted to contain the same concentration of total protein. The protein samples with 2X 4% SDS sample buffer were loaded onto a SDS-PAGE gel, subjected to electrophoresis, and then transferred to a polyvinylidene difluoride membrane (Millipore, MA). The membrane was probed with primary antibody [rabbit anti-leptin receptor (1 : 500, Abcam, Cambridge, MA), rabbit anti-NR_1 receptor (1 : 500, Santa Cruz Biotechnology, Santa Cruz, CA), or rabbit anti-glyceraldehyde 3-phosphate dehydrogenase (GAPDH; 1 : 2000, Santa Cruz Biotechnology)] overnight and then probed with secondary antibody (peroxidase-conjugated anti-rabbit IgG, 1 : 5000, Pierce). An enhanced chemiluminescence substrate (Pierce) was applied to the membrane, followed by an exposure within an UVP system (UVP BioImaging, Upland, CA) for visualization. Kodak 1D software (Kodak, NY) was used to quantify the signal. The expression of protein was calculated as the ratio of intensity of the leptin receptor and NR_1 receptor, respectively, relative to the intensity of GAPDH band.

2.9. Leptin Receptor and NMDA NR_1 Receptor Immunohistochemistry. The rats were anesthetized with pentobarbital (65 mg/kg) and transcardially perfused with heparinized saline followed by 4% paraformaldehyde in 0.1 M sodium phosphate buffer. The brain was removed and postfixed in 4% paraformaldehyde solution and then placed in 30% sucrose. 30 μm brain sections were cut with a cryostat and preserved in the cryoprotectant.

Two groups of sections (control and T2D, $n = 4$/group) were incubated with 10% normal donkey serum for 1 hour and then incubated with primary antibody against the leptin receptor (anti-goat, 1 : 200, Santa Cruz Biotechnology) or NR_1 receptor (anti-goat, 1 : 200, Santa Cruz Biotechnology) with the neuronal marker microtubule-associated protein 2 (MAP2, anti-mouse, 1 : 200, Abcam) or glial marker glial fibrillary acidic protein (GFAP, anti-mouse, 1 : 200, BD Pharmingen, San Jose, CA) overnight at 4°C. After washing, the sections were incubated with Cy3-conjugated donkey anti-goat secondary antibody (1 : 200) and Cy2-conjugated donkey anti-mouse secondary antibody (1 : 400, Jackson ImmunoResearch, West Grove, PA) for 2 hours at room temperature. After washing and drying, the sections were cover-slipped with fluoromount-G (SouthernBiotech, Birmingham, AL). Distribution of the leptin receptor or NR_1 receptor with MAP2 or GFAP immunofluorescence, respectively, within the ARCN and PVN was viewed using an Olympus fluorescence microscope equipped with a digital camera (QImaging, Canada).

2.10. Statistical Analysis. Data are presented as means ± SE. The data were subjected to one-way ANOVA followed by comparison for individual group differences with the Newman-Keuls test. Statistical significance was indicated by a value of $P < 0.05$.

3. Results

3.1. General Data. T2D was induced by a combination of both HFD and injection of low-dose STZ. Table 1 illustrates the general characteristics of control and T2D rats used in these experiments. After 12–14 weeks of the treatments (HFD and STZ injection), the body weight and weight of the retroperitoneal fat pad were significantly higher in T2D rats. The T2D rats also show decreased brown adipose tissue. The plasma glucose level and plasma leptin were significantly higher in T2D rats than in control rats. The insulin sensitivity index was significantly decreased in the T2D rats compared with control rats. These data indicated that HFD and low-dose STZ induced hyperglycemia, hyperleptinemia, hyperlipidemia, and insulin resistance in T2D rats mimicking T2D in humans.

The basal RSNA and 24 h urinary norepinephrine levels were significantly increased in T2D rats, suggesting that there was an increased overall sympathetic tone in the T2D rats (Table 1). However, there were no significant differences in basal MAP and HR between control and T2D rats.

3.2. Responses to Microinjection of Leptin into the ARCN or PVN. In anesthetized rats, microinjections of leptin (5 ng ~ 100 ng) into the ARCN or PVN induced increases in RSNA (ARCN: 37 ± 6%; PVN: 35 ± 8% at 100 ng), MAP (ARCN: 25 ± 3 mmHg; PVN: 17 ± 3 mmHg at 100 ng), and HR (ARCN: 51 ± 6 bpm; PVN: 41 ± 6 bpm at 100 ng) (Figure 2). Prior microinjections of NMDA receptor antagonist AP5 (16 pmol) into the ARCN or PVN significantly reduced a leptin-induced increase in RSNA (ARCN: 12 ± 2% versus 37 ± 6%, $P < 0.05$; PVN: 11 ± 4% versus 35 ± 8% at 100 ng, $P < 0.05$), MAP (ARCN: 8 ± 1 mmHg versus 25 ± 3 mmHg; PVN: 2 ± 1 mmHg versus 17 ± 3 mmHg at

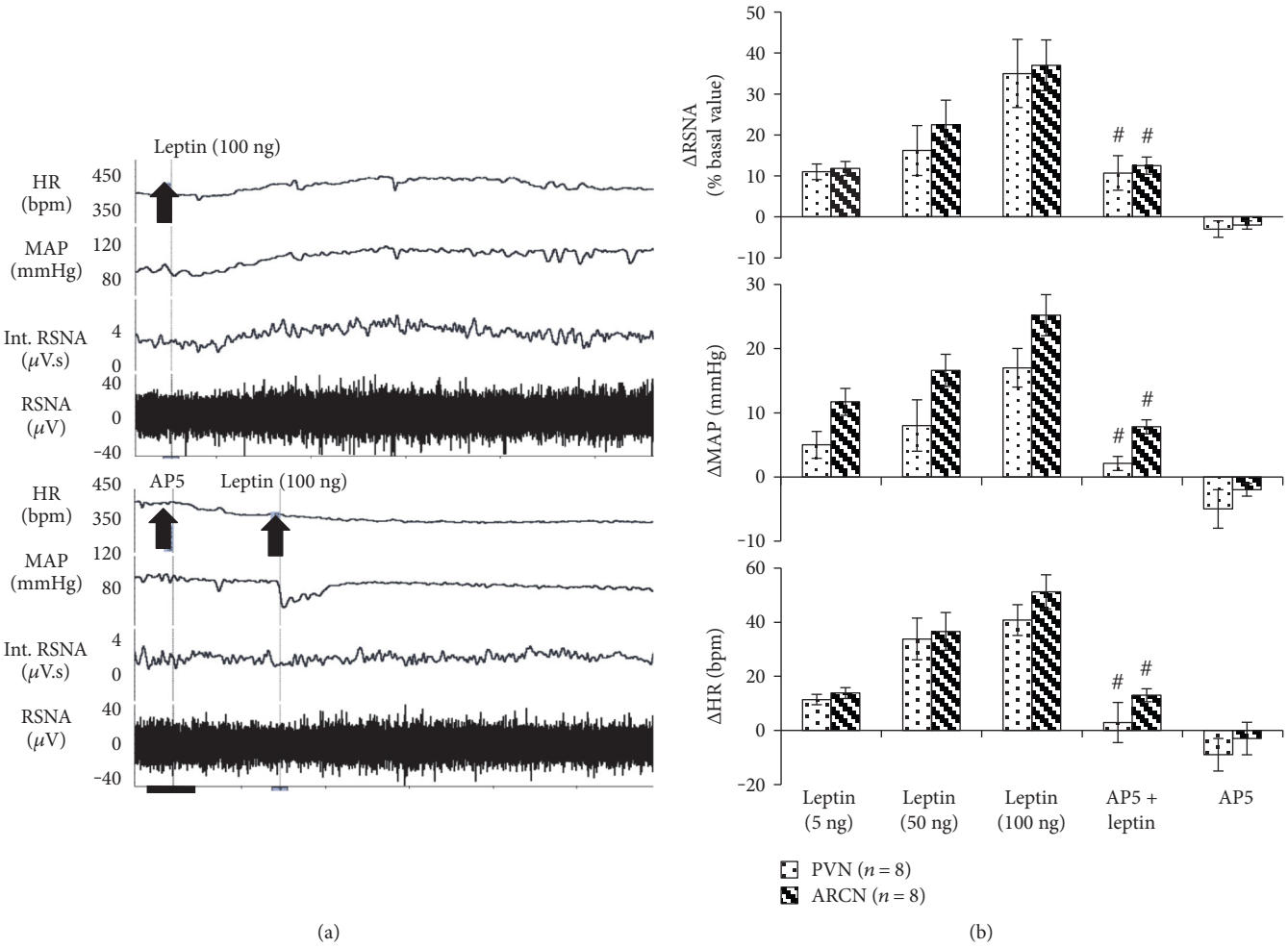

Figure 2: Renal sympathetic nerve activity (RSNA), mean arterial pressure (MAP), and heart rate (HR) responses to microinjection of leptin with/without preadministration of AP5 in the PVN or ARCN. $^{\#}P < 0.05$ versus control group without AP5 administration. (a) A representative tracer of RSNA, MAP, and HR responses to microinjection of leptin with/without preadministration of AP5 in the PVN; bar = 1 min. (b) Mean changes in RSNA, MAP, and HR to microinjection of leptin (5–100 ng) with preadministration of AP5 (16 pmol) in the PVN or ARCN. $^{\#}P < 0.05$ versus leptin group without AP5.

100 ng, $P < 0.05$), and HR (ARCN: 13 ± 2 bpm versus 51 ± 6 bpm, $P < 0.05$; PVN: 3 ± 7 bpm versus 41 ± 6 bpm at 100 ng, $P < 0.05$).

3.3. Knockdown of the Leptin Receptor Inhibits NMDA-Induced Responses in the ARCN. Administration of NMDA (100 pmol) in the ARCN and PVN elicited increases in RSNA, MAP, and HR in both control and T2D groups (Figure 3). Microinjection of NMDA elicited significant increases in RSNA (ARCN: 38 ± 6%; PVN: 49 ± 7%), MAP (ARCN: 14 ± 6 mmHg; PVN: 16 ± 4 mmHg), and HR (ARCN: 22 ± 8 bpm; PVN: 35 ± 9 bpm) in control rats. The RSNA, MAP, and HR responses were significantly enhanced in T2D rats compared to the control rats, reaching 59 ± 4%, 25 ± 4 mmHg, and 43 ± 7 bpm, respectively, in the ARCN (Figure 3(a)) and 76 ± 11%, 25 ± 4 mmHg, and 63 ± 7 bpm, respectively, in the PVN ($P < 0.05$) (Figure 3(b)). Knockdown of the leptin receptor with siRNA in the ARCN and PVN significantly inhibited an NMDA-induced increase in RSNA in the ARCN (Figure 3(a)), but not in the PVN (Figure 3(b)), in both control and T2D rats (ARCN: 16 ± 4% versus 38 ± 6% in control and 20 ± 3% versus 59 ± 4% in T2D, $P < 0.05$), MAP (ARCN: 6 ± 1 mmHg versus 14 ± 3 mmHg in control and 8 ± 2 mmHg versus 25 ± 4 mmHg in T2D, $P < 0.05$), and HR (ARCN: 11 ± 3 bpm versus 22 ± 8 bpm in control and 19 ± 8 bpm versus 43 ± 7 bpm in T2D, $P < 0.05$).

3.4. Brain Histology. Figure 1 illustrates the brain histological data. Among the 32 injections within the ARCN or PVN area, 16 injection sites belong to normal group rats, 8 injection sites belong to control group rats, and 8 injection sites belong to T2D rats. A total of 6 injections missed intended injection sites.

3.5. Leptin Enhanced Intracellular Ca^{2+} Influx to Glutamate in Both Neuronal and Astrocytic Cell Lines. Figure 4 illustrates the effects of leptin on intracellular Ca^{2+} ($[Ca^{2+}]_i$) responses to glutamate in cultured neuronal NG108 and astrocytic C6 cells. Although basal $[Ca^{2+}]_i$ was not

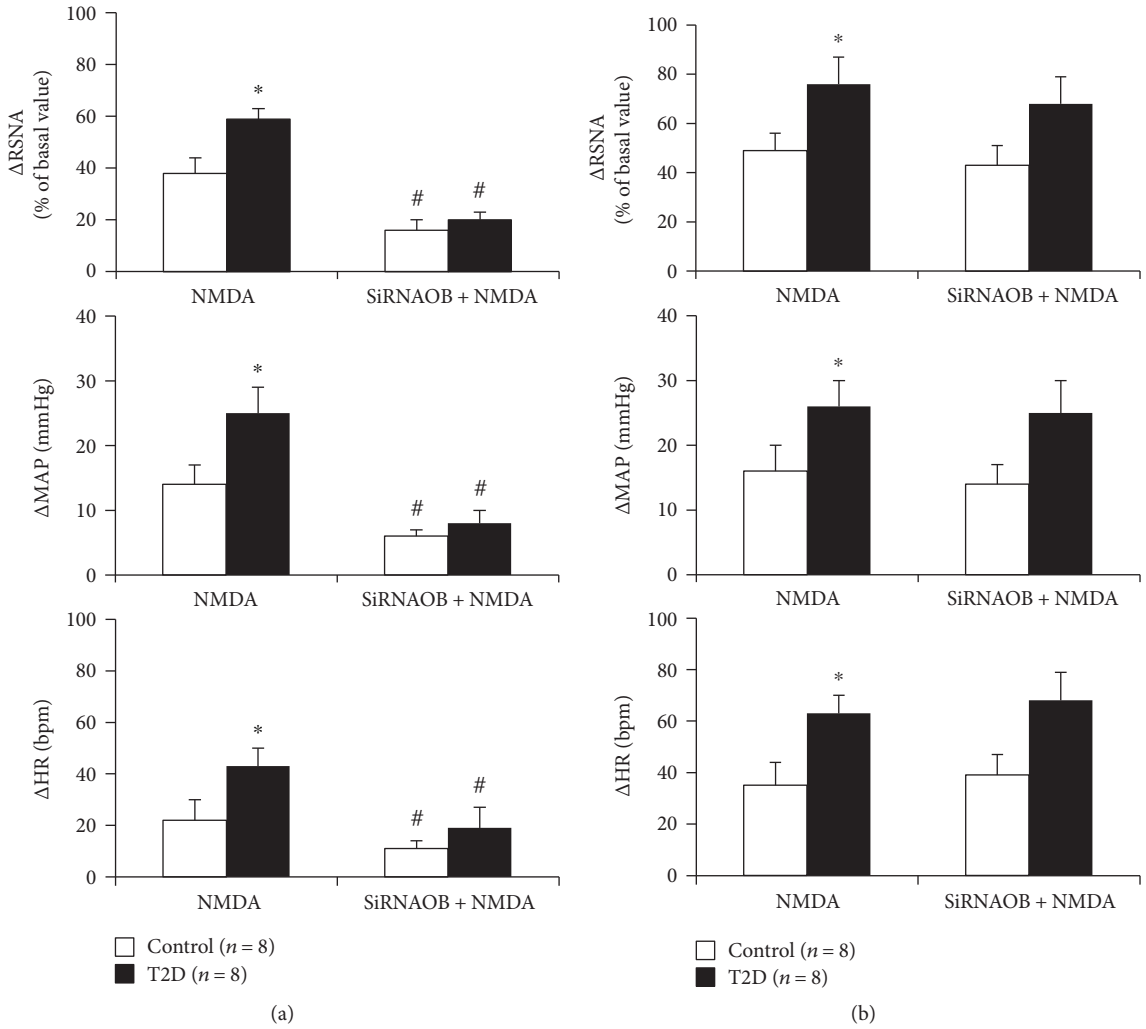

Figure 3: Renal sympathetic nerve activity (RSNA), mean arterial pressure (MAP), and heart rate (HR) responses to microinjection of NMDA (100 pmol) into the ARCN (a) or PVN (b) after knockdown of the leptin receptor with siRNA (siRNAOB) in the ARCN or PVN in control and T2D rats. $^{*}P < 0.05$ versus control group; $^{\#}P < 0.05$ versus group without siRNA knockdown.

significantly altered by treatment with 5 μM leptin, responses to glutamate were significantly affected. In the control group (untreated cells, $n = 12$), 1 μM glutamate caused a rapid $[Ca^{2+}]_i$ increase that peaked at 2.6 ± 0.3 in neurons and 0.35 ± 0.06 in astrocytes, followed by a decline in $[Ca^{2+}]_i$ (Figure 4(b)). Compared with responses of untreated cells, the peak of the $[Ca^{2+}]_i$ response to glutamate was enhanced significantly in cells treated with leptin ($n = 12$). The magnitude of the peak response increased by 69% in leptin-treated neuronal cells (4.4 ± 0.5, $P < 0.05$) and 60% in astrocytic cells (0.56 ± 0.08, $P < 0.05$) (Figure 4(c)). The plateau phase of the response in both neuronal and astrocytic cells had no significant difference with leptin treatment.

3.6. Increased Leptin Receptor and NMDA NR_1 Protein Expression in the ARCN and PVN in T2D Rats. Western blotting analysis showed 100 kDa bands representing the leptin receptor and 115 kDa bands representing the NR_1 receptor in the ARCN and PVN of control and T2D rats. T2D rats had significantly higher protein level of the leptin receptor (ratio of intensity: 1.06 ± 0.14 versus 0.54 ± 0.11, $P < 0.05$) and NR_1 receptor (ratio of intensity: 0.43 ± 0.06 versus 0.24 ± 0.03, $P < 0.05$) in the ARCN (Figure 5). In the PVN, both leptin receptor and NR_1 receptor protein expressions were also significantly increased in the T2D compared to the control rats (ratio of intensity—leptin receptor: 1.23 ± 0.21 versus 0.49 ± 0.11; NR_1 receptor: 0.55 ± 0.09 versus 0.20 ± 0.08, $P < 0.05$).

As an in situ confirmation of the alteration in the leptin receptor and NR_1 receptor within the ARCN and PVN, the immunofluorescence for leptin receptors (Figure 6) and NR_1 receptors (Figure 7) was found increased in the ARCN and PVN from rats with T2D compared with control rats. Both leptin receptor and NR_1 receptor immunofluorescent signals were colocalized with the neuronal marker MAP2 within the ARCN and the PVN (Figures 6(a) and 7(a)). Leptin receptor immunofluorescent signals were also colocalized with the glial cell marker GFAP within the ARCN and the PVN (Figure 6(b)). However, NR_1 receptor immunofluorescent signals were not colocalized with GFAP within the ARCN and the PVN (Figure 7(b)).

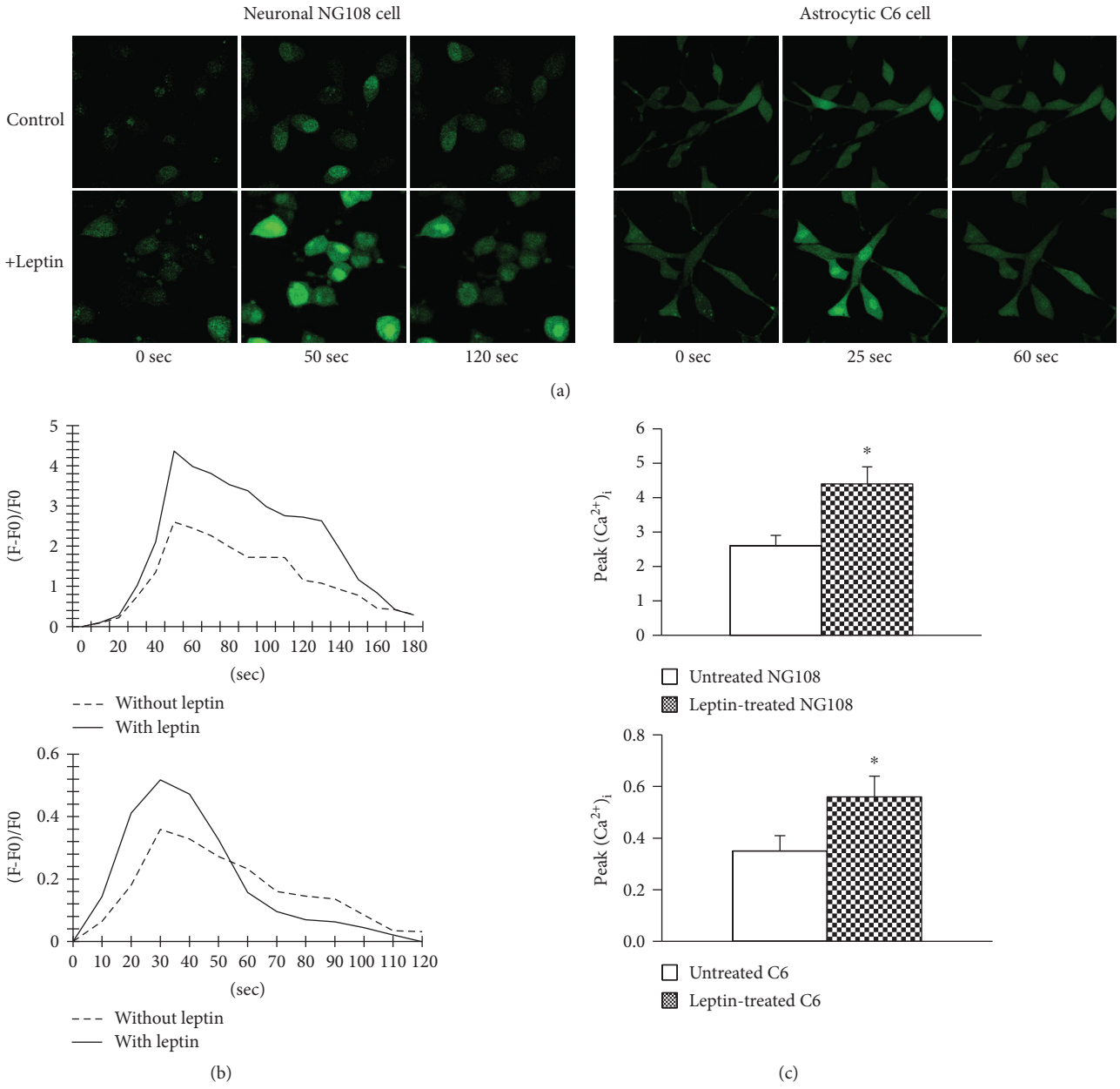

FIGURE 4: (a) Representative confocal images showing Ca^{2+} green fluorescent changes to glutamate (1 μM) in neuronal NG108 and astrocytic C6 cells with/without leptin pretreatment. (b) Time-dependent responses of mean $[Ca^{2+}]_i$ to glutamate in each treatment group. (c) Summary data showing peak $[Ca^{2+}]_i$ in each treatment group. $^*P < 0.05$ versus untreated group.

4. Discussion

In the present study, we have demonstrated that microinjections of leptin into the ARCN or PVN induce increases in RSNA, MAP, and HR. Prior microinjections of NMDA receptor antagonist AP5 blunted the leptin-induced increases in RSNA, MAP, and HR. Knockdown of leptin receptor expression with siRNA inhibited NMDA-induced increases in RSNA, MAP, and HR in the ARCN but not in the PVN. In *in vitro* studies, preincubation of neuronal NG108 cells with leptin induced a robust increase in intracellular Ca^{2+} green fluorescence when the cells were challenged with glutamate. Furthermore, in high-fat diet and low-dose STZ-induced T2D rats, we found that leptin receptor and NMDA NR_1 receptor expressions in the ARCN and PVN were significantly increased. Taken together, these results show that within these hypothalamic nuclei, leptin-glutamate signaling regulates the sympathetic activation. This may contribute to the sympathoexcitation commonly observed in obesity-related T2D.

Adipose tissue-released leptin exerts an influence on many physiologic processes, including food intake, thermoregulation, fertility, sympathetic nerve activation, renal function, blood vessel tone, and blood pressure. The role of leptin in activating sympathetic drive has been highlighted in many reviews [23–25]. In the whole animal studies, we have observed that microinjections of leptin into the ARCN or PVN induce an

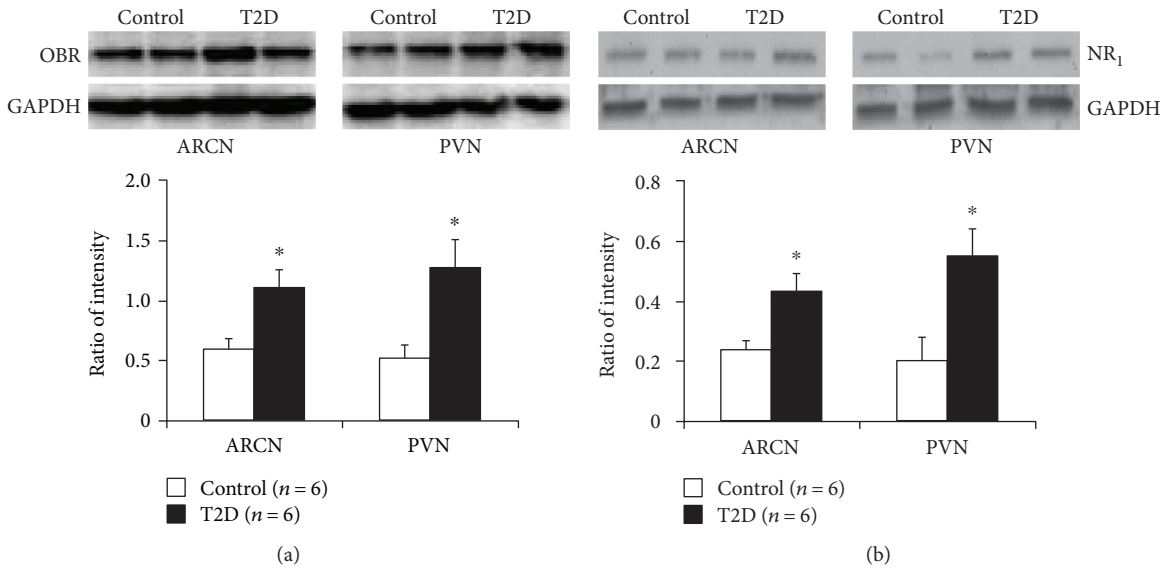

Figure 5: (a) Representative gel of leptin receptor (OBR) and mean protein expressions in the ARCN and PVN in control and T2D rats. $^*P < 0.05$ versus control group. (b) Representative gel of NMDA receptor (NR_1) and mean protein expressions in the ARCN and PVN in control and T2D rats. $^*P < 0.05$ versus control group.

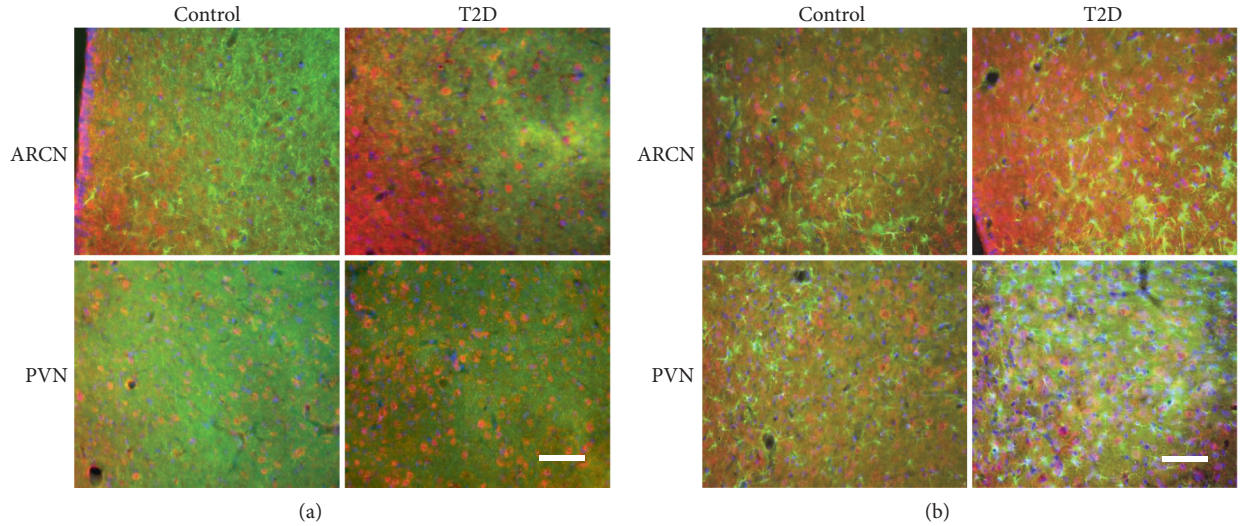

Figure 6: (a) Immunofluorescent photomicrographs from the sections of the ARCN and PVN region stained for the leptin receptor (red), neuronal marker microtubule-associated protein 2 (MAP2 in green), and 4′,6-diamidino-2-phenylindole (DAPI in blue) in a control and a T2D rat. (b) Immunofluorescent photomicrographs from the sections of the ARCN and PVN region stained for the leptin receptor (red), glial marker glial fibrillary acidic protein (GFAP in green), and DAPI (blue) in a control and a T2D rat. Bar = 100 μm.

increase in RSNA, MAP, and HR. This is consistent with reports that intracerebroventricular- (ICV-) administered leptin increases sympathetic nerve activity to the kidney [26, 27].

The hypothalamic ARCN has been shown to regulate energy balance and blood pressure [27]. Stimulation of the ARCN with leptin and glutamate elicits increases in RSNA and MAP [13]. The hypothalamic PVN is one of the major preautonomic centers that directly control sympathetic outflow in the central nervous system [28]. Stimulation of PVN has been shown to elicit an increased discharge from several sympathetic nerves, including renal, adrenal, and splanchnic nerves [29–31]. Studies indicate that the ARCN is a gateway for the action of insulin and leptin on sympathetic activity [32]. The ARCN-to-PVN circuit involved in energy homeostasis is directly and tonically controlled by leptin in a multinodal fashion [5]. Neurons in the ARCN express leptin receptors and play an important role in transmitting the leptin signal to the PVN neurons. The ARCN-PVN projection appears to be overactive in diabetic rats [33].

In the central nervous system, leptin appears to exert its effects on sympathetic activity and blood pressure through a number of mediators. A novel interaction between

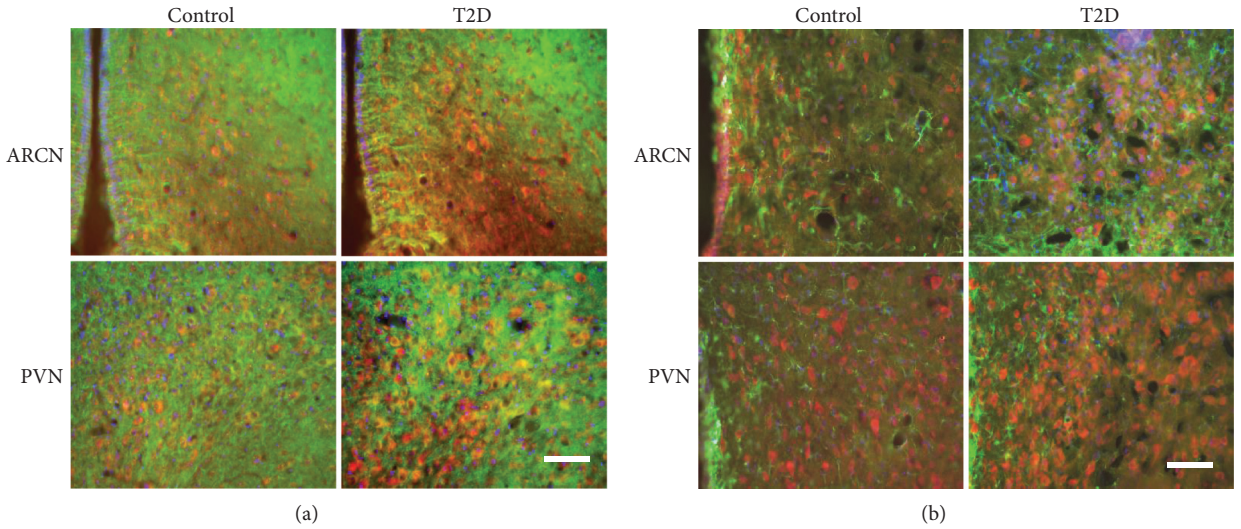

Figure 7: (a) Immunofluorescent photomicrographs from the sections of the ARCN and PVN region stained for NMDA receptor 1 (NR_1 in red), MAP2 (green), and DAPI (blue) in a control and a T2D rat. (b) Immunofluorescent photomicrographs from the sections of the ARCN and PVN region stained for NR_1 (red), GFAP (green), and DAPI (blue) in a control and a T2D rat. Bar = 100 μm.

angiotensin-II and leptin in the control of sympathetic nerve activity, brown adipose tissue thermogenesis, and body weight has been reported recently [34, 35]. Leptin also regulates PVN neurons indirectly, by binding to receptors in the ARCN and regulating the release of neural effectors like glutamate from first-order neurons onto preautonomic neurons in the PVN [16]. Glutamate NR_1 is markedly augmented in the PVN of diabetic rats [15]. The precise mechanisms of leptin-glutamate signaling within the hypothalamus that lead to sympathoexcitation in T2D remain to be determined.

Both leptin and glutamate are important neuromodulators in the central nervous system. High glutamatergic tone has been shown in several hypersympathetic disease conditions, such as diabetes, hypertension, and chronic heart failure [14, 15, 36]. Our data has shown that central leptin-induced increases in RSNA, MAP, and HR were attenuated by glutamate NMDA receptor antagonist AP5 in both the ARCN and PVN. These data support the concept of a brain leptin-glutamate interaction in which the brain glutamate mechanism facilitates leptin-induced increases in sympathetic nerve activity. Both the ARCN and PVN are possible sites for the leptin-glutamate interaction. When we knock down the leptin receptor, a central NMDA-induced increase in RSNA, MAP, and HR was attenuated in the ARCN but not in the PVN. This suggests that leptin facilitates NMDA-induced increases in sympathetic nerve activity in the ARCN. However, in the PVN, NMDA-mediated sympathetic activation is more dominant and appears to be likely more independent of leptin signaling.

By confocal calcium image, in cultured neuronal NG108 cells and astrocytic C6 cells, we have observed that preincubation with leptin for 24 hours induced a robust increase in intracellular Ca^{2+} green fluorescence when the cells were challenged with glutamate compared to the control group without leptin pretreatment. The responses occurred immediately after leptin administration followed by a rapid return to baseline. Leptin caused a robust increase in glutamate-induced calcium signaling in both cultured neurons and astrocytes, confirming functional changes in neurons and astrocytes induced by leptin via a glutamate receptor.

The hypothalamus is an extremely heterogeneous tissue comprised of astrocytes, oligodendrocytes, microglia, endothelial cells, ependymal cells and numerous neuronal subgroups [37]. Astrocytes have recently emerged as an active component of various complex central mechanisms, and it is now clear that their role in the brain is by no means limited to just providing structural and metabolic support to neurons. Astrocytes can affect neuronal activity in a variety of ways. This may include the release of glutamate, ATP, or other signaling molecules [38]. Astrocytes are possible cellular substrates of angiotensin (1–7) that affect local metabolism and microcirculation in the RVLM, resulting in changes in the activity of RVLM presympathetic neurons and hence blood pressure [39]. Regulation of tonic GABA inhibitory function, presympathetic neuronal activity, and sympathetic outflow from the PVN is shown to be modulated by astrocytic GABA transporters [40]. Leptin receptor mRNA and protein are observed in both astrocytes and neurons in the rat hypothalamus [41]. It has been reported that metabolic changes in obese mice can rapidly alter leptin receptor expression and astrocytic activity. The leptin receptor is responsible for leptin-induced calcium signaling in astrocytes [42].

In the T2D rat model, we have observed that 12–14 weeks of HFD and single low-dose STZ injection produces hyperglycemia, hyperleptinemia, hyperlipidemia, and insulin resistance in the rat. Hyperleptinemic condition might be implicated in generating the elevation of sympathoexcitation in T2D rats. We have observed that leptin receptor and NMDA NR_1 protein levels in the ARCN and PVN tissues were upregulated in T2D rats compared to the control rats. This result suggests that upregulation of leptin receptors and NMDA receptor within the hypothalamus may be one possible mechanism for the enhanced endogenous

leptin-glutamate-mediated excitatory action on sympathetic outflow in T2D. Furthermore, double-labeling immunohistochemistry analysis showed that both neurons and astrocytes in the hypothalamus expressed leptin receptors while NMDA NR_1 receptors were only localized on the neurons. The results imply alterations of leptin receptor expression and astrocytic activity within the ARCN and PVN in T2D rats. Determining exactly which specific cell types activate leptin signaling may yield novel and critical clues to the mechanisms related to the altered neurohumoral drive during T2D.

5. Conclusion

These studies provide evidence that within the hypothalamic nuclei, leptin-glutamate signaling regulates sympathetic activation. This altered mechanism/s within the PVN may contribute to the increased renal sympathetic neural activity observed in T2D. These results provide a potential target for the treatment of enhanced sympathoactivation commonly observed in T2D.

Conflicts of Interest

The authors declare that they have no conflicts of interest.

References

[1] P. Bjorntorp, G. Holm, and R. Rosmond, "Hypothalamic arousal, insulin resistance and type 2 diabetes mellitus," *Diabetic Medicine*, vol. 16, no. 5, pp. 373–383, 1999.

[2] A. M. Sharma and V. T. Chetty, "Obesity, hypertension and insulin resistance," *Acta Diabetologica*, vol. 42, Supplement 1, pp. S3–S8, 2005.

[3] K. Rahmouni and W. G. Haynes, "Leptin and the central neural mechanisms of obesity hypertension," *Drugs of Today (Barcelona, Spain)*, vol. 38, no. 12, pp. 807–817, 2002.

[4] D. J. Ewing, "Diabetic autonomic neuropathy and the heart," *Diabetes Research and Clinical Practice*, vol. 30, pp. S31–S36, 1996.

[5] Y. D. Lin, K. L. Hsu, E. T. Wu et al., "Autonomic neuropathy precedes cardiovascular dysfunction in rats with diabetes," *European Journal of Clinical Investigation*, vol. 38, no. 9, pp. 607–614, 2008.

[6] K. R. Ward, J. F. Bardgett, L. Wolfgang, and S. D. Stocker, "Sympathetic response to insulin is mediated by melanocortin 3/4 receptors in the hypothalamic paraventricular nucleus," *Hypertension*, vol. 57, no. 3, pp. 435–441, 2011.

[7] Y. Ao, M. Ko, A. Chen et al., "Potent hyperglycemic and hyperinsulinemic effects of thyrotropin-releasing hormone microinjected into the rostroventrolateral medulla and abnormal responses in type 2 diabetic rats," *Neuroscience*, vol. 169, no. 2, pp. 706–719, 2010.

[8] L. J. Prior, N. Elkelis, J. A. Armitage et al., "Exposure to a high-fat diet alters leptin sensitivity and elevates renal sympathetic nerve activity and arterial pressure in rabbits," *Hypertension*, vol. 55, no. 4, pp. 862–868, 2010.

[9] K. Rahmouni, C. D. Sigmund, W. G. Haynes, and A. L. Mark, "Hypothalamic ERK mediates the anorectic and thermogenic sympathetic effects of leptin," *Diabetes*, vol. 58, no. 3, pp. 536–542, 2009.

[10] A. L. Mark, K. Rahmouni, M. Correia, and W. G. Haynes, "A leptin-sympathetic-leptin feedback loop: potential implications for regulation of arterial pressure and body fat," *Acta Physiologica Scandinavica*, vol. 177, no. 3, pp. 345–349, 2003.

[11] K. Matsumura, I. Abe, T. Tsuchihashi, and M. Fujishima, "Central effects of leptin on cardiovascular and neurohormonal responses in conscious rabbits," *American Journal of Physiology. Regulatory, Integrative and Comparative Physiology*, vol. 278, pp. R1314–R1320, 2000.

[12] M. Ghamari-Langroudi, D. Srisai, and R. D. Cone, "Multinodal regulation of the arcuate/paraventricular nucleus circuit by leptin," *Proceedings of the National Academy of Sciences of the United States of America*, vol. 108, no. 1, pp. 355–360, 2011.

[13] T. Nakamura, S. Bhatt, and H. N. Sapru, "Cardiovascular responses to hypothalamic arcuate nucleus stimulation in the rat: role of sympathetic and vagal efferents," *Hypertension*, vol. 54, no. 6, pp. 1369–1375, 2009.

[14] Y. F. Li, K. G. Cornish, and K. P. Patel, "Alteration of NMDA NR1 receptors within the paraventricular nucleus of hypothalamus in rats with heart failure," *Circulation Research*, vol. 93, no. 10, pp. 990–997, 2003.

[15] Y. Luo, C. Kaur, and E. A. Ling, "Neuronal and glial response in the rat hypothalamus-neurohypophysis complex with streptozotocin-induced diabetes," *Brain Research*, vol. 925, no. 1, pp. 42–54, 2002.

[16] A. J. Irving, L. Wallace, D. Durakoglugil, and J. Harvey, "Leptin enhances NR2B-mediated N-methyl-D-aspartate responses via a mitogen-activated protein kinase-dependent process in cerebellar granule cells," *Neuroscience*, vol. 138, no. 4, pp. 1137–1148, 2006.

[17] H. Zheng, X. Liu, Y. Li, P. K. Mishra, and K. P. Patel, "Attenuated dopaminergic tone in the paraventricular nucleus contributing to sympathoexcitation in rats with type 2 diabetes," *American Journal of Physiology-Regulatory, Integrative and Comparative Physiology*, vol. 306, no. 2, pp. R138–R148, 2014.

[18] H. Zheng, W. G. Mayhan, K. R. Bidasee, and K. P. Patel, "Blunted nitric oxide-mediated inhibition of sympathetic nerve activity within the paraventricular nucleus in diabetic rats," *American Journal of Physiology-Regulatory, Integrative and Comparative Physiology*, vol. 290, no. 4, pp. R992–R1002, 2006.

[19] A. C. Kleiber, H. Zheng, H. D. Schultz, J. D. Peuler, and K. P. Patel, "Exercise training normalizes enhanced glutamate-mediated sympathetic activation from the PVN in heart failure," *American Journal of Physiology. Regulatory, Integrative and Comparative Physiology*, vol. 294, pp. R1863–R1872, 2008.

[20] S. M. Harlan, D. A. Morgan, K. Agassndian et al., "Ablation of the leptin receptor in the hypothalamic arcuate nucleus abrogates leptin-induced sympathetic activation," *Circulation Research*, vol. 108, no. 7, pp. 808–812, 2011.

[21] T. Kawabe, K. Kawabe, and H. N. Sapru, "Tonic gamma-aminobutyric acid-ergic activity in the hypothalamic arcuate nucleus is attenuated in the spontaneously hypertensive rat," *Hypertension*, vol. 62, no. 2, pp. 281–287, 2013.

[22] M. Palkovits and M. Brownstein, "Brain microdissection techniques," in *Brain Microdissection Techniques*, A. E. Cuello, Ed., John Wiley & Sons, Chichester, 1983.

[23] G. A. Head, K. Lim, B. Barzel, S. L. Burke, and P. J. Davern, "Central nervous system dysfunction in obesity-induced hypertension," *Current Hypertension Reports*, vol. 16, no. 9, p. 466, 2014.

[24] A. L. Mark, "Selective leptin resistance revisited," *American Journal of Physiology-Regulatory, Integrative and Comparative Physiology*, vol. 305, no. 6, pp. R566–R581, 2013.

[25] G. Z. Kalil and W. G. Haynes, "Sympathetic nervous system in obesity-related hypertension: mechanisms and clinical implications," *Hypertension Research*, vol. 35, no. 1, pp. 4–16, 2012.

[26] J. C. Dunbar, Y. G. Hu, and H. Q. Lu, "Intracerebroventricular leptin increases lumbar and renal sympathetic nerve activity and blood pressure in normal rats," *Diabetes*, vol. 46, pp. 2040–2043, 1997.

[27] K. Rahmouni and D. A. Morgan, "Hypothalamic arcuate nucleus mediates the sympathetic and arterial pressure responses to leptin," *Hypertension*, vol. 49, no. 3, pp. 647–652, 2007.

[28] A. M. Strack, W. B. Sawyer, J. H. Hughes, K. B. Platt, and A. D. Loewy, "A general pattern of CNS innervation of the sympathetic outflow demonstrated by transneuronal pseudorabies viral infections," *Brain Research*, vol. 491, pp. 156–162, 1989.

[29] H. Kannan, Y. Hayashida, and H. Yamashita, "Increase in sympathetic outflow by paraventricular nucleus stimulation in awake rats," *The American Journal of Physiology*, vol. 256, pp. R1325–R1330, 1989.

[30] T. Y. Katafuchi, Y. Oomura, and M. Kurosawa, "Effects of chemical stimulation of paraventricular nucleus on adrenal and renal nerve activity in rats," *Neuroscience Letters*, vol. 86, pp. 195–200, 1988.

[31] J. Deering and J. H. Coote, "Paraventricular neurones elicit a volume expansion-like change of activity in sympathetic nerves to the heart and kidney in the rabbit," *Experimental Physiology*, vol. 85, pp. 177–186, 2000.

[32] R. A. Dampney, "Arcuate nucleus - a gateway for insulin's action on sympathetic activity," *The Journal of Physiology*, vol. 589, Part 9, pp. 2109-2110, 2011.

[33] H. M. Frankish, S. Dryden, D. Hopkins, Q. Wang, and G. Williams, "Neuropeptide Y, the hypothalamus, and diabetes: insights into the central control of metabolism," *Peptides*, vol. 16, no. 4, pp. 757–771, 1995.

[34] C. N. Young, D. A. Morgan, S. D. Butler et al., "Angiotensin type 1a receptors in the forebrain subfornical organ facilitate leptin-induced weight loss through brown adipose tissue thermogenesis," *Molecular Metabolism*, vol. 4, no. 4, pp. 337–343, 2015.

[35] A. M. Hilzendeger, D. A. Morgan, L. Brooks et al., "A brain leptin-renin angiotensin system interaction in the regulation of sympathetic nerve activity," *American Journal of Physiology. Heart and Circulatory Physiology*, vol. 303, no. 2, pp. H197–H206, 2012.

[36] D. P. Li, Q. Yang, H. M. Pan, and H. L. Pan, "Pre- and postsynaptic plasticity underlying augmented glutamatergic inputs to hypothalamic presympathetic neurons in spontaneously hypertensive rats," *The Journal of Physiology*, vol. 586, no. 6, pp. 1637–1647, 2008.

[37] G. R. Gordon, K. J. Iremonger, S. Kantevari, G. C. Ellis-Davies, B. A. MacVicar, and J. S. Bains, "Astrocyte-mediated distributed plasticity at hypothalamic glutamate synapses," *Neuron*, vol. 64, no. 3, pp. 391–403, 2009.

[38] T. Okada, S. Shimizu, M. Wakamori et al., "Molecular cloning and functional characterization of a novel receptor-activated TRP Ca2+ channel from mouse brain," *The Journal of Biological Chemistry*, vol. 273, no. 17, pp. 10279–10287, 1998.

[39] F. Guo, B. Liu, S. Lane et al., "Astroglia are a possible cellular substrate of angiotensin(1-7) effects in the rostral ventrolateral medulla," *Cardiovascular Research*, vol. 87, no. 3, pp. 578–584, 2010.

[40] J. B. Park, J. Y. Jo, H. Zheng, K. P. Patel, and J. E. Stern, "Regulation of tonic GABA inhibitory function, presympathetic neuronal activity and sympathetic outflow from the paraventricular nucleus by astroglial GABA transporters," *The Journal of Physiology*, vol. 587, Part 19, pp. 4645–4660, 2009.

[41] H. Hsuchou, W. Pan, M. J. Barnes, and A. J. Kastin, "Leptin receptor mRNA in rat brain astrocytes," *Peptides*, vol. 30, no. 12, pp. 2275–2280, 2009.

[42] H. Hsuchou, Y. He, A. J. Kastin et al., "Obesity induces functional astrocytic leptin receptors in hypothalamus," *Brain*, vol. 132, Part 4, pp. 889–902, 2009.